

# Optimal process design across process hierarchies for the efficient utilization of renewable energy sources

**Dissertation**  
zur Erlangung des akademischen Grades

**Doktoringenieur**  
**(Dr.-Ing.)**

von M.Sc. Dominik Schack  
geboren am 16. April 1987 in Celle

genehmigt durch die Fakultät für Verfahrens- und Systemtechnik der Otto-von-Guericke-Universität Magdeburg

Promotionskommission: Jun.-Prof. Dr.-Ing. Alba Dieguez-Alonso (Vorsitz)  
Prof. Dr.-Ing. Kai Sundmacher (Gutachter)  
Prof. Dr.-Ing. Mirko Skiborowski (Gutachter)  
Prof. Dr.-Ing. Peter Pfeifer (Gutachter)

eingereicht am: 06. April 2021  
Promotionskolloquium am: 06. September 2021



## Abstract

Without strong efforts and effective climate protection measures, the world's population will have only a few more years to achieve the goals announced in the Paris Agreement. As one of the largest consumers of energy and thus a large contributor of harmful greenhouse gas emissions, the chemical industry bears a special responsibility for a successful energy transition. Consequently, one of the major goals of the chemical industry is to replace fossil raw materials with renewable resources by using sustainable process technologies. For a significant CO<sub>2</sub> reduction, the massive use of renewable energies by implementation of Renewables-to-Chemicals (R2Chem) production systems is of key importance. The principal step of R2Chem-concepts is the electrochemical splitting of water into hydrogen and oxygen via electrolysis and the subsequent utilization and/or storage of hydrogen. Since in many areas, (synthetic) hydrocarbons will still be required in future, also sustainable carbon sources have to be identified. Carbon capture and utilization (CCU) technologies seem to be very attractive since they offer the possibility to close the carbon cycle by recycling the bounded carbon atom in the CO<sub>2</sub> molecule.

Initially, this dissertation evaluates different target molecules by introducing the storage efficiency as the ratio of the stored energy content to the total energy input required via the R2Chem pathway. Methanol proves to be an optimal target molecule due to its advantageous carbon-hydrogen feed ratio and beneficial storage properties. It is shown that the main energy consumption is caused by the electrolysis of water, although the carbon source also has a significant influence: The use of CCU and the direct capture of CO<sub>2</sub> from the air increases the energy demand significantly compared to concentrated CO<sub>2</sub> sources such as flue gases from power plants. While theoretically the annual methanol production in Germany could be covered by the available electricity from renewable energies, the consumption (and thus the reduction potential) of CO<sub>2</sub> is only 0.2 % of the annual emissions. This shows that not only the substitution of fossil raw material and energy sources but also an increase in the energy efficiency of the processes involved is crucial for a successful transition to a more sustainable chemical production.

In order to increase the overall efficiency of the processes, challenges must be faced at different process hierarchies. While at the production system level, more general questions and early-

stage decisions in chemical production networks are addressed, at the plant and process unit level the focus is on the detailed optimization of chemical processes and process units. In the context of this dissertation the FluxMax approach was developed as a scale-independent network approach for process design and synthesis and simultaneous heat integration. The basic idea of the FluxMax approach is an effective decoupling of process-related non-linearities from the subsequent network flow optimization by discretizing the thermodynamic state space. The discretization allows the representation of chemical processes across different length scales, which enables the transformation of a non-linear process optimization problem into a convex flow optimization task on a defined network graph. The chemical process is represented as a directed graph, with nodes corresponding to thermodynamic substances, elementary processes and heat and work utilities. While each mixture is uniquely defined by thermodynamic coordinates, the elementary processes are uniformly described by stoichiometric equations. The edges connecting the nodes correspond to the mass and energy flows and are decision variables of the optimization problem. Consequently, the FluxMax approach can be divided into three steps: i) discretization of the thermodynamic state space; ii) modeling of the elementary processes; and iii) formulation and solution of the flow optimization problem. The FluxMax approach was developed in collaboration with Georg Liesche at the Max Planck Institute Magdeburg.

Using the methanol synthesis process as a case study, the FluxMax approach was applied to different levels of the process hierarchy. First, the FluxMax approach was applied at the production system level for the systematic analysis of different feedstocks and energy sources. It is shown that an acceptable trade-off between costs and emissions can be achieved by using natural gas as raw material source if the required energy is supplied from renewable sources. However, a net consumption of CO<sub>2</sub> of the entire production system is only possible if renewable energy sources are used and at the same time CO<sub>2</sub> is used as a raw material source. With the use of fossil fuels, a significant carbon footprint is unavoidable due to high indirect CO<sub>2</sub> emissions from the energy supply (electricity, heat). Thus, in addition to economic challenges of using CO<sub>2</sub> as feedstock also the ecological impact strongly depends on the energy source used.

Secondly, the FluxMax approach was applied at the plant level by representing the overall process of methanol production through the elementary processes of reaction, separation, heating/cooling, mixing and compression. As a result of the simultaneous consideration of heat integration, an energy-optimized process configuration is identified that outperforms the configuration identified in a sequential design procedure. The simultaneous approach results in a heat saving potential of almost 99 % compared to 88 % in the sequential approach. This result underlines the need for a simultaneous approach to identify energy efficient processes that lead to significant reductions in CO<sub>2</sub> emissions.



Thirdly, the FluxMax approach was used for the design of distillation columns, as these account for the largest contribution to the total energy consumption of chemical processes due to their high heat demand. The representation of a distillation process by elementary processes results in additional degrees of freedom for optimization compared to classical column modeling approaches. The energy-optimized configuration is a column with improved heat transfer between vapor and liquid streams. MESH equations are used for the validation of the FluxMax design, as they represent the state-of-the-art in process modeling tools. While the new design reduces the energy requirements by up to 64 % compared to the classic design, additional heat exchange area is required to exploit the energy saving potential. A multi-objective optimization – energy demand vs. heat exchange area – was performed to determine the optimal trade-off between energy demand and capital costs related to heat exchange area to be installed. The highly energy-efficient designs identified by the FluxMax approach can be realized in practice by horizontal columns or modularized container solutions.

The results presented in this dissertation demonstrate the versatility of the FluxMax approach, which uses a unique description of each type of chemical conversion process. Consequently, the approach is applicable to any level of the process hierarchy. In particular, the representation of the chemical process by elementary processes – resulting in increased degrees of freedom – and the simultaneous consideration of heat integration and process design make the FluxMax approach a powerful tool for the design of chemical processes on different length scales. At different levels of the process hierarchy, it is demonstrated that highly energy-efficient processes can be designed that can contribute to a reduction in the energy consumption of the chemical industry. Nevertheless, the results also show the limits of the chemical industry's potential in terms of reducing global energy consumption and the corresponding GHG emissions. However, the chemical industry needs to be considered in a sector-coupled perspective, as the chemical industry has a major impact on other sectors: from the sustainable production of alternative fuels to the sustainable production of consumer goods.



## Zusammenfassung

Auch bei stärksten Anstrengungen und wirksamen Klimaschutzmaßnahmen wird die Weltbevölkerung nur noch wenige Jahre Zeit haben, die im Pariser Abkommen angekündigten Ziele zu erreichen. Als einer der größten Energieverbraucher und damit als erheblicher Verursacher schädlicher Treibhausgasemissionen trägt die chemische Industrie eine besondere Verantwortung für eine erfolgreiche Energiewende. Infolgedessen ist es eines der Hauptziele der chemischen Industrie, fossile Rohstoffe durch nachwachsende Rohstoffe zu ersetzen, indem nachhaltige Prozesstechnologien eingesetzt werden. Für eine signifikante CO<sub>2</sub>-Reduzierung ist die massive Nutzung erneuerbarer Energien zur Herstellung von Chemikalien durch die Einführung von Renewables-to-Chemicals (R2Chem) Produktionssystemen von zentraler Bedeutung. Der wichtigste Schritt von R2Chem-Konzepten ist die elektrochemische Spaltung von Wasser in Wasserstoff und Sauerstoff durch Elektrolyse und die anschließende Nutzung und/oder Speicherung von Wasserstoff. Da in vielen Bereichen auch in Zukunft (synthetische) Kohlenwasserstoffe benötigt werden, müssen ebenfalls nachhaltige Kohlenstoffquellen identifiziert werden. Carbon Capture and Utilization (CCU) Technologien scheinen sehr attraktiv zu sein, da sie die Möglichkeit bieten, den Kohlenstoffkreislauf durch Recycling des im CO<sub>2</sub>-Molekül gebundenen Kohlenstoffatoms zu schließen.

In dieser Arbeit werden zunächst verschiedene Zielmoleküle evaluiert, indem die Speichereffizienz als Verhältnis des gespeicherten Energieinhalts zum Gesamtenergieeinsatz, der über den R2Chem-Pfad benötigt wird, eingeführt wird. Methanol erweist sich aufgrund seines vorteilhaften Kohlenstoff-Wasserstoff-Verhältnisses und vorteilhafter Speichereigenschaften als optimales Zielmolekül. Es wird gezeigt, dass der Hauptenergieverbrauch durch die Elektrolyse von Wasser verursacht wird, obwohl auch die Kohlenstoffquelle einen bedeutenden Einfluss hat: Der Einsatz von CCU und die direkte Abscheidung von CO<sub>2</sub> aus der Luft erhöht den Energiebedarf im Vergleich zu konzentrierten CO<sub>2</sub>-Quellen, wie z.B. Rauchgasen aus Kraftwerken, erheblich. Während theoretisch die jährliche Methanolproduktion in Deutschland durch den verfügbaren Strom aus erneuerbaren Energien gedeckt werden könnte, liegt der Verbrauch (und damit das Reduktionspotenzial) von CO<sub>2</sub> nur bei 0,2 % der jährlichen Emissionen. Dies zeigt, dass nicht nur die Substitution fossiler Energieträger,

sondern auch die Steigerung der Energieeffizienz der beteiligten Prozesse entscheidend für einen erfolgreichen Übergang zu einer nachhaltigeren Chemieproduktion ist.

Um die Gesamteffizienz der Prozesse zu steigern, müssen technische Verbesserungsmaßnahmen auf verschiedenen Ebenen ergriffen werden. Während auf der Verbundebene allgemeinere Fragen und strategische Entscheidungen bezüglich chemischer Produktionsnetzwerke beantwortet werden, liegt der Schwerpunkt auf der Ebene einzelner Anlagen sowie Prozesseinheiten auf der detaillierten Optimierung der chemischen Prozesse und Prozesseinheiten. Im Rahmen dieser Dissertation wurde der FluxMax Approach als skalunenabhängiger Netzwerkansatz für Prozessdesign und -synthese unter simultaner Berücksichtigung von Wärmeintegration entwickelt. Die Grundidee des FluxMax Approach ist eine effektive Entkopplung der prozessbedingten Nichtlinearitäten von der nachfolgenden Flussoptimierung durch Diskretisierung des thermodynamischen Zustandsraums. Die Diskretisierung erlaubt die Darstellung chemischer Prozesse über verschiedene Längenskalen hinweg, was die Umwandlung eines nichtlinearen Prozessoptimierungsproblems in eine konvexe Flussoptimierungsaufgabe auf einem definierten Netzwerkgraphen ermöglicht. Der chemische Prozess wird als gerichteter Graph dargestellt, wobei die Knoten den thermodynamischen Substanzen, den Elementarprozessen, den Wärmebereitstellungseinrichtungen sowie dem elektrischen Netz entsprechen. Während jede chemische Mischung eindeutig durch thermodynamische Koordinaten definiert ist, werden die Elementarprozesse einheitlich durch stöchiometrische Gleichungen beschrieben. Die Kanten, die die Knoten verbinden, entsprechen den Massen- und Energieströmen, die Entscheidungsgrößen des Optimierungsproblems sind. Folglich kann der FluxMax Approach in drei Schritte unterteilt werden: i) Diskretisierung des thermodynamischen Zustandsraums; ii) Modellierung der Elementarprozesse; und iii) Formulierung und Lösung des Flussoptimierungsproblems. Der FluxMax Approach wurde in Zusammenarbeit mit Georg Liesche am Max-Planck-Institut Magdeburg entwickelt.

Anhand der Methanolsynthese als Beispielprozess wurde der FluxMax Approach auf verschiedenen Ebenen der Prozesshierarchie angewandt. Zunächst wurde der FluxMax Approach auf der Verbundebene für die systematische Analyse verschiedener Rohstoffe und Energiequellen eingesetzt. Es wird gezeigt, dass ein guter Kompromiss zwischen Kosten und Emissionen durch die Verwendung von Erdgas als Rohstoffquelle erreicht werden kann, wenn die benötigte Energie aus erneuerbaren Quellen geliefert wird. Ein Nettoverbrauch des gesamten Produktionssystems von  $\text{CO}_2$  ist jedoch nur möglich, wenn erneuerbare Energiequellen eingesetzt werden und gleichzeitig  $\text{CO}_2$  als Rohstoffquelle genutzt wird. Bei der Nutzung fossiler Energieträger ist ein negativer  $\text{CO}_2$ -Fußabdruck aufgrund hoher indirekter  $\text{CO}_2$ -Emissionen aus der Energieversorgung (Strom, Wärme) unvermeidbar. Neben den ökonomischen Herausforderungen bei der Nutzung von  $\text{CO}_2$  als Rohstoffquelle hängen daher auch die ökologischen Auswirkungen stark von der eingesetzten Energiequelle ab.

Zweitens wurde der FluxMax Approach auf der Anlagenebene angewandt, indem der Gesamtprozess der Methanolproduktion durch die elementaren Prozesse Reaktion, Separation, Erhitzung/Kühlung, Mischen und Verdichtung repräsentiert wurde. Als Ergebnis der simultanen Betrachtung der Wärmeintegration wird eine energieoptimierte Prozesskonfiguration identifiziert, die die in einem sequenziellen Prozess identifizierte Konfiguration hinsichtlich ihrer Energieeffizienz übertrifft. Der simultane Ansatz ergibt ein Wärmeeinsparungspotenzial von fast 99 % im Vergleich zu nur 88 % beim klassischen sequentiellen Ansatz, was die Notwendigkeit eines simultanen Ansatzes unterstreicht, um energieeffiziente Prozesse zu identifizieren, die zu signifikanten Reduzierungen der CO<sub>2</sub>-Emissionen führen.

Drittens wurde der Ansatz für die Auslegung von Destillationskolonnen verwendet, da diese aufgrund ihres hohen Wärmebedarfs den größten Beitrag zum Gesamtenergieverbrauch chemischer Prozesse leisten. Die Darstellung eines Destillationsprozesses durch Elementarprozesse führt im Vergleich zu klassischen Kolonnenmodellierungsansätzen zu erhöhten Freiheitsgraden für die Optimierung. Die energieoptimierte Konfiguration ist eine Kolonne mit verbessertem Wärmeübergang zwischen Dampf- und Flüssigkeitsströmen. Für die Validierung des FluxMax-Designs werden die MESH-Gleichungen verwendet, da sie den Stand der Technik in Prozesssimulationstools darstellen. Während der integrierte Designansatz den Energiebedarf im Vergleich zum klassischen Design um bis zu 64 % reduziert, ist zusätzliche Wärmeaustauschfläche erforderlich, um das Energieeinsparungspotenzial auszuschöpfen. Eine Mehrzieloptimierung – Energiebedarf vs. Wärmeaustauschfläche – wurde durchgeführt, um den optimalen Kompromiss zwischen Energiebedarf und Kapitalkosten in Bezug auf die Wärmeaustauschfläche zu ermitteln. Die durch den FluxMax Approach identifizierten energieeffizienten Designs können in der Praxis durch horizontale Kolonnen oder modularisierte Containerlösungen realisiert werden.

Die in dieser Arbeit vorgestellten Ergebnisse zeigen die Vielseitigkeit des FluxMax Approaches, der eine einheitliche Beschreibung für verschiedene Arten von chemisch-physikalischen Wandlungsprozessen verwendet. Folglich ist der Ansatz auf jeder Ebene der Prozesshierarchie anwendbar. Insbesondere die Darstellung des chemischen Prozesses durch Elementarprozesse – was zu erhöhten Freiheitsgraden führt – und die simultane Berücksichtigung von Wärmeintegration und Prozessdesign machen den FluxMax Approach zu einem leistungsfähigen Werkzeug für den Entwurf chemischer Prozesse auf verschiedenen Längenskalen. Es wird gezeigt, dass extrem energieeffiziente Prozesse entworfen werden können, die zu einer Reduzierung des Energieverbrauchs der chemischen Industrie beitragen können. Dennoch zeigen die Ergebnisse auch die Grenzen des Potenzials der chemischen Industrie in Bezug auf die Reduzierung des globalen Energieverbrauchs und der entsprechenden Emissionen auf. Die chemische Industrie muss jedoch in einer sektorgekoppelten Perspektive betrachtet werden, da die chemische Industrie einen großen Einfluss auf andere Sektoren hat: von der nachhaltigen Produktion alternativer Kraftstoffe bis hin zur nachhaltigen Produktion von Konsumgütern.



## Preface

In the context of this dissertation, several publications were prepared, six of which are partly included in this manuscript. The chapters containing parts of these publications are listed in the following.

- The FluxMax approach as a length-scale independent process design and synthesis method is based on various publications prepared in the context of this thesis. The version presented in **Chapter 3** was largely taken from Schack et al. [1]. Additional heat integration constraints were first derived in Schack et al. [2]. Parts were also published in Liesche et al. [3].
- The systematic analysis of the influence of different raw materials and energy sources on the specific production costs and the specific CO<sub>2</sub>-emissions of the methanol production network presented in **Chapter 4** is based on Schack et al. [4]. However, the results presented in this thesis were recalculated for a current cost scenario. Furthermore, some of the results as well as discussions were also published in Schack et al. [5].
- **Chapter 5** demonstrates the application of the FluxMax approach at the plant level and emphasizes the need for simultaneous consideration of heat integration during the actual process design task. The presented results are taken from Schack et al. [1]. However, the results were recalculated taking into account the additional heat integration constraints introduced in Schack et al. [2].
- The application of the FluxMax approach at the process unit level is presented in **Chapter 6**. The design optimization of distillation columns using the FluxMax approach was first demonstrated in Schack et al. [6], and the chapter is largely based on the detailed analysis performed in Schack et al. [2].

[1] **Schack, D.**, Liesche, G., Sundmacher, K.: The FluxMax approach: Simultaneous flux optimization and heat integration by discretization of thermodynamic state space illustrated on methanol synthesis process, *Chemical Engineering Science*, 215, 115382, **2020**. doi:10.1016/j.ces.2019.115382

- [2] **Schack, D.**, Jastram, A., Liesche, G., Sundmacher, K.: Energy-efficient distillation processes by additional heat transfer derived from the FluxMax approach, *Frontiers in Energy Research*, 8, 134, **2020**. doi:10.3389/fenrg.2020.00134
- [3] Liesche, G., **Schack, D.**, Sundmacher, K.: The FluxMax approach for simultaneous process synthesis and heat integration: production of hydrogen cyanide, *AIChE Journal*, 65(7), e16554, **2019**. doi:10.1002/aic.16554
- [4] **Schack, D.**, Rihko-Struckmann, L., Sundmacher, K.: Linear programming approach for structure optimization of Renewable-to-Chemicals (R2Chem) production networks, *Industrial & Engineering Chemistry Research*, 57(30), 9889–9902, **2018**. doi:10.1021/acs.iecr.7b05305
- [5] **Schack, D.**: R2Chem: Renewables to valuable chemicals and fuels, *MPI Magdeburg Report 2017 – 2018*, 42–43, Magdeburg, Germany, **2019**.
- [6] **Schack, D.**, Liesche, G., Sundmacher, K.: Simultaneous heat and mass flow optimization of a distillation column applying the FluxMax approach, *Chemical Engineering Transactions*, 76, 337–342, **2019**. doi:10.3303/CET1976057



# Contents

<b>Abstract</b>	<b>iii</b>
<b>Zusammenfassung</b>	<b>vii</b>
<b>Preface</b>	<b>xi</b>
<b>Nomenclature</b>	<b>xvii</b>
<b>1 Introduction</b>	<b>1</b>
1.1 Motivation . . . . .	1
1.2 Central research questions . . . . .	3
1.3 Structure of this dissertation . . . . .	4
<b>2 Renewables-to-Chemicals</b>	<b>7</b>
2.1 Target molecules in the context of R2Chem . . . . .	7
2.2 Evaluation of storage efficiency of target molecules . . . . .	10
2.3 Chapter summary . . . . .	16
<b>3 Scale-independent network approach for process design and synthesis</b>	<b>19</b>
3.1 Literature review . . . . .	19
3.2 The FluxMax approach . . . . .	21
3.2.1 Directed graph representation of chemical process networks . . . . .	22
3.2.2 Formulation of node conservation laws . . . . .	25
3.2.3 Heat integration model . . . . .	27
3.2.4 Formulation of the optimization problem . . . . .	31
3.3 Chapter summary . . . . .	33
<b>4 Production system level</b>	<b>35</b>
4.1 Literature review . . . . .	36
4.1.1 Knowledge-based approaches . . . . .	36
4.1.2 Optimization-based approaches . . . . .	38
4.2 Application of FluxMax approach to the production system level . . . . .	40
4.3 Case study . . . . .	42

---

4.3.1	Methanol production network . . . . .	42
4.3.2	Formulation of the optimization problem . . . . .	43
4.4	Results . . . . .	48
4.4.1	Evaluation of different feedstock and energy sources . . . . .	49
4.4.2	Analysis of combined feedstock sources . . . . .	53
4.4.3	Multi-objective optimization . . . . .	56
4.5	Chapter summary . . . . .	57
<b>5</b>	<b>Plant level</b>	<b>59</b>
5.1	Literature review . . . . .	59
5.2	Application of FluxMax approach to the plant level . . . . .	61
5.3	Case study . . . . .	63
5.3.1	Methanol synthesis process . . . . .	64
5.3.2	Formulation of the optimization problem . . . . .	70
5.4	Results . . . . .	72
5.4.1	Comparison of sequential and simultaneous process synthesis . . . . .	72
5.4.2	Optimal utility network . . . . .	79
5.4.3	Identification of optimal process designs . . . . .	81
5.5	Chapter summary . . . . .	84
<b>6</b>	<b>Process unit level</b>	<b>85</b>
6.1	Literature review . . . . .	85
6.2	FluxMax approach for distillation processes . . . . .	88
6.2.1	Directed graph representation of distillation processes . . . . .	88
6.2.2	Heat integration model . . . . .	89
6.3	Case Study . . . . .	90
6.3.1	Methanol-water separation . . . . .	90
6.3.2	Formulation of optimization problems . . . . .	92
6.4	Results . . . . .	95
6.4.1	Application to conventional distillation design tasks . . . . .	95
6.4.2	Energy-efficient designs by additional heat transfer . . . . .	99
6.4.3	Implementation of the improved heat transfer . . . . .	102
6.5	Chapter summary . . . . .	104
<b>7</b>	<b>Conclusions</b>	<b>107</b>
7.1	Summary . . . . .	107
7.2	FluxMax approach . . . . .	108
7.3	Production system level . . . . .	109
7.4	Plant level . . . . .	111
7.5	Process unit level . . . . .	112

---

7.6	Outlook . . . . .	113
<b>Appendix A Thermodynamic data</b>		<b>115</b>
<b>Appendix B Supplement to Chapter 2</b>		<b>119</b>
<b>Appendix C Supplement to Chapter 4</b>		<b>121</b>
C.1	Linear fitting parameters for investment cost estimation . . . . .	121
C.2	Elementary processes at production system level . . . . .	121
<b>Appendix D Supplement to Chapter 5</b>		<b>125</b>
D.1	Overview of elementary processes . . . . .	125
D.2	Formulation of the linear program . . . . .	127
D.3	Temperature levels of utilities . . . . .	129
D.4	Discretization of thermodynamic state space . . . . .	129
<b>Appendix E Supplement to Chapter 6</b>		<b>131</b>
E.1	Distillation column design by MESH equations . . . . .	131
E.1.1	MESH equations for classic column design . . . . .	131
E.1.2	Extension of MESH equations . . . . .	132
<b>References</b>		<b>135</b>
<b>List of Figures</b>		<b>153</b>
<b>List of Tables</b>		<b>157</b>
<b>Publications and statements of authorship</b>		<b>159</b>
<b>Schriftliche Erklärung</b>		<b>165</b>



# Nomenclature

## Latin Symbols

<b>A</b>	Coefficient matrix of constraints	
$a, b$	Fitting parameters for investment cost estimation	
$A^{\text{HX}}$	Heat exchanger area	$\text{m}^2$
$A_\alpha, B_\alpha, C_\alpha$	Antoine parameters of $\alpha$ in Chapter 6	
$A_\alpha, B_\alpha, C_\alpha, D_\alpha, E_\alpha$	Shomate parameters in Appendix A	
$A_j$	Elementary process of absorption	
<b>b</b>	Vector of right-hand sides	
<b>c</b>	Vector of cost factors	
$C$	Cost contribution in Chapter 4	$\text{€ a}^{-1}$
$c_{\text{CO}_2}$	$\text{CO}_2$ price	$\text{€ t}_{\text{CO}_2}^{-1}$
$c_s$	Specific costs	$\text{€ t}_{\text{CH}_3\text{OH}}^{-1}$
$c_{p,\alpha}$	Molar isobaric heat capacity of $\alpha$	$\text{J mol}^{-1}\text{K}^{-1}$
<b>C</b>	Carbon atom	
<b>C</b>	Cold stream in Chapter 3	
$C_j$	Elementary process of compression	
$D_j$	Elementary process of heating/cooling	
$E_\alpha^{\text{stored}}$	Energy content of $\alpha$	$\text{kW}$
$E_{\text{CO}_2}$	$\text{CO}_2$ emissions	$\text{t a}^{-1}$
$E_j^{\text{in}}$	Energy input of process step $j$	$\text{kW}$
$e_j^{\text{in}}$	Specific energy demand of process step $j$	$\text{kJ mol}^{-1}$
$e_s$	Specific carbon dioxide emission	$\text{t}_{\text{CO}_2} \text{ t}_{\text{CH}_3\text{OH}}^{-1}$
$E_j$	Elementary process node $j$	

$\tilde{f}$	Adjusted objective function for $\ell_1$ -norm-regularization	
$f$	Objective function	
$g(\varphi)$	Inequality constraints	
$G_j$	Elementary process of a generic process	
$\Delta h_v$	Enthalpy of evaporation	$\text{kJ mol}^{-1}$
$\Delta h_{f,\alpha}$	Enthalpy of formation of $\alpha$	$\text{kJ mol}^{-1}$
$\Delta h_{u,\alpha}^{\text{mass}}$	Gravimetric lower heating value	$\text{MJ kg}^{-1}$
$\Delta h_{u,\alpha}^{\text{mol}}$	Molar lower heating value	$\text{MJ mol}^{-1}$
$\Delta_R h^\ominus$	Standard enthalpy of reaction	$\text{kJ mol}^{-1}$
$\Delta_R h_{(E_j)}$	Enthalpy of reaction of elementary process $E_j$	$\text{kJ mol}^{-1}$
$h(\varphi)$	Equality constraints	
$h_\alpha$	Molar enthalpy of $\alpha$	$\text{kJ mol}^{-1}$
H	Hot stream in Chapter 3	
H	Hydrogen atom	
$j$	process step $j$	
$k^{\text{HX}}$	Heat transfer coefficient	$\text{W m}^{-2}\text{K}$
$L_j$	Elementary process of mixing	
$m$	Heat exchanger $m$	
$M_\alpha$	Molar mass of $\alpha$	$\text{kg mol}^{-1}$
$M_i$	Thermodynamic substance node $i$	
$\dot{\mathbf{N}}$	Vector of mass fluxes	$\text{mol s}^{-1}$
$\dot{N}$	Mass flux	$\text{mol s}^{-1}$
$n$	Distillation tray $n$	
$n_C$	Number of pure components	
$n_{\text{HX}}$	Total number of inter-tray heat exchangers	
$n_{\text{pb}}$	Payback period	a
$n_{\text{tray}}$	Total number of distillation trays	
N	Nitrogen atom	
O	Oxygen atom	
$p$	Pressure	Pa
$p_0$	Reference pressure	Pa
$p_1, p_2$	Linear regression parameters for investment cost estimation	

$p_{\alpha}^{\text{sat}}$	Saturation pressure of $\alpha$	Pa
$\dot{\mathbf{Q}}$	Vector of heat fluxes	kW
$\dot{Q}$	Heat flux	kW
$R$	Ideal gas constant	$\text{J mol}^{-1}\text{K}^{-1}$
$r$	Reflux ratio	-
$R_j$	Elementary process of reaction	
$\Delta s_{f,\alpha}$	Entropy of formation of $\alpha$	$\text{J mol}^{-1}\text{K}^{-1}$
$\Delta_{R^S(E_j)}$	Entropy of reaction of elementary process $E_j$	$\text{J mol}^{-1}\text{K}$
$s_{\alpha}$	Molar entropy of $\alpha$	$\text{J mol}^{-1}\text{K}^{-1}$
$S_j$	Elementary process of separation	
$S_k$	Work utility node $k$	
$\Delta T_m$	Logarithmic mean temperature difference	K
$\Delta T_{\min}$	Minimum temperature difference of heat transfer	K
$T$	Temperature	K
$T_0$	Reference temperature	K
$U_l$	Utility node $l$	
$\dot{\mathbf{W}}$	Vector of work fluxes	kW
$\dot{W}$	Work flux	kW
$\mathbf{x}$	Vector of molar fractions	-
$x$	Molar fraction	-
$x$	Liquid stream in MESH equations in Appendix E	
$y_n$	Integer variable associated with distillation tray $n$	
$y$	Vapor stream in MESH equations in Appendix E	
$z$	Interest rate	-
$z$	Dimension of the thermodynamic state space in Chapter 3	
$z$	Feed stream in MESH equations in Appendix E	

### Greek Symbols

$\alpha$	Pure substance	
$\dot{\mathbf{\Gamma}}$	Vector of process extent numbers	$\text{mol s}^{-1}$
$\dot{\Gamma}$	Process extent number	$\text{mol s}^{-1}$
$\zeta_z$	Thermodynamic coordinate of $z$ -th dimension	

$\eta$	Efficiency factor of work consumption	-
$\eta_j^{\text{th}}$	Thermodynamic efficiency of process step $j$	
$\eta_{\text{comp}}^{\text{C}_j}$	Compression efficiency	-
$\eta_{(\text{E}_j)}^{\text{in}}$	Energy conversion efficiency	-
$\eta_{\alpha}^{\text{storage}}$	Storage efficiency of $\alpha$	-
$\eta_{\text{ec}}$	Energy conversion efficiency	-
$\eta_{\text{ht}}$	Heat transfer efficiency	-
$\eta_j$	Conversion efficiency of process step $j$	-
$\lambda$	Regularization parameter of $\ell_1$ -norm-regularization	-
$\dot{\xi}$	Extent of reaction	$\text{mol s}^{-1}$
$\rho$	Mass density	$\text{kg m}^{-3}$
$\varphi$	Vector of decision variables	
$\varphi$	Molar heat duty	$\text{kJ mol}^{-1}$
$\varphi_i$	Decision variable	
$\chi$	Generalized stoichiometric coefficient	
$\psi_{(\text{S}_j)}^{(\text{M}_i)}$	Total split ratio of separator $\text{S}_j$	-
$\omega$	Molar work duty	$\text{kJ mol}^{-1}$

### Indices

$\ominus$	Standard condition
AS	Air separation
B	Boiling point
bot	Bottom stage
comp	Compression
conv	Conversion
D	Dew point
EL	Electrolysis
el	Electric
eq	Equality
ext	External flux
F	Flash inlet
feed	Feed stage



---

H,r	Heat removal
H,s	Heat supply
I	Investment
in	Inlet flux
int	Internal flux
iq	Inequality
lb	Lower bound
liq	Liquid
loss	Losses
mass	Gravimetric
max	Maximum
min	Minimum
mol	Molar
out	Outlet flux
P	Purchase
rev	Reversible
top	Top stage
ub	Upper bound
util	Utility
vap	Vapor
vol	Volumetric

**Other Symbols**

$\mathcal{A}$	Set of all pure substances $\alpha$
$\mathcal{E}$	Set of elementary process nodes $E_j$
$\mathcal{F}$	Set of all fluxes
$\mathcal{K}$	Set of all permutations of internally heat transferring streams
$\mathcal{M}$	Set of all thermodynamic substance nodes $M_i$
$\mathcal{S}$	Set of work utility nodes $S_k$
$\mathcal{U}$	Set of utility nodes $U_l$

**Acronyms**

AC	Ambient conditions
----	--------------------

---

ACES	Advanced process for cost and energy saving
ADM1	Anaerobic digestion model No. 1
BBEx	Branch and bound with exergy analysis
BMA	Hydrogen cyanide from methane and ammonia, Ger.: <i>Blausäure aus Methan und Ammoniak</i>
CAPEX	Capital expenditure
CCS	Carbon capture and storage
CCU	Carbon capture and utilization
DECHEMA	German Society for Chemical Engineering and Biotechnology, Ger.: <i>Deutsche Gesellschaft für Chemische Technik und Biotechnologie</i>
DME	Dimethyl ether
DR	Dry reforming
EC	Electrochemical
EPF	Elementary process function
EPN	Elementary process node
EU	European Union
FEHE	Feed effluent heat exchanger
FMA	FluxMax Approach
GHG	Greenhouse gas
GWP	Global Warming Potential
HIDiC	Heat integrated distillation column
HPPO	Hydrogen Peroxide to Propylene Oxide
HT	High temperature
HTW	High temperature Winkler process, Ger.: <i>Hochtemperatur Winkler Verfahren</i>
HX	Heat exchanger
IDEAS	Infinite-dimensional state-space
IEA	International Energy Agency
IPPC	Intergovernmental Panel on Climate Change
LCA	Life cycle assessment
LHV	Lower heating value
LOHC	Liquid organic hydrogen carriers
LP	Linear programming

---

LT	Low temperature
MESH	Mass, equilibrium, summation, energy balances in enthalpy form
MILP	Mixed integer linear programming
MINLP	Mixed integer non-linear programming
MPI	Max Planck Institute
MSW	Municipal solid waste
NIST	National Institute of Standards and Technology
NLP	Non-linear programming
OME	Poly(oxymethylene) dimethyl ether
OPEX	Operational expenditure
ORC	Organic Rankine cycles
PEM	Polymer electrolyte membrane
PEN	Process extent number
PMB	Partial molar balance
PNFA	Process Network Flux Analysis
PSE	Process systems engineering
R2Chem	Renewables-to-Chemicals
RNFA	Reaction Network Flux Analysis
RWGS	Reverse water gas shift
SR	Steam reforming
TAC	Total annualized costs
TSN	Thermodynamic substance node
UN	Utility node
UNFCCC	United Nations Framework Convention on Climate Change
USA	United States of America
WCEC	World Congress of Chemical Engineering
WUN	Work utility node



# Chapter 1

## Introduction

### 1.1 Motivation

While the climate of the earth has always been characterized by cold and warm epochs, there is clear evidence that anthropogenic global warming is unprecedented in the industrial era [1]. In 1992, the international environmental agreement United Nations Framework Convention on Climate Change (UNFCCC) was adopted, which obliged the signatory states, including the European Union (EU) and the United States of America (USA), to take measures against anthropogenic climate change and to reduce harmful greenhouse gas (GHG) emissions. The UNFCCC was expanded by the Kyoto Protocol, which introduced three flexible mechanisms, including the introduction of an emissions trading system. With the Kyoto Protocol, which was adopted in 1997 and came into force in 2005, the industrialized countries committed themselves for the first time to the legally binding goal of reducing GHG emissions. Compared to 1990, emissions are to be reduced by 5.2 % in the period 2008-2012. The EU committed to reduce its overall emissions by 8 %, which meant a reduction of 21 % for Germany [2]. After a first successful period, the treaty was extended in 2012 and committed the signatory states to further reduce their GHG emissions by 18 % by 2020. The EU (20 %) and Germany (40 %) had even more ambitious targets. In addition, the German energy concept (Ger.: *Energiekonzept*) aimed to reduce emissions by 80 %, which means almost GHG-neutrality. In order to achieve these targets, primary energy demand is to be reduced gradually by 20 % by 2020 and by 50 % by 2050 compared to the reference year 2008 [3]. While the Kyoto Protocol was only adopted by the industrialized countries, the Paris Agreement, which was adopted in 2016, was signed by all countries worldwide by 2017 – until the USA later denounced it. The agreement aimed to reduce the effects of climate change and to keep the global temperature increase below 2 °C – or even better below 1.5 °C – compared to the pre-industrial era [4]. In 2019, the European Commission announced the European Green Deal, a set of policy

initiatives intended to achieve net greenhouse gas emissions of zero by 2050 and make Europe the first climate neutral continent [5].

However, the deceptive sense that mankind is on the right track due to the successful implementation of environmental measures and compliance with initial climate targets is misleading. There is an urgent need for further action. In 2018, the United Nations Intergovernmental Panel on Climate Change (IPCC) published a study which indicated a remaining carbon dioxide CO<sub>2</sub> budget of only 460 Gt<sub>CO<sub>2</sub></sub> to maintain a 66 % probability of meeting the 1.5 °C climate target [6]. To date, the budget has been further reduced to about 320 Gt<sub>CO<sub>2</sub></sub>, leaving only 7.5 years if CO<sub>2</sub> emissions remain at today's level [7]. Even the 2 °C will not be reached if emissions are not significantly reduced within the next 25 years. As a result, there is a growing awareness in societies around the world that blames policy makers for slow and insufficient action. In particular, The younger generation fears the destruction of the basis of life [8].

Most GHG emissions are caused by energy consumption, of which industry is the second largest contributor after the transport sector. German industry alone accounts for 28.9 % of the total energy consumption [9]. In a study from 2017, the German Society for Chemical Engineering and Biotechnology (DECHEMA) stated that the chemical industry is the largest industrial energy consumer (19 %) and the third largest GHG emitter in Europe [10]. Although they analyzed that there has been a tremendous improvement in energy efficiency – since 1990, energy consumption has been reduced by 22 % (resulting in a 59 % reduction in GHG gases) while chemical production has increased by 78 % – they see a further reduction potential of 20-30 Mt<sub>CO<sub>2</sub></sub> through energy efficiency measures. Similar conclusions are drawn by the International Energy Agency (IEA) [11]. Additional emission reductions can be achieved by considering the use of alternative raw materials, such as biomass or CO<sub>2</sub> [12, 13], or the electrification of chemical processes [14]. This is achieved through Power-to-X processes [15–21] by using surplus electrical energy for the production of chemicals. However, electrification through electricity from renewable energy sources is not sufficient to achieve the required reduction of CO<sub>2</sub> emissions, but renewable raw materials must be taken into account. For this reason, the term Renewables-to-Chemicals (R2Chem) is used throughout this dissertation instead of Power-to-X.

In conjunction with the chemical industry, it is the responsibility of research to develop alternative processes. At the 10th World Congress of Chemical Engineering (WCEC) 2017 in Barcelona, several presidents of leading chemical engineering associations signed the Barcelona Declaration [22]. There they declared that they would dedicate their research to the major global challenges. This led to the recognition of the need for novel methods and computer-based tools capable of meeting the challenges ahead, in particular the ability to consider different scales of chemical processes [23]. It is also essential to rethink the energy

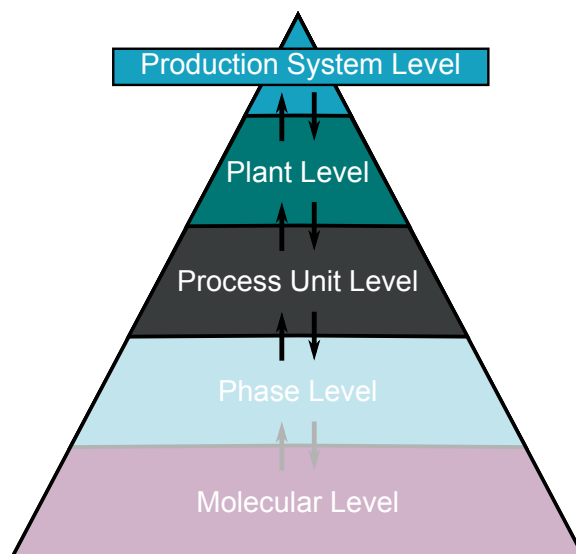


**Fig. 1.1** Schematic illustration of the process hierarchies considered in the context of this dissertation.

consumption of the chemical industry by combining process integration approaches, such as heat integration, with process systems engineering (PSE) methods to support the solution of real world problems [24].

## 1.2 Central research questions

In view of the global challenges mentioned above, this dissertation aims to provide a scientific basis for future decisions in the context of R2Chem as well as potential solutions for the design and synthesis of energy-efficient processes. For this purpose, suitable computer-based tools are developed and applied to urgent topics, which can be summarized by the following five central research questions, which are to be answered in this dissertation:

- (I) Which target molecule should be produced via the R2Chem pathway in order to use energy from renewable sources as efficiently as possible?
- (II) What are the optimal raw materials and conversion technologies to produce the desired target molecule both economically efficiently and environmentally friendly?
- (III) Can the chemical industry become a carbon sink under economic viewpoints?
- (IV) What is the most energy-efficient process flowsheet for converting raw materials into the desired product while making optimal use of synergies between individual process units?
- (V) Are there highly energy-efficient unit designs that lead to lower energy consumption than conventional designs?

In order to answer the research questions raised above, considerations at different levels of the process hierarchy are necessary, as they involve different degrees of complexity. Fig. 1.1 illustrates the process hierarchies as used in the PSE group of the Max Planck Institute (MPI) Magdeburg from the (lower) molecular level to the (upper) production system level. Indicated by the shading of the two lower levels, only the three upper levels are considered in the thesis : i) production system level, ii) plant level and iii) process level.

**Production system level:** At the production system level, entire chemical production networks (Ger.: *Verbund*) are considered. The focus is on the systematic planning and analysis of the total consumption of energy and raw materials as well as on the evaluation of the corresponding chemical conversion technologies. The level is characterized by little knowledge and decisions at an early stage, e.g. as a basis for strategic decisions for political decision makers.

**Plant level:** At the plant level, chemical processes are considered which consist of individual process units such as reactors, separators and heat exchangers. A more detailed knowledge of the processes is required, which enables process design and synthesis as well as flowsheet optimization. Methods for process intensification, such as energy integration, become crucial in order to make optimal use of synergy effects.

**Process unit level:** At the process unit level, individual process units are designed. While shortcut models are often used at the upper levels to reduce computational complexity, rigorous and computationally expensive models are usually used for unit design. The focus is on identifying more (energy) efficient designs.

Based on the definitions of the process hierarchies, it becomes obvious that the research questions (I), (II) and (III) require a systematic analysis of a multitude of possibilities and are answered at the production system level. In contrast, (IV) is associated with the plant level, since a more detailed knowledge of the process is crucial, and (V) is answered at the process unit level.

### 1.3 Structure of this dissertation

Fig. 1.2 provides a graphical illustration of this dissertation, which consists of seven chapters including the introduction. In the following, the content of each chapter is outlined, highlighting the research questions raised above:

Chapter 2 introduces the concept of R2Chem and gives an overview of several target molecules that are frequently discussed in the context of R2Chem. To answer the first research question (I), storage efficiency is introduced as the ratio of the stored energy content to the total energy input required via the R2Chem pathway. The results of this chapter set the roadmap



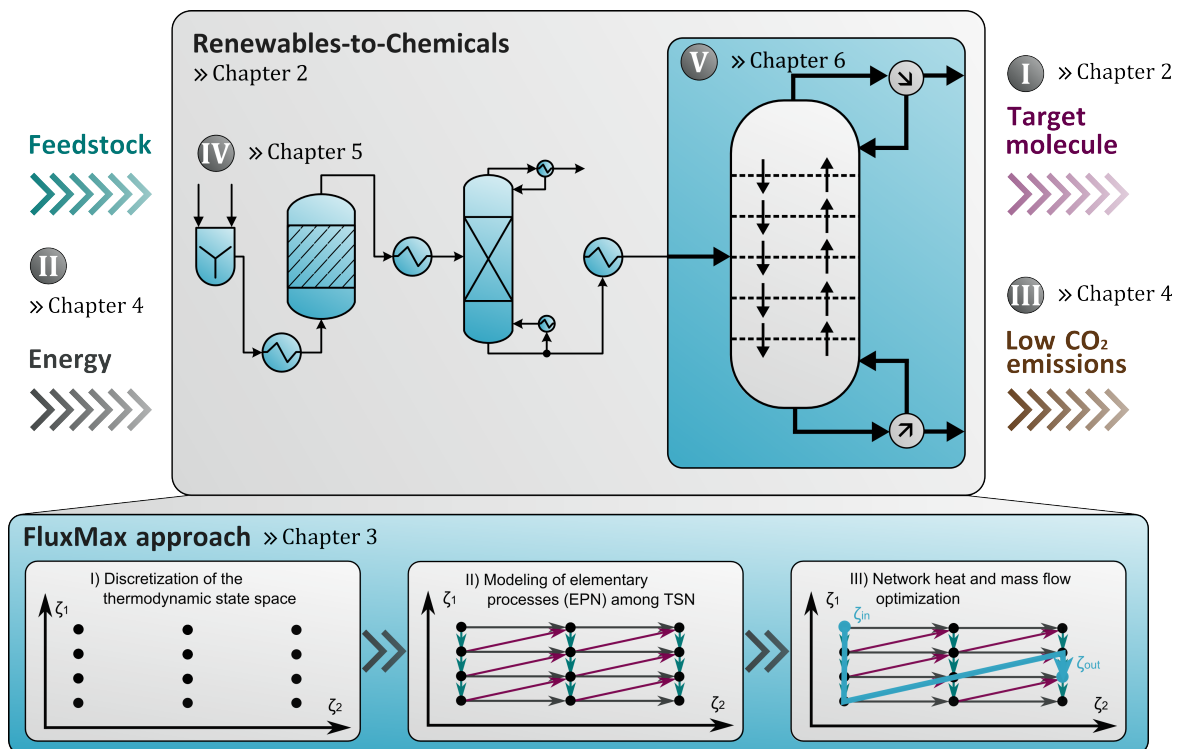


**Fig. 1.2** Dissertation in a nutshell: Schematic illustration of the structure of this dissertation and indication of the research questions answered.

for the following chapters, especially the selection of methanol as a case study. It is shown that not only the substitution of fossil raw materials and energy sources, but also an increase in the energy efficiency of the processes involved is crucial for a successful transition to a more sustainable chemical production.

As the research questions made clear, several levels of the process hierarchy have to be considered. As a consequence, Chapter 3 presents the scale-independent FluxMax approach for process design and synthesis, which was developed in cooperation with Georg Liesche at the MPI Magdeburg. In particular, the key feature of effective decoupling of process-based non-linearities from the flux optimization problem and the simultaneous consideration of heat integration during the design task is highlighted. Two approaches for heat integration – direct and indirect – are presented, which enable heat integration by introducing additional inequality constraints.

Chapter 4 applies the FluxMax approach at the production system level to address research questions (II) and (III). Using the methanol synthesis process as a case study, the influence of different raw materials and energy sources on specific production costs and specific CO<sub>2</sub> emissions is systematically investigated. The tradeoff between economic and ecological

efficiency is analyzed by applying a multi-objective function. It is shown that economically competitive production processes can be designed using renewable energies.

The research question (IV) is addressed in Chapter 5 by applying the FluxMax approach to the plant level. Energy-efficient process designs are identified as energy consumption turns out to be the main cost driver. The simultaneous approach of considering heat integration during the design tasks is compared to the classical sequential approach, where the process is designed first and then the heat integration potential is calculated by applying a pinch-based method. As a result of the simultaneous consideration of heat integration, an energy-optimized process configuration is identified, which outperforms the configuration determined in a sequential process.

In Chapter 6 the FluxMax approach is applied to the energy-intensive distillation process to answer the last research question (V). The representation of the distillation process by elementary processes leads to larger degrees of freedom for optimization compared to classical column modeling approaches based on the MESH equations. The energy-optimized configuration is a column with improved heat transfer between vapor and liquid streams, which can reduce energy requirements by up to 64 % compared to conventional design. However, there is a tradeoff as the energy saving potential requires additional heat exchangers, which is analyzed by multi-objective optimization.

In the final Chapter 7 the main findings of this dissertation are summarized and put into the broader context of energy transition. Moreover, an outlook on further research and open questions is given.

## Chapter 2

# Renewables-to-Chemicals

A key step in the R2Chem context is the electrochemical splitting of water into hydrogen and oxygen by electrolysis and the subsequent utilization of hydrogen as shown in Fig. 2.1. Since in many areas, for example the transportation sector, (synthetic) hydrocarbons will still be needed in the future, sustainable carbon sources must also be identified. In addition, nitrogen-based molecules, such as ammonia, are possible target molecules.

After a broad overview of possible target molecules discussed in the context of R2Chem, the storage efficiency – the ratio of stored energy content and energy required for production – is introduced and discussed for each of the target molecules under consideration. The first research question (I) is addressed on the basis of storage efficiency: Which target molecule should be produced via the R2Chem pathway in order to use energy from renewable sources as efficiently as possible?

### 2.1 Target molecules in the context of R2Chem

As the principal step of R2Chem processes is the production of hydrogen  $H_2$  via electrolysis [25–27],  $H_2$  itself is often discussed as an optimal storage molecule for surplus electrical energy, which could lead to a defossilification of the chemical industry [28, 29]. As shown in Tab. 2.1,  $H_2$  has a favorable gravimetric lower heating value  $LHV^{mass}$ , but due to its low molecular weight the volumetric  $LHV^{vol}$  is very poor. Rihko-Struckmann et al. [30] calculated power-to-power efficiencies of 36.4 % for the use of hydrogen as a storage molecule, if  $H_2$  is reconverted into electricity by a combined cycle power plant. However, the direct storage of hydrogen is very demanding, since the storage of  $H_2$  in tanks usually requires pressures of about 700 bar [31]. Nevertheless, there are also publications dealing with the design of cryogenic hydrogen tanks for aircraft applications [32]. Liquid organic hydrogen carriers LOHC are a promising way to overcome the challenges of storage. Hydrogenation produces a

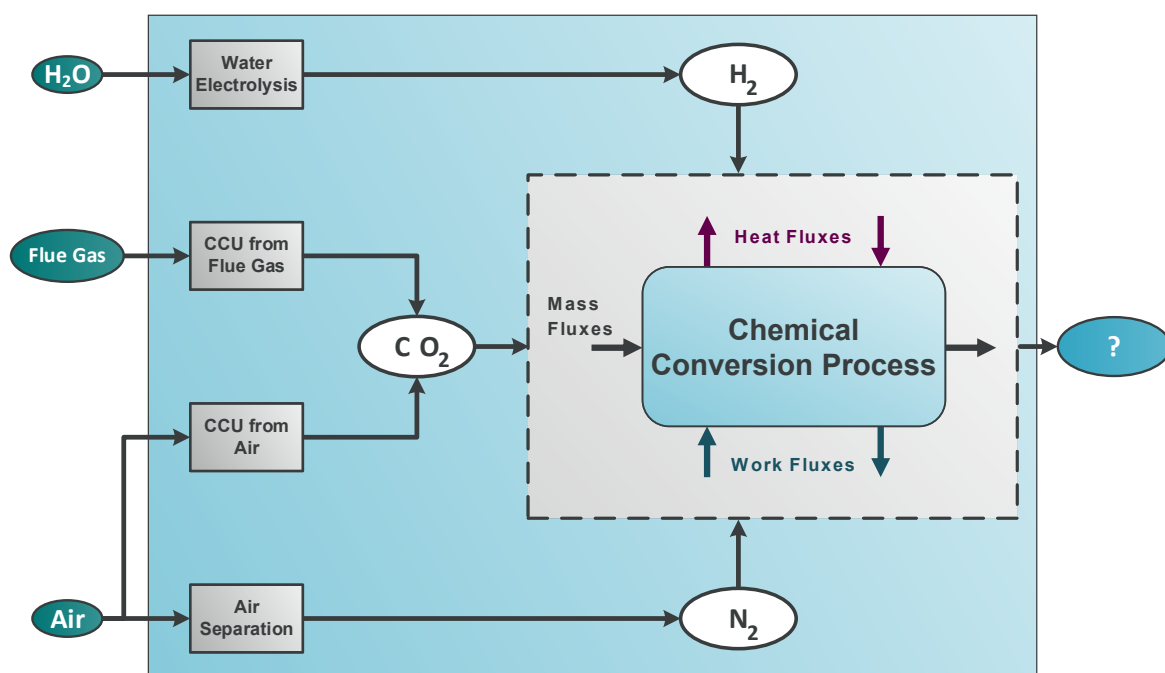


**Fig. 2.1** Schematic illustration of the R2Chem concept to store electrical energy by chemical conversion of valuable chemicals.

**Tab. 2.1** Overview on different storage molecules.

Molecule	Formula	LHV <sup>mass</sup>	LHV <sup>vol</sup>	Reactants	Product	State of matter
		MJ/kg	MJ/Nm <sup>3</sup>	CO <sub>2</sub> :H <sub>2</sub> :N <sub>2</sub>	C:H:N	
Hydrogen	H <sub>2</sub>	120.0	10.8	0:1:0	0:2:0	gaseous
Formaldehyde	CH <sub>2</sub> O	17.3	23.4	1:2:0	1:2:0	gaseous
Methane	CH <sub>4</sub>	50.0	35.7	1:4:0	1:4:0	gaseous
DME	C <sub>2</sub> H <sub>6</sub> O	28.4	58.3	1:3:0	1:3:0	gaseous
Formic Acid	HCOOH	4.6	5.6×10 <sup>3</sup>	1:1:0	1:2:0	liquid
Methanol	CH <sub>3</sub> OH	19.9	15.7×10 <sup>3</sup>	1:3:0	1:4:0	liquid
Ethanol	C <sub>2</sub> H <sub>5</sub> OH	27.8	21.1×10 <sup>3</sup>	1:3:0	1:3:0	liquid
OME <sub>1</sub>	C <sub>3</sub> H <sub>8</sub> O <sub>2</sub>	23.1	20.0×10 <sup>3</sup>	3:8:0	3:8:0	liquid
OME <sub>3-5</sub>	C <sub>3</sub> H <sub>8</sub> O <sub>2</sub>	23.1	20.0×10 <sup>3</sup>	3:8:0	3:8:0	liquid
Decane	C <sub>10</sub> H <sub>22</sub>	44.6	32.6×10 <sup>3</sup>	10:31:0	5:11:0	liquid
Ammonia	NH <sub>3</sub>	18.6	14.1	0:3:1	0:3:1	gaseous
Urea	CH <sub>4</sub> N <sub>2</sub> O	9.1	12.0×10 <sup>3</sup>	1:3:1	1:4:2	solid

liquid compound that can be dehydrogenated again later if  $H_2$  or electrical energy is required. Important example systems are toluene-methylcyclohexane [33, 34] or N-ethylcarbazole [35]. In addition to publications on the design of efficient hydrogenation-dehydrogenation cycles [29], there are also publications on applications in residential and commercial buildings [36] or in the transportation sector [33, 35].

In recent years much attention was paid to the further conversion of hydrogen into synthetic hydrocarbons, which has the advantage of operating with molecules with favorable gravimetric  $LHV_s^{\text{mass}}$  as well as beneficial storage capabilities [37, 38]. In most R2Chem applications, the simplest hydrocarbon methane  $CH_4$  is discussed as the target molecule. Uebbing et al. [39] calculated a power-to-power efficiency of 23.4 % for methane from  $CO_2$  and hydrogen produced by water electrolysis. Besides the increased volumetric heating value, as shown in Tab. 2.1, the simple distribution via the natural gas grid makes  $CH_4$  suitable as storage molecule. In addition,  $CH_4$  offers a wide range of applications: use as chemical intermediate, heat supply by combustion or as fuel in the transportation sector. In the context of energy storage, dynamic operation of methanation processes comes into the focus of interest due to the fluctuating availability of renewable energies. In particular, the exothermic nature of the reaction requires a sophisticated design and control strategy [40]. Not only electrical surplus energy but also biomass as energy carrier might be a feedstock for R2Chem processes with  $CH_4$  as storage molecule. Biomass – energy crops or organic waste – can be converted into mixtures of  $CH_4$  and carbon dioxide  $CO_2$  by anaerobic digestion. The ADM1 model developed by [41], is often used to design the reactor [42] or to study different types of biomass as feedstock [43]. In order to increase the  $CH_4$  yield – while simultaneously reducing  $CO_2$  emissions – biological methanation by adding additional hydrogen to the reactor was also investigated [44].

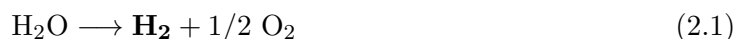
Due to their significantly higher volumetric  $LHV^{\text{vol}}$ , liquids become also more favorable as storage molecules than gases. Besides formic acid [45, 46], methanol is of particular interest. Similar to methane, a future energy economy based on methanol is often proposed due to the simple and well-known synthesis chemistry and the wide range of possible applications [38]. Possible applications are the use as an important basic chemical and possible fuel substitute in fuel cell vehicles or vehicles with internal combustion engines. The reconversion into electrical power seems unsuitable, since the power-to-power efficiency of approx. 17 % is poor [30]. Nevertheless, methanol is very often regarded as a key molecule for the storage of electrical surplus energy [38, 47, 48]. It was also shown that an economically competitive production process can be designed under uncertain market situations [49].

Other alternative fuels are also frequently discussed. In particular, the bio-based production of ethanol is often considered [50, 51] or even technically applied as fuel or fuel-blend for Otto engine vehicles. Furthermore, dimethyl ether DME [52] and poly(oxymethylene) dimethyl

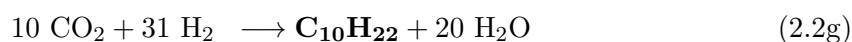
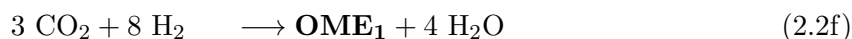
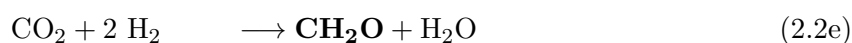
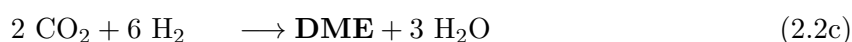
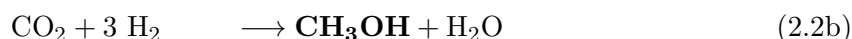
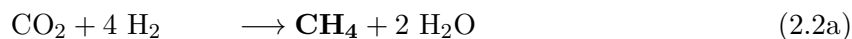
ethers OME [53–56] are highly discussed as diesel substitutes in recent years. Due to the easy handling resulting from the low adaptation of conventional internal combustion engines and the improved combustion properties compared to conventional diesel (almost no NOx and soot emissions) OMEs seem to be attractive fuels for the future. As a consequence of new developments in catalysis, which enable a direct electrochemical synthesis of ammonia – as an alternative to the classical Haber-Bosch-process – nitrogen-based storage systems utilizing ammonia NH<sub>3</sub> also came into the focus of interest [45].

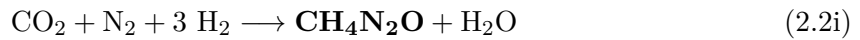
## 2.2 Evaluation of storage efficiency of target molecules

R2Chem processes are often motivated by their ability to store volatile renewable energies [15, 40]. Reasons for storing energy are diverse: electricity peaks in times of low energy demands, or a spacial and/or temporary difference of energy supply and demand (e.g. in the transportation sector). While it is true that the conversion of chemicals has many advantages over the direct storage of electricity – higher capacities and lower self-discharge rates [57] – one crucial drawback becomes obvious: each conversion step inevitably causes losses resulting in a decreased storage efficiency. Therefore, often hydrogen as storage molecule is postulated [35, 58] as it has the lowest conversion chain when produced from water by electrolysis as shown in Eq. (2.1).



However, due to its low volumetric energy content (see Table 2.1) and poor transportation properties resulting in high storage pressures and self-discharge rates, the further conversion into hydrocarbons or nitrogen compounds under the usage of CO<sub>2</sub> or N<sub>2</sub> is proposed. Eq. (2.2) lists the net reaction equations for the conversion of the storage molecules given in Table 2.1 from H<sub>2</sub>, CO<sub>2</sub>, and N<sub>2</sub> where the target molecules are highlighted in bold font.





The overall conversion chain for the chemical energy storage is illustrated in Fig. 2.2. Starting from water the available electrical energy is used to produce hydrogen via water electrolysis. To further process  $\text{H}_2$  chemically by one of the conversion processes given in Eq. (2.2), sources for the key intermediates  $\text{H}_2$  or  $\text{N}_2$  have to be found. While  $\text{CO}_2$  can be separated from flue gases of industrial sites and fossil-fired power plants, in the near to mid future carbon capture from air becomes an important carbon source [59]. Already today, the state-of-the-art process to gain pure  $\text{N}_2$  is air separation [60].

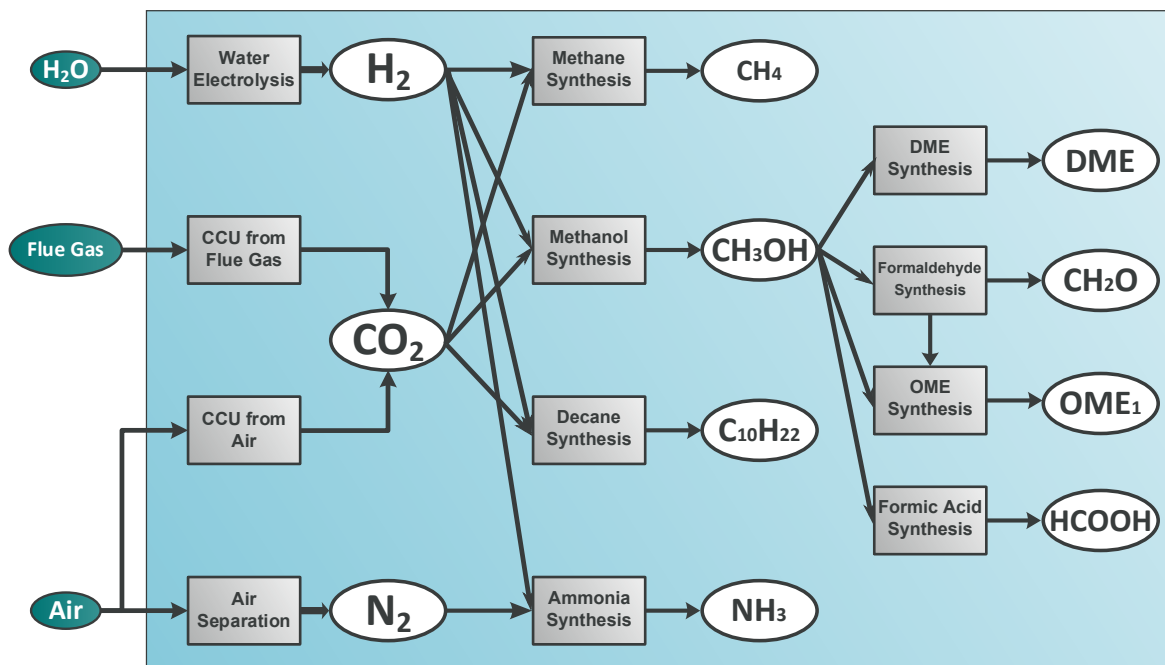


**Fig. 2.2** Schematic illustration of the conversion chain to produce valuable chemicals via the R2Chem pathway.

In recent years, numerous publications in the field of Carbon Capture and Utilization (CCU) have been published. An overview of  $\text{CO}_2$  capture from air is given in Goepfert et al. [61] with the aim of promoting air as a future renewable carbon source. In addition to direct carbon capture from air, the indirect utilization of  $\text{CO}_2$  by means of biomass is also discussed. Abanades et al. [62] analyzed manufacturers of fuels from  $\text{CO}_2$  to contrast CCU with Carbon Capture and Storage (CCS) technologies. They found significantly higher mitigation costs for CCU than for CCS and stressed the resulting restrictions for  $\text{CO}_2$  conversion processes. Similar conclusions were drawn by Krekel et al. [59], who performed a techno-economic assessment of the  $\text{CO}_2$  separation processes from air by analyzing key process parameters,

such as specific costs, work demand, and cyclability. They emphasized the high costs for direct CO<sub>2</sub> separation from air, which are often underestimated in other studies. They concluded, however, that CO<sub>2</sub> air separation might be a long-term option, although it is currently not economically competitive with CCU from coal fired power plants. Besides technical issues, Offermann-van Heek et al. [63] analysed the social acceptance of different carbon capture technologies and emphasized the importance of relevant information provided to society in order to achieve social acceptance.

In order to compare the different storage molecules and conversion pathways, the storage efficiency  $\eta_{\alpha}^{\text{storage}}$  for each molecule  $\alpha$  is defined as ratio of energy content of the molecule  $E_{\alpha}^{\text{stored}}$  and sum of the single energy inputs  $E_j^{\text{in}}$  of all required process steps  $j$ :

$$\eta_{\alpha}^{\text{storage}} = \frac{E_{\alpha}^{\text{stored}}}{\sum_j E_j^{\text{in}}} \quad (2.3)$$

Herein,  $E_{\alpha}^{\text{stored}}$  is expressed by the molar lower heating value  $\Delta h_{\text{u},\alpha}^{\text{mol}}$ :

$$E_{\alpha}^{\text{stored}} = \Delta h_{\text{u},\alpha}^{\text{mol}} \dot{N}_{\alpha}, \quad (2.4)$$

which can be calculated by the mass related lower heating value  $\Delta h_{\text{u},\alpha}^{\text{mass}}$  listed in Tab. 2.1 and the molar mass  $M_{\alpha}$  of the molecule  $\alpha$ :

$$\Delta h_{\text{u},\alpha}^{\text{mol}} = \Delta h_{\text{u},\alpha}^{\text{mass}} M_{\alpha} \quad (2.5)$$

The total electrical energy input is determined by the energy demand  $E_j^{\text{in}}$  of the individual process steps  $j$  along the conversion chain.

$$\sum_j E_j^{\text{in}} = \dot{N}_{\text{H}_2} e_{\text{EL}}^{\text{in}} + \dot{N}_{\text{CO}_2} e_{\text{CCU}}^{\text{in}} + \dot{N}_{\text{N}_2} e_{\text{AS}}^{\text{in}} + \dot{N}_{\alpha} e_{\text{conv}}^{\text{in}} \quad (2.6)$$

Herein, Eqs. (2.1) and (2.2) determine the stoichiometrically required molar fluxes of hydrogen  $\dot{N}_{\text{H}_2}$ , carbon dioxide  $\dot{N}_{\text{CO}_2}$ , and nitrogen  $\dot{N}_{\text{N}_2}$  in relation to the flux of the final storage molecule  $\dot{N}_{\alpha}$ . In literature, there is a multitude of energetic assessments of different target molecules [64, 39, 65, 66, 59, 67], where the specific energy demand  $e_j^{\text{in}}$  of step  $j$  is either reported directly or in form of a conversion efficiency  $\eta_j$  determining the ratio of energy content stored in the product and energy required – in form of the energy content of the reactants  $\Delta h_{\text{u},\beta}^{\text{mol}} \dot{N}_{\beta}$  as well as the energy input  $e_j \dot{N}_{\alpha}$ :



**Tab. 2.2** Overview on the conversion efficiencies.

Stoichiometry		Efficiency $\eta_j$	Reference
H <sub>2</sub> O	→ H <sub>2</sub> + 1/2 O <sub>2</sub>	0.70	[68, 64]
CO <sub>2</sub> + 4 H <sub>2</sub>	→ CH <sub>4</sub> + 2 H <sub>2</sub> O	0.76	[39]
CO <sub>2</sub> + 3 H <sub>2</sub>	→ CH <sub>3</sub> OH + H <sub>2</sub> O	0.84	[65]
2 CO <sub>2</sub> + 6 H <sub>2</sub>	→ DME + 3 H <sub>2</sub> O	0.75	calculation based on [65]
CO <sub>2</sub> + H <sub>2</sub>	→ HCOOH	0.83	calculation based on [69, 65]
CO <sub>2</sub> + 2 H <sub>2</sub>	→ CH <sub>2</sub> O + H <sub>2</sub> O	0.58	[65]
3 CO <sub>2</sub> + 8 H <sub>2</sub>	→ OME <sub>1</sub> + 4 H <sub>2</sub> O	0.68	[65]
10 CO <sub>2</sub> + 31 H <sub>2</sub>	→ C <sub>10</sub> H <sub>22</sub> + 20 H <sub>2</sub> O	0.70	[68]
1/2 N <sub>2</sub> + 3/2 H <sub>2</sub>	→ NH <sub>3</sub>	0.52	[66]

**Tab. 2.3** Overview of specific energy inputs required for CCU and air separation.

Process step	Specific energy input $e_j$	Reference
CCU from air / kJ <sub>el</sub> /mol <sub>CO<sub>2</sub></sub>	161	[59]
CCU from flue gas / kJ <sub>el</sub> /mol <sub>CO<sub>2</sub></sub>	42	[67]
Air separation	25	[70]

$$\eta_j = \frac{E_\alpha^{\text{stored}}}{\Delta h_{u,\beta}^{\text{mol}} \dot{N}_\beta + e_j \dot{N}_\alpha} \quad (2.7)$$

In Tab. 2.2 the reported conversion efficiencies  $\eta_j$  are listed as well as specific energy duties  $e_j$  in Tab. 2.3. Own calculations of energy efficiencies are based on Appendix B.

The resulting storage efficiencies  $\eta_\alpha^{\text{storage}}$  of the target molecules considered are shown in Fig. 2.3. To highlight the different energy requirements caused by the carbon source – CCU from flue gas or direct air capture – both CO<sub>2</sub> sources are depicted separately. It is evident that most of the energy consumption that leads to a reduction in efficiency is caused by chemical transformation – in particular electrolysis – and carbon capture has only a minor impact on the total energy consumption. Nevertheless, it is important to mention that the social acceptance of R2Chem pathways is essentially influenced by carbon capture [63].

As expected, the highest efficiency of 0.7 is reached for H<sub>2</sub>, since, apart from the water electrolysis, no losses occur due to further conversion. Consequently, the carbon source has no influence on the efficiency because no carbon is needed for the production of H<sub>2</sub>. The next best alternatives are methanol (up to 0.57) and formic acid (up to 0.54) in the case of CO<sub>2</sub> capture from flue gas, which only require a further conversion step. While CH<sub>3</sub>OH remains the second best candidate also for direct air capture, the efficiency of formic acid drops significantly. The reason for this is the low C:H ratio of the reactants of only 1:1 for the production of formic acid (Tab. 2.1). As a result, the production is more sensitive to

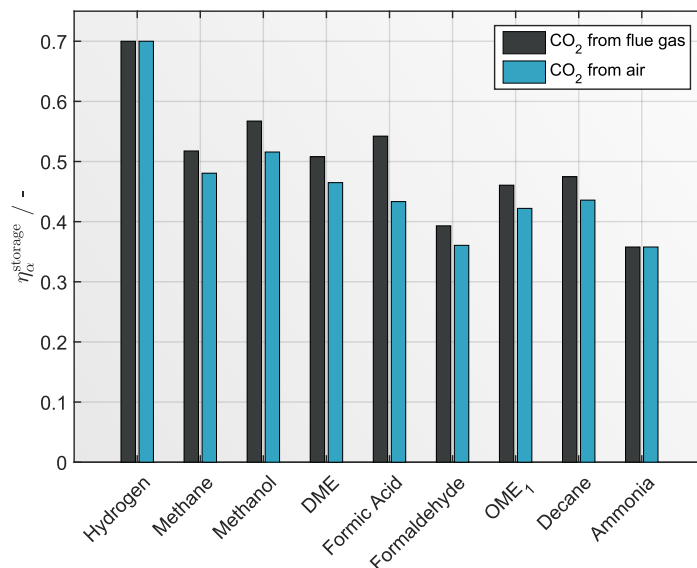


**Fig. 2.3** Storage efficiency of different target molecules for two carbon dioxide sources: capturing from flue gas and direct air capturing.

the carbon source and is less dominated by hydrogen production compared to the other molecules.

Although CH<sub>4</sub> requires only one additional conversion step like methanol and formic acid, the storage efficiency is lower due to the high amount of H<sub>2</sub> needed for the synthesis of CH<sub>4</sub> (four moles of H<sub>2</sub> compared to only three moles of H<sub>2</sub> for the synthesis of methanol). This leads to an additional energy requirement, which is however not stored in the target molecules. The additionally generated H<sub>2</sub> molecule produces the undesired by-product H<sub>2</sub>O (see Eq. (2.2a)), which leads to the same C:H ratio in the target products CH<sub>4</sub> and CH<sub>3</sub>OH.

Besides H<sub>2</sub> there is only one other molecule that does not show any influence of the carbon source: ammonia NH<sub>3</sub>. While no CO<sub>2</sub> is needed for the synthesis, there is a need for N<sub>2</sub>, which requires the very energy-intensive air separation. In combination with the rather poor lower heating value, NH<sub>3</sub> turns out to be the energetically worst target molecule (together with formaldehyde).

The other molecules – DME, OME<sub>1</sub> and decane – have a lower storage efficiency compared to CH<sub>3</sub>OH. However, they may be interesting for another reason: Similar to CH<sub>3</sub>OH they are discussed as fuel substitutes. While CH<sub>3</sub>OH can be used as a gasoline substitute, the derivatives DME and OME<sub>1</sub> are possible substitute fuels for diesel engines [12, 71]. Since the OME derivatives with chain lengths between 3-5 OME<sub>3-5</sub> are more similar to diesel with regard to combustion properties, current fuel research concentrates on mixtures of OME<sub>3-5</sub> instead of OME<sub>1</sub> [53, 72]. Due to additional conversion steps, however, the storage efficiency

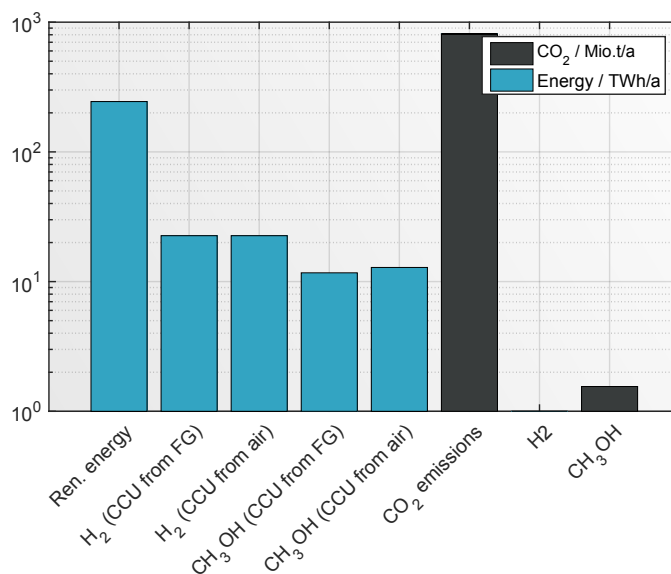


**Fig. 2.4** Comparison of annual renewable energy available in Germany and CO<sub>2</sub> emissions with annual productions of H<sub>2</sub> and CH<sub>3</sub>OH.

decreases by about 9 % compared to OME<sub>1</sub> [65, 72]. Synthetic decane could be an important ingredient in substitute jet fuels. While there may be applications that favor the use of these molecules, the focus of this dissertation is on methanol because of its more beneficial storage efficiency.

In addition, methanol is often discussed in literature as an important energy storage molecule in R2Chem applications [38, 73]. The reasons for assigning methanol such an important role are diverse [74, 75, 38]. First, methanol is an industrially important commodity and the reaction chemistry is well-declared [76]. The conversion of carbon dioxide and hydrogen generated by electrolysis is an auspicious way to store so-called electrical surplus energy [30, 48]. In particular, the low global warming potential was highlighted by König et al. [77]. In the context of energy conversion, methanol is a C<sub>1</sub> molecule to bound CO<sub>2</sub> in a one step reaction with H<sub>2</sub> produced from renewable resources. While this also applies to methane, methanol is a liquid at ambient conditions. This is very advantageous when it comes to storage and handling, especially for mobility purposes where methanol can be used as a direct gasoline substitute.

In the following, besides the production of H<sub>2</sub>, the production of CH<sub>3</sub>OH from renewable energies and CO<sub>2</sub> will be further analyzed. The annual production in 2018 for Germany was 1.13 Mio. t/a for CH<sub>3</sub>OH and 5,237 Mio. m<sup>3</sup>/a for H<sub>2</sub> [78]. Using the storage efficiencies (Fig. 2.3) and the specific CO<sub>2</sub> demand (Tab. 2.1), the total energy and CO<sub>2</sub> demand required to cover the annual production is calculated. Fig. 2.4 illustrates the energy and CO<sub>2</sub> demand

for CH<sub>3</sub>OH and H<sub>2</sub>. In addition, for the year 2019, the electricity available in Germany from renewable energies of 244.3 TWh [79] and the total CO<sub>2</sub> emissions of 811 Mio. t/a [80] are shown for comparison. A logarithmic scale is used for the ordinate, as the orders of magnitude differ strongly.

22.6 TWh/a are required for H<sub>2</sub> and between 11.7 and 12.9 TWh/a for CH<sub>3</sub>OH – depending on the CO<sub>2</sub> source – to cover the entire annual production in Germany on the R2Chem pathway shown in Fig. 2.1. As a result, the total energy demand could be met from renewable sources, since the available amount is about one order of magnitude higher. While no CO<sub>2</sub> is needed for H<sub>2</sub>, the production of CH<sub>3</sub>OH would reduce the atmospheric CO<sub>2</sub>. However, Fig. 2.4 shows that only 1.55 Mio. t/a CO<sub>2</sub> are needed to cover the annual methanol production in Germany, which is only 0.2 % of the annual German CO<sub>2</sub> emissions.

From Fig. 2.4 it becomes clear that merely shifting the raw material – from fossil to renewable resources – is not sufficient as a single measure to effectively reduce CO<sub>2</sub>-emissions. Even if all available renewable energy were used for the production of chemicals, only about 4 % of the annual CO<sub>2</sub> emissions could be used and thus removed from the atmosphere. This leads to three consequences for a successful CO<sub>2</sub> reduction: i) the capacity of energy from renewable sources must be drastically increased, ii) the chemical industry must support other energy sectors, especially the transportation sector, through sector coupling, and iii) the energy efficiency of chemical conversion processes must be improved. While the first two consequences are out of the scope of this dissertation, the last requirement – increasing the energy efficiency of chemical processes – is the focus of the following chapters of this dissertation. To successfully increase energy efficiency, the performance of chemical processes must be analyzed and optimized across different length scales and process hierarchies. In particular, the intelligent use of synergies between different parts of the process needs to be elaborated, which requires, for example, the identification and exploitation of the full heat integration potential. This is the aim of the scale-independent FluxMax approach for process design and synthesis, which is presented in the following chapter and then applied to three examples based on different process hierarchies using methanol as target molecule.

## 2.3 Chapter summary

This chapter introduced the concept of R2Chem, which uses electricity from renewable energy sources – preferably surplus energy – to produce hydrogen by electrolysis, which is directly used or further processed by converting H<sub>2</sub> together with CO<sub>2</sub> or N<sub>2</sub> into valuable chemicals. After presenting possible target molecules, which are often discussed in the context of R2Chem, the storage efficiency was introduced as a measure of the energy content stored in the target molecule in relation to the required input energy. Using the storage efficiency the first research question (I) was addressed: It was shown that besides H<sub>2</sub> (70 %) also

CH<sub>3</sub>OH has an advantageous storage efficiency of almost 57 % in case CO<sub>2</sub> is captured from flue gas. Although the efficiency is lower, CH<sub>3</sub>OH is an ideal target molecule because of the better storage and transport properties – CH<sub>3</sub>OH is liquid at ambient conditions. In addition, methanol is an important base chemical, which is the starting point for many synthesis processes as shown in Fig. 2.2. As a consequence, CH<sub>3</sub>OH is selected as central application considered in the next chapters.

The analysis of the limitations of R2Chem processes given by the amount of energy available from renewable sources showed that theoretically enough energy is available to cover the entire annual production of both H<sub>2</sub> and CH<sub>3</sub>OH via the R2Chem pathway. However, the consumption of CO<sub>2</sub> would merely amount to 0.2 % of the total German CO<sub>2</sub> emissions, and a maximum of about 4 % could be achieved if all energy from renewable sources were used for R2Chem processes. This leads to three key messages: There is a need for i) increased capacity of renewable energy, ii) improved sector coupling strategies and iii) highly energy efficient processes across all process hierarchies.

In particular, the last key message forms the roadmap for the following chapters of this dissertation.



## Chapter 3

# Scale-independent network approach for process design and synthesis

The transition to a more sustainable chemical industry requires the design of energy- and cost-optimized processes at different levels of the process hierarchy, as shown in Fig. 1.2. The FluxMax approach is a process design and synthesis methodology for chemical processes on different length scales. Its key feature is the simultaneous mass flow optimization and heat integration by discretization of the thermodynamic state space. The introduction of nodes corresponding to chemical mixtures, elementary processes and utilities allows the representation of each chemical process as a directed graph, effectively decoupling process-based non-linearities from the optimization problem. The heat integration is taken into account by additional constraints.

After an overview of the design methods published in recent years, the formulation of the FluxMax approach is derived in this chapter.

### 3.1 Literature review

In the context of energy transition, one of the major goals of the chemical industry is to substitute fossil feedstock with sustainable technologies and the use of renewable resources. But even if the focus is on the substitution of feedstock, an increase in efficiency is crucial for a successful transition to a more sustainable production of chemicals [11]. In order to enhance the overall process efficiency, challenges must be faced at different levels of process hierarchy as shown in Fig. 1.1. While at the production system level, more general questions and early stage decisions of chemical production networks are addressed [74, 81, 82], at the plant

level, the aim is the identification of optimal process configurations, that consists of single process units, such as reactors, separators, and heat exchangers [83, 84, 39]. In contrast, at the process unit level the performance of the single units is the main aspect [85, 86].

The methodology of Elementary Process Functions (EPF) was proposed by Freund and Sundmacher [87] with focus on reactor design. In a multi-step approach, a matter element was tracked in the thermodynamic state space and an optimal trajectory was calculated. In a final step, the optimal trajectory was used as the basis for the invention of a real process. In contrast to classic design approaches, process elementary process functions are used rather than conventional unit operations to represent chemical processes. The methodology was successfully applied to catalytic gas phase reactions [88] and multiphase reactors [89, 85]. Recent developments based on this methodology also enable the design of so-called tolerant chemical reactors capable of processing multiple raw materials [90].

For the design of process and production systems, mixed integer formulation are often used to account for the binary decision whether an alternative is active or not [91, 81, 92]. A graph-theoretical approach that represents a chemical process as a network of nodes and edges leading to a mixed-integer optimization problem was presented by Friedler et al. [93]. Recently, Ryu and Maravelias [94] proposed a mixed integer linear programming (MILP) model that uses a discrete temperature grid for the process synthesis problem. In addition, they showed how non-uniform grids can reduce the complexity of large scale problems.

However, there are also approaches that avoid binary decision variables. Kim et al. [95] analyzed optimal strategies for converting biomass into fuels. A (continuous) linear programming (LP) formulation was derived by considering the yield as a parameter, which led to a linear dependency on the production capacity. Within the IDEAS framework, the chemical process is divided into a distribution network and process operator. The linearization of the feasible region was also applied previously and results in an infinite linear program which allows the identification of a global lower bound [96].

A key issue of process design and synthesis methodologies is the consideration of heat integration to enhance the energy-efficiency of chemical processes. Pinch analysis is widely used to identify optimal heat exchanger networks for a given process structure, which consists of hot and cold heat streams [97]. In this context, hot streams are defined as streams to be cooled and cold streams to be heated. However, pinch analysis cannot be applied directly to a simultaneous optimization approach, as the heat duties are decision variables and thus not known a priori. As a consequence, often a subsequent procedure is proposed in literature: first the flow problem is optimized without consideration of heat integration and subsequently a pinch-based analysis is performed to identify the heat integration potential [98, 83, 99]. These approaches may not identify the overall mass-related and energetic optimum [100]. To identify the global mass-related and energetic optimum, a simultaneous procedure is crucial



that solves simultaneously the flow problem under consideration of heat integration. This is the aim of the FluxMax approach that is introduced in the following.

## 3.2 The FluxMax approach

The general idea of the FluxMax approach (FMA) is an effective decoupling of process-based non-linearities from the subsequent network flux optimization by discretization of the thermodynamic state space. The discretization allows the representation of chemical processes across different lengthscales, which enables the transformation of a non-linear process optimization problem into a convex flux optimization on a defined network graph. The FluxMax approach can be divided into three steps that are illustrated in Fig. 3.1:

- i) discretization of the thermodynamic state space,
- ii) modeling of elementary process functions, and
- iii) formulation and solution of the flux optimization problem.

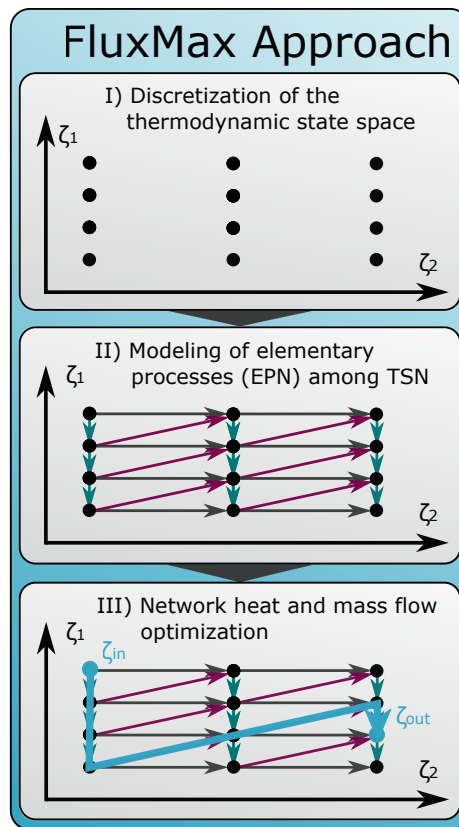


**Fig. 3.1** Illustration of the three-step FluxMax approach for unit and process design with simultaneous heat integration: discretization of thermodynamic state space (I), modeling of elementary processes (II), and formulation and solution of the flow optimization (III); the thermodynamic state space is spanned by its thermodynamic coordinates  $\zeta_z$ , where  $z$  denotes the number of dimension.

The first step comprises the discretization of the thermodynamic state space into thermodynamic state points (Fig. 3.1 (top)). In this way, it is possible to calculate the non-linear thermodynamic potentials, such as enthalpy and entropy, a priori. In a second step, the discrete state points are connected by elementary process functions as shown in Fig. 3.1 (center). Depending on the type of design application, these elementary process functions represent micro changes in the thermodynamic state space that are combined into process units or fully engineered process units such as distillation columns, reactors and other apparatuses. Thus, the FluxMax approach is applicable to different levels of complexity. Characteristic quantities of the elementary process functions, such as specific energy demands, can be calculated a priori, because the linked thermodynamic state points are predefined. Thereby, the non-linear preprocessing is fully decoupled from the third step: the network flux optimization under simultaneous consideration of heat integration (Fig. 3.1 (bottom)). The feasible region of the flux optimization is linear in terms of the fluxes that are decision variables.

The discretization of the thermodynamic state space and the introduction of a generalized process extent variable allow the direct application of the approach to any kind of process design and synthesis problem. In addition, the introduction of inequalities enables the simultaneous consideration of heat integration as integrated part of the flux optimization problem, which ensures the consideration of both the temperature levels and the heat fluxes actually transferred. In the following, the directed graph concept and the model formulation of the FluxMax approach are presented. Particularly, the heat integration model is emphasized, which enables direct and indirect heat integration.

### 3.2.1 Directed graph representation of chemical process networks

The decoupling of non-linear preprocessing and subsequent flux optimization is achieved by representing the chemical process network as directed graph (digraph) that consists of nodes and edges. Also Friedler et al. [93] used a graph representation and introduced material and operating nodes [101]. In contrast, the FluxMax approach distinguishes between four types of nodes (or vertices). Firstly, there are thermodynamic substance nodes (TSN)  $M_i \in \mathcal{M}$  where  $\mathcal{M}$  is the set of all TSNs. TSN represent discrete state points in the thermodynamic state space. Secondly, there is the set of elementary process nodes (EPN)  $\mathcal{E}$  containing all elementary process nodes  $E_j \in \mathcal{E}$  at which any kind of chemical or physical interaction among TSNs takes place. The third group of nodes are utility nodes (UN)  $U_l \in \mathcal{U}$  to provide heating and cooling. Herein,  $\mathcal{U}$  is the set of possible utilities at different temperatures. A fourth group of nodes – the work utility nodes (WUN)  $S_k$  – are contained in the set  $\mathcal{S}$ . The WUNs represent the electrical grid that supplies the required electrical power or distribute the generated power, in case of power generating processes.

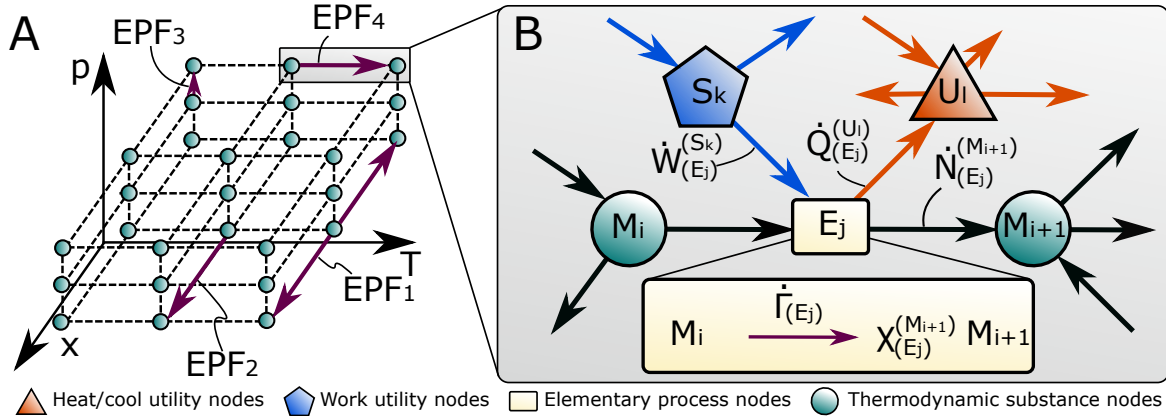


**Fig. 3.2** Grid of thermodynamic state points (A) in the thermodynamic state space with  $p$ ,  $T$  and  $x$  coordinates. Thermodynamic substance nodes (green) are linked via elementary process functions (magenta): isobaric isothermal separation (EPF<sub>1</sub>); isobaric isothermal reaction (EPF<sub>2</sub>); isobaric cooling (EPF<sub>3</sub>); and isobaric heating (EPF<sub>4</sub>). The digraph representation for EPFs that link two TSN (green circles)  $M_i$  and  $M_{i+1}$  via an elementary process node  $E_j$  (yellow rectangle) is illustrated on the right (B). Work utility nodes (blue pentagon) and heat utility nodes (red triangle) supply the EPN with duties. Work fluxes (blue arrows), heat fluxes (red arrows) and molar fluxes (black arrows) link the four node types. The conversion is described by a stoichiometric equation that is characterized by the generalized process extent number  $\dot{\Gamma}_{(E_j)}$ .

The nodes are connected by edges, that represent the mass and energy fluxes desired to be determined. The set of all fluxes is denoted as  $\mathcal{F}$ .

### Thermodynamic substance nodes

Thermodynamic substance nodes  $M_i$  are discrete points in the thermodynamic state space. As a consequence, a TSN is clearly defined by its thermodynamic coordinates  $\zeta_z$ , where  $z$  corresponds to a considered coordinate of the thermodynamic state space. Examples of thermodynamic coordinates are molar composition  $[x_1, x_2, \dots, x_n]^T$ , temperature  $T$ , and pressure  $p$ . For each temperature, pressure or composition change a new TSN is introduced. The thermodynamic potentials, such as enthalpy or entropy, are calculated a priori from the coordinates of the TSN by use of (non-linear) thermodynamic equations of state.

In order to move from one TSN  $M_i$  to another TSN  $M_{i+1}$ , elementary process functions (EPF) are introduced. In Fig. 3.2 (A) four different elementary process functions are illustrated for the transformation from one TSN to another: isobaric isothermal separation (EPF<sub>1</sub>), isobaric isothermal reaction (EPF<sub>2</sub>), isothermal compression (EPF<sub>3</sub>), and isobaric heating (EPF<sub>4</sub>).

### Elementary process nodes

Elementary process nodes  $E_j$  are introduced to describe the elementary process functions that enable the chemical transformation among TSNs. The mass fluxes, which are illustrated

as black arrows in Fig. 3.2 (B), connect an elementary process node with at least two TSNs. Stoichiometric equations are formulated to describe the transformation between TSNs analogously to transformations between pure substances  $\alpha \in \mathcal{A}$ . Hereby,  $\mathcal{A} \subset \mathcal{M}$  is the set of pure substances, which are a special case of TSN. As shown in Fig. 3.2 (B) the generalized stoichiometric coefficients are denoted as  $\chi_{(E_j)}^{(M_i)}$ . Similarly to the extent of reaction  $\dot{\xi}$  that is frequently used for the description of the progress of a chemical reaction, a generalized process extent number (PEN)  $\dot{\Gamma}$  is introduced that links all participating TSN of an elementary process node. It can be interpreted as the extent of the elementary process  $E_j$ :

$$d\dot{\Gamma}_{(E_j)} := \chi_{(E_j)}^{(M_i)} d\dot{N}_{(E_j)}^{(M_i)} \quad (3.1)$$

From Eq. (3.1) follows that  $\dot{\Gamma}_{(E_j)} = 0$  if the transformation along  $E_j$  is inactive. Contrary to the extent of the reaction that directly affects the outlet composition of a reactor, the PENs can be considered as a scaling variable that allows an elegant formulation of the flow problem by relating each flow of an EPN to a unique PEN.

In addition, heat and work fluxes, illustrated as blue and red arrows, connect EPNs with utility nodes.

### Utility nodes

Utility nodes  $U_l$  are introduced to provide the heating and cooling demands of the EPNs. UNs are considered as reservoirs of heat at a constant temperature level. The external heating and cooling requirements are fulfilled by at least two UNs at sufficiently low and high temperature, respectively. In case of indirect heat integration, which is introduced in section 3.2.3, the UNs are additionally used to enable the heat integration.

The work utility nodes  $S_k$  provide the external power demand.

### Edges representing mass- and energy fluxes

In a directed graph the nodes are connected with edges. These edges can be weighted or limited in a subsequent optimization problem. In the FluxMax approach, there are two types of edges. Firstly, there are edges corresponding to mass fluxes that connect at least two TSNs with an elementary process node. As shown in Fig. 3.2 (B) these fluxes are either external or internal mass fluxes (black arrows). In case of external fluxes, the fluxes are a consequence of initially provided substances, which are desired to be transformed within the chemical process, or the final products, which leave the overall process. In contrast, internal mass fluxes are fluxes among elementary processes and thus in- and outlet flows of the EPNs.

Secondly, there are heat and work fluxes that connect the UNs and WUNs with EPNs as illustrated as red and blue arrows in Fig. 3.2 (B).

### 3.2.2 Formulation of node conservation laws

In this section, the conservation laws of the introduced nodes are presented, that are used as equality constraints in the subsequently formulated flux optimization problem. For the thermodynamic substance nodes only mass balances are formulated, because the thermodynamic state of a TSN is clearly determined by its thermodynamic coordinates. For utility nodes only energy balances are formulated as they are not connected to mass fluxes. In contrast, for the elementary process nodes both mass and energy balances have to be formulated. The energy balances for the WUNs are omitted as their task is only to provide the external work flows. These fluxes are corresponding to the power supply or generation of the EPNs and are considered as external fluxes in the energy balances of  $E_j$ .

Once the elementary processes are described with stoichiometric equations that link TSNs, mass and energy balances for each elementary process node  $E_j$  can be formulated. In contrast to the formulation of partial mass balances for each substance in classical modeling approaches, mass balances for TSN are formulated directly by making use of the process extent number  $\dot{\Gamma}$ : all balances have a similar format because they link one TSN  $M_i$  with the PEN for each elementary process  $E_j$  via their stoichiometric coefficients  $\chi_{(E_j)}^{(M_i)}$ :

$$0 = -\text{sgn} \left( \chi_{(E_j)}^{(M_i)} \right) \dot{N}_{(E_j)}^{(M_i)} + \chi_{(E_j)}^{(M_i)} \dot{\Gamma}_{(E_j)} \quad \forall E_j \in \mathcal{E}; \forall M_i \in \mathcal{M} \quad . \quad (3.2)$$

The energy demands of  $E_j$  are expressed by the specific molar heat ( $\varphi$ ) and work ( $\omega$ ) duties, which are calculated a priori by suitable (non-linear) models. The generic system of three equations that constitutes the energy balancing scheme for unit  $E_j$  is formulated as:

$$0 = \left( -\omega_{(E_j)}^{\text{in}} + \omega_{(E_j)}^{\text{out}} \right) \dot{\Gamma}_{(E_j)} + \dot{W}_{(E_j)}^{\text{ext, in}} - \dot{W}_{(E_j)}^{\text{ext, out}} \quad (3.3a)$$

$$0 = \left[ \varphi_{(E_j)}^{\text{out}} + \left( 1 - \eta_{(E_j)}^{\text{in}} \right) \omega_{(E_j)}^{\text{in}} + \left( \frac{1}{\eta_{(E_j)}^{\text{out}}} - 1 \right) \omega_{(E_j)}^{\text{out}} \right] \dot{\Gamma}_{(E_j)} - \sum_{U_l \in \mathcal{U}} \dot{Q}_{(U_l)}^{(E_j)} \quad (3.3b)$$

$$0 = -\varphi_{(E_j)}^{\text{in}} \dot{\Gamma}_{(E_j)} + \sum_{U_l \in \mathcal{U}} \dot{Q}_{(E_j)}^{(U_l)} \quad (3.3c)$$

$$\forall E_j \in \mathcal{E}$$

where  $\dot{Q}_{(U_l)}^{(E_j)}$ ,  $\dot{Q}_{(E_j)}^{(U_l)}$ ,  $\dot{W}_{(E_j)}^{\text{ext, out}}$ ,  $\dot{W}_{(E_j)}^{\text{ext, in}} \in \mathbb{R}_0^+$ . The superscript of an internal flow  $\dot{Q}_{(E_j)}^{(U_l)}$  or  $\dot{Q}_{(U_l)}^{(E_j)}$  indicates the node from which it originates and the subscript indicates its destination node. It is important to note, that these heat fluxes correspond directly to the external heating and cooling supply if no heat integration is considered:  $\sum \dot{Q}_{(E_j)}^{(U_l)} = \dot{Q}_{(E_j)}^{\text{ext, in}}$  and  $\sum \dot{Q}_{(U_l)}^{(E_j)} = \dot{Q}_{(E_j)}^{\text{ext, out}}$ .

The reason to split the overall energy balance into three balances is that in this way the consideration of a dedicated entropy balance is avoided: Eq. (3.3a) determines the external work fluxes  $\dot{W}_{(E_j)}^{\text{ext, in}}$  and  $\dot{W}_{(E_j)}^{\text{ext, out}}$ , which depend on the molar work demand  $\omega_{(E_j)}^{\text{in}}$  or generation  $\omega_{(E_j)}^{\text{out}}$  of  $E_j$ . Eq. (3.3b) determines the cooling requirement of  $E_j$ , that consists of three contributions: cooling duty  $\varphi_{(E_j)}^{\text{out}}$  e.g. due to condensation and cooling duties resulting from waste heat for work in- and output flows which is accounted for by means of two efficiency factors  $\eta_{(E_j)}^{\text{in}}$  and  $\eta_{(E_j)}^{\text{out}}$ :

$$\eta_{(E_j)}^{\text{in}} := \frac{\omega_{(E_j)}^{\text{in, rev}}}{\omega_{(E_j)}^{\text{in}}} \quad \text{and} \quad \eta_{(E_j)}^{\text{out}} := \frac{\omega_{(E_j)}^{\text{out}}}{\omega_{(E_j)}^{\text{out, rev}}} \quad (3.4)$$

The third Eq. (3.3c) determines the heating demand  $\dot{Q}_{(E_j)}^{(U_l)}$  of  $E_j$ , which depends on the molar heat duty  $\varphi_{(E_j)}^{\text{in}}$ .

After introducing balances for the EPNs, the mass balances for thermodynamic state nodes are formulated as:

$$0 = \sum_{E_j \in \mathcal{E}} \text{sgn} \left( \chi_{(E_j)}^{(M_i)} \right) \dot{N}_{(E_j)}^{(M_i)} + \dot{N}_{\text{ext, in}}^{(M_i)} - \dot{N}_{\text{ext, out}}^{(M_i)} \quad \forall M_i \in \mathcal{M} \quad (3.5)$$

taking into account all internal mass fluxes  $\dot{N}_{(E_j)}^{(M_i)}$  that link  $E_j$  and  $M_i$  as well as external mass fluxes that provide the initial reactants  $\dot{N}_{\text{ext, in}}^{(M_i)}$  or release the final products  $\dot{N}_{\text{ext, out}}^{(M_i)}$ . The sign of the stoichiometric coefficient  $\chi_{(E_j)}^{(M_i)}$  denotes the direction of the internal mass flux between  $E_j$  and  $M_i$ . No energy balances are required for TSNs, as the thermodynamic state of all fluxes that are connected with a TSN is equal by definition. As a consequence, two TSNs are not linked directly.

In contrast, for each utility node  $U_l$  an energy balance has to be formulated, which simplifies to a single heat balance:

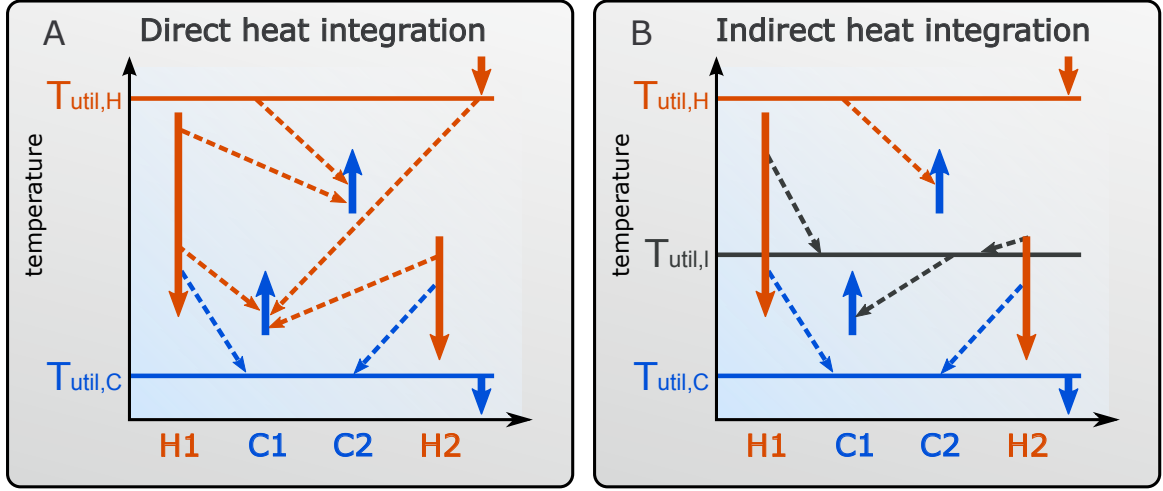


**Fig. 3.3** Schematic illustration of direct and indirect heat integration; A) direct heat integration: hot (H) and cold streams (C) interact directly, utilities are only used to provide external heating and cooling at sufficiently high  $T_{util,H}$  and low temperature  $T_{util,C}$ ; B) indirect heat integration: introduction of additional utilities at intermediate temperatures  $T_{util,I}$  that facilitate heat integration.

$$0 = \sum_{E_j \in \mathcal{E}} \left( \dot{Q}_{(U_l)}^{(E_j)} - \dot{Q}_{(E_j)}^{(U_l)} \right) + \dot{Q}_{(U_l)}^{ext,in} - \dot{Q}_{(U_l)}^{ext,out} \quad \forall U_l \in \mathcal{U} \quad (3.6)$$

The sum of all heat fluxes that enter a utility  $U_l$  – heat fluxes  $\dot{Q}_{(U_l)}^{(E_j^{out})}$  from  $E_j$  and externally provided heat fluxes  $\dot{Q}_{(U_l)}^{ext,in}$  – have to be equal to all heat fluxes that leave a utility  $U_l$  – heat fluxes  $\dot{Q}_{(E_j^{in})}^{(U_l)}$  to  $E_j$  and externally released heat fluxes  $\dot{Q}_{(U_l)}^{ext,out}$ .

### 3.2.3 Heat integration model

While in other approaches the feasibility of heat integration needs to be ensured a priori [102, 103], the FluxMax approach ensures the feasibility by introducing inequality constraints that enables the simultaneous heat integration. In this way, the internally transferred heat flux is limited, which ensures an adequate calculation of the actual heat integration potential. The presented constraints enable direct – among entities – as well as indirect – via utilities – heat integration.

While for direct heat integration, the heat is directly transferred among entities (Fig. 3.3 A), indirect heat integration utilizes the utility nodes to enable heat integration (Fig. 3.3 B). The maximum amount of internally transferable heat depends on the temperature levels of cold and hot streams. Analogous to pinch analysis, cold streams require heat whereas hot streams provide heat. Three distinct temperature domains can be distinguished, that determine the heat integration possibility depending on the minimum temperature difference  $\Delta T_{min}$  and the in- and outlet temperatures of hot streams  $T_{H,in}$  and  $T_{H,out}$ , or of cold streams  $T_{C,in}$

**Tab. 3.1** Temperature conditions for for classification of heat integration possibility.

Domain	Condition	Heat Integration
<i>Cold Fluxes</i>		
I	i) $T_{H,in}^{\max} \geq T_{C,out} + \Delta T_{\min}$	total
II	i) $T_{H,in}^{\max} < T_{C,out} + \Delta T_{\min}$ ii) $T_{H,in}^{\max} > T_{C,in} + \Delta T_{\min}$	partial
III	i) $T_{H,in}^{\max} \leq T_{C,in} + \Delta T_{\min}$	infeasible
<i>Hot Fluxes</i>		
I	i) $T_{C,in}^{\min} + \Delta T_{\min} \leq T_{H,out}$	total
II	i) $T_{C,in}^{\min} + \Delta T_{\min} < T_{H,in}$ ii) $T_{C,in}^{\min} + \Delta T_{\min} > T_{H,out}$	partial
III	i) $T_{C,in}^{\min} + \Delta T_{\min} \geq T_{H,in}$	infeasible

and  $T_{C,out}$ , respectively: domain I: total heat integration possible, domain II: partial heat integration possible, and domain III: heat integration infeasible. The temperature conditions and classification of hot and cold fluxes are listed in Tab. 3.1.

Tab. 3.1 shows that a cold stream can be completely heated internally (provided that sufficiently large heat fluxes are available) by hot streams (domain I) if the maximum inlet temperature  $T_{H,in}^{\max}$  of the corresponding hot streams is higher than the cold outlet stream temperature and a minimum temperature difference  $\Delta T_{\min}$ , that ensures a sufficiently large driving force. In contrast, heat integration is infeasible if the cold inlet stream temperature is larger than the hot inlet stream temperature. In the other cases (domain II), the cold stream can be partially heated internally. An analogous classification can be done for hot streams that have to be cooled internally by cold streams depending on the minimum inlet temperature of cold streams  $T_{C,in}^{\min}$  (Tab. 3.1).

The internal heat fluxes that supply heat to a cold EPN  $E_j$  are denoted as  $\dot{Q}_{(E_j)}^{(k_{mj}^H)}$ , while  $\dot{Q}_{(k_{mj}^C)}^{(E_j)}$  originate from a hot EPN  $E_j$ . Hereby,  $k_{mj}^H \in \mathcal{E}, k_{mj}^C \in \mathcal{E}$  for direct heat integration and  $k_{mj}^H \in \mathcal{U}, k_{mj}^C \in \mathcal{U}$  for indirect heat integration. For stream combinations that belong to domain I, no inequality has to be formulated, because the heating or cooling demand of the corresponding EPN can be completely provided internally. However, for combinations that belong to domain II the maximum amount of transferable heat has to be quantified. Two subsets of  $\mathcal{F}$  are introduced: i) the subset  $\mathcal{F}_{II}^{H,E_j} := \{\dot{Q}_{(E_j)}^{(k_{mj}^H)} \in \mathbb{R}_0^+ \mid \text{case II satisfied}\}$  that contains all the internal heat fluxes that supply heat to a cold EPN  $E_j$ ; and ii) the subset  $\mathcal{F}_{II}^{E_j,C} := \{\dot{Q}_{(k_{mj}^C)}^{(E_j)} \in \mathbb{R}_0^+ \mid \text{case II satisfied}\}$  that contains all the internal heat fluxes that release heat from a hot EPN  $E_j$ . The first subset  $\mathcal{F}_{II}^{h,E_j}$  is used to formulate an inequality for every combination of cold EPN  $E_j^{\text{in}}$  and possibly interacting hot streams that belong to domain II:



$$0 \leq \frac{T_{H,in}^{\max} - T_{C,in,(E_j)} - \Delta T_{\min}}{T_{C,out,(E_j)} - T_{C,in,(E_j)}} \varphi_{(E_j)}^{\text{in}} \dot{\Gamma}_{(E_j)} - \sum_{k_{mj}^H \in \mathcal{K}_m^H} \dot{Q}_{(E_j)}^{(k_{mj}^H)} \quad \forall \dot{Q}_{(E_j)}^{(k_{mj}^H)} \in \mathcal{K}_m^H \quad (3.7)$$

Herein,  $\varphi_{(E_j)}^{\text{in}}$  denotes the specific heat demand of  $E_j^{\text{in}}$  and  $T_{\text{Hot,in}}^{\max}$  the maximum inlet temperature of the possibly interacting hot streams.  $\mathcal{K}_m^H \subset \mathcal{K}^H = \{k_{mj}^H\}$  denotes the  $m$ -th row of the set of all permutations of  $\mathcal{F}_{\text{II}}^{H,E_j}$ , that determine all possibly interacting streams of cold EPN  $E_j$ . Illustrated for an example of three possible interacting hot streams ( $H_1, H_2, H_3$ ) the set of permutations  $\mathcal{K}^H$  equals to:

$$\mathcal{K}^H = \left\{ \begin{array}{ccc} H_1 & & \\ & H_2 & \\ & & H_3 \\ H_1 & H_2 & \\ H_1 & & H_3 \\ & H_2 & H_3 \\ H_1 & H_2 & H_3 \end{array} \right\} \quad (3.8)$$

In the same way, an inequality for every combination of hot EPN  $E_j$  and possibly interacting cold streams is introduced by using the specific excess of heat  $\varphi_{(E_j)}^{\text{out}}$ , the minimum inlet temperature of possibly interacting cold streams  $T_{C,in}^{\min}$ , the subset  $\mathcal{F}_{\text{II}}^{E_j,C}$ , and the corresponding set of permutations  $\mathcal{K}^C$ , according to Eq. (3.8):

$$0 \leq \frac{T_{H,in,(E_j)} - T_{C,in}^{\min} - \Delta T_{\min}}{T_{H,in,(E_j)} - T_{H,out,(E_j)}} \varphi_{(E_j)}^{\text{out}} \dot{\Gamma}_{(E_j)} - \sum_{k_{mj}^C \in \mathcal{K}_m^C} \dot{Q}_{(E_j)}^{(k_{mj}^C)} \quad \forall \dot{Q}_{(E_j)}^{(k_{mj}^C)} \in \mathcal{K}_m^C \quad (3.9)$$

The maximum inlet temperature of possibly interacting hot streams  $T_{H,in}^{\max}$  and the minimum inlet temperature of possibly interacting cold streams  $T_{C,in}^{\min}$  are calculated by comparing the temperatures of the interacting partner streams as shown in Eqs. (3.10a) and (3.10b).

$$T_{H,in}^{\max} = \max_{k \in \mathcal{K}_H} (T_{k,in}) \quad (3.10a)$$

$$T_{C,in}^{\min} = \min_{k \in \mathcal{K}_C} (T_{k,in}) \quad (3.10b)$$

The inequalities introduced in Eq. (3.9) do not take into account in which order a hot stream transfers its heat to distinct cold streams if more than one partner stream is possible. Similar conditions apply to cold streams that are connected to more than one hot stream (Eq. (3.7)).

It becomes obvious that the available heat that can be transferred to the second cold stream is lower than to the first cold stream since the energetic content of the hot stream is steadily decreasing. Therefore, two additional inequalities for all hot  $\mathcal{F}_{\text{II}}^{H,E_j}$  and cold streams  $\mathcal{F}_{\text{II}}^{E_j,C}$  are introduced to account for the energy content actually available.

$$0 \leq \frac{T_{k,\text{in}} - T_{C,\text{in},(E_j)} - \Delta T_{\text{min}}}{T_{C,\text{out},(E_j)} - T_{C,\text{in},(E_j)}} \left( \varphi_{(E_j)}^{\text{in}} \dot{\Gamma}_{(E_j)} - \sum_{\substack{l \in \mathcal{F}^{H,E_j} \\ l \neq k}} \dot{Q}_{(E_j)}^{(l)} - \dot{Q}_{(E_j)}^{\text{ext},\text{in}} \right) - \dot{Q}_{(E_j)}^{(k)} \quad \forall k \in \mathcal{F}^{H,E_j} \quad (3.11a)$$

$$0 \leq \frac{T_{H,\text{in},(E_j)} - T_{k,\text{in}} - \Delta T_{\text{min}}}{T_{H,\text{in},(E_j)} - T_{H,\text{out},(E_j)}} \left( \varphi_{(E_j)}^{\text{out}} \dot{\Gamma}_{(E_j)} - \sum_{\substack{l \in \mathcal{F}^{E_j,C} \\ l \neq k}} \dot{Q}_{(l)}^{(E_j)} - \dot{Q}_{(E_j)}^{\text{ext},\text{out}} \right) - \dot{Q}_{(k)}^{(E_j)} \quad \forall k \in \mathcal{F}^{E_j,C} \quad (3.11b)$$

After introducing the general heat integration model, in the following two different approaches – direct and indirect heat integration – are presented, which mainly differ in the considered sets of permutations  $\mathcal{K}_H$  and  $\mathcal{K}_C$  of possibly interacting hot or cold streams, respectively.

### Direct heat integration among elementary process nodes

In case of direct heat integration, the UNs provide the external heating and cooling at sufficient high and low temperature as shown in Fig. 3.3 A. Thus, according to the classification in three domains the heat fluxes that link UNs and EPNs belong to domain I. To enable internal heat transfer, additional heat flux variables  $\dot{Q}_{(E_i)}^{(E_j)}$  and  $\dot{Q}_{(E_j)}^{(E_i)}$ , that link two EPNs directly, have to be added to the energy balances:

$$0 = \left( -\omega_{(E_j)}^{\text{in}} + \omega_{(E_j)}^{\text{out}} \right) \dot{\Gamma}_{(E_j)} + \dot{W}_{(E_j)}^{\text{ext},\text{in}} - \dot{W}_{(E_j)}^{\text{ext},\text{out}} \quad (3.12a)$$

$$0 = \left[ \varphi_{(E_j)}^{\text{out}} + \left( 1 - \eta_{(E_j)}^{\text{in}} \right) \omega_{(E_j)}^{\text{in}} + \left( \frac{1}{\eta_{(E_j)}^{\text{out}}} - 1 \right) \omega_{(E_j)}^{\text{out}} \right] \dot{\Gamma}_{(E_j)} - \sum_{U_i \in \mathcal{U}} \dot{Q}_{(U_i)}^{(E_j)} - \sum_{E_i \in \mathcal{E}} \dot{Q}_{(E_i)}^{(E_j)} \quad (3.12b)$$

$$0 = -\varphi_{(E_j)}^{\text{in}} \dot{\Gamma}_{(E_j)} + \sum_{U_i \in \mathcal{U}} \dot{Q}_{(E_j)}^{(U_i)} + \sum_{E_i \in \mathcal{E}} \dot{Q}_{(E_j)}^{(E_i)} \quad (3.12c)$$

$$\forall E_j \in \mathcal{E}$$

whereby according to Fig. 3.3 A, the assumption of only two utility nodes – one at sufficient high, and one at sufficient low temperature – can be made, which results in:

$$\sum_{U_i \in \mathcal{U}} \dot{Q}_{(E_j)}^{(U_i)} = \dot{Q}_{(E_j)}^{\text{ext, in}} \quad (3.13a)$$

$$\sum_{U_i \in \mathcal{U}} \dot{Q}_{(U_i)}^{(E_j)} = \dot{Q}_{(E_j)}^{\text{ext, out}} \quad (3.13b)$$

Adding the newly introduced internal heat flux variables in every energy balance, as shown in Eq. (3.12), and the introduction of inequalities (Eqs. (3.7) and (3.9)), facilitates the simultaneous consideration of heat integration as a part of the optimization problem. However, the number of inequalities increases drastically due to the increasing combinatorial complexity caused by the increasing number of EPNs. Therefore, in the next section indirect heat integration via utilities is presented.

### Indirect heat integration via utility nodes

In chemical production plants, heat is usually not transferred directly among individual process units, but via a network of utilities. Utilities are considered as reservoirs of heat at a constant temperature, such as steam at a specific pressure, or a sufficiently large water reservoir (e.g. a river). Depending on the temperature levels of heat demanding or heat supplying EPN, respectively, the utilities serve either as heat source or sink, as shown in Fig. 3.3.

In contrast to direct heat integration, further utility nodes at intermediate temperatures are considered as shown in Fig. 3.3 B. As a consequence, the heat fluxes  $\dot{Q}_{(E_j)}^{(U_i)}$  and  $\dot{Q}_{(U_i)}^{(E_j)}$  that link UNs and EPNs may belong also to domain II and III. Therefore, additional inequalities have to be formulated for combinations that belong to domain II, according to Eqs. (3.7) and (3.9). However, the newly introduced heat flux variables are limited by the number of UNs considered (two heat flux variables for each UN) and are therefore strongly limited compared to the direct heat integration approach. In this way, the complexity of the resulting optimization problem is reduced drastically, since the number of utilities considered is lower than the number of EPNs, which result in a significant reduction of considered inequalities.

#### 3.2.4 Formulation of the optimization problem

The equality and inequality constraints result from the conservation laws and the heat integration conditions, respectively. All constraints are linear in terms of the fluxes – mass, heat, and work – which are the decision variables of the optimization problem. The general formulation of an optimization problem with linear constraints is given in Eq. (3.14).

$$\begin{aligned}
\min_{\boldsymbol{\varphi}} \quad & f(\boldsymbol{\varphi}) \\
\text{s.t.} \quad & \mathbf{A}_{\text{eq}}\boldsymbol{\varphi} = \mathbf{b}_{\text{eq}} \\
& \mathbf{A}_{\text{iq}}\boldsymbol{\varphi} \leq \mathbf{b}_{\text{iq}} \\
& \boldsymbol{\varphi}_{\text{lb}} \leq \boldsymbol{\varphi} \leq \boldsymbol{\varphi}_{\text{ub}}
\end{aligned} \tag{3.14}$$

Herein,  $f$  is the objective function and  $\boldsymbol{\varphi} = (\dot{\mathbf{N}}, \dot{\mathbf{\Gamma}}, \dot{\mathbf{Q}}, \dot{\mathbf{W}})^\top$  denotes the vector of all decision variables, namely mass fluxes  $\dot{\mathbf{N}}$ , heat fluxes  $\dot{\mathbf{Q}}$ , work fluxes  $\dot{\mathbf{W}}$ , and generalized process extent numbers  $\dot{\mathbf{\Gamma}}$ .

The equality constraints, that are described by the coefficient matrix  $\mathbf{A}_{\text{eq}}$  and the vector of right-hand sides  $\mathbf{b}_{\text{eq}}$ , contain all energy and mass balances of TSNs, EPNs, and UNs. In addition,  $\mathbf{A}_{\text{eq}}$  contains the information of the coupling of the nodes, that result from the generalized utilization of stoichiometric equations.

The temperature constraints, that result from heat integration are summarized by the coefficient matrix of inequalities  $\mathbf{A}_{\text{iq}}$  and corresponding right hand sides  $\mathbf{b}_{\text{iq}}$ . The coefficient matrices,  $\mathbf{A}_{\text{eq}}$  and  $\mathbf{A}_{\text{iq}}$ , and the solution vectors,  $\mathbf{b}_{\text{eq}}$  and  $\mathbf{b}_{\text{iq}}$ , as well as the lower  $\boldsymbol{\varphi}_{\text{lb}}$  and upper bounds  $\boldsymbol{\varphi}_{\text{ub}}$  vary depending on the chosen application.

### $\ell_1$ -norm-regularization

In general the identified solution of the optimization problem given in Eq. (3.14) does not have to be unique. This even applies for linear objective functions  $f(\boldsymbol{\varphi}) = \mathbf{c}^\top \boldsymbol{\varphi}$  that weight the decision variables  $\boldsymbol{\varphi}$  with constant cost factors  $\mathbf{c}$ . While it is true that the optimum of a linear programming problem is always a global optimum [104], there may be different vectors  $\boldsymbol{\varphi}$  leading to the global optimum. In the context of process synthesis, this is in particular the case if more than one possible process configuration affects the objective function in the same way or if specific fluxes are not considered – and thus not penalized – in the objective function  $f$ . The  $\ell_1$ -norm-regularization can be used to identify the most sparse solution vector by adding an additional penalty term [105]. As a consequence, all fluxes that are not penalized in the objective function are set to zero if possible. The augmented objective function  $\tilde{f}$  is defined in the following:

$$\tilde{f}(\boldsymbol{\varphi}) = f(\boldsymbol{\varphi}) + \lambda \|\boldsymbol{\varphi}\|_1 \tag{3.15}$$

Herein,  $\lambda \geq 0$  is the regularization parameter and  $\|\boldsymbol{\varphi}\|_1 = \sum_i |\varphi_i|$  the  $\ell_1$ -norm of  $\boldsymbol{\varphi}$ . If the lower bound of the decision variables  $\boldsymbol{\varphi}_{\text{lb}}$  equals zero (non-negativity condition) than the penalty term simplifies to the weighed sum of all decision variables  $\varphi_i$ , shown for a linear objective function in the following:

$$\tilde{f}(\boldsymbol{\varphi}) = \mathbf{c}^\top \boldsymbol{\varphi} + \boldsymbol{\lambda}^\top \boldsymbol{\varphi}, \quad \boldsymbol{\varphi}, \boldsymbol{\lambda} \geq \mathbf{0} \quad (3.16)$$

Although in the following chapters, for readability reasons, only the actual objective functions  $f(\boldsymbol{\varphi})$  are presented, which are applied to the corresponding case studies, in each case a suitable  $\ell_1$ -norm-regularization is applied to identify the most sparse solution.

### 3.3 Chapter summary

In this chapter the FluxMax approach for process design and synthesis under consideration of heat integration by discretization of the thermodynamic state space is presented. The introduction of thermodynamic state nodes (TSN), elementary process nodes (EPN), utility nodes (UN), and work utility nodes (WUN) enables the representation of the chemical process as a directed graph, with the edges corresponding to the mass and energy fluxes to be optimized. All mixtures in the process are uniquely determined by thermodynamic coordinates and thus assigned to a distinct TSN. The EPNs facilitate the thermodynamic state change between the TSNs. Therefore each elementary process is described uniformly. By introducing a generalized process extent number, a stoichiometric equation is formulated for each type of elementary process. The generalized process extent number is also used to formulate a continuous flux optimization problem that identifies the optimal pathway within the discretized thermodynamic state space. The discretization of the thermodynamic state space effectively decouples the process based non-linearities from the network optimization problem, which result in a linear feasible region. By adding additional inequality constraints, heat integration is considered as integrated part of the flux optimization.

In addition to the key features of the simultaneous consideration of heat integration and the unified representation of any chemical process as directed graph by introducing generalized stoichiometric equations, the FluxMax approach has a further important aspect: the FluxMax approach is independent of the considered process scale. The EPNs can correspond to: i) whole processes for the optimization of chemical production networks on production system level, ii) process units for the optimization of chemical processes on plant level, or iii) elementary processes for the optimization of process units. This is enabled by the unified description of any type of chemical transitions by stoichiometric equations introducing generalized stoichiometric coefficients  $\chi_{(E_j)}^{(M_i)}$ . The energetic requirements – heating, cooling, and power supply – are considered by specific heat  $\varphi$  and work  $\omega$  duties, which can be evaluated by suitable (non-linear) models a priori. In this way, it is also possible to overlap different scales by using rigorous models to describe elementary processes of particular interest, while lumped models are used for less important elementary processes.



## Chapter 4

# Production system level

The production system level is the top level of the process hierarchy considered in this dissertation (see Fig. 1.1). This level is characterized by a small knowledge basis about the processes involved and therefore deals with questions in a broader context and with decisions to be taken at an early stage: Strategic and future design decisions are evaluated rather than detailed process optimizations. Consequently, conversion processes are treated as black boxes, as shown in Fig. 4.1. In the context of energy conversion, two central research questions arise which can be answered at the production system level (see section 1.2): (II) What are optimal raw materials and conversion technologies to produce the desired target molecule both economically efficiently and environmentally friendly, and (III) can the chemical industry become a carbon sink under economic constraints? The challenge of answering both key questions is the need to identify economically competitive production processes while at the same time significantly reducing valuable renewable energy.

The economic measure considered in this work includes both the operational (OPEX) and capital (CAPEX) expenditures of the entire production network. Therefore, the specific production costs of methanol introduced in [106] and the annualized investment costs derived in [107] are used. In addition, a penalty term for carbon dioxide emissions is considered, which was first introduced in [82]. The specific CO<sub>2</sub> emissions, which are caused by both direct and indirect emissions depending on the energy source used [82], are used as an ecological measure.

Within the context of this dissertation, the FluxMax approach was applied at the production system level for the systematic analysis of the different feedstocks and energy sources of the formic acid [108] and the methanol [82] production network. The latter is the basis of the results presented in this chapter, after a literature review of process alternative evaluation approaches that are applicable at the production system level.

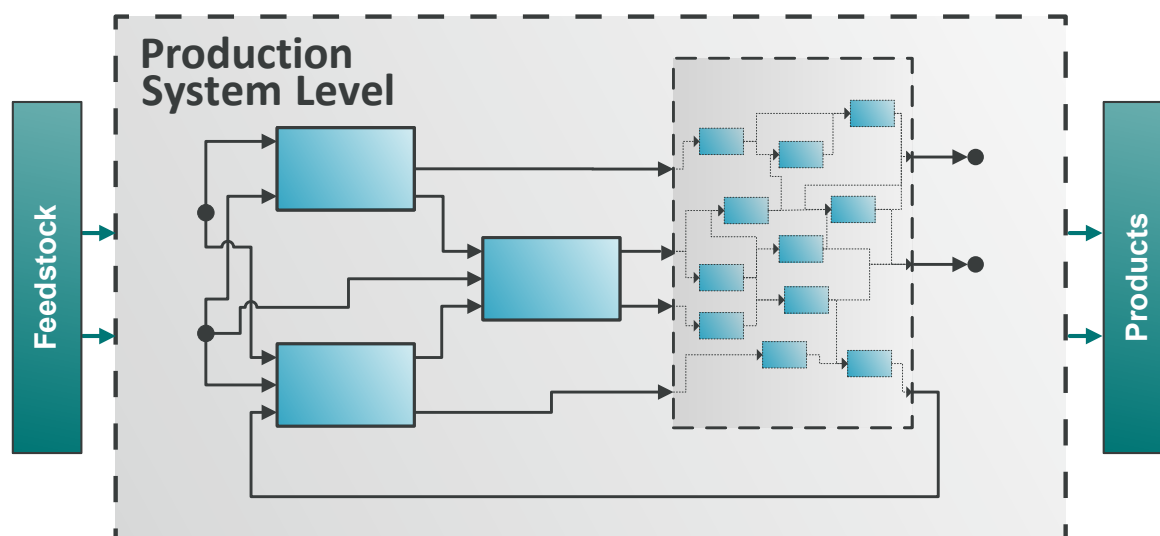


Fig. 4.1 Schematic illustration of the process design task at the production system level.

## 4.1 Literature review

This section provides a broad overview of evaluation approaches for identifying optimal process pathways and optimal target molecules that were reported in the literature in recent years. There are a large number of possible evaluation criteria. These include energy efficiency, global warming potential, greenhouse gas emissions and economic costs. Schlögl [109] underlined the outstanding strategic role of chemical energy conversion technologies for improved sustainability and the importance of increasing energy efficiency through energy integration. Two main types of approaches to identify optimal process pathways and optimal storage molecules can be found in the literature. On the one hand, there are optimization-based approaches that apply different objective functions. On the other hand, there are knowledge-based methods, such as life cycle assessment (LCA). In the following, knowledge-based approaches are presented first, followed by optimization-based approaches.

### 4.1.1 Knowledge-based approaches

Knowledge-based approaches are an efficient way to easily evaluate a variety of possible pathways and molecules. In general, they are characterized by simple implementation, as they do not require superstructure modeling and omit complex mathematical model formulations. In addition, they have a high degree of flexibility with regard to different types of evaluation criteria. Otto et al. [74] listed CO<sub>2</sub> conversion technologies for the production of bulk and fine chemicals. Key parameters such as CO<sub>2</sub>-avoidance potential, relative added value, and the independence of fossil reactants were introduced for the evaluation of bulk chemicals that could also be suitable as storage molecules. As a result, methanol was identified as one optimal target molecule. Also Roh et al. [110] proposed a methodological framework for the



development of CO<sub>2</sub>-conversion processes aiming at the substitution of non-CO<sub>2</sub> utilizing processes or products. By introducing three criteria – demand availability, CO<sub>2</sub> reduction feasibility, and economic feasibility – they investigated a methanol plant and evaluated the feasibility of a CO<sub>2</sub>-based fuel production that is strongly dependent on the raw material.

Using CO<sub>2</sub> as feedstock is a smart way of reducing total CO<sub>2</sub>-emission, or even achieving net consumption. However, it is not sufficient to develop the CO<sub>2</sub>-conversion process but suitable CO<sub>2</sub>-sources must also be found. An assessment of algal based CCU technology pathways was carried out by Arnold et al. [111]. Criteria such as CCU potential, resource demand and investment risk were used to assess conversion pathways in a techno-economic analysis using Monte Carlo simulations. As a result, they identified processes consisting of algal biodiesel-production and biomass liquefaction. As the transportation sector accounts for a significant part of CO<sub>2</sub> emissions, the evaluation of production pathways from biomass to fossil fuel substitutes was subject of many publications. Bidy et al. [112] compared the production costs for a fuel-only production from biomass with a combined production of fuel and chemicals. They concluded that the minimum selling price for the produced fuel can be drastically decreased if the coproduced chemical has an appropriate value and an adequate market size: Using lignocellulose as biomass, the minimum selling price can roughly be halved if the valuable co-product is succinic acid. In Hoppe et al. [113] the Global Warming Potential (GWP) of production processes for the synthesis of natural gas for the use in transportation and in chemical industry was evaluated. CO<sub>2</sub>-based methane production with wind power showed the lowest GWP. In a further publication, methane was identified as target molecule with lowest – or even negative – GWP by applying LCA [114]. However, the authors expose the strong influence of the hydrogen source on the overall resource efficiency.

In general, an increasing number of papers have been published in recent years that use LCA as a tool to evaluate process pathways and target molecules. Some of them are briefly discussed in the following. One of the mostly cited article in the field of life cycle assessment in recent years was written by Sternberg and Bardow [37]. They performed a systematic evaluation of energy storage systems on the basis of data for various countries, including the USA and Germany. Sternberg et al. [115] also examined the production of CO<sub>2</sub>-based C<sub>1</sub> chemicals and identified formic acid as optimal target molecule with maximum environmental impact reduction, followed by carbon monoxide and methanol. Deutz et al. [65] discussed the effect of using oxymethylene ethers (OME<sub>n</sub>) as a diesel blend on a more sustainable transport sector. Using CO<sub>2</sub>-based methanol as the raw material, they compared the conventional conversion pathway via formaldehyde with a novel direct route and could show that the direct route significantly increases the exergy efficiency. GWP impact and the NO<sub>x</sub> and soot emissions are also significantly reduced by the substitution of 24 mass-% of fossil diesel with OME<sub>n</sub>. A study by Reiter and Lindorfer [116] evaluating the GWP of H<sub>2</sub> and CH<sub>4</sub> production from renewable electricity showed a large GWP reduction potential. However,

they emphasized that the current electricity mix of EU countries would lead to a high GWP. In addition, the CO<sub>2</sub> source strongly influences the ecological impact if the previously bound CO<sub>2</sub> is released again, e.g. as a result of combustion processes.

#### 4.1.2 Optimization-based approaches

The multitude of approaches dealing with the identification of optimal process pathways or storage molecules is formulated as a mathematic optimization problem. In almost all publications economic objective functions – costs minimization or profit maximization – and/or ecological objective functions – minimization of greenhouse gas emissions or maximization of energy efficiency – were applied. Parajuli et al. [117] gave a comprehensive overview of sustainable pathways and evaluation methodologies for biorefineries. In the following, selected articles are presented in more detail. First, studies on biorefineries are presented, followed by publications focusing on other topics.

Kim et al. [95] examined strategies for converting biomass into fuel by breaking down the entire process into intermediate subprocesses. Formulating a linear programming (LP) problem facilitated the identification of the most convenient mass flux distribution. The developed framework was demonstrated for the production of ethanol from woody biomass. A similar case study was considered by Giuliano et al. [118]. They examined a multi-product biorefinery – levulinic acid, succinic acid, and ethanol – from wooden biomass by introducing a discretization method in order to obtain MILP formulation from the mixed integer non-linear program (MINLP) master problem. An economic optimization was carried out, followed by a sensitivity analysis which showed that the optimal flowsheet depends strongly on the considered economic scenario and the plant size. Martin and Grossmann [50] also investigated the production of ethanol from solid biomass, namely by gasification of switchgrass. A three step MINLP approach using shortcut models was presented, consisting of optimization of the flowsheet, heat integration and economic analysis. Direct gasification, steam reforming, removal of excess hydrogen and ethanol synthesis were found to be the optimal process configurations. Another multi-product biorefinery system was investigated by Zondervan et al. [119]. The optimal process pathway for the production of ethanol, butanol, succinic acid, and blends of these compounds with fossil fuels was analyzed. The resulting MINLP was solved and discussed for different objective functions – yield maximization as well as costs and waste minimization. The method can be used for fast scanning of different process alternatives and was exemplified for both single-product and multi-product plants. In contrast to ethanol as biofuel, Onel et al. [120] examined process configurations for the production of Fischer-Tropsch fuels and olefins from biomass and natural gas. A global optimization framework was introduced to solve the MINLP and to identify the optimal target molecule. As a result, co-production of liquid fuels and olefins was reported, whereby the profit is increased for higher olefin production levels. Voll and Marquardt [81] introduced the concept

of Reaction Network Flux Analysis (RNFA) as a MILP based rapid screening approach for chemical production networks to identify promising pathways to produce biofuels. Maronese et al. [121] proposed an Integer-Cut Constraint method applied to a MILP formulation to rank biorefinery conversion pathways. Through the detailed simulation of each conversion unit and the subsequent mass flux optimization by interconnecting the units in a superstructure, a comparison between competing strategies was possible. As an illustrative case study, various biomass-to-fuel technologies were evaluated on the basis of data for the Swiss market. Another MILP formulation can be found in Kokossis et al. [98] who introduced a digraph approach for the integrated design of biorefineries. They optimized the mass flux distribution and then performed a pinch analysis to account for the energy demand and to design a heat exchanger network. Due to the high number of publications in the field of biorefinery optimization, Cheali et al. [122] established a data collecting and management approach. By formulating an integrated thermodynamic and biochemical biorefinery superstructure, a generic modeling approach was achieved which led to a MINLP formulation. Taking into account model parameters such as reaction yield, utility consumption and separation efficiency, a large database with almost 3,000 possible biorefinery pathways was created. This database was made public for benchmarking and application in optimization-based superstructure approaches.

While many publications deal with the optimization of biorefineries, there are also many articles dealing with non-biological processes. A design methodology for energy systems that integrates classical branch and bound with exergy analysis (BBEx) was proposed by Hartono et al. [91]. Instead of solving the relaxed NLP subproblems of a MINLP, the residual exergy at intermediate nodes was calculated. Comparisons with branch and bound as well as total enumeration showed a significant improvement in computing time for the case study of a wood-based fuel cell system. A systematic methodology for designing sustainable CO<sub>2</sub> utilization processes was published by Roh et al. [75]. Their three step approach – reaction pathway synthesis, superstructure generation, and optimal pathway determination – enables the determination of economically profitable processes that mitigate CO<sub>2</sub>. The method was illustrated with the CO<sub>2</sub>-based production of methanol. It was shown that replacing an existing methanol plant with an integrated process can lead to a more sustainable production. A MINLP-based framework has been proposed for the production of liquid fuels from municipal solid waste (MSW) by Niziolek et al. [123]. A rigorous deterministic global branch and bound algorithm was used to optimize the production system of Fischer-Tropsch and other liquid fuels via methanol production routes. First results indicated that the production of fuels from MSW was economically competitive with petroleum-based processes. In a further study Niziolek et al. [124] examined the nationwide supply chain of MSW-to-liquid-fuels for the United States. The economic competitiveness of break-even oil

prices between USD 64 and 77 was demonstrated, making MSW a promising raw material for fuel production.

## 4.2 Application of FluxMax approach to the production system level

The production system level is characterized by coarse process information only and supports deriving strategic decisions. This leads to two assumptions: i) only pure components are considered, and ii) the conversion processes are considered as black boxes whose chemical conversion is described by a net stoichiometric equation. Consequently, the discretization of the thermodynamic state space is also very coarse. Only one TSN  $M_i$  is introduced for each pure component  $i = \alpha \in \mathcal{A}$  occurring in the production network. The temperature and pressure are set to a reference temperature  $T_0$  and a reference pressure  $p_0$  for all TSNs.

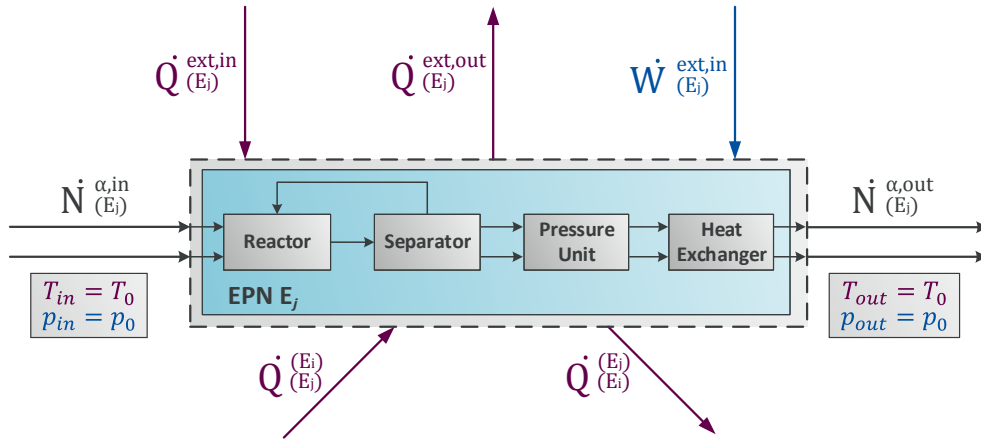


**Fig. 4.2** Mass conversion along the edges; schematic illustration of a single process consisting of reaction, separation and auxiliary operations used for temperature and pressure adjustment.

Fig. 4.2 shows the black box representation of an EPN  $E_j$ , which transforms pure components that enter and leave the EPN under reference conditions. Temperature and pressure changes as well as all auxiliary processes are considered within the EPNs. The temperature and pressure level of each EPN itself is assumed to be the average process temperature and pressure. Tab. C.1 lists typical operating windows of the considered processes. Depending on the constant temperature levels, the EPNs can transfer heat internally according to the direct heat integration approach, introduced in section 3.2.3. Due to the restriction to pure components and the consideration of both reaction and separation within the EPNs, at the production system level, the generalized stoichiometric coefficients  $\chi_{(E_j)}^{(M_i)}$  correspond to the stoichiometric coefficients  $\nu_{\alpha}^{(j)}$  of the EPNs shown in Tab. C.1 of the  $j$ -th conversion process.

$$\chi_{(E_j)}^{(M_i)} = \nu_{\alpha}^{(j)} \quad (4.1)$$

In addition to the generalized stoichiometric coefficients, the specific molar heat  $\varphi$  and energy  $\omega$  duties must be known to fully describe an EPN. The specific duties are calculated by formulating enthalpy and entropy balances for each EPN  $E_j$ . While the enthalpy balances correspond to the first law of thermodynamics and thus determine the total energy demand, the entropy balances indicate the ratio between heat-related and work-related energy demand. No work output fluxes are considered, since no work generating processes are considered in this case study (see Tab. C.1). Due to the same inlet and outlet conditions – temperature and pressure – of  $E_j$ , the steady-state enthalpy balance is expressed by means of the enthalpy of reaction  $\Delta_R h_{(E_j)}$ :

$$0 = -\Delta_R h_{(E_j)} \dot{\Gamma}_{(E_j)} + \dot{Q}_{(E_j)}^{\text{ext,in}} - \dot{Q}_{(E_j)}^{\text{ext,out}} + \sum_{E_i \in \mathcal{E}} \left( \dot{Q}_{(E_j)}^{(E_i)} - \dot{Q}_{(E_i)}^{(E_j)} \right) + \dot{W}_{(E_j)}^{\text{ext,in}} \quad \forall E_j \in \mathcal{E} \quad (4.2)$$

Similarly, an entropy balance is formulated for each EPN. Using the energy conversion efficiency  $\eta_{(E_j)}^{\text{in}}$  introduced in Eq. (3.4) to estimate the irreversible entropy production and the entropy of the reaction  $\Delta_R s_{(E_j)}$  of each EPN  $E_j$  the following balance is derived:

$$0 = -\Delta_R s_{(E_j)} \dot{\Gamma}_{(E_j)} - \frac{1}{T_{E_j}} \left( \dot{Q}_{(E_j)}^{\text{ext,in}} - \dot{Q}_{(E_j)}^{\text{ext,out}} + \sum_{E_i \in \mathcal{E}} \left( \dot{Q}_{(E_j)}^{(E_i)} - \dot{Q}_{(E_i)}^{(E_j)} \right) \right) - \frac{1}{T_{E_j}} \left( 1 - \eta_{(E_j)}^{\text{in}} \right) \dot{W}_{(E_j)}^{\text{ext,in}} \quad \forall E_j \in \mathcal{E} \quad (4.3)$$

As  $\dot{\Gamma}_{(E_j)}$  determines the process extent of  $E_j$ , from Eqs. (4.2) and (3.12) follow for the molar duties for heating  $\varphi_{(E_j)}^{\text{in}}$  and cooling  $\varphi_{(E_j)}^{\text{out}}$  as well as for electrical work demand  $\omega_{(E_j)}^{\text{in}}$ :

$$\varphi_{(E_j)}^{\text{in}} - \varphi_{(E_j)}^{\text{out}} + \eta_{(E_j)}^{\text{in}} \omega_{(E_j)}^{\text{in}} = \Delta_R h_{(E_j)} \quad \forall E_j \in \mathcal{E} \quad (4.4)$$

Similar, Eqs. (4.2) and (4.3) are used to express the specific heat demands by the entropy of reaction:

$$\varphi_{(E_j)}^{\text{in}} - \varphi_{(E_j)}^{\text{out}} = T_{E_j} \Delta_R s_{(E_j)} \quad (4.5)$$

From Eqs. (4.4) and (4.5) follow for the specific work demand:

$$\omega_{(E_j)}^{\text{in}} = \frac{\Delta_R h_{(E_j)} - T_{E_j} \Delta_R s_{(E_j)}}{\eta_{(E_j)}^{\text{in}}} \quad (4.6)$$

Eqs. (4.5) and (4.6) determine the specific energy requirements. However, a degree of freedom is left, which is why the equations are added as additional constraints to the optimization problem. In this way, the minimum energy requirement is calculated, fulfilling both the first and second law of thermodynamics.

## 4.3 Case study

### 4.3.1 Methanol production network

The methanol production network constitutes the case study for the application of the FluxMax approach at the production system level. The methanol molecule consists of one carbon, one oxygen and four hydrogen atoms. In principle, these atoms can be provided by any other molecule containing C, O or H. However, methanol is industrially produced from synthesis gas consisting mainly of CO, CO<sub>2</sub> and H<sub>2</sub>. The conventional feedstock for synthesis gas production is based on fossil resources, such as coal or natural gas, and steam reforming and coal gasification are the main process technologies for conversion. On the other hand, renewable sources and corresponding technologies are also taken into account here to enable a sustainable production system via a R2Chem path. Promising technologies are anaerobic digestion of biomass and the subsequent reforming step, the use of electrical energy for the electrochemical splitting of water into hydrogen and oxygen, and the use of carbon dioxide as carbon source. Therefore, the reverse water gas shift (RWGS) process or carbon dioxide electrolysis are also moving into the focus of interest. Tab. C.1 lists the conversion processes that are considered in this analysis.

For the evaluation of the economic and ecological impacts of the methanol production, two measures – specific costs  $c_s$  in €/t<sub>CH<sub>3</sub>OH</sub> and specific carbon dioxide emission  $e_s$  in t<sub>CO<sub>2</sub></sub>/t<sub>CH<sub>3</sub>OH</sub> – are introduced. Both measures are influenced by the production process (in the form of equipment costs and energy demand) and by the resources used (in the form of energy-specific costs and energy-specific emissions). The raw material sources, costs and CO<sub>2</sub> emissions for energy supply are given in Tab. 4.1.

Tab. 4.1 shows that sources with lower specific CO<sub>2</sub> emissions tend to have higher specific costs. Only the use of nuclear energy features both low costs and low emissions. However, due to the political decision to phase out nuclear power plants by 2022 [125] this energy source is not a future option for Germany. It also does not take into account follow-up costs,

**Tab. 4.1** Comparison of different energy sources, their costs and associated CO<sub>2</sub> emissions.

Energy Source Unit	Costs ct/kWh	CO <sub>2</sub> -emission g/kWh	References
<i>Electrical energy</i>			
Lignite	3.3	1025	[126–128]
Bituminous coal	2.8	925	[126–128]
Natural gas	4.2	475	[126–128]
Biomass	9.6	100*	[126–128]
German power-mix	5.9**	535	[126, 127, 129]
Nuclear energy	3.5	10	[126–128]
Water	10.2	10.5	[126–128]
Photovoltaic	30	50	[126–128]
Wind (onshore)	10.1	11	[126–128]
Wind (offshore)	13.1	11	[126–128]
<i>Heat supply</i>			
Lignite	1.3	410	[126–128]
Bituminous coal	1.1	370	[126–128]
Natural gas	2.3	260	[126–128]
Biomass	5.3	55*	[126–128]
German power-mix	6.2**	565	[126, 127, 129]
Wind (onshore)	10.7	11.5	[126–128]
Wind (offshore)	13.8	11.5	[126–128]

\* CO<sub>2</sub>-consumption during biomass growth is not considered

\*\* Calculated for German power mix [125]

e.g. from final disposal, which would ultimately lead to increased costs for the use of nuclear energy.

For the analysis a production scenario with an annual production of 100,000 t<sub>CH<sub>3</sub>OH</sub>/a was defined and Tab. 4.2 lists all specifications and conditions. The costs of CO<sub>2</sub> emissions were set to 25 €/t<sub>CO<sub>2</sub></sub>, which is the current exchange-traded price of CO<sub>2</sub> for European emission allowances [130]. As a further restriction, no emission of carbon monoxide (CO) is desired because of its toxicity. Thus, all the CO generated by the total production is assumed to either be consumed or oxidized to CO<sub>2</sub>.

### 4.3.2 Formulation of the optimization problem

In the following the optimization problem based on the FluxMax formulation is derived. The generalized stoichiometric coefficients  $\chi_{(E_j)}^{(M_i)}$  and the specific energy constraints  $\varphi$  and  $\omega$  introduced in section 4.2 are used to formulate the linear equality constraints. The inequality constraints are derived from the direct heat integration approach and corresponding temperature constraints, introduced in section 3.2.3. The lower  $\varphi_{lb}$  and the upper bounds  $\varphi_{ub}$  correspond to the scenario (Tab. 4.2) and are specified in Tab. 4.3.

Tab. 4.2 Definition of scenario.

Parameter	Symbol	Unit	Value
<i>Operational conditions</i>			
Plant capacity	$\dot{N}_{\text{ext,out}}^{(\text{MCH}_3\text{OH,out})}$	t <sub>CH<sub>3</sub>OH/a</sub>	100,000
Safety constraint	$\dot{N}_{\text{ext,out}}^{(\text{MCO}_2,\text{out})}$	t <sub>CO/a</sub>	0
Reference temperature	$T_0$	K	298.15
Reference pressure	$p_0$	bar	1
<i>Efficiencies</i>			
Power generation	$\eta_{\text{ec}}$	-	0.35
Heat supply	$\eta_{\text{ht}}$	-	0.85
<i>Economics</i>			
Rate of interest	$z$	%	6
Payback time	$n_{\text{pb}}$	a	20
<i>Heat Exchange</i>			
Heat exchanger area costs	$c_{\text{HX}}$	€/m <sup>2</sup>	200
Heat transfer coefficient	$k^{\text{HX}}$	W/m <sup>2</sup> K	50
Minimum temperature difference	$\Delta T_{\text{min}}$	K	10
<i>Emissions</i>			
CO <sub>2</sub> -certificate price	$c_{\text{CO}_2}$	€/t <sub>CO<sub>2</sub></sub>	25

Tab. 4.3 Lower and upper bounds.

Description	Lower Bound	Upper Bound
Non-negativity conditions	$\mathbf{0} \leq (\dot{\mathbf{N}}, \dot{\mathbf{\Gamma}}, \dot{\mathbf{Q}}, \dot{\mathbf{W}})^{\top}$	
Minimum input mass fluxes	$\dot{N}_{\text{ext,in}}^{\text{min}} \leq \dot{N}_{\text{ext,in}}$	
Minimum output mass fluxes	$\dot{N}_{\text{ext,out}}^{\text{min}} \leq \dot{N}_{\text{ext,out}}$	
Maximum input mass fluxes		$\dot{N}_{\text{ext,in}} \leq \dot{N}_{\text{ext,in}}^{\text{max}}$
Maximum output mass fluxes		$\dot{N}_{\text{ext,out}} \leq \dot{N}_{\text{ext,out}}^{\text{max}}$



This analysis aims at the identification of the configuration with minimum costs for each combination of feedstock and energy source – heating/cooling and electricity. This is achieved by using an economic objective function, namely the *Total Annualized Cost* (TAC). Related to the payback period  $n_{pb}$  of the chemical production plant and the average interest rate  $z$  during this period, TAC measures the annual costs. The TAC is composed of costs for raw material purchase  $C_P$ , for heat supply  $C_{H,s}$ , heat removal  $C_{H,r}$ , power supply  $C_{E,s}$ , penalty costs for CO<sub>2</sub> emissions  $C_{CO_2}$ , heat transfer costs  $C_{HX}$ , and investment costs  $C_I$ .

$$\text{TAC} = C_P + C_{H,s} + C_{H,r} + C_{E,s} + C_{CO_2} + \frac{(C_{HX} + C_I)z}{1 - (z + 1)^{-n}} \quad (4.7)$$

TACs can be divided into operational and capital costs. In contrast to the operational costs, which are caused by the operation of the production process, the capital costs arise from the investment. The individual contributions of the objective function (Eq. (4.7)) are derived below. In particular, the linear model approach for estimating the capital costs is presented.

### Modeling the operational costs

The operational costs are variable costs and depend on the process conditions. In addition to the costs of the reactants, which are directly related to the consumption of raw materials, energy consumption also causes expenses. The following costs factors are introduced to weight the different costs contributions:

$$\text{purchase costs } c_\alpha^P \text{ of the raw materials } \alpha: \quad C_P = \sum_{\alpha \in \mathcal{A}} c_\alpha^P \cdot \dot{N}_{\text{ext,in}}^{(\alpha)} \quad (4.8)$$

$$\text{heat supply costs } c^{H,s}: \quad C_{H,s} = \sum_{E_j \in \mathcal{E}} c^{H,s} \cdot \dot{Q}_{(E_j)}^{\text{ext,in}} \quad (4.9)$$

$$\text{heat removal costs } c^{H,r}: \quad C_{H,r} = \sum_{E_j \in \mathcal{E}} c^{H,s} \cdot \dot{Q}_{(E_j)}^{\text{ext,out}} \quad (4.10)$$

$$\text{work supply costs } c^{E,s}: \quad C_{E,s} = \sum_{E_j \in \mathcal{E}} c^{H,s} \cdot \dot{W}_{(E_j)}^{\text{ext,in}} \quad (4.11)$$

### Modeling the investment costs

The investment costs  $C_I$  typically depend on the size of the production capacity. For costs estimation several correlations are available in the literature [131–133]. A correlation defined by Lange [134] between the energy losses of a chemical production plant and the corresponding investment costs is applied here [107]. This correlation is given in Eq. (4.12).

$$C_I^{\text{Lange}} = a (E_{\text{loss}})^b \quad (4.12)$$

According to Lange [134]  $a$  and  $b$  are regression parameters ( $a = 3.0$ ,  $b = 0.84$ ),  $E_{\text{loss}}$  [MW] is the energy loss and  $C_I$  [ $10^6$  USD] are the investment costs. The energy loss (Eq. (4.14)) is defined as the difference between the lower heating values  $\Delta h_{\text{u},\alpha}^{(\text{E}_j)}$  of the reactants including required energy input and the lower heating values of the products. This correlation allows a quite reliable estimation of the investment costs, especially if the process is far from being heat-neutral and has low energy losses [134]. Lange also emphasizes an almost linear dependence of investment costs on energy loss. This is also illustrated in Fig. C.1. Therefore the investment costs are linearized according to Eq. (4.13), whereby the linear fitting parameters  $p_1$  and  $p_2$  are determined by curve fitting for an estimated plant capacity as derived in the Appendix C.

$$c_1^{(\text{E}_j)} = p_1 E_{\text{loss}}^{(\text{E}_j)} + p_2 \quad \forall \text{E}_j \in \mathcal{E} \quad (4.13)$$

The energy loss  $E_{\text{loss}}^{(\text{E}_j)}$  of each EPN  $\text{E}_j$  is calculated as follows:

$$E_{\text{loss}}^{(\text{E}_j)} = \sum_{\alpha \in \mathcal{A}} \left( \text{sgn}(\nu_{\alpha}^{(\text{E}_j)}) \dot{N}_{(\text{E}_j)}^{(\alpha)} \Delta h_{\text{u},\alpha}^{(\text{E}_j)} + \dot{N}_{(\text{E}_j)}^{\text{fuel}} \Delta h_{\text{u},\text{fuel}}^{(\text{E}_j)} \right) \quad \forall \text{E}_j \in \mathcal{E} \quad (4.14)$$

The molar flow of the fuel is directly related to the required heat and power demand. Due to heat transfer losses and also losses due to energy conversion efficiency factors,  $\eta_{\text{ht}}$  and  $\eta_{\text{ec}}$  are introduced.

$$\dot{N}_{(\text{E}_j)}^{\text{fuel}} = \frac{\dot{Q}_{(\text{E}_j)}^{\text{fuel}}}{\Delta h_{\text{u},\text{fuel}}^{(\text{E}_j)}} \quad \forall \text{E}_j \in \mathcal{E} \quad (4.15)$$

$$\dot{Q}_{(\text{E}_j)}^{\text{fuel}} = \frac{1}{\eta_{\text{ht}}} \left( \dot{Q}_{(\text{E}_j)}^{\text{ext,in}} + \sum_{U_l \in \mathcal{U}} \dot{Q}_{(\text{E}_j)}^{(U_l)} + \sum_{E_i \in \mathcal{E}} \dot{Q}_{(\text{E}_j)}^{(E_i)} \right) + \frac{1}{\eta_{\text{ec}}} \dot{W}_{(\text{E}_j)}^{\text{ext,in}} \quad \forall \text{E}_j \in \mathcal{E} \quad (4.16)$$

Finally, the total investment costs  $C_I$  of the entire production network system are then estimated by summation of the single contributions of the individual EPN  $\text{E}_j$ :

$$C_I = \sum_{\text{E}_j \in \mathcal{E}} p_1 \sum_{\alpha \in \mathcal{A}} \text{sgn}(\nu_{\alpha}^{(\text{E}_j)}) \dot{N}_{(\text{E}_j)}^{(\alpha)} \Delta h_{\text{u},\alpha}^{(\text{E}_j)} + \sum_{\text{E}_j \in \mathcal{E}} p_1 \left( \frac{1}{\eta_{\text{ht}}} \left( \dot{Q}_{(\text{E}_j)}^{\text{ext,in}} + \sum_{U_l \in \mathcal{U}} \dot{Q}_{(\text{E}_j)}^{(U_l)} + \sum_{E_i \in \mathcal{E}} \dot{Q}_{(\text{E}_j)}^{(E_i)} \right) + \frac{1}{\eta_{\text{ec}}} \dot{W}_{(\text{E}_j)}^{\text{ext,in}} \right) + p_2 \quad (4.17)$$

### Modeling the internal heat transfer costs

It is assumed that the internal heat transfer costs depend linearly on the heat exchanger area  $A_{(\text{E}_j)}^{\text{HX}}$ .

$$C_{\text{HX}}^{(\text{E}_j)} = c_{\text{HX}} A_{(\text{E}_j)}^{\text{HX}} \quad (4.18)$$

Hereby  $C_{\text{HX}}^{(\text{E}_j)}$  denotes the total costs of the heat exchanger and  $c_{\text{HX}}$  the area-specific costs in €/m<sup>2</sup>. The heat exchanger area  $A_{(\text{E}_j)}^{\text{HX}}$  for each EPN  $\text{E}_j$  can be calculated using the internally transferred heat flows and the heat transfer coefficient  $k^{\text{HX}}$ :

$$A_{(\text{E}_j)}^{\text{HX}} = \frac{1}{k^{\text{HX}}} \left( \sum_{\text{E}_i \in \mathcal{E}} \frac{\dot{Q}_{(\text{E}_j)}^{(\text{E}_i)}}{\Delta T_{\text{m},(\text{E}_j)}^{(\text{E}_i)}} + \sum_{\text{U}_l \in \mathcal{U}} \frac{\dot{Q}_{(\text{E}_j)}^{(\text{U}_l)}}{\Delta T_{\text{m},(\text{E}_j)}^{(\text{U}_l)}} \right) \quad (4.19)$$

The logarithmic mean temperature difference  $\Delta T_{\text{m}}$  depends on the temperature differences at both ends of the heat exchanger  $\Delta T_1$  and  $\Delta T_2$ . For the calculation of temperature differences the heating (in case of heat receiving processes) or cooling down to the reference level (in case of heat releasing processes) is taken into account.

$$\Delta T_{\text{m}} = \frac{\Delta T_1 - \Delta T_2}{\ln \Delta T_1 - \ln \Delta T_2} \quad (4.20)$$

Using Eqs. (4.18) and (4.19) the costs of the heat exchanger area required to transfer the internal heat flows are calculated for each EPN  $\text{E}_j$ :

$$C_{\text{HX}}^{(\text{E}_j)} = \frac{c_{\text{HX}}}{k^{\text{HX}}} \left( \sum_{\text{E}_i \in \mathcal{E}} \frac{\dot{Q}_{(\text{E}_j)}^{(\text{E}_i)}}{\Delta T_{\text{m},(\text{E}_j)}^{(\text{E}_i)}} + \sum_{\text{U}_l \in \mathcal{U}} \frac{\dot{Q}_{(\text{E}_j)}^{(\text{U}_l)}}{\Delta T_{\text{m},(\text{E}_j)}^{(\text{U}_l)}} \right) \quad \forall \text{E}_j \in \mathcal{E} \quad (4.21)$$

Finally, the total heat transfer costs are calculated by adding up the heat exchanger areas of all elementary processes  $\text{E}_j$ :

$$C_{\text{HX}} = \sum_{\text{E}_j \in \mathcal{E}} \frac{c_{\text{HX}}}{k^{\text{HX}}} \left( \sum_{\text{E}_i \in \mathcal{E}} \frac{\dot{Q}_{(\text{E}_j)}^{(\text{E}_i)}}{\Delta T_{\text{m},(\text{E}_j)}^{(\text{E}_i)}} + \sum_{\text{U}_l \in \mathcal{U}} \frac{\dot{Q}_{(\text{E}_j)}^{(\text{U}_l)}}{\Delta T_{\text{m},(\text{E}_j)}^{(\text{U}_l)}} \right) \quad (4.22)$$

### Modeling the penalty term for CO<sub>2</sub> emissions

In addition to the capital and operational costs introduced above, costs caused by the CO<sub>2</sub> emissions  $E_{\text{CO}_2}$  must also be included in the costs estimation. They can be associated with

CO<sub>2</sub> certificate costs for carbon dioxide emissions. It is intended to limit emissions through the mandatory purchase of CO<sub>2</sub> allowances, the price of which is subject to a political decision. The emission itself is composed on the one hand directly of the stoichiometrically co-produced carbon dioxide from the production network  $\dot{N}_{\text{ext,out}}^{(\text{MCO}_2)}$  and on the other hand of the CO<sub>2</sub>-emissions caused by the energy consumption, which in turn is influenced by the process configuration and also by the energetic efficiencies of the process: the lower the efficiency, the more energy is required. If the energy demand cannot be met internally, the external source causes the energy specific carbon dioxide emission  $e_{\text{CO}_2}$ . Therefore, a combination of political penalty, identification of a suitable and sustainable source and finally improvement of the technology influences the costs caused by the CO<sub>2</sub>-emissions.

$$E_{\text{CO}_2} = e_{\text{CO}_2, \dot{Q}} \cdot \sum_{U_i \in \mathcal{U}} \dot{Q}_{(U_i)}^{\text{ext,in}} + e_{\text{CO}_2, \dot{W}} \cdot \sum_{E_j \in \mathcal{E}} \dot{W}_{(E_j)}^{\text{ext,in}} + \dot{N}_{\text{ext,out}}^{(\text{MCO}_2)} \quad (4.23)$$

Eq. (4.23) considers both the direct emission  $\dot{N}_{\text{ext,out}}^{(\text{MCO}_2)}$  and the indirect emissions caused by the energy supply  $(\dot{Q}_{(U_i)}^{\text{ext,in}}, \dot{W}_{(E_j)}^{\text{ext,in}})$  of all elementary processes  $E_j$ . By multiplying the process-related carbon dioxide emissions with a price  $c_{\text{CO}_2}$  for CO<sub>2</sub> – which is assumed here as the certificate price – the penalty costs caused by CO<sub>2</sub> emissions are determined:

$$C_{\text{CO}_2} = c_{\text{CO}_2} E_{\text{CO}_2} \quad (4.24)$$

## 4.4 Results

For the methanol production network, a systematic evaluation of the different raw material sources as well as the different energy sources is carried out using the FluxMax approach. The different possible sources for both raw material and energy are shown in Tab. 4.1. Fossil based energy sources such as coal and natural gas as well as renewable energy sources such as biomass, wind and photovoltaic are considered. In addition, the current German electricity mix and nuclear energy are analyzed for the transition period. For the carbon raw material, fossil and renewable sources are considered, i.e. lignite and bituminous raw materials, natural gas, biomass and CO<sub>2</sub>. The CO<sub>2</sub> source is not further specified in the following analysis, but it is assumed that CO<sub>2</sub> is purchased for the price of the CO<sub>2</sub> certificate given in Tab. 4.2.

The first measure – specific methanol production costs – is determined directly by solving the linear program and dividing the TAC of the optimal process configuration by the methanol product flow. For also evaluating the second measure – specific carbon dioxide emission – Eq. (4.23) is divided by the methanol product flow to calculate the specific CO<sub>2</sub> emissions  $e_{\text{CO}_2}$  of the entire production process.

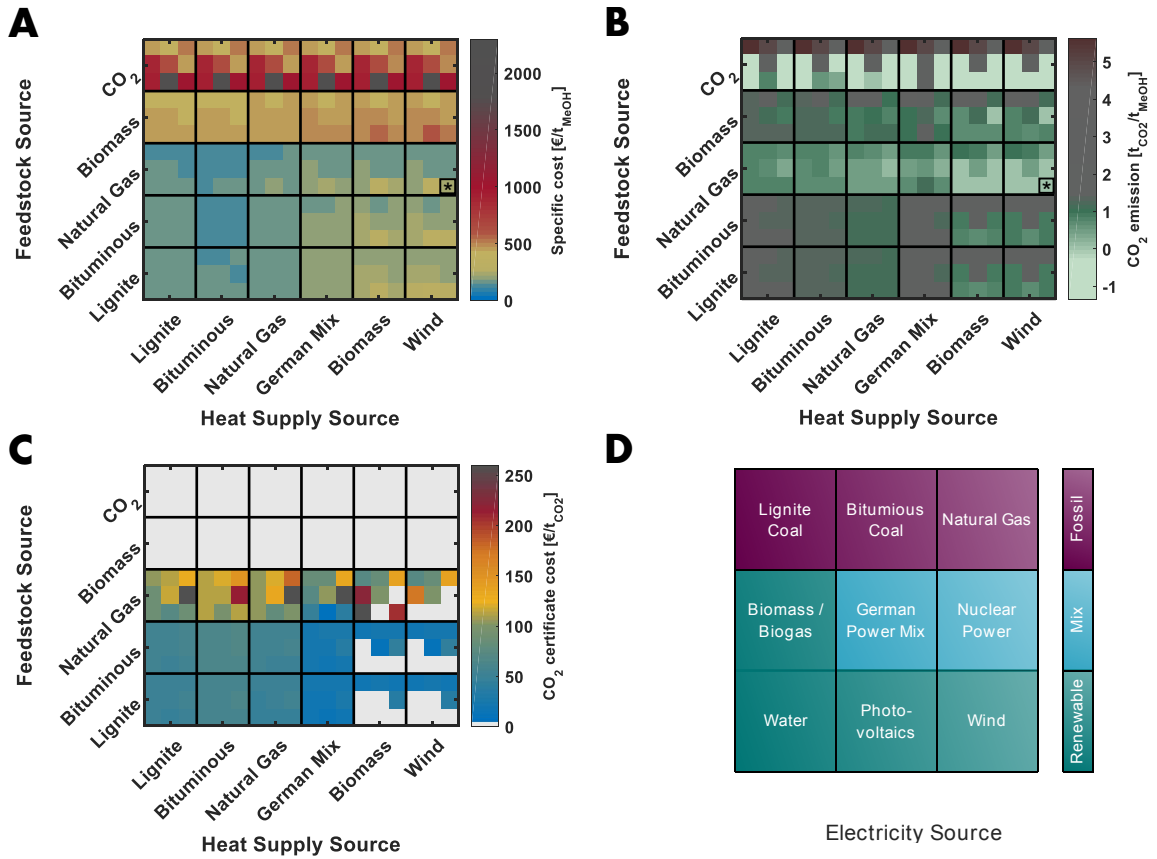


**Fig. 4.3** Systematically evaluation of the influence of different sources for feedstock, heat and power supply on the specific production costs (A) and on the specific CO<sub>2</sub> emissions (B); evaluation of required CO<sub>2</sub> certificate costs to support low emission processes (C); order of clustered power sources (D); element of reference configuration for further analysis marked with \*.

#### 4.4.1 Evaluation of different feedstock and energy sources

First, the dependence of the measures – specific methanol production costs  $c_s$  and specific CO<sub>2</sub> emissions  $e_s$  – on the different feedstock and energy sources is investigated. Therefore, the cost-optimal configuration is systematically determined for each combination of feedstock, heat and power source as listed in Tab. 4.1. The results of  $c_s$  and  $e_s$  depending on the sources of feedstock and energy are shown in Fig. 4.3. The nine different energy sources can be roughly classified into three categories: fossil (coal and natural gas), renewable (biomass, hydro, photovoltaic, and wind), and a mix category characterizing the transition period (German electricity mix and nuclear energy). The specific costs (Fig. 4.3 A) and specific emissions (Fig. 4.3 B) as a function of feedstock and energy source are shown in a mosaic pattern plot. The different raw material sources, shown on the vertical axis, and heat sources, shown on the horizontal axis, form the frame of the mosaic. Within the frames, the nine possible power sources are grouped together in a 3×3 mosaic pattern, with each element

corresponding to one of the nine power sources under consideration. The order of the different current sources in the mosaic pattern is shown in Fig. 4.3 D.

The specific CO<sub>2</sub> emissions vary in a range from about  $-1.3$  to  $5.7$   $t_{\text{CO}_2}/t_{\text{CH}_3\text{OH}}$ , where a negative value means that more CO<sub>2</sub> is consumed in the production process than is emitted, which is possible if CO<sub>2</sub> is used as raw material. However, then the specific costs are above  $934$  €/t<sub>CH<sub>3</sub>OH</sub>, while for the other sources of raw materials considered only costs between  $121$  and  $538$  €/t<sub>CH<sub>3</sub>OH</sub> were observed, which is in good agreement with other published results [135].

Neglecting first CO<sub>2</sub> as a feedstock, one can observe that the specific costs of fossil feedstocks are only 25 – 40 % of the costs of biomass as a feedstock. It is also found that the use of coal – lignite or bituminous – results in slightly higher specific costs than natural gas. Similar observations can be made for the different heat and power sources. The switch from fossil sources to renewable energy sources leads to higher specific costs. However, a stronger impact on costs was found for the heat source than for the electricity source. This is due to the fact that for the methanol production network – with the exception of CO<sub>2</sub> as raw material – classical petrochemical processes are preferable, which leads to a higher heat demand than electricity demand. In terms of specific CO<sub>2</sub> emissions, the processes using coal either as raw material or as energy source have the highest emissions, but these can be drastically reduced by using renewable energy sources. However, this is not the case for biomass, as it produces higher emissions than fossil natural gas. This is due to the fact that the anaerobic digestion of biomass to biogas produces the coupled by-product CO<sub>2</sub>, which is emitted when no further use is realised. In this context it is important to note that in other studies [128, 10] the coupled CO<sub>2</sub> production in a biogas plant is often not considered negatively, because CO<sub>2</sub> is consumed during the growth of the biomass. This assumption of climate neutrality would result in drastically lower carbon footprints of biomass processes.

The challenges of a further use of the produced CO<sub>2</sub> become evident when looking at the results in Fig. 4.3 for CO<sub>2</sub> as raw material. A large amount of energy is required because CO<sub>2</sub> has to be chemically activated to convert it to methanol. This leads to high costs and also the specific CO<sub>2</sub> emissions depend strongly on the energy source. It is shown that on the one hand the lowest emissions or even a net consumption of CO<sub>2</sub> can be achieved if renewable sources are used for energy supply. On the other hand, however, the highest emissions are observed when the required energy is provided by fossil sources. Therefore it is important to emphasize that only the use of renewable energy sources leads to a net consumption of CO<sub>2</sub>. This also means that the often discussed electrification of chemical processes [136] only makes sense if sufficient renewable energy is available. In particular, the current German electricity mix as an energy source would lead to net carbon emissions, although CO<sub>2</sub> is consumed as

feedstock. In this case the indirect emissions caused by the energy demand are higher than the direct CO<sub>2</sub> consumption.

In view of the results of this analysis, it can be stated that natural gas is advantageous both as a raw material and as an energy source. The specific emissions are in a range of 0.02  $t_{\text{CO}_2}/t_{\text{CH}_3\text{OH}}$  when wind is considered as an energy source and 0.73  $t_{\text{CO}_2}/t_{\text{CH}_3\text{OH}}$  when the required power is based on coal. Only the use of CO<sub>2</sub> as a raw material results in lower emissions. Natural gas also performs well in terms of specific costs. The lowest achievable costs of 121 €/t<sub>CH<sub>3</sub>OH</sub> are attained by using natural gas as raw material. The highest costs for natural gas of 331 €/t<sub>CH<sub>3</sub>OH</sub> are even lower than the best results for biomass as feedstock.

It was found that methanol production for natural gas as a raw material source can achieve almost zero carbon dioxide emissions if the energy demand is covered by renewable energies. For further investigations, the configuration with natural gas as raw material source and wind as heat and power supply was chosen as reference case. This configuration is marked with an asterisk (\*) in Fig. 4.3 and shows specific costs of 266 €/t<sub>CH<sub>3</sub>OH</sub> and specific CO<sub>2</sub> emissions of 0.02  $t_{\text{CO}_2}/t_{\text{CH}_3\text{OH}}$ . In Fig. 4.3 C the theoretical prices of CO<sub>2</sub> certificates are analyzed, which are necessary to make the reference configuration cost-optimal. A resulting certificate price of zero means that either the corresponding configuration has a lower emission than the reference configuration (e.g. for some CO<sub>2</sub> processes with a net consumption of CO<sub>2</sub>) or the configuration cannot become cost-optimal independently of the certificate price. This is the case for configurations with biomass-fed processes, which are more expensive, although the specific emissions are higher than in the reference case.

Even though the certificate price rose significantly in recent years [130], it becomes clear that the current certificate price level of about 25 €/t<sub>CO<sub>2</sub></sub> is still not sufficient to promote renewable energies. From the analysis, prices in the order of about 50 – 150 €/t<sub>CO<sub>2</sub></sub> result to achieve comparable specific production costs for fossil- and renewable-based production. This is in line with other studies that also estimate the need for CO<sub>2</sub> certificate prices in the range of 50 – 110 €/t<sub>CO<sub>2</sub></sub> by 2050 to meet the climate targets [137].

Not only the information on costs and emissions obtained in the previous analyses is crucial, but also the structure of the production network. Structural information is provided directly by the FluxMax approach, since all mass and energy flows are decision variables of the LP. In this way, the optimal flow distribution of all internal and external flows is determined. Each element in Fig. 4.3 corresponds to a particular process configuration. These configurations differ in the sources for raw material and energy supply or in the overall process structure and the processes involved. In Fig. 4.4, for each type of raw material source (coal, natural gas, biomass and CO<sub>2</sub>) the configuration with the lowest specific production costs (left column, bluish background) and additionally the cost-optimal configuration which simultaneously shows the lowest CO<sub>2</sub> emission (right column, greenish background) is shown. Since the

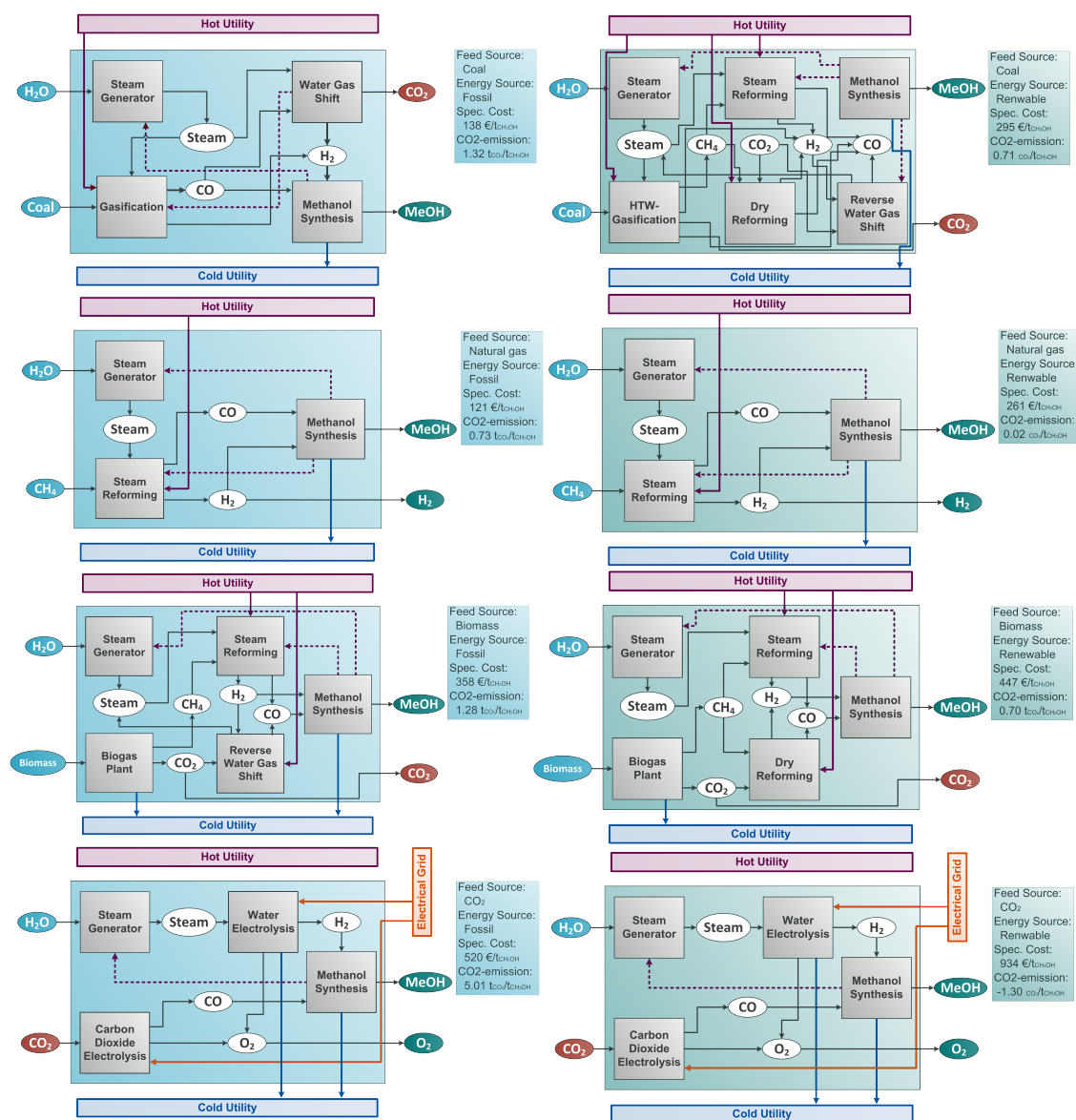


**Fig. 4.4** Schematic illustration of optimal process configurations for the different feedstock sources coal (1st row), natural gas (2nd row), biomass (3rd row) and CO<sub>2</sub> (4th row); depicted are the overall costs-optimal configurations with blue background (left column) and the renewable energy-based configurations with lowest specific CO<sub>2</sub> emission with green background (right column).



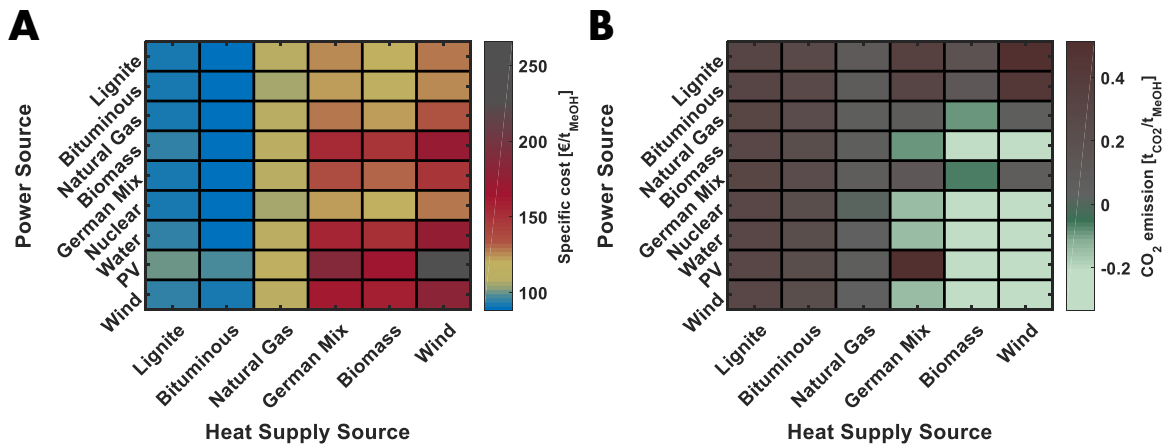


**Fig. 4.5** Evaluation of the influence of energy supply sources on the specific costs (left) and on the CO<sub>2</sub> emissions (right).

process structures are the same for configurations with lignite or bituminous feedstock, no distinction is made in the following according to the type of coal.

As can also be seen from the mosaic plots (Fig. 4.3), coal and biomass processes have direct CO<sub>2</sub> emissions, which is mainly the reason for the high specific emissions. One process – the methanol synthesis process – is present in each optimized process configuration and will be examined in more detail in the following chapters. At least one other process is required for the conversion of the feedstock, depending on the source of the raw material. In the case of coal it is coal gasification, in the case of natural gas it is a reforming process and for biomass it is anaerobic digestion to form methane. Considering CO<sub>2</sub> as feedstock, electrochemical electrolysis processes appear to provide CO and H<sub>2</sub> from CO<sub>2</sub> or H<sub>2</sub>O. For the electrochemical processes, the electrical grid is shown as the power supply in addition to the heating utilities. But electrical energy is also required for the other processes, e.g. for adjusting the pressure levels. In these cases the electricity demand is rather low compared to the heating/cooling demand and therefore not shown in Fig. 4.4.

#### 4.4.2 Analysis of combined feedstock sources

So far, the different sources of raw materials were analyzed individually. In addition, in the following the impact of the different sources of energy on both measures is examined in case all sources of raw materials are available at the same time. Fig. 4.5 shows the specific costs (Fig. 4.5 A) as well as the specific emissions (Fig. 4.5 B) depending on the heat source (horizontal axis) and the energy source (vertical axis).

As expected, the inverse relationship between costs and emissions can be observed. The specific costs are in a range of about 106 to 277 €/t<sub>CH<sub>3</sub>OH</sub> and thus significantly lower compared to the single feedstock analysis. An even greater difference is seen in the specific emissions,

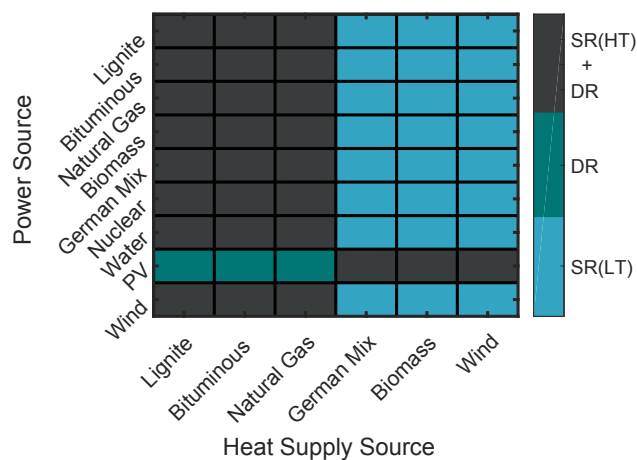


**Fig. 4.6** Analysis of the reforming processes for the conversion of methane into synthesis gas for each combination of heat and power source.

which lie between  $-0.34$  and  $0.67 \text{ t}_{\text{CO}_2}/\text{t}_{\text{CH}_3\text{OH}}$ . The lowest  $\text{CO}_2$  emissions were achieved when renewable sources such as wind and biomass are used for heating. However, in these cases the specific costs are high. Also the use of the current German electricity mix as a heat source by electric heating leads to low emissions if an electricity source with low emissions is used at the same time, which is unexpected when considering Tab. 4.1. To investigate the reason, an analysis of the optimal reforming processes for the conversion of methane to synthesis gas was carried out. Fig. 4.6 shows the optimal reforming processes for each combination of heat and power source. It can be seen that three different combinations of reforming processes are obtained ((A) a combination of high temperature steam reforming (SR(HT) and dry reforming (DR), (B) dry reforming, (C) low temperature steam reforming). With the exception of the use of electricity from photovoltaics, the power source has no influence on the choice of the reforming process. In general, the configuration (A) is optimal for fossil-based heat supply sources, while renewable sources and also the German electricity mix favor the low temperature steam reforming process. The corresponding process structures are shown in Fig. 4.7. For all combinations of heat and power sources a simultaneous use of natural gas and  $\text{CO}_2$  as raw material source is optimal. For fossil heat sources the classical high-temperature steam reforming process is used to convert methane into synthesis gas. At high temperatures, the endothermic steam reforming process is favoured according to Le Chatelier's principle. Consequently, the performance of the low-temperature steam reforming process is worse compared to the classical process, which leads to a higher energy demand for the subsequent separation. However, more available internal heat provided by the methanol synthesis can be transferred internally as the heat for the low temperature process ( $450 \text{ }^\circ\text{C}$ ) is required at a lower temperature level compared to the high temperature process ( $> 900 \text{ }^\circ\text{C}$ ). Therefore, the low-temperature steam reforming process is preferred for heat supply based

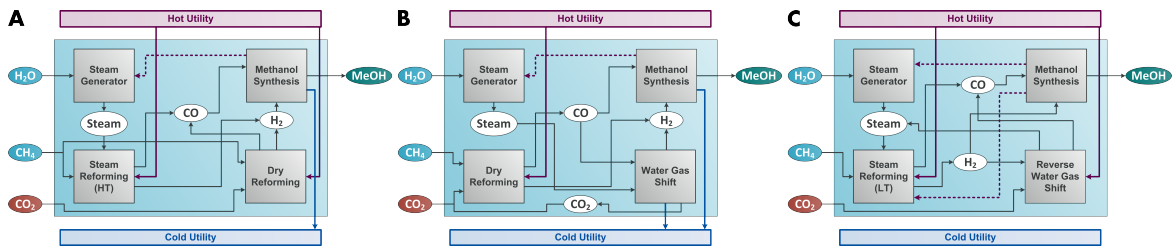


**Fig. 4.7** Flowsheets of the optimal process configuration for the methanol synthesis using methane and carbon dioxide as feedstock sources depending on different reforming processes; (A) combination of high temperature steam reforming and dry reforming; (B) dry reforming and water gas shift; (C) low temperature steam reforming and reverse water gas shift.

on renewable resources, since the additional costs for the increased electricity demand is lower than the reduction of external heat supply costs. Only for process configurations using electricity from photovoltaics, a shift to a more electrified process is not optimal due to the high price of electricity from photovoltaics, as shown in Tab. 4.1.

Analysis of the three different possible process configurations, as illustrated in Fig. 4.7, shows that 25 % of the carbon atoms in the final methanol molecule are provided by CO<sub>2</sub>. The chemical activation of CO<sub>2</sub> to convert it into other products requires a high amount of energy. Therefore a second high-energy reactant is needed to provide some of the energy. The second reactant is either methane, which together with CO<sub>2</sub> is converted to synthesis gas in a dry reforming process, or together with hydrogen in a reverse water gas shift process. The low-temperature steam reforming process (Fig. 4.6 C) becomes optimal only if the costs of heat supply are significantly higher than the costs of electricity. It can be seen that in the case of a heat supply from renewable sources, which causes high heat supply costs, no cooling utility is required, since all available heat from the methanol process is transferred internally. In the case of a fossil-based heat supply, the available heat from the methanol synthesis process is partially released to the environment, as the costs for the internal heat transfer become more expensive at low temperatures than the external heat supply.

Looking at the results for methane as the only feedstock source (Fig. 4.4), it becomes clear why the combined use of methane and CO<sub>2</sub> as feedstock source is advantageous. Hydrogen was formed in excess, resulting in an additional outlet stream and is therefore available for the conversion of synthesis gas when CO<sub>2</sub> is present as a second reactant.

While the analysis was performed at a price of CO<sub>2</sub> of 25 €/t<sub>CO<sub>2</sub></sub> it can be shown that the simultaneous use of natural gas and carbon dioxide as feedstock is also optimal for certificate prices up to 40 €/t<sub>CO<sub>2</sub></sub>. However, it is important to note that this study assumes that CO<sub>2</sub> has to be purchased as a raw material for the certificate price, which makes it an expensive feedstock with rising certificate prices. Nevertheless, the combined use of natural gas and

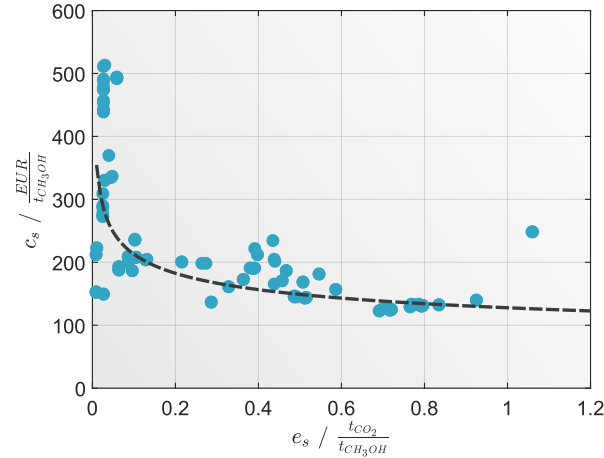


**Fig. 4.8** Pareto optimal curve of multiobjective optimization problem using natural gas as feedstock source and each combination of heat and power source for methanol synthesis.

CO<sub>2</sub> is a promising option, especially in the transition period from fossil resources to a production only from renewables.

#### 4.4.3 Multi-objective optimization

In the results obtained, the inverse relationship between costs and emissions can be observed. In most cases, methanol-specific production costs increase with decreasing specific carbon dioxide emissions or vice versa. Therefore, a tradeoff between specific costs (Eq. (4.7)) and specific CO<sub>2</sub>-emissions (Eq. (4.23)) is necessary. Mathematically speaking, this leads to a multi-criteria optimization problem. By introducing the factor  $w \in [0, 1]$ , which weights the two competing objectives, a multi-objective function can be formulated.

$$f(\varphi) = w\text{TAC} + (1 - w) c_{\text{CO}_2} E_{\text{CO}_2} \quad (4.25)$$

Considering the results already presented, it is evident that natural gas as a raw material source already represents a reasonable compromise between costs and emissions. Therefore, for natural gas as feedstock, the FluxMax approach was solved with respect to the multi-objective function Eq. (4.25) for each combination of heat and power sources and weighting factors between 0 and 1. The resulting Pareto plot of the multi-objective optimization problem is shown in Fig. 4.8.

The specific CO<sub>2</sub> emission  $e_s$  is shown on the horizontal axis and the specific costs  $c_s$  on the vertical axis. Each cyan dot in Fig. 4.8 corresponds to an optimal process configuration obtained by solving the multi-objective linear program. The black dashed curve is obtained by curve fitting and identifies the approximation of the Pareto optimum curve. Each point along

the Pareto curve represents the optimal compromise between the two objectives. Although the data points are scattered, there is a clear trend of increasing specific costs for decreasing specific emissions. Especially for very low emissions, which are smaller than  $0.05 \text{ t}_{\text{CO}_2}/\text{t}_{\text{CH}_3\text{OH}}$ , the costs increase dramatically. However, in the range between 0.05 and  $1 \text{ t}_{\text{CO}_2}/\text{t}_{\text{CH}_3\text{OH}}$  the slope of the curve is quite flat. This means that, if natural gas is used as a raw material, there is a high reduction potential of  $\text{CO}_2$  emissions at a comparatively small costs increase. Such a costs increase could easily be compensated by a political decision to increase the price of  $\text{CO}_2$  certificates.

## 4.5 Chapter summary

In order to manage the transition successfully towards a more sustainable production system for chemicals, industry will need not only to utilize renewable feedstocks and energy, but also to increase the energy efficiency of existing fossil-based technologies. For a fair assessment of the economic and ecological impacts, a systematic comparison of all combinations of feedstock and energy sources as well as process technologies is necessary. Due to the multitude of alternative raw materials and process technologies, there are many different potential pathways to converting renewables into valuable target products.

For the target product methanol, the specific costs and specific  $\text{CO}_2$  emissions of a multitude of fossil and renewable-based feedstocks as well as energy sources were systematically evaluated. The economic objective function contains the Total Annualized Costs (TAC) and penalty terms for direct and indirect  $\text{CO}_2$  emissions. In this way, the FluxMax approach identified the cost-optimal process structure and the associated  $\text{CO}_2$  emissions for each combination of feedstock and energy source considered. A net consumption of  $\text{CO}_2$  by the overall production system is possible if renewable energy sources are exploited and  $\text{CO}_2$  is used as a feedstock source at the same time. If fossil energy sources are used, a significant carbon footprint is unavoidable due to the high indirect  $\text{CO}_2$  emissions from the energy supply (electricity, heat). Thus, not only the economic challenge of using  $\text{CO}_2$  as a raw material, but also the ecological impact depends strongly on the energy source used.

Addressing the second research question (II), it was shown that using natural gas as a feedstock source leads to a very good trade-off between production costs and emissions, especially if the required energy comes from renewable sources. A multi-objective optimization of the two competing objectives – costs and emissions – for natural gas-fed processes resulted in a Pareto plot. It becomes obvious that it is possible to significantly reduce the  $\text{CO}_2$  emissions while costs increase only slightly. Only if almost emission-free configurations are desired the costs rise drastically. Therefore, the theoretical price of  $\text{CO}_2$  certificates were further analyzed, which would be required to make almost emission-free configurations cost-optimal. Depending on the energy source used, certificate prices in the range of 50 to  $150 \text{ €/t}_{\text{CO}_2}$

(current price: 25 €/t<sub>CO<sub>2</sub></sub>) were calculated. The third research question (III) was also addressed in this chapter. It must be noted that from an economic point of view, the chemical industry cannot become a carbon sink under the current costs scenarios. The only way to achieve net consumption is to use CO<sub>2</sub> as raw material, which leads to high costs caused by the tremendous energy demand.

The case study presented, showed the main advantage of the FluxMax approach, that is its ability to quickly determine an optimal process system within a superstructure wherein many alternative process configurations are embedded. The main outcome is the fact that a net consumption of CO<sub>2</sub>, and thus a real reduction of atmospheric CO<sub>2</sub>, is only possible if the energy is provided entirely by renewable energies. However, this results not only in high economic challenges due to high electricity prices, but also in the reliability of production systems at a low technological readiness level. An economically viable alternative to drastically reduce CO<sub>2</sub>-emissions in the transition period is a combination of fossil-based natural gas and CO<sub>2</sub>-fed process with simultaneous use of renewable energy supply.

On the production system level, however, only the interactions between entire chemical plants can be analyzed and optimized due to the black box assumption. Consequently, it is necessary to break down the entire process box into subunits such as reactors, separators and auxiliary units in order to determine the optimal process design. This is the goal of the next chapter – the application of the FluxMax approach to the plant level – where the methanol synthesis process is further analyzed and designed in more detail.

# Chapter 5

## Plant level

The plant level is characterized by a more detailed consideration of the chemical conversion process compared to the production system level. Therefore, unit operations, such as reaction, separation, and mixing, that are associated with a chemical process are considered explicitly, as illustrated in Fig. 5.1. This enables detailed process design tasks addressing the fourth key research question (IV): What is the most energy-efficient process flowsheet for converting raw materials into the desired product while making optimal use of synergies between individual process units? Smart heat integration strategies are crucial to identify highly energy-efficient processes. Of particular importance is the simultaneous consideration of heat integration during the actual process design task.

In the context of this dissertation, the FluxMax approach was applied at the plant level to diverse case studies [138, 139]. The application to the methanol synthesis process [139] constitutes the basis of this chapter.

### 5.1 Literature review

In this section an overview is given on process design methodologies and case studies applied at the plant level. A sharp distinction between methodologies applicable to the production system level and the plant level is often hardly possible, and some of the literature presented in the review chapter of the production system level may also be applicable to the plant level. In order to avoid an unnecessary overlap, in the following the focus is on heat integration and the way the heat integration potential is considered during the design task.

While in many bio-based applications, heat integration is often not of key interest, as the temperatures are too low [119, 81, 95], in most publications, heat integration and corresponding energy reduction potentials are in the main focus. In general, there are

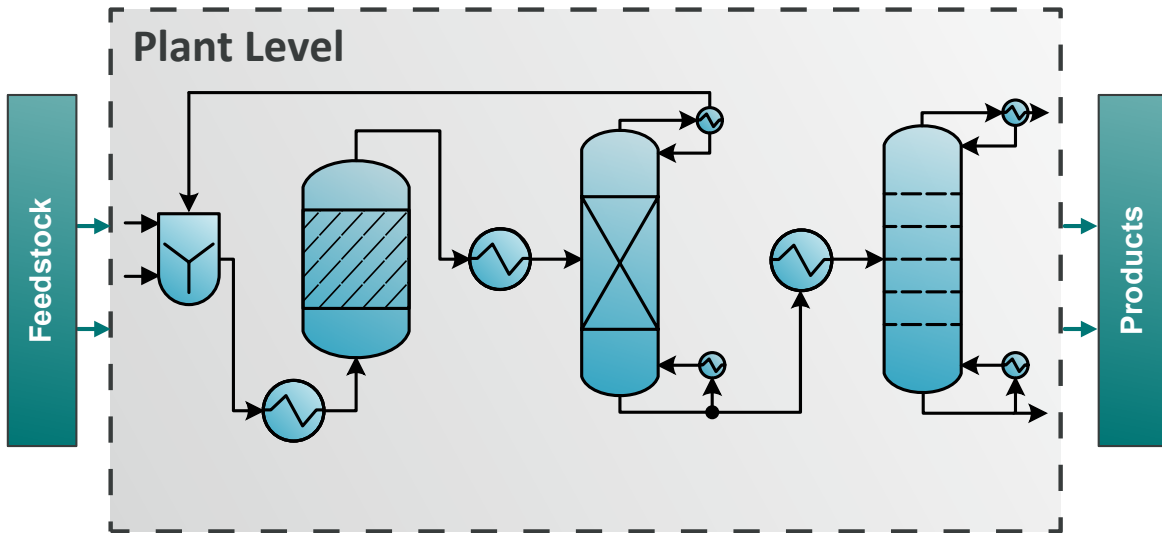


**Fig. 5.1** Schematic illustration of the process design task at the plant level.

two different approaches to consider heat integration within optimization based design methodologies: in a sequential procedure, or in an simultaneous procedure. In case of the sequential approach the flow optimization is solved first and subsequently a pinch-based analysis is performed to evaluate the heat integration potential [98, 83, 99]. Ulonska et al. [83] extended the RNFA concept introduced by Voll and Marquardt [81] to the process level (PNFA) by using reactor and separator shortcut models to estimate the total energy demand and to evaluate biorefinery process pathways. The heat integration potential of the optimal solution was taken into account by conducting a pinch analysis subsequently. As an outcome, they identified ethanol and iso-butanol as optimal bio-based fuels. The study of the entire biomass supply chain showed that co-production of ethanol and iso-butanol could increase the expected profit [140]. The PNFA was also used to compare bio-based fuel production pathways with e-fuels using hydrogen generated by electrical energy. One outcome was the lower global warming potential but higher costs of e-fuels compared to bio-based production pathways [77]. The advantage of a sequential procedure is that the complexity of the optimization is usually decreased because no additional constraints have to be considered to account for the heat integration. However, the sequential procedure does not ensure the identification of energy-optimal processes [100].

To guarantee the identification of the optimal process configuration a simultaneous procedure has to be followed, in which the heat integration is part of the flow optimization problem [141, 142, 100]. The idea of the model proposed by Duran and Grossmann [100] is to consider all feasible and non-feasible pinch combinations within the optimization problem and to identify the feasible pinch by maximization of the total utility requirements. As the number of additional constraints grows rapidly for complex systems, which makes the solution of



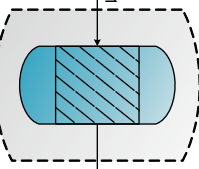
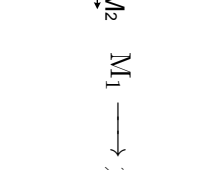
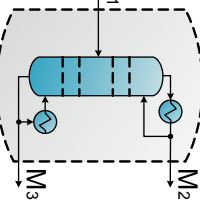
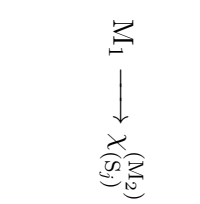
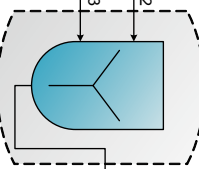
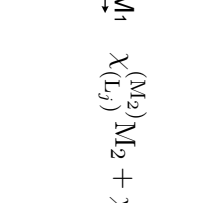
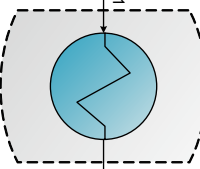
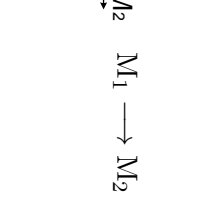
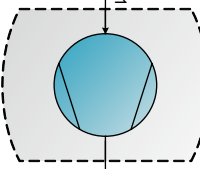
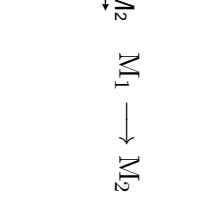
the MINLP problem increasingly difficult to solve, the model was further developed, e.g. by splitting the heat flows into dedicated zones, in which heat integration is allowed [143–145, 84]. The increasing complexity is also the limiting factor in the p-graph approach of Friedler et al. [93]. They ended up with over 10,000 possible heat exchangers in their MILP formulation of a relative simple superstructure of a single reactor and three separation stages [146]. The infinitely dimensional state space (IDEAS) framework, which was first proposed by Wilson and Manousiouthakis [96], might help to overcome the challenges of a large complexity, as they iteratively solve a linear program. In this way, the global optimum is approximated by increasing the dimension at each iteration. Later, heat integration was also included in their studies [147, 102]. The pre-selection of possible heat transferring streams, however, need to be done a-priori.

In recent years the possibility of so-called Organic Rankine Cycles (ORC) has aroused interest because they enable the utilization of low temperature heat fluxes to generate electrical energy [148–150]. Yu et al. [148] developed a techno-economic optimization approach under simultaneous consideration of heat integration for multiple waste heat streams. The NLP approach was illustrated with a refinery process and the sensitivity of the solution to the parameters, electricity price and utility cost, was discussed. To identify optimal ORC structures, Kermani et al. [150] introduced a bi-level optimization methodology, which includes architectural features such as turbine-bleeding, re-heating, and transcritical cycles. In the first level, the working fluid and operation conditions are optimized by applying a genetic algorithm, while in the second level the deterministic MILP model determines the optimal architecture and equipment size.

## 5.2 Application of FluxMax approach to the plant level

In contrast to the production system level, at the plant level not only pure substances, but also mixtures of chemical compounds are considered. Those mixtures originate either from the mixing of pure compounds or from chemical transitions, e.g. thermodynamic limitations of the reaction. Consequently, the mixtures may not only differ in the composition but also in the energetic state – different temperatures or pressures. According to the FluxMax approach, the mixtures are represented as thermodynamic substance nodes of a distinct thermodynamic state  $(\mathbf{x}, T, p)$ . Elementary processes are used to describe a particular path in the thermodynamic state space associated with a particular chemical transition. For each elementary process a distinct elementary process node  $E_j$  is introduced which is described by a stoichiometric equation characterized by stoichiometric coefficients  $\chi_{(E_j)}^{(M_i)}$  as well as specific energy demands for heat ( $\varphi$ ) and power ( $\omega$ ). At the plant level, the elementary processes correspond to unit operations, such as reaction, separation, mixing, heating, or compression. Tab. 5.1 gives an overview about the unit operations, used in the case study here. For each

**Tab. 5.1** Overview of generalized stoichiometric equations and corresponding unit operations of elementary processes considered in this case study.

EPPN	Stoichiometry	Unit operation	TSNs
	$M_1 \longrightarrow \chi_{(R_j)}^{(M_2)} M_2$	isobaric reaction	$M_1(\mathbf{x}_1, T_1, p_1), M_2(\mathbf{x}_2, T_2, p_1)$
	isothermal reaction	$M_1(\mathbf{x}_1, T_1, p_1), M_2(\mathbf{x}_2, T_1, p_2)$	
	$M_1 \longrightarrow \chi_{(S_j)}^{(M_2)} M_2 + \chi_{(S_j)}^{(M_3)} M_3$	isobaric separation	$M_1(\mathbf{x}_1, T_1, p_1), M_2(\mathbf{x}_2, T_2, p_1), M_3(\mathbf{x}_3, T_3, p_1)$
	isothermal separation	$M_1(\mathbf{x}_1, T_1, p_1), M_2(\mathbf{x}_2, T_1, p_2), M_3(\mathbf{x}_3, T_1, p_3)$	
	$\chi_{(L_j)}^{(M_2)} M_2 + \chi_{(L_j)}^{(M_3)} M_3 \longrightarrow M_1$	isobaric mixing	$M_1(\mathbf{x}_1, T_1, p_1), M_2(\mathbf{x}_2, T_2, p_1), M_3(\mathbf{x}_3, T_3, p_1)$
	isothermal mixing	$M_1(\mathbf{x}_1, T_1, p_1), M_2(\mathbf{x}_2, T_1, p_2), M_3(\mathbf{x}_3, T_1, p_3)$	
	$M_1 \longrightarrow M_2$	isobaric heating	$M_1(\mathbf{x}_1, T_1, p_1), M_2(\mathbf{x}_1, T_2, p_1)$
	isobaric cooling	$M_1(\mathbf{x}_1, T_1, p_1), M_2(\mathbf{x}_1, T_2, p_1)$	
	$M_1 \longrightarrow M_2$	isothermal compression	$M_1(\mathbf{x}_1, T_1, p_1), M_2(\mathbf{x}_1, T_1, p_2)$
	isenthalpic expansion	$M_1(\mathbf{x}_1, T_1, p_1), M_2(\mathbf{x}_1, T_1, p_2)$	

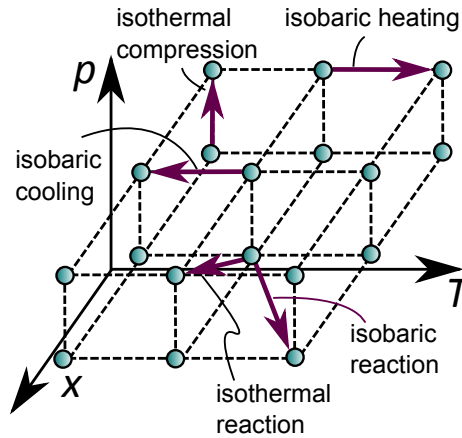


**Fig. 5.2** Schematic illustration of selected EPNs in the discretized thermodynamic state space.

type of EPN, a distinct stoichiometric equation – and thus stoichiometric coefficients  $\chi_{(E_j)}^{(M_i)}$  – is formulated.

Besides information on the stoichiometry, Tab. 5.1 denotes also the thermodynamic state of the TSNs. It becomes obvious that these TSNs do not only depend on the type of EPN but also on the operational mode: for a given input TNS  $M_1(\mathbf{x}_1, T_1, p_1)$  of a reactor, an isobaric operation mode results in a different output state  $M_2(\mathbf{x}_2, T_2, p_1)$  than an isothermic operation mode  $M_2(\mathbf{x}_2, T_1, p_2)$  as indicated in Fig. 5.2.

As a consequence also the specific energy duties  $\varphi$  and  $\omega$  differ accordingly and depend strongly on the case study considered. While the actual values for  $\chi_{(E_j)}^{(M_i)}$ ,  $\varphi$  and  $\omega$  are therefore derived and calculated later after the introduction of the case study, the stoichiometric data given in Tab. 5.1 is sufficient to formulate the conservation laws introduced in section 3.2.2, that serve as equality constraints in the subsequent optimization problem. For selected elementary processes, the resulting balance equations are given in Tab. D.1.

### 5.3 Case study

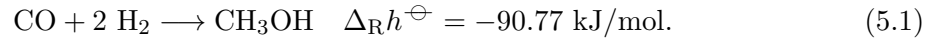
While the focus of the previous chapter was on analyzing the specific methanol production costs and the corresponding CO<sub>2</sub> emissions, this chapter examines in more detail the production process of methanol synthesis at the plant level. Therefore, the following six elementary processes are considered to model the methanol synthesis process: i) isothermal isobaric reaction, ii) isothermal isobaric separation, iii) isothermal compression, iv) isenthalpic expansion, v) isobaric heating and cooling, and vi) isothermal isobaric mixing.

### 5.3.1 Methanol synthesis process

First, the modeling of the elementary processes and the determination of the stoichiometric coefficients  $\chi_{(E_j)}^{(M_i)}$  as well as specific energy duties –  $\varphi$  and  $\omega$  – are presented. Subsequently, the attainable region of the entire thermodynamic state space – which has to be discretized – is derived by applying the equilibrium limitations of the reactor.

#### Isothermal isobaric reaction

The reaction is the most important part of the process as the chemical conversion of the reactants into the desired product takes place here. While pressure and temperature remain constant during the elementary reaction process, the chemical composition changes according to Eq. (5.1). For simplification no side reactions are considered, resulting in only one reaction equation.



The concept of TSNs enables the use of only two TSNs to describe the reaction given in Eq. (5.1): one for the input and one for the output mixture, resulting in Eq. (5.2):



The stoichiometric coefficient of the elementary process  $\text{R}_j$   $\chi_{(\text{R}_j)}^{(\text{M}_2)}$  is a function of the stoichiometric coefficients of the reaction  $\nu_{\alpha}$  and the extent of reaction  $\dot{\xi}$ . In contrast to  $\chi_{(\text{R}_j)}^{(\text{M}_2)}$ , the stoichiometric coefficients of the reaction  $\nu_{\alpha}$  are not related to TSNs but to the pure chemical substances  $\alpha \in \mathcal{A}$ . While  $\nu_{\alpha}$  is fixed due to the reaction equation (see Eq. (5.1)), discrete values for  $\dot{\xi}$  denote the reactor outlet TSNs in the thermodynamic state space. The stoichiometric coefficient  $\chi_{(\text{R}_j)}^{(\text{M}_2)}$  is defined as ratio between outlet and inlet flows:

$$\chi_{(\text{R}_j)}^{(\text{M}_2)} := \frac{\sum_{\alpha \in \mathcal{A}} \dot{N}_{\text{ext,out}}^{(\alpha)}}{\sum_{\alpha \in \mathcal{A}} \dot{N}_{\text{ext,in}}^{(\alpha)}}, \quad (5.3)$$

where  $\dot{N}_{\text{ext,out}}^{(\alpha)}$  and  $\dot{N}_{\text{ext,in}}^{(\alpha)}$  are the inlet and outlet molar fluxes of the pure components  $\alpha \in \mathcal{A}$ . The outlet molar fluxes can be expressed by  $\dot{N}_{\text{ext,in}}^{(\alpha)}$  and the extent of reaction  $\dot{\xi}$ , which gives the following equation:

$$\chi_{(R_j)}^{(M_i)} = 1 + \frac{\sum_{\alpha \in \mathcal{A}} \nu_{\alpha} \dot{\xi}}{\sum_{\alpha \in \mathcal{A}} \dot{N}_{\text{ext,in}}^{(\alpha)}} \quad (5.4)$$

The outlet mole fractions  $x_{\alpha}^{(M_2)}$  are obtained by solving the partial mass balances of the pure components  $\alpha$ :

$$x_{\alpha}^{(M_2)} = \frac{x_{\alpha}^{(M_1)} + \frac{\nu_{\alpha} \dot{\xi}}{\sum_{\alpha \in \mathcal{A}} \dot{N}_{\text{ext,in}}^{(\alpha)}}}{1 + \frac{\sum_{\alpha \in \mathcal{A}} \nu_{\alpha} \dot{\xi}}{\sum_{\alpha \in \mathcal{A}} \dot{N}_{\text{ext,in}}^{(\alpha)}}} \quad \forall \alpha \in \mathcal{A} \quad (5.5)$$

For a normalized inlet flow of 1 mol/s, the outlet composition depends only on the discrete extent of reaction  $\dot{\xi}$  and the inlet mole fractions  $x_{\alpha}^{(M_1)}$ , which simplifies Eq. (5.5):

$$x_{\alpha}^{(M_2)} = \frac{x_{\alpha}^{(M_1)} + \nu_{\alpha} \dot{\xi}}{1 + \sum_{\alpha \in \mathcal{A}} \nu_{\alpha} \dot{\xi}} \quad \forall \alpha \in \mathcal{A} \quad (5.6)$$

Since the reactor operates under isothermal and isobaric conditions, the temperature and pressure of the reactor inlet flows equal the reactor outlet flows. However, the reaction requires cooling as the reaction is exothermic ( $\Delta_{\text{R}} h < 0$ ). The specific cooling duty  $\varphi_{(R_j)}^{\text{out}}$  of  $R_j$  is calculated by the enthalpy differences of the reactor inlet and outlet:

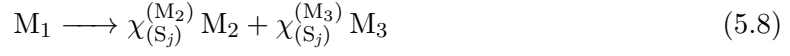
$$\varphi_{(R_j)}^{\text{out}} = h_{(R_j)}^{\text{in}} - h_{(R_j)}^{\text{out}} \quad \forall R_j \in \mathcal{E}. \quad (5.7)$$

In Eq. 5.7 the enthalpies  $h_{(R_j)}^{\text{in}} = h_{(R_j)}^{\text{in}}(T_{\text{in}}^{\text{R}_j})$  and  $h_{(R_j)}^{\text{out}} = h_{(R_j)}^{\text{out}}(T_{\text{out}}^{\text{R}_j})$  depend only on the temperatures if ideal gas behavior is assumed. Thus, the enthalpies can be calculated a priori by suitable equations of state (see Appendix A) because the inlet and outlet temperatures are discretized and predefined according to the FluxMax formulation.

Furthermore,  $\varphi_{(R_j)}^{\text{in}}$ ,  $\omega_{(R_j)}^{\text{in}}$ , and  $\omega_{(R_j)}^{\text{out}}$  equal zero since the reaction does neither require heating nor electrical power is generated or consumed.

### Isothermal isobaric separation

A separator  $S_j$  with one input and two output molar flows is considered for an arbitrary mixture of  $n_C$  pure substances  $\alpha \in \mathcal{A}$ . The separator is described by the stoichiometric equation:



where the subscript of the stoichiometric coefficients  $\chi_{(S_j)}^{(M_i)}$  denotes the elementary process and the superscript denotes the corresponding TSN  $M_i$ . The stoichiometric coefficients  $\chi_{(S_j)}^{(M_i)}$  are equivalent to the total split ratios  $\psi_{(S_j)}^{(M_i)}$ :  $\chi_{(S_j)}^{(M_2)} \equiv \psi_{(S_j)}^{(M_2)}$  and  $\chi_{(S_j)}^{(M_3)} \equiv \psi_{(S_j)}^{(M_3)}$ . The total split ratios are determined by the partial mass balances of the pure substances  $\alpha$

$$x_{\alpha}^{(M_1)} = \psi_{(S_j)}^{(M_2)} x_{\alpha}^{(M_2)} + \psi_{(S_j)}^{(M_3)} x_{\alpha}^{(M_3)} \quad \forall \alpha \in \mathcal{A}, S_k \in \mathcal{S} \quad (5.9)$$

wherein  $x_{\alpha}^{(M_i)}$  denotes the molar composition of  $\alpha$  of  $M_i$  and  $\psi_{(S_j)}^{(M_i)}$  the total split ratio. In addition, summation conditions for  $x_{\alpha}^{(M_i)}$  and  $\psi_{(S_j)}^{(M_i)}$  have to be fulfilled:

$$1 = \sum_{\alpha \in \mathcal{A}} x_{\alpha}^{(M_i)} \quad \forall M_i \in \mathcal{M} \quad (5.10)$$

$$1 = \psi_{(S_j)}^{(M_2)} + \psi_{(S_j)}^{(M_3)}. \quad (5.11)$$

The total split ratio e.g. for the flow of TSN  $M_2$  is defined as  $\psi_{(S_j)}^{M_2} = \dot{N}_{M_2} / \dot{N}_{M_1}$  and corresponds to the stoichiometric coefficients in Eq. (5.9).

In this study, the separator is regarded as a isothermal flash which ideally separates the product methanol and the unconverted reactants by condensation. It is assumed that methanol is completely liquified when the separation temperature is below the boiling temperature of methanol. The pressure dependence of the boiling temperature is expressed by the Clausius Clapeyron equation, which can be approximated for ideal gases as follows [151]:

$$\frac{1}{p} dp = \frac{\Delta h_v}{RT^2} dT \quad (5.12)$$

In Eq. (5.12)  $\Delta h_v$  expresses the enthalpy of evaporation and  $R$  the ideal gas constant. In Fig. 5.3 the resulting boiling temperature  $T_{\text{CH}_3\text{OH}}^{\text{boil}}$  of methanol is illustrated as a function of pressure.

Due to the assumption of an ideal split between liquid methanol and gaseous reactants, the stoichiometric coefficients simplify to

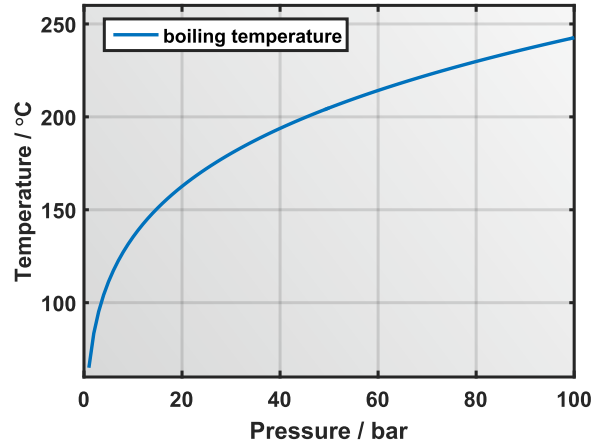


**Fig. 5.3** Boiling temperature of methanol as a function of the pressure.

$$\chi_{(S_j)}^{(M_2)} = x_{\text{CH}_3\text{OH}}^{(M_1)} \quad (5.13)$$

$$\chi_{(S_j)}^{(M_3)} = 1 - x_{\text{CH}_3\text{OH}}^{(M_1)} \quad (5.14)$$

wherein  $M_1$  is compound by pure  $\text{CH}_3\text{OH}$  and  $M_2$  corresponds to the unreacted gaseous compounds. Thus, the outlet compositions correspond to  $x_{\text{CH}_3\text{OH}}^{(M_2)} = 1$  for  $M_2$  and the initial inlet composition of the reactants for  $M_3$ .

During the isothermal isobaric separation the energetic states remain constant, which results in no specific energy duties:  $\varphi_{(S_j)}^{\text{in}} = \varphi_{(S_j)}^{\text{out}} = \omega_{(S_j)}^{\text{in}} = \omega_{(S_j)}^{\text{out}} = 0$ .

### Isothermal compression

An isothermal compressor  $C_j$  converts one TSN  $M_1$  into another TNS  $M_2$  at higher pressure. The stoichiometric coefficients  $\chi_{(C_j)}^{(M_i)}$  equal unity as the number of moles does not change during the compression.



While the molar composition  $[x_1, x_2, \dots, x_i]^\top$  and the temperature  $T_{\text{in}}^{C_j} = T_{\text{out}}^{C_j}$  remain constant, the pressure  $p_{\text{out}}^{C_j}$  at the compressor outlet is increased. The specific work duty of the elementary compression process depends on the phase – liquid or gaseous – of the inlet mixture, that is described by the TSN  $M_1$ .

Assuming ideal gas behavior, the required technical work duty  $\omega_{(C_j)}^{\text{in, gas}}$  of  $C_j$  is for a gaseous inlet mixture

$$\omega_{(C_j)}^{\text{in,gas}} = \frac{RT_{\text{in}}^{C_j}}{\eta_{\text{comp}}^{C_j}} \ln \left( \frac{p_{\text{out}}^{C_j}}{p_{\text{in}}^{C_j}} \right) \quad \forall C_j \in \mathcal{E} \quad (5.16)$$

where  $R$  is the ideal gas constant and  $\eta_{\text{comp}}^{C_j}$  is the compression efficiency.

For a liquid inlet mixture the following equation is given

$$\omega_{(C_j)}^{\text{in,liq}} = \frac{M_{\text{in}}^{C_j}}{\eta_{\text{comp}}^{C_j} \rho_{\text{in}}^{C_j}} (p_{\text{out}}^{C_j} - p_{\text{in}}^{C_j}) \quad \forall C_j \in \mathcal{E} \quad (5.17)$$

where  $M_{\text{in}}^{C_j}$  is the molar mass and  $\rho_{\text{in}}^{C_j}$  the density of the inlet mixture. As a consequence of the energy conservation law, the specific cooling duty  $\varphi_{(C_j)}^{\text{out}}$  equals the specific work duty  $\omega_{(C_j)}^{\text{in}}$ .

$$\varphi_{(C_j)}^{\text{out}} = \begin{cases} \omega_{(C_j)}^{\text{in,gas}} & \text{if } T \geq T_{\text{CH}_3\text{OH}}^{\text{boil}} \\ \omega_{(C_j)}^{\text{in,liq}} & \text{if } T < T_{\text{CH}_3\text{OH}}^{\text{boil}} \end{cases} \quad \forall C_j \in \mathcal{E} \quad (5.18)$$

There is neither power generated nor heat fluxes required:  $\varphi_{(C_j)}^{\text{in}} = \omega_{(C_j)}^{\text{out}} = 0$ .

### Isenthalpic expansion

The isenthalpic valve  $V_j$  transfers TSN  $M_1$  into another TNS  $M_2$  by expanding the pressure. For expansion, the molar composition remains constant, resulting in the following stoichiometric equation:



The expansion is considered as a valve, resulting in an isenthalpic operation. Thus the enthalpy remains constant:  $\varphi_{(V_j)}^{\text{in}} = \varphi_{(V_j)}^{\text{out}} = \omega_{(V_j)}^{\text{in}} = \omega_{(V_j)}^{\text{out}} = 0$ .

### Isobaric heating and cooling

Economizers  $D_j$  with one inlet and one outlet flux change the temperature between TSN  $M_1$  ( $T_{\text{in}}^{D_j}$ ) and TSN  $M_2$  ( $T_{\text{out}}^{D_j}$ ). The stoichiometric equations to represent cooling and heating are trivial because the stoichiometric coefficients  $\chi_{(D_j)}^{(M_i)}$  are equal to unity.





Depending on the sign of the enthalpy difference, the economizer  $D_j$  operates as heater ( $h^{\text{in}} - h^{\text{out}} < 0$ ) or as cooler ( $h^{\text{in}} - h^{\text{out}} > 0$ ). The resulting heating  $\varphi_{(D_j)}^{\text{in}}$  or cooling duties  $\varphi_{(D_j)}^{\text{out}}$  are determined as follows:

$$\varphi_{(D_j)}^{\text{in}} = h_{(D_j)}^{\text{out}} - h_{(D_j)}^{\text{in}} \geq 0 \quad \forall D_j \in \mathcal{E} \quad (5.21)$$

$$\varphi_{(D_j)}^{\text{out}} = h_{(D_j)}^{\text{in}} - h_{(D_j)}^{\text{out}} \geq 0 \quad \forall D_j \in \mathcal{E}. \quad (5.22)$$

where the enthalpies again depend on the temperature:  $h_{(D_j)}^{\text{out}} = h_{(D_j)}^{\text{out}}(T_{\text{out}}^{D_j})$ ,  $h_{(D_j)}^{\text{in}} = h_{(D_j)}^{\text{in}}(T_{\text{in}}^{D_j})$ ,  $h_{(D_j)}^{\text{in}} = h_{(D_j)}^{\text{in}}(T_{\text{in}}^{D_j})$ , and  $h_{(D_j)}^{\text{out}} = h_{(D_j)}^{\text{out}}(T_{\text{out}}^{D_j})$ .

Since no power is consumed or generated, the molar work duties  $\omega_{(D_j)}^{\text{in}} = \omega_{(D_j)}^{\text{out}} = 0$  equal zero.

### Isothermal isobaric mixing

The isothermal isobaric mixer  $L_j$  connects two inlet fluxes, corresponding to TSNs  $M_2$  and  $M_3$ , with one outlet flux, corresponding to TSN  $M_1$ . Assuming ideal mixing behavior, no enthalpy change due to mixing is taken into account. Thus the temperature remains constant and no energy balances need to be formulated:  $\varphi_{(L_j)}^{\text{in}} = \varphi_{(L_j)}^{\text{out}} = \omega_{(L_j)}^{\text{in}} = \omega_{(L_j)}^{\text{out}} = 0$ . However, the molar composition changes according to the following stoichiometric equation:



where the subscripts of the stoichiometric coefficients  $\chi_{(L_j)}^{(M_i)}$  denote the mixer  $L_j$  and the superscript the TSNs  $M_i$ . The stoichiometric coefficients  $\chi_{(L_j)}^{(M_i)} = \chi_{(L_j)}^{(M_i)}(x_{\alpha}^{(M_1)}, x_{\alpha}^{(M_2)}, x_{\alpha}^{(M_3)})$  depend on the molar compositions  $x_{\alpha}^{(M_i)}$  of pure substances that define the three TSNs  $M_1$ ,  $M_2$ ,  $M_3$  and can be calculated in the same way as illustrated for the stoichiometric coefficients of separation processes.

### Attainable region

In addition to the technical applied operation conditions, the thermodynamic feasibility has to be taken into account. Fig. 5.4 shows the pressure dependence of the chemical equilibrium and the boiling temperature  $T_{\text{CH}_3\text{OH}}^{\text{boil}}$  of methanol as a function of the pressure. The attainable process conditions are depicted as magenta area. While the maximum amount of methanol in the reactor outlet is determined by the chemical equilibrium (Fig. 5.4 A), the minimum

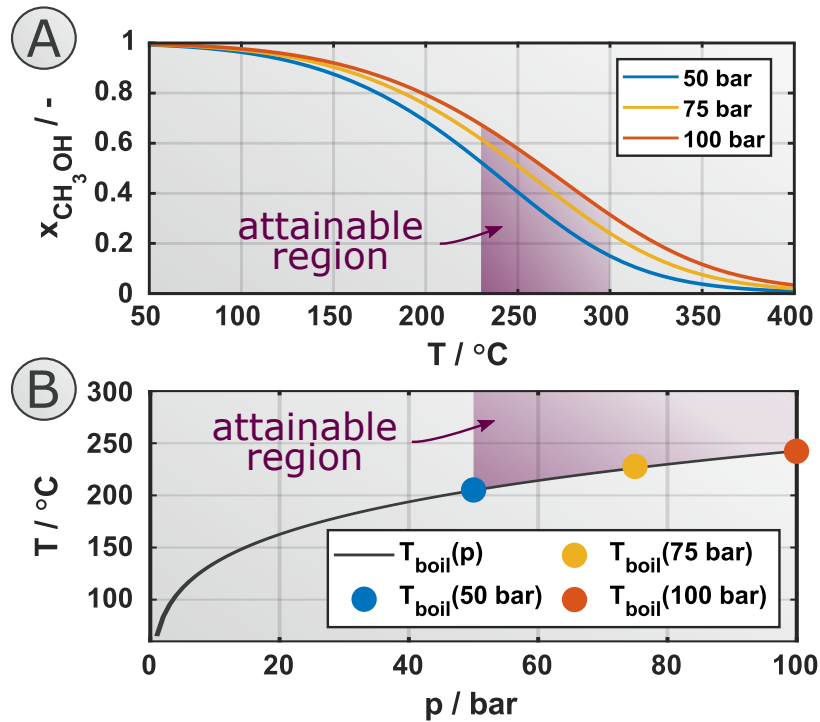


**Fig. 5.4** Illustration of the pressure dependence of the chemical equilibrium molar fraction of methanol in the reactor  $x_{\text{CH}_3\text{OH}}$  (A) and of the boiling temperature of methanol (B); the feasible region for the methanol synthesis reaction is depicted as magenta area.

reaction temperature is characterized by the boiling temperature (Fig. 5.4 B) to ensure that methanol is gaseous.

Due to the simplified reaction system, the reactor outlet flow only consists of condensable methanol and non-condensable, unconverted reactants. As a consequence, the separation can be considered as condensation of methanol. Thus, the separation temperature is set to the boiling temperature of methanol (Fig. 5.4 B) at the corresponding pressure.

The annual production of pure methanol is desired to be 100,000  $t_{\text{CH}_3\text{OH}}/\text{a}$ . The specification of the case study considered are summarized in Tab. 5.2.

### 5.3.2 Formulation of the optimization problem

The conservation laws and temperature conditions for heat integration, introduced in section 3.2.2 and 3.2.3, are equality and inequality constraints of the optimization problem. As the constraints are linear in terms of the decision variables, the feasible region is convex. As a consequence, the identification of a global optimum is guaranteed for a convex objective function.

**Tab. 5.2** Definition of scenario.

Parameter	Symbol	Unit	Value
<i>Operational conditions</i>			
Plant capacity	$\dot{N}_{\text{CH}_3\text{OH},\text{out}}$	$t_{\text{CH}_3\text{OH}/\text{a}}$	100,000
Minimum temperature difference	$\Delta T_{\text{min}}$	K	20
<i>Feedstock specifications</i>			
Temperature	$T_{\text{in}}$	°C	25
Pressure	$p_{\text{in}}$	bar	1
<i>Feedstock composition</i>			
Hydrogen	$x_{\text{H}_2}^{\text{in}}$	-	2/3
Carbon monoxide	$x_{\text{CO}}^{\text{in}}$	-	1/3
Methanol	$x_{\text{CH}_3\text{OH}}^{\text{in}}$	-	0
<i>Efficiencies</i>			
Compression	$\eta_{\text{comp}}^{C_j}$	-	0.5

One of the major cost drivers in the field of Renewable-to-Chemicals applications is the energy demand. In order to become more competitive compared to fossil-based processes, the energy efficiency of the processes must be increased. This study uses the FluxMax approach to identify energy optimal process configurations. The objective function  $f$  is therefore to minimize the total external energy duty – sum of external heating, cooling, and electrical energy – which is linear in terms of the fluxes:

$$f = \sum_{U_l \in \mathcal{U}} \dot{Q}_{(E_j)}^{(U_l)} + \sum_{U_l \in \mathcal{U}} \dot{Q}_{(U_l)}^{(E_j)} + \sum_{E_j \in \mathcal{E}} \dot{W}_{(E_j)}^{\text{ext},\text{in}} \quad (5.24)$$

A compact form of the linear objective function is given in terms of the decision variables  $\varphi = (\dot{\mathbf{N}}, \dot{\mathbf{\Gamma}}, \dot{\mathbf{Q}}, \dot{\mathbf{W}})^\top$ , where  $\dot{\mathbf{N}}, \dot{\mathbf{\Gamma}}, \dot{\mathbf{Q}}, \dot{\mathbf{W}} \in \mathcal{F}$  are row vectors:

$$f(\varphi) = \mathbf{c}^\top \varphi, \quad (5.25)$$

where the entries of the cost vector  $\mathbf{c}^\top = (\mathbf{c}_{\dot{\mathbf{N}}}, \mathbf{c}_{\dot{\mathbf{\Gamma}}}, \mathbf{c}_{\dot{\mathbf{Q}}}, \mathbf{c}_{\dot{\mathbf{W}}})$  are as follows:  $\mathbf{c}_{\dot{\mathbf{N}}} = \mathbf{c}_{\dot{\mathbf{\Gamma}}} = \mathbf{0}$  and  $\mathbf{c}_{\dot{\mathbf{Q}}^{\text{ext}}} = \mathbf{c}_{\dot{\mathbf{W}}^{\text{ext},\text{in}}} = \mathbf{1}$ . The resulting linear program, applying the objective function Eq. (5.24) and the constraints introduced in sections 3.2.2 and 3.2.3 is presented in the Appendix (Eq. (D.3)).

## 5.4 Results

### 5.4.1 Comparison of sequential and simultaneous process synthesis

This section emphasizes not only the influence of heat integration on the optimal pathway, but also the need of a simultaneous consideration of heat and mass flux optimization. A benchmark scenario is defined, which follows the sequential procedure, in which the flow problem is optimized without consideration of heat integration first and the heat integration potential is subsequently evaluated with the help of pinch-based analysis [98, 83, 99].

Subsequently, the FluxMax approach is applied to the same benchmark scenario. The two heat integration approaches presented in section 3.2.3 – direct and indirect heat integration – are compared and discussed.

#### Benchmark scenario: A sequential procedure

In the benchmark scenario, the energy-optimal (Eq.(5.24)) pathway is identified if the feedstock – hydrogen and carbon monoxide – is fed into the process at a temperature of 25 °C and a pressure of 1 bar and the product – pure methanol – has to be delivered at 25 °C and 50 bar. Since in this first analysis the flux optimization is decoupled from heat integration, the energy duties have to be provided completely from external sources.

The elementary processes introduced in section 5.3.1 are used to discretize the five-dimensional thermodynamic state space (molar fractions of the components  $x_{\text{CO}}$ ,  $x_{\text{H}_2}$ ,  $x_{\text{CH}_3\text{OH}}$ ; temperature  $T$ ; and pressure  $p$ ). To illustrate the results in a three-dimensional state space representation, the molar fractions of carbon monoxide and hydrogen are omitted in Fig. 5.5. The TSNs corresponding to the feedstock and product are marked as a magenta and a green circle, respectively. In addition, the elementary processes are illustrated as cyan thin lines connecting the discrete TSNs, illustrated as black circles. For this first analysis, the thermodynamic state space is discretized in a coarse grid (45 TSNs) to obtain a benchmark scenario that allows the comparison with direct heat integration among entities. This is because the fineness of the discretization is limited in case of direct heat integration, since the number of constraints increases drastically if the number of entities increases, as stated in section 3.2.3.

The discrete options for the reaction are two different reaction temperatures – 230 °C and 300 °C – and reactor outlet compositions –  $x_{\text{CH}_3\text{OH}}$  : 0.10, 0.21, 0.35 and 0.51 (if within the attainable region depicted in Fig. 5.4) – leading to different separation tasks. Depending on the pressure of the different separation inlet compositions resulting from different reaction outlet compositions, the separation temperature is set to the corresponding boiling temperature of methanol (Fig. 5.4 B). To adjust the required temperature and pressure levels, heating and

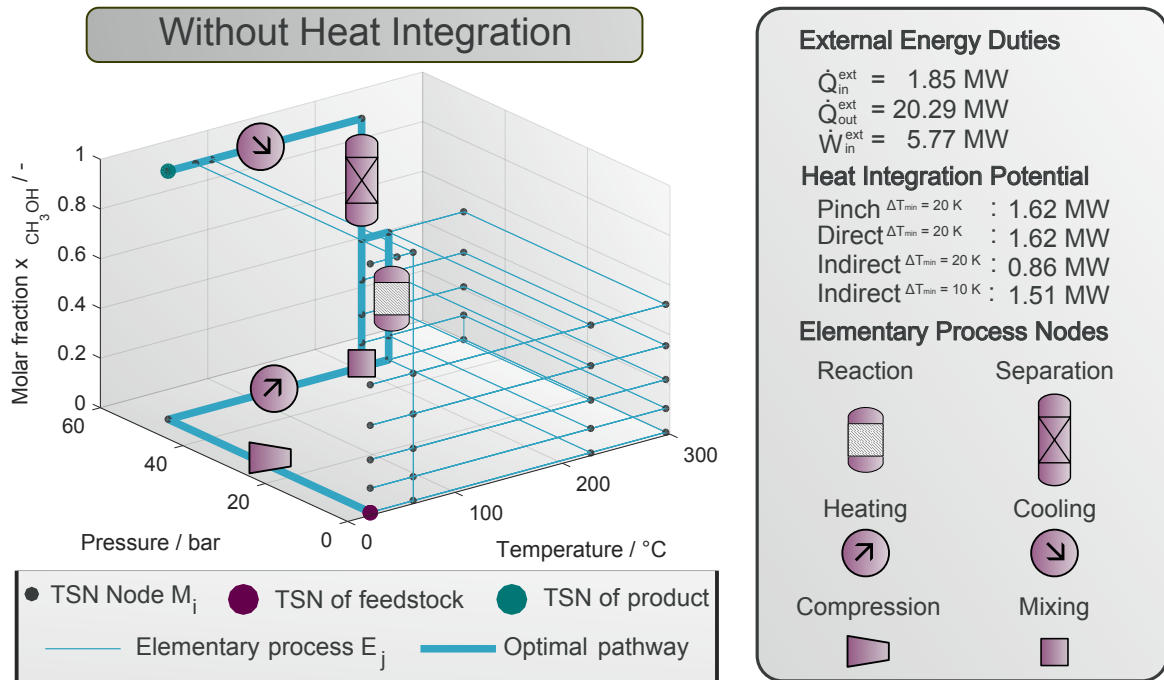


**Fig. 5.5** Optimal pathway of benchmark case in the discretized state space; corresponding elementary processes are represented along the path.

cooling as well as compression and expansion between TSNs are considered, as illustrated in Fig. 5.5 with thin blue lines along the temperature and pressure axis, respectively.

The optimal path (bold cyan line) within the thermodynamic state space for the benchmark scenario is shown in Fig. 5.5. The different elementary processes – reaction, separation, heating, cooling, compression, and mixing – are also assigned to the corresponding path. First, the reactants – hydrogen and carbon monoxide – are mixed under ambient conditions. The mixing itself, however, is not visible in the state space representation of Fig. 5.5, since only the molar fraction of the product is depicted, which does not allow a differentiation of the individual TSNs of the raw materials. The feedstock mixture is then compressed to a pressure of 50 bar and heated to the reaction temperature of 230 °C. The EPN at lower temperature of 230 °C is selected because less heating – of the feedstock – and cooling – of the reaction and products – are required compared to a reaction at 300 °C. The reaction is performed up to the maximum amount of about 51 mol-% methanol, as the total energy requirement – heating, cooling, and power – is smaller than for the reactor outlet with a lower methanol content. In this case, either the unconverted reactants would have to be reheated to the reaction temperature after product separation – resulting in increased heating demand – or the initial feedstock flow would have to be increased – resulting in a higher heating demands as well as higher cooling and power demand due to increased compression requirements. The reaction mixture, which contains of about 51 mol-% methanol is cooled

to condensate the methanol in the separator at 205 °C, which corresponds to the boiling temperature of methanol at 50 bar. While the unconverted feedstock is recycled, the pure methanol is finally cooled to the desired temperature of 25 °C.

The optimal pathway requires a total energy duty of about 27.91 MW, which is about 1.85 MW for heating, 20.29 MW for cooling, and 5.77 MW for electrical energy. Cooling and electrical energy demands are much higher than the heating demand, since the heating is only required to bring the feedstock to reactor inlet temperature, while cooling is required to cool the product, the exothermic reactor and the compressor. However, the external heating demand can still be further decreased if heat integration is taken into account. For the benchmark scenario a pinch analysis for the identified optimal configuration was performed to evaluate the heat integration potential, resulting in a maximum internally transferable heat flux of approximately 1.62 MW.

In addition, the heat integration potential for the optimized configuration is investigated using the direct heat integration approach – among entities – and the indirect heat integration approach – using utilities, introduced in section 3.2.3. The comparison of the pinch result with the prediction of the FluxMax approach shows that the consideration of direct heat integration leads to the same heat integration potential of 1.62 MW. In contrast, the consideration of indirect heat integration slightly underestimates the heat integration potential. Since heat fluxes can only be transferred to or from utilities at distinct temperature levels, the calculated internal heat flux depends on the selected temperature levels of the utilities. In addition, the desired minimum temperature difference  $\Delta T_{\min}$  influences the calculation of the heat integration potential for the different methods differently. While two heat fluxes – one hot, one cold – interact directly in the classical pinch analysis and in consideration of heat integration among entities, the two heat fluxes interact indirectly via the utilities in consideration of utilities. Thus  $\Delta T_{\min}$  is considered twice, because the hot flux transfers the heat in a first step to the utility – considering  $\Delta T_{\min}$  – and then in a second step to the cold flux. In order to improve the comparability of all presented heat integration methods, the calculated internal heat fluxes for the case of considering utilities are not only presented for  $\Delta T_{\min} = 20$  K, but also for  $\Delta T_{\min} = 10$  K, which leads to heat integration potentials of 0.86 MW and 1.51 MW, respectively.

Since the elementary processes in the thermodynamic state space represent unit operations, the optimal process configuration can also be illustrated as a flowsheet of process units. Fig. 5.6 A shows the optimal process configuration of the benchmark scenario identified by a sequential procedure. The process units – mixer, compressor, heater/cooler, reactor, and separator – are connected by mass fluxes, which are represented as black arrows. The heat fluxes are represented by red arrows and the work fluxes by blue arrows. The thickness of the red and blue arrows corresponds to the amount of the energy flux, represented by the

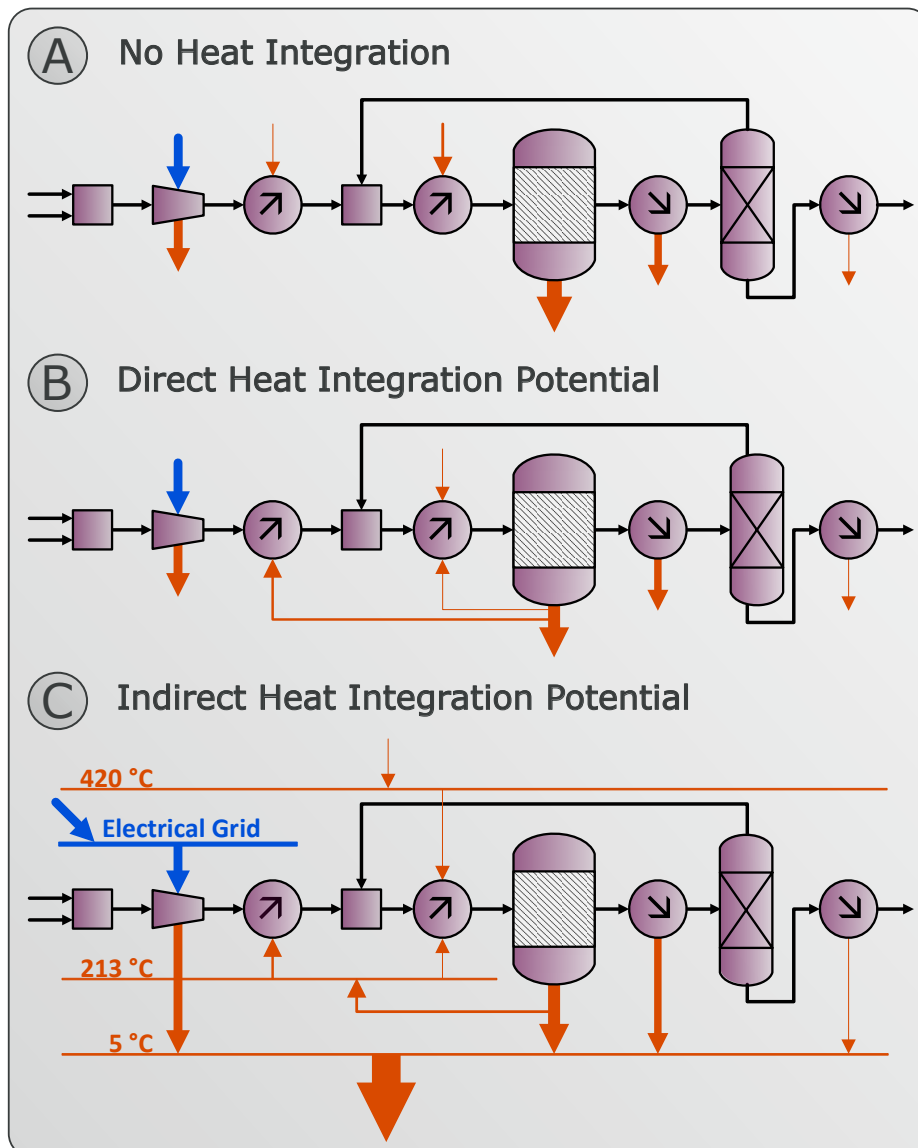


**Fig. 5.6** Schematic illustration of the optimal process configurations of the benchmark scenario obtained in a sequential procedure; optimal flowsheet if no heat integration is taken into account (A); additionally the heat integration potentials for direct (B) and indirect heat integration (C) are shown.

corresponding arrow: a thick arrow indicates a high amount energy required or released, while a thin arrow indicates a low amount of energy. As the orientation of the arrows denotes the direction of the fluxes, it can be seen that electrical energy is required only for the operation of the compressor and heating only for preheating the reactor inlet stream, which consists of initially provided reactants and unconverted reactants separated and recycled from the reactor outlet. The heat integration potential – identified by the classical pinch analysis and by the proposed direct and indirect method – results from the possibility to partially utilize the excess heat of the reactor. The resulting heat flux distributions are shown in Fig. 5.6 B and C. It is evident that in both cases a part of the excess heat of the reactor is used to preheat the reactants. The first heater, which heats the reactants to the temperature of 205 °C – corresponding to the mixing point of initial reactants and recycled, unconverted reactants – is completely fed by the internal heat flux and the heat demand of the second heater, which heats the reactants to reaction temperature, is reduced by about 89.0 % for direct heat integration and by about 86.5 % for indirect heat integration. This results in overall percentage reduction in external heat duty of 90.3 % and 87.4 %, respectively.

While direct heat integration – Fig. 5.6 B – uses the excess heat of the reactor directly to preheat the feedstock, indirect heat integration – Fig. 5.6 C – uses a network of utilities. According to pinch analysis, the external heat fluxes are provided at the maximum temperature and released at the minimum temperature. This concept of using excess heat of the reactor to preheat the feed is also applied in reality and is referred to as feed heat exchanger (FEHE) [152–154].

The first important result is that the FluxMax approach is able to identify the well-known and widely used concept of FEHE if applied in a sequential procedure. However, the strength of the FluxMax approach lies in its ability to simultaneously optimize the flow problem while taking into account heat integration, which can lead to new, non-intuitive, process designs. Therefore, the simultaneous approach is examined in more details in the following.

### **FluxMax: A simultaneous approach**

With the benchmark scenario defined above, the influence of simultaneous consideration of heat integration as an integrated part of the overall optimization problem is investigated. In addition, the advantages and limitations of the two proposed methods – direct and indirect – heat integration are presented and discussed.

Fig. 5.7 shows the optimal pathways for the benchmark scenario considering the two heat integration methods presented in section 3.2.3. When analyzing the results, two things are apparent. First, the consideration of direct and indirect heat integration identifies identical process configurations. And secondly, the newly identified process configuration differs



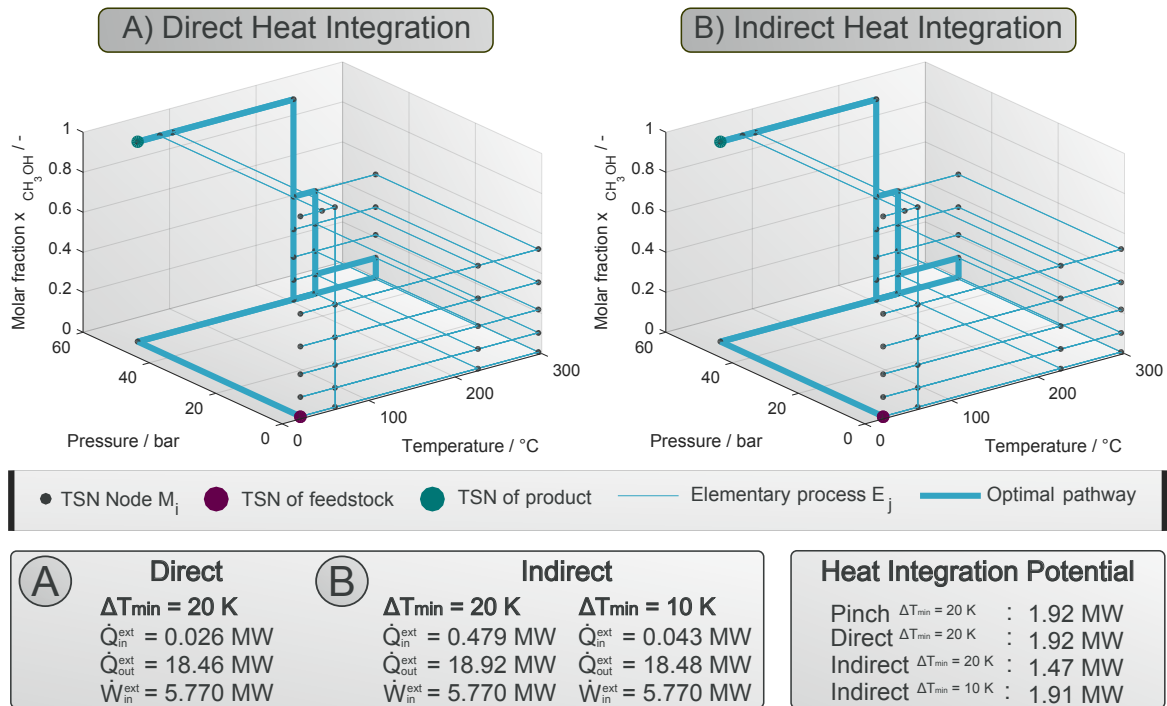


**Fig. 5.7** Optimal pathway in discretized state space obtained in a simultaneous procedure; optimal pathways for direct (A) and indirect heat integration (B); in addition, external energy demands and heat integration potentials are given.

from the optimal process configuration identified in the sequential procedure (Fig. 5.5) of decoupling the flux optimization from the determination of the heat integration potential.

In the newly identified optimal configuration, the reaction is not only carried out at the lower temperature of 230 °C, but also in a parallel reaction at the higher temperature of 300 °C, since in this way the total energy demand is minimized. However, since the chemical equilibrium shifts towards the reactants at higher temperatures, the reaction is only carried out up to a methanol content of mol-10 % at elevated temperatures. Although the net heating demand is increased by the additional preheating of the reactants, an even higher amount of heat resulting from the excess heat of the reactor at 300 °C and the cooling of the reactor outlet can be integrated internally. The consideration of direct heat integration leads to a similar total energy requirement of about 24.26 MW (0.026 MW for heating, 18.46 MW for cooling, and 5.77 MW electrical energy) as the consideration of indirect heat integration. The following energy duties are calculated depending on the minimum temperature difference  $\Delta T_{\min}$  i) for  $\Delta T_{\min} = 20 \text{ K}$ : 0.479 MW for heating, 18.92 MW for cooling, and 5.77 MW electrical energy, and ii) for  $\Delta T_{\min} = 10 \text{ K}$ : 0.043 MW for heating, 18.48 MW for cooling, and 5.77 MW electrical energy. While the total energy duty is dominated by the cooling of the reactor and the electrical energy demand, which is the same as for the benchmark case, the heating plays only a minor role for the methanol synthesis process. Compared to the

**Tab. 5.3** Overview of the external heating and cooling duties of the sequential and simultaneous approach and corresponding saving potentials.

Energy flux	No HI	Sequential			Simultaneous		
		direct	indirect	pinch	direct	indirect	pinch
<i>External duties</i>							
external heating / MW	1.850	0.230	0.340	0.230	0.026	0.043	0.026
external cooling / MW	20.290	18.670	18.780	18.670	18.460	18.480	18.460
electrical work / MW	5.770	5.770	5.770	5.770	5.770	5.770	5.770
total energy / MW	27.910	23.960	24.890	24.670	24.256	24.293	24.256
<i>Savings</i>							
saving in total energy / %	0	11.6	10.8	11.6	13.1	13.0	13.1
saving in heating / %	0	87.6	81.6	87.6	98.6	97.7	98.6

benchmark case, this only leads to a small improvement in the heating demand reduction. However, it was shown that the FluxMax approach identifies new process configurations when heat integration is considered as a part of the flux optimization. To validate the obtained results, a common pinch analysis is applied to the novel configuration leading to a heat integration potential of 1.92 MW. While the available heat integration potential was slightly underestimated for indirect heat integration (1.47 MW or 1.91 MW, respectively), direct heat integration (1.92 MW) corresponds exactly to the pinch result.

This proves that the internally transferable heat fluxes for the new configuration are increased compared to the benchmark configuration, as shown in Tab. 5.3. This is a very important result as it underlines the need for a simultaneous procedure and the ability of the FluxMax approach to identify globally optimal process configurations for a given thermodynamic state space discretization. In particular, if the energy duty depends stronger on the heating duty than in the case scenario under consideration, the FluxMax approach can be a powerful tool for designing new, non-intuitive, process configurations [138]. The energy saving potentials listed in Tab. 5.3 support the latter statement. While the FluxMax approach enables the identification of process structures that almost completely save the total heat demand (approx. 99 % for the simultaneous procedure compared to 88 % of the sequential procedure), the total energy savings for the considered case study are only slightly increased from approx. 11 % to approx. 13 %, since the external cooling duty remains high after exploitation of the heat integration potential.

The optimum that is identified for indirect heat integration depends on the number of utilities considered and their temperature levels. The dependency of the number of utilities on the result is analyzed in section 5.4.2. It can be stated, however, that even a coarse discretization was able to identify a configuration with increased internally integrated heat fluxes. As a consequence, only the indirect heat integration approach is used in the following, since the

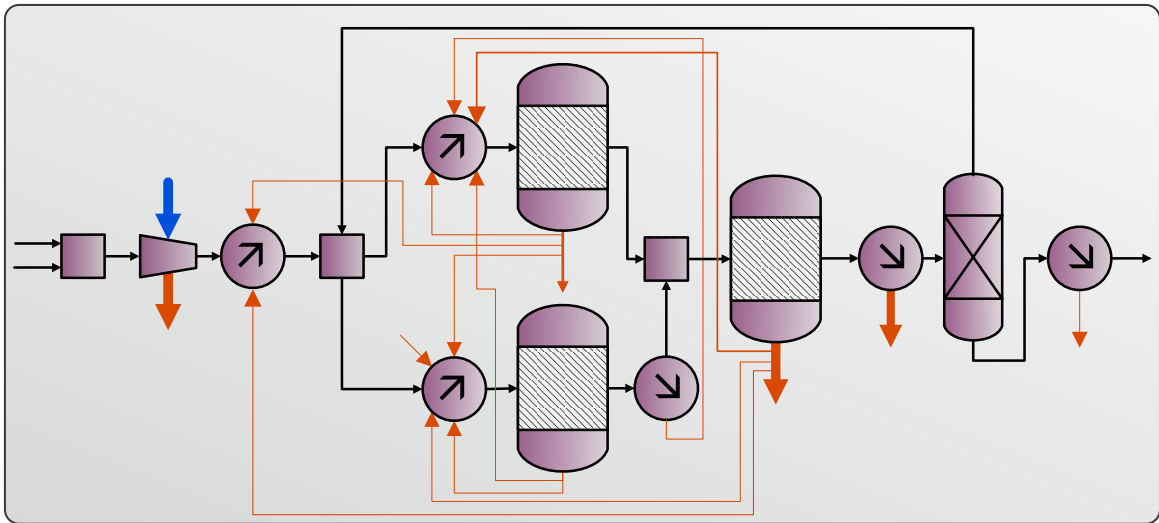


**Fig. 5.8** Schematic illustration of the optimal process configurations obtained in a simultaneous procedure; for better clarity, only the flowsheet is shown, taking direct heat integration into account.

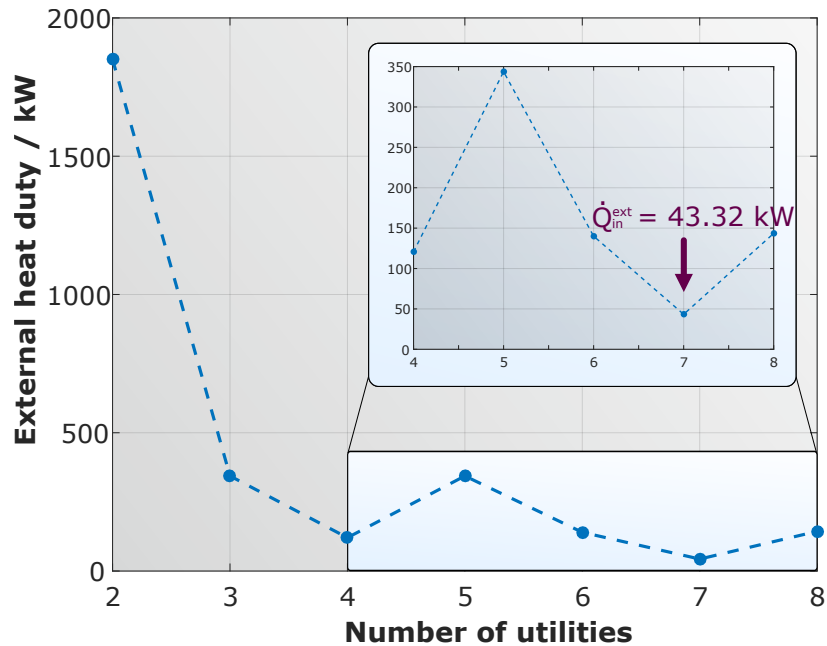
computational effort is significantly lower compared to the direct approach, which allows a finer discretization of the thermodynamic state space.

Fig. 5.8 shows the flowsheet representation for the optimal trajectory found in the thermodynamic state space. For better visibility the energy flux distribution resulting from consideration of indirect heat integration is omitted and only the flowsheet with direct heat integration is displayed. However, the following statements on Fig. 5.8 also apply to the case of indirect heat integration, since the general flowsheets are interchangeable. The parallel reaction at an elevated temperature requires an additional heater to provide the reactants at higher reaction temperatures and an additional cooler to cool the reaction outlet – with a methanol content of about 10 % – to the reaction temperature of the first reactor to be further converted at lower temperature. Besides this change in the reaction part of the process, the other process units correspond to the configuration of the benchmark process, shown in Fig. 5.6.

It can be seen that the excess heat of the parallel reactor at higher temperature and of the new cooler is completely integrated internally. In this way, the reactants entering the first reactor, can be better preheated by internal heat fluxes.

#### 5.4.2 Optimal utility network

The FluxMax approach guarantees the identification of the global optimum if a convex objective function is used, because all constraints are linear in terms of the decision variables as a direct result of the formulation of the FluxMax approach. However, the result depends strongly on the selected discretization of the thermodynamic state space. In the previous



**Fig. 5.9** Illustration of the external heating requirement as a function of the number of utilities considered.

section, a coarse grid was used to better visualize the results and reduce the computational time – in particular when applying the direct heat integration approach. In this section, the effect of the discretization of utility temperatures of the indirect heat integration approach is analyzed.

The internally transferred heat depends strongly on the predefined temperature levels of the considered utilities. Since external energy fluxes are also provided or released via utilities for the indirect heat integration approach, the minimum number of utilities equals two: one utility at a sufficiently low temperature to provide the external cooling and one utility at sufficiently high temperature to provide the external heating, respectively. Fig. 5.9 illustrates the external heat duty for the scenario introduced above as a function of the number of utilities considered. The temperatures of the utilities are equidistantly distributed between 5 °C and 420 °C and are listed in Tab. D.2.

For the consideration of only two utilities no internal heat transfer is possible and the external heat duty corresponds to the heat duty calculated for the benchmark process (see also Fig. 5.5). If one considers utilities at a temperature between these outer limits, the external heating duty is reduced as a result of the internal heat integration potential. It is evident, however, that an increase of considered utilities does not necessarily mean a decrease in external heat duty. The reason for this is that not (only) the number of considered utilities, but also the particular temperature is decisive for a high heat integration potential. Due to the equidistant distribution of the temperature levels considered an additional utility

**Tab. 5.4** Utilities and their corresponding temperatures used in the study.

Utility	1	2	3	4	5	6	7
Temperature / °C	5	74	143	213	282	351	420

influences all the other temperatures of the remaining utilities. In other words: While the probability of a higher heat integration potential estimated by the indirect approach increases with an increased number of utilities considered, even a low number of utilities can lead to a maximum heat integration potential if dedicated temperature levels are chosen.

For the scenario defined above, an optimal number of seven utilities is found, resulting in the external heat duty of 43.32 kW. But also the consideration of only four utilities already leads to an acceptable result. Since an increase in the number of utilities considered could lead to an increase in costs – which are not considered in this study – the choice of the actual number of utilities considered in an industrial application may differ. To obtain the energy minimal results for this case study, however, the utility number is set to seven, as listed in Tab. 5.4.

In addition to illustrating the impact of the number of utilities, the results presented demonstrate another key feature of the FluxMax approach: the optimization of utility networks. In the case study under consideration, in the optimal configuration, three utilities – 5 °C, 213 °C, and 420 °C – are selected from the options listed in Tab. 5.4. Thus, the FluxMax approach generally enables the identification of the optimal temperature levels of the utilities by introducing a multitude of utility nodes, which provide heating or cooling at different temperatures. Particularly when considering distinct cost for the external heat fluxes to provide heating or cooling at distinct temperature levels, further interesting optimization tasks are facilitated.

### 5.4.3 Identification of optimal process designs

In the previous sections of this chapter, the FluxMax approach was applied to a coarse discretization of the thermodynamic state space. In this way, key features – such as the simultaneous consideration of heat integration – were demonstrated while maintaining an intuitive understanding of the obtained results. In this section, the focus is on the process optimization, which requires a finer discretization of the thermodynamic state space.

The discretization of the whole thermodynamic state space is not done equidistantly, since there is a distinct operating window for each elementary process. The methanol synthesis reaction is normally performed between temperatures of 230 °C and 300 °C and in a pressure range of 50 bar to 100 bar [76]. Therefore, the reaction conditions were discretized within the technically applied range: the pressure at which the reaction can take place in steps of 10 bar and the temperature in steps of 10 °C. The extent of reaction was discretized in such

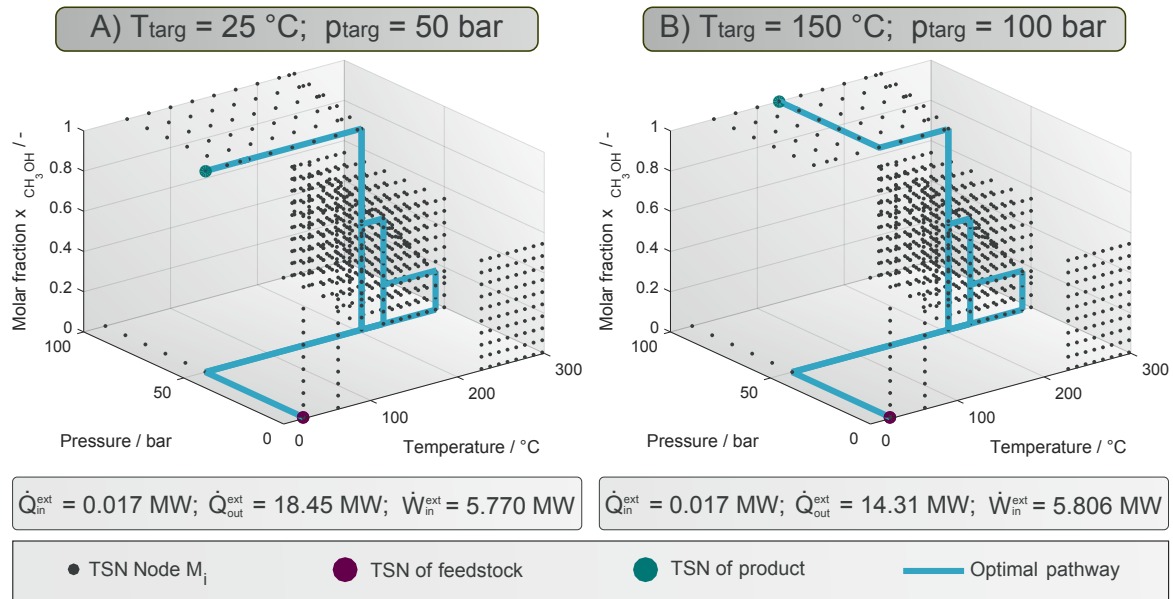


**Fig. 5.10** Optimal pathway in discretized state space for cases A)  $T_{\text{targ}} = 25\text{ }^{\circ}\text{C}$ ,  $p_{\text{targ}} = 50\text{ bar}$  and B)  $T_{\text{targ}} = 150\text{ }^{\circ}\text{C}$ ,  $p_{\text{targ}} = 100\text{ bar}$ .

a way that discrete molar fractions of methanol between zero and chemical equilibrium – in 0.06 steps – were achieved. To separate the reactor outlet, the product stream must be cooled to the condensation temperature of methanol to be flashed into liquid methanol and gaseous, unconverted reactants. The condensation temperatures as a function of the pressure is calculated by the Clausius Clapeyron equation (Eq. (5.12)). The resulting discretized thermodynamic state space (810 TSNs) and possible elementary processes, that connect the TSNs, are shown in the Appendix D in Fig. D.1.

For the identification of process pathways that optimally convert the feedstock into the desired product specifications, only indirect heat integration was considered in order to enable an finer discretization. The number of utility nodes, that provide the external energy duties and enable the internal heat transfer, is set to seven according to Table 5.4.

The initial reactants are supplied at ambient conditions –  $25\text{ }^{\circ}\text{C}$  and  $1\text{ bar}$  – and an annual production of  $100,000\text{ t}_{\text{CH}_3\text{OH}}/\text{a}$  pure methanol is desired. Two different product specifications are examined: case A) ambient target temperature and mildly increased pressure of the product ( $T_{\text{targ}} = 25\text{ }^{\circ}\text{C}$ ,  $p_{\text{targ}} = 50\text{ bar}$ ); and case B) elevated target temperature and pressure of the product ( $T_{\text{targ}} = 150\text{ }^{\circ}\text{C}$ ,  $p_{\text{targ}} = 100\text{ bar}$ ). The specifications of case A are the same as for the benchmark scenario. In case B, the methanol is desired to be delivered at increased temperature and pressure, which may correspond to the case, that methanol is not the final product but an intermediate, that needs to be further processed.

The optimal pathways in the discretized thermodynamic state space are illustrated in Fig. 5.10. In contrast to previously presented results, the connections between TSNs, that represents the possible elementary process functions, are omitted for better readability. The optimal trajectories are again depicted as cyan line.

Before analyzing the two cases in detail, it can be seen that the desired product specification only affects the downstream part of the process. Both cases have in common that the initial reactants are mixed, then compressed to the lowest possible reaction pressure of 50 bar and heated to be converted in two parallel reactors. Most of the reaction is performed at the lowest possible reaction temperature of 230 °C, while a second reactor is performed at evaluated temperature of 290 °C. The parallel reaction at evaluated temperature allows the utilization of the excess reactor heat fluxes to preheat the reactants as described in section 5.4.1 and shown in Fig. 5.8. Both reactions are carried out to the maximum extent at the corresponding temperature (Fig. 5.4), resulting in an outlet methanol fraction  $x_{\text{CH}_3\text{OH}}$  of the low temperature reactor of about 52.5 % and of about 19 % of the high temperature reactor. While in this case the achieved reactor outlet fractions correspond to the chemical equilibrium composition, it is important to mention that the FluxMax approach in general also facilitates the use of kinetic reactor models [138]. The high temperature reactor outlet stream is cooled and further converted in the low temperature reactor. Subsequently, the overall reactor outlet stream is cooled to meet the condensation temperature to separate the unconverted reactants. The unconverted reactants are recycled, while the pure methanol is brought to the desired product specification in a final step.

Case A results in almost the same optimal configuration that was found when the FluxMax approach was applied to the benchmark case (Fig. 5.7). Due to the finer discretization, however, the parallel reaction is performed at a slightly lower temperature of 290 °C. As can be seen in Fig. 5.10, the energy duties can be further reduced in this way, because the amount of external heat duty to preheat the reactant inlet stream of the second reactor is smaller compared to the benchmark process. The finer discretization of the elementary reaction process improves the identified optimum. The improvement is very small yet, thus in this study an even finer discretization was omitted.

The case B differs with regard to the desired target temperature and the target pressure, which requires additional compression, resulting in increased power consumption. Although the excess heat of compression must be cooled, the overall cooling duty is smaller compared to case A, because the product only has to be cooled to 150 °C. Interestingly, however, the reaction is carried out at a pressure of 50 bar not directly at target pressure of 100 bar. The reason is that compression of one mole of liquid methanol requires less power than compression of three moles of gaseous reactants – 1 mole of CO and 2 mole of H<sub>2</sub>.

The presented results demonstrate that the FluxMax approach can be used for process design tasks by optimizing the mass and energy fluxes. Once the thermodynamic state space is discretized and elementary processes are defined, the desired reactant and product specifications are easily adjustable. As a result, the FluxMax approach is very versatile in the analysis and optimization of different scenarios.

## 5.5 Chapter summary

Resource efficiency is a key performance aspect in the chemical industry for both economic and ecological reasons. However, often the design of chemical processes or units and the corresponding heat integration, is divided into two design phases: a flow optimization to identify an optimal design and the subsequent evaluation of the heat integration potential. This procedure cannot guarantee the identification of the global resource optimum, which increases the need for a method that can do both simultaneously. This is the aim of the FluxMax approach that discretizes the thermodynamic state space.

The FluxMax approach was applied to the methanol synthesis process, which is of great significance for applications in the field of Renewable-to-Chemicals. A linear objective function – minimizing total energy demand – was used, resulting in a purely linear optimization problem. Addressing the fourth research question (IV), it was shown that the FluxMax approach identifies energy-optimal process configurations that outperform configurations identified in a sequential procedure: The simultaneous approach resulted in a heat savings potential of almost 99 % compared to 88 % in a sequential approach. This was achieved by a parallel reaction at elevated temperature, which improved the heat integration potential significantly. This highlights the key outcome of this chapter: the importance of a simultaneous approach for designing energy efficient processes leading to low carbon emissions. The complexity of the optimization problem was drastically reduced by the introduction of an indirect heat integration approach. The validation with classical pinch analysis proved the applicability of the FluxMax approach to identify novel, non-intuitive process configurations. Furthermore, the possibility of optimizing the utility network resulting directly from the introduction of utility nodes was demonstrated.

The whole study showed also the necessity for further work since the separation was only regarded as a simple split of condensable methanol from the gaseous compounds by condensation. In technical applications, however, the product purification is often responsible for the largest proportion of the overall energy demand of the overall process. Therefore, distillation processes – as the most frequently applied thermal separation technology – are further investigated in the next chapter to optimize the energy-intensive downstream part of the methanol synthesis process in more detail.



# Chapter 6

## Process unit level

Rather than entire processes at the plant level, the focus of this chapter is on the design of individual process units as illustrated by the example of a distillation column in Fig. 6.1. Consequently, the key research question at this level is (V): Are there highly energy-efficient unit designs that lead to lower energy consumption than conventional designs?

In the context of the dissertation the proof-of-concept for the application to the compressor cascade and the reactor part of the methanol synthesis process was demonstrated on the process unit level [155]. Furthermore, the ability to design classical distillation columns [156] was demonstrated as well as the ability to identify new, unconventional designs with minimal energy consumption by using additional degrees of freedom [157]. The latter two publications served as a basis for this chapter.

After a literature review of distillation design and synthesis approaches, the FluxMax formulation for distillation processes is derived, followed by a presentation of the case study of methanol-water separation, which applies two objective functions to identify the most energy-efficient design and the minimum stage configuration. Furthermore, an extension of the classical modeling approach based on the MESH equations is derived. This serves as a benchmark for the results obtained with the FluxMax formulation. Finally, the designs obtained with the FluxMax approach and based on the MESH equations are compared.

### 6.1 Literature review

In order to achieve the ambitious goal of greenhouse gas emission neutrality within the European Union by 2050, the chemical industry is required to reduce drastically carbon dioxide emissions [158]. In addition to the substitution of raw materials by renewable resources, an increase in material and energy efficiency would reduce greenhouse gas emissions. A

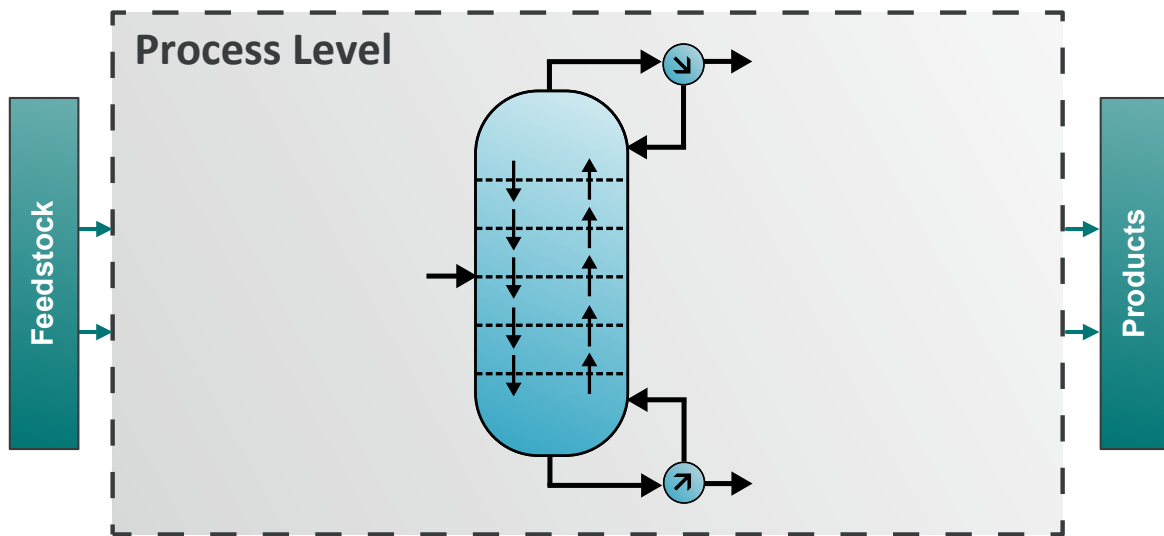


**Fig. 6.1** Schematic illustration of the process unit design task at the process level.

critical aspect for the resource efficiency of chemical processes is product purification due to the high energy demand and low energy efficiency of distillation columns [159]. Especially the backmixing of already separated streams within the column and large temperature differences in reboiler and condenser lead to large energy losses [160]. As a consequence, many papers were published in recent years that aim to identify energy optimal distillation column designs. Most of these publications are based either on shortcut methods such as the Fenske-Underwood-Gilliland method [161–163] or on rigorous tray-by-tray model formulations [164]. Bausa et al. [165] introduced a shortcut method using a new energy efficiency criterion by determining the pinch points of both column sections. In this way the minimum energy demand of non-ideal multi-component mixtures are estimated efficiently. Another shortcut method was proposed by Adiche and Vogelpohl [166], which allows the design of distillation columns for the separation of azeotropic mixtures. Caballero and Grossmann [167] provided a broad overview of the optimization of both individual distillation columns and distillation processes. Halvorsen and Skogestad [160] focused on energy-efficient distillation arrangements such as thermally coupled divided wall columns or multi-effect columns with additional heat transfer by pressure adjustment, which are particularly suitable for the modernization of existing plants. Ledezma-Martinez et al. [168] investigated crude oil distillation plants and showed that a preflash unit can reduce the heat demand. Jiang et al. [169] compared different process intensification strategies for multi-component distillation and investigated the possibility of using synergy effects to design distillation systems that are both energetically and economically efficient. In particular, the reduction potential by thermal coupling and simultaneous heat and mass integration is emphasized [170]. An overview of heat integrated distillation columns (HIDiC) is given by Nakaiwa et al. [171]. HIDiCs are a special configuration of multi-effect columns that allow internal heat transfer from the rectifying

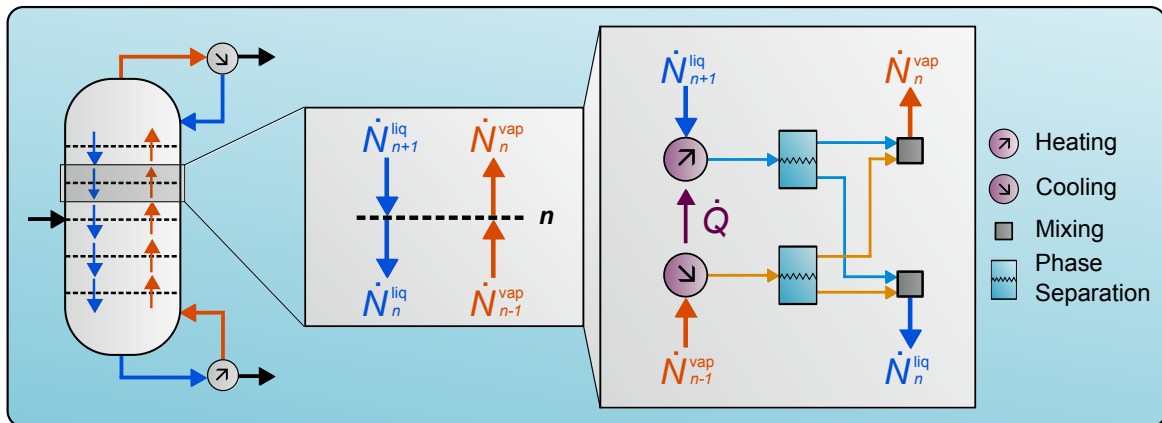


**Fig. 6.2** Representation of the overall distillation process as a sequence of elementary processes mixing (grey), heating/cooling (magenta) and flash separation (cyan) as well as single tray fluxes.

section to the stripping section. In combination with the use of heat pumps this leads to significant energy savings [172]. The use of heat pumps is also the focus of the selection scheme proposed by Kiss et al. [173]. The scheme identifies the most promising technologies for a given separation task. Similarly, an enumeration-based framework by Cui et al. [174] evaluates a variety of multi-effect processes, using shortcut methods to enable quick decision making [175]. In the literature there are further surrogate models that try to overcome challenges posed by dynamic operations [176] or the need for global optimization [86]. In contrast, Waltermann and Skiborowski [177] proposed a superstructure approach based on rigorous modeling to identify economically attractive distillation processes. In addition to the strong need for methods that allow a fast and efficient selection of different alternatives, there is also a necessity for process synthesis approaches to generate promising process alternatives. Papalexandri and Pistikopoulos [178] introduced a modular representation framework using a mass and heat exchange superstructure for process synthesis, which was also applied to distillation processes [179]. Shah and Kokossis [180] invented a synthesis framework that replaced the superstructure with a supertask representation. Since these methods are often only valid for ideal mixtures, Brüggemann and Marquardt [181] proposed a rapid screening approach for non-ideal mixtures, in which the distillation alternatives are ordered according to a suitable measure, such as energy consumption. A graph-theoretical approach that represents a chemical process as a network of nodes and edges leading to a mixed-integer optimization problem was presented by Friedler et al. [93]. In another work, this concept was used to solve separation network synthesis problems [182]. In contrast, Holiastos and Manousiouthakis [102] used an infinite dimensional linear programming approach to identify globally optimal distillation network designs.

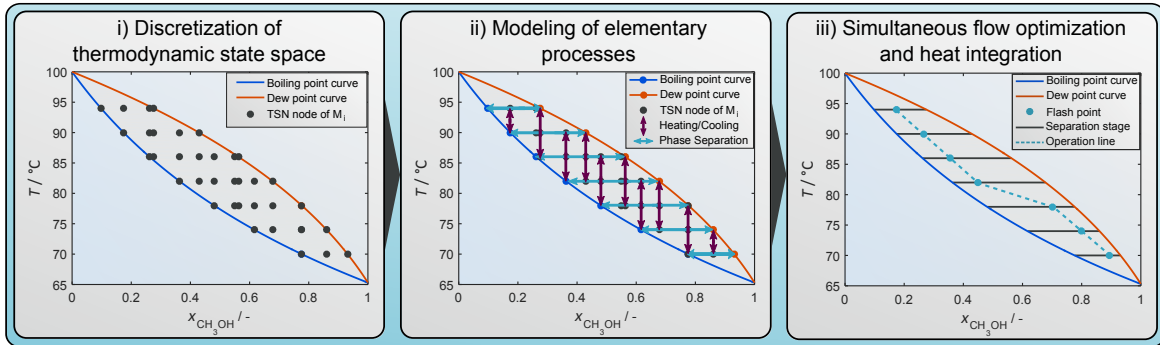


Fig. 6.3 Schematic illustration of the FluxMax approach for distillation column design.

## 6.2 FluxMax approach for distillation processes

Fig. 6.2 shows the representation of the distillation process by the elementary processes mixing, heating, cooling and phase separation. In a distillation column the mixing of hot vapor and cold liquid stream results in a distinct mixing temperature of each tray  $n$  that enables the phase separation. The FluxMax approach considers each flux separately: The hot vapor stream  $\dot{N}_{n-1}^{\text{vap}}$  has to be cooled to meet the tray temperature, and the cold liquid stream  $\dot{N}_{n+1}^{\text{liq}}$  has to be heated accordingly. Then, the phase separation of both streams takes place and the new vapor and liquid fractions are mixed together accordingly. The resulting liquid  $\dot{N}_n^{\text{liq}}$  and vapor  $\dot{N}_n^{\text{vap}}$  streams leave tray  $n$  and enter the neighboring trays.

Following the general idea of the FluxMax approach, the distillation design task can be divided into three steps as shown in Fig. 6.3: i) discretization of the thermodynamic state space, ii) modeling of the transitions between discrete state points, and iii) simultaneous flow optimization and heat integration.

### 6.2.1 Directed graph representation of distillation processes

In case of an isobaric distillation process, the thermodynamic state space is characterized by the thermodynamic coordinates temperature  $T$  and molar compositions  $x_\alpha$  of the components  $\alpha \in \mathcal{A}$ . According to Fig. 6.3, two types of EPNs are required, corresponding to the elementary processes of heating/cooling and phase separation. It is important to mention that no unique EPN is required for the mixing process as only mixtures with identical thermodynamic coordinates are mixed. Thus the TSNs themselves can be interpreted as mixers. The generalized stoichiometric coefficients for heating and cooling equal unity ( $M_1 \rightarrow M_2$ ), as the number of moles remains constant. The stoichiometric equation for each elementary phase separation process  $S_j$  is given as follows:



According to Chapter 5 the stoichiometric coefficients  $\chi_{(S_j)}^{(M_i)}$  are determined by the following equation system, where  $x_{\alpha,F}$  denotes the molar composition of component  $\alpha$  of the phase separator inlet flux, and  $x_{\alpha,B}$ ,  $x_{\alpha,D}$  denote the corresponding compositions at the boiling (B) and dew (D) point curves at phase change temperature:

$$x_{\alpha,F} = \chi_{(S_j)}^{(M_2)} x_{\alpha,B} + \chi_{(S_j)}^{(M_3)} x_{\alpha,D} \quad (6.2)$$

$$1 = \chi_{(S_j)}^{(M_2)} + \chi_{(S_j)}^{(M_3)} \quad (6.3)$$

Here it is assumed that the phase separator outlet is described by the vapor-liquid equilibrium. In general, non-ideal effects corresponding to efficiency losses or degradation effects could also be included, e.g. by introducing efficiency factors.

While there is no energy demand for the elementary process of phase separation, the specific heating  $\varphi_{(D_j)}^{\text{in}}$  or cooling  $\varphi_{(D_j)}^{\text{out}}$  demands are calculated from the enthalpy differences according to Eqs. (5.21) and (5.22).

### 6.2.2 Heat integration model

Again, the two different heat integration approaches – direct and indirect – are analyzed. Indirect heat integration refers to the use of UNs at a predefined temperature that provide the internal heat transfer. In contrast, the direct approach considers the direct coupling of hot and cold streams. This is shown in Fig. 6.4, where the blue and red curves correspond to the boiling point and dew point curves, respectively, and the blue and red arrows correspond to the liquid and vapor flows.

The choice of the heat integration approach – direct or indirect – as well as the number of utilities impact the degrees of freedom of the subsequent optimization. Fig. 6.4 A illustrates how the FluxMax approach enables the design of classic distillation columns by introducing a dedicated UN for each discrete flash temperature: For an assumed minimum temperature driving force of  $\Delta T_{\text{min}} = 0$ , a single column tray is represented. The magenta arrows in Fig. 6.4 A indicate the internal heat transfer from hot vapor stream (red arrow) towards cold liquid stream (blue arrow) via the corresponding UN.

Fig. 6.4 B shows how the consideration of additional utilities – with predefined temperatures between tray temperatures – increases the heat transfer options and thus the degrees of freedom. The additional UNs enable the heat transfer between vapor and liquid flows entering and leaving the same two trays  $n$  and  $n + 1$  as well as the classical transfer between vapor and liquid flow entering the same tray  $n$ . The consideration of an infinite number of utilities is

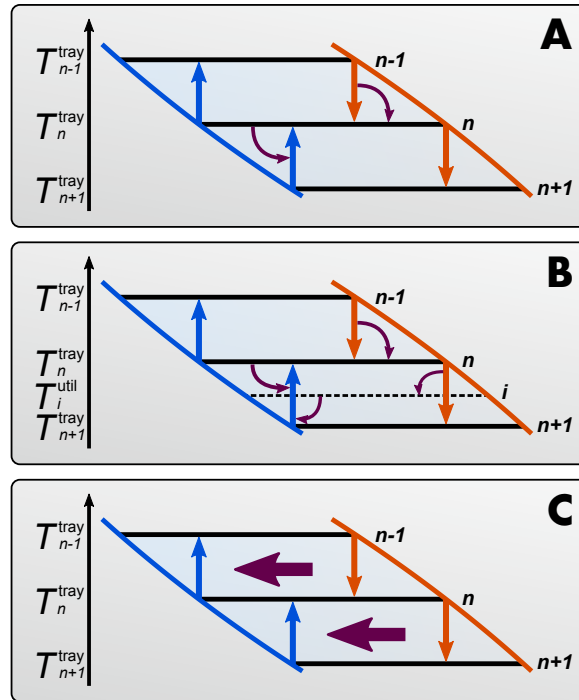


**Fig. 6.4** Schematic illustration of the heat integration model: For classic distillation columns by consideration of one utility for each tray (A), and for the exploitation of additional degrees of freedom: Applying indirect heat integration (B), and direct heat integration (C).

equivalent to the direct heat integration approach, where the hot vapor stream can transfer its heat directly to the cold liquid stream as illustrated in Fig. 6.4 C. While the direct approach leads to an increased computational effort, the calculation of the heat integration potential corresponds to the reduction potential obtained by pinch analysis – and thus to the maximum thermodynamically achievable – as shown in Chapter 5. In contrast, the indirect approach limits the computational complexity, but is only an approximation of the thermodynamically possible energy reduction potential.

## 6.3 Case Study

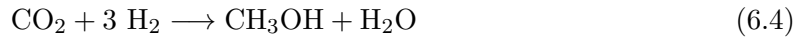
In this section the case study – the methanol-water separation – is introduced, followed by the derivation of the resulting optimization problems for both the FluxMax as well as the MESH formulation.

### 6.3.1 Methanol-water separation

Eq. (6.4) shows the reaction equation of the direct methanol synthesis from carbon dioxide and water, which can be regarded as a combination of the reverse water-gas-shift reaction and the carbon monoxide synthesis process [76].

**Tab. 6.1** Scenario definition of methanol-water separation.

parameter	symbol	unit	value
operating pressure	$p$	bar	1
feed temperature	$T^{\text{feed}}$	°C	80
bottom temperature	$T^{\text{bot}}$	°C	93.52
top temperature	$T^{\text{top}}$	°C	67.83
feed composition	$x_{\text{CH}_3\text{OH}}^{\text{feed}}$	-	0.50
bottom composition	$x_{\text{CH}_3\text{OH}}^{\text{bot}}$	-	0.10
top composition	$x_{\text{CH}_3\text{OH}}^{\text{top}}$	-	0.95



While the obvious advantage lies in the direct use of the greenhouse gas  $\text{CO}_2$ , the coupled by-production of  $\text{H}_2\text{O}$  is an unavoidable shortcoming that requires a downstream separation of the reactor output stream, even if all other possible side reactions – such as the production of higher alcohols or ethers [76] – are neglected. The unconverted gaseous reactants can be easily separated and recycled by cooling the reactor output stream and condensing the methanol-water mixture. However, a mixture of methanol and water is chemically unavoidable and must be further separated.

This separation task constitutes the case study of this chapter. Thereby, the focus is on the identification of non-conventional distillation designs with increased energy efficiency by exploiting the additional degrees of freedom provided by the consideration of additional heat integration possibilities introduced in section 6.2.2. The specifications of the scenario under consideration are listed in Tab. 6.1, assuming that the products are saturated liquid or vapor streams.

Following the three step procedure of the FluxMax approach introduced in section 3.2 and illustrated in Fig. 6.3 for distillation processes, the thermodynamic state space is discretized. The relevant thermodynamic state space for the isobaric binary separation of methanol and water is defined by the temperature  $T$  and the molar fractions of methanol  $x_{\text{CH}_3\text{OH}}$  and water  $x_{\text{H}_2\text{O}}$ . In addition, the entire thermodynamic state space is further limited by the vapor-liquid equilibrium which determines the attainable region. Assuming ideal conditions in both liquid and vapor phase, the boiling point curve which bounds the attainable region is computed as follows:

$$p = \sum_{\alpha \in \mathcal{A}} x_{\alpha} p_{\alpha}^{\text{sat}} \quad (6.5)$$

**Tab. 6.2** Antoine parameters for pure water and methanol for the relevant temperature range.

$\alpha$	$A_\alpha$	$B_\alpha$	$C_\alpha$	$T_{\text{low}}/K$	$T_{\text{up}}/K$	Reference
Water	4.6543	1435.264	-64.848	255.9	373	[183]
Methanol	5.2041	1581.341	-33.500	288.1	356.8	[184]

where  $p$  is the operation pressure and  $p_\alpha^{\text{sat}}$  the saturation pressure of component  $\alpha$ . The corresponding dew point curve is calculated by the equilibrium condition (Eq. (E.2)) and the definition of the equilibrium constant  $K_\alpha := y_\alpha/x_\alpha$ . Herein,  $x_\alpha$  and  $y_\alpha$  denote the liquid and vapor fraction, respectively.

$$K_\alpha = \frac{p_\alpha^{\text{sat}}}{p} \quad (6.6)$$

The saturation pressure depends on the temperature and can be expressed by the semi-empirical Antoine equation:

$$\log_{10} p_\alpha^{\text{sat}} = A_\alpha - \frac{B_\alpha}{T + C_\alpha} \quad (6.7)$$

The Antoine parameters  $A_\alpha$ ,  $B_\alpha$ , and  $C_\alpha$  for pure water and methanol are listed in Tab. 6.2. They are valid if the pressure is given in bar and the temperatures in K.

### 6.3.2 Formulation of optimization problems

Based on the model presented in the previous section, the optimization problem is derived in this section. In addition, the design optimization problem based on the MESH equations is introduced for validation purposes.

#### FluxMax formulation

The FluxMax approach is applied to two different objective functions: i) minimization of the number of separation trays ( $f^I$ ), and ii) minimization of the total energy duties ( $f^{II}$ ). The number of trays is minimal if the liquid reflux stream from the condenser to the top tray is maximized. According to the FluxMax formulation, this liquid reflux stream corresponds to the sum of all liquid fluxes  $\dot{N}_{(D_j)}^{\text{liq,top}}$  that are heated at the lowest tray temperature under consideration by means of the heater  $D_j \in \mathcal{E}$ .

$$f^I(\varphi) = - \sum_{D_j \in \mathcal{E}} \dot{N}_{(D_j)}^{\text{liq,top}} \quad (6.8)$$



The second objective function  $f^{\text{II}}$  seeks to identify the most energy efficient column design and can be written as sum of external heating  $\dot{Q}_{(U_i)}^{\text{ext,in}}$  and cooling duties  $\dot{Q}_{(U_i)}^{\text{ext,out}}$ , which are desired to be minimized:

$$f^{\text{II}}(\varphi) = \sum_{U_i \in \mathcal{U}} \dot{Q}_{(U_i)}^{\text{ext,in}} + \sum_{U_i \in \mathcal{U}} \dot{Q}_{(U_i)}^{\text{ext,out}} \quad (6.9)$$

A key parameter of distillation columns is the reflux ratio  $r$ , which is defined as ratio between liquid reflux stream from the condenser and the total top product stream  $\dot{N}_{\text{top}}$ :

$$r = \sum_{D_j \in \mathcal{E}} \frac{\dot{N}_{(D_j)}^{\text{liq,top}}}{\dot{N}_{\text{top}}} \quad (6.10)$$

### MESH formulation

The results that are obtained from the FluxMax formulation of the column design problem are benchmarked with results that are obtained from the solution of the MESH equations. With the MESH equations, the distillation column design is addressed using a tray-by-tray formulation [164]. The characteristic of the MESH equations is the solution of mass (M), equilibrium (E), summation (S) and energy balance in its enthalpy form (H) for each tray. Each tray is considered as equilibrium stage, which means that vapor and liquid flows leave the tray at thermodynamic equilibrium. Fig. 6.5 A illustrates the flows interacting with trays  $n$  and  $n + 1$ . An overall distillation column for a binary mixture with reboiler and condenser duties has five degrees of freedom that are typically fixed using the feed condition as well as top and bottom product specifications. If heating and cooling duties can be theoretically provided at each tray, the degrees of freedom are increased by  $n_{\text{tray}} - 2$  where  $n_{\text{tray}}$  is the total number of trays including reboiler and condenser trays. Thus the tray temperatures can be set to any desired values.

Optimizing the tray temperature for a given feed and top/bottom product specification leads to the optimization problem in Eq. (6.12) where all mass fluxes between trays, tray duties and tray temperatures are decision variables that are contained in the vector  $\varphi = (\dot{N}^{\text{feed}}, \dot{N}^{\text{liq}}, \dot{N}^{\text{vap}}, \dot{Q}_n^{\text{ext}}, \dot{Q}_n^{\text{out}}, \mathbf{T}_n)^\top$ .  $\dot{N}^{\text{feed}}$  is the vector of feed mass fluxes that is not illustrated in Fig. 6.5. The objective function is the sum of external heating  $\dot{Q}_n^{\text{ext}}$  and cooling  $\dot{Q}_n^{\text{out}}$  requirements (Eq. (6.11)) of all trays  $n$  which is a linear objective function.

$$f(\varphi) = \sum_{n=1}^{n_{\text{tray}}} \dot{Q}_n^{\text{ext}} + \sum_{n=1}^{n_{\text{tray}}} \dot{Q}_n^{\text{out}} \quad (6.11)$$

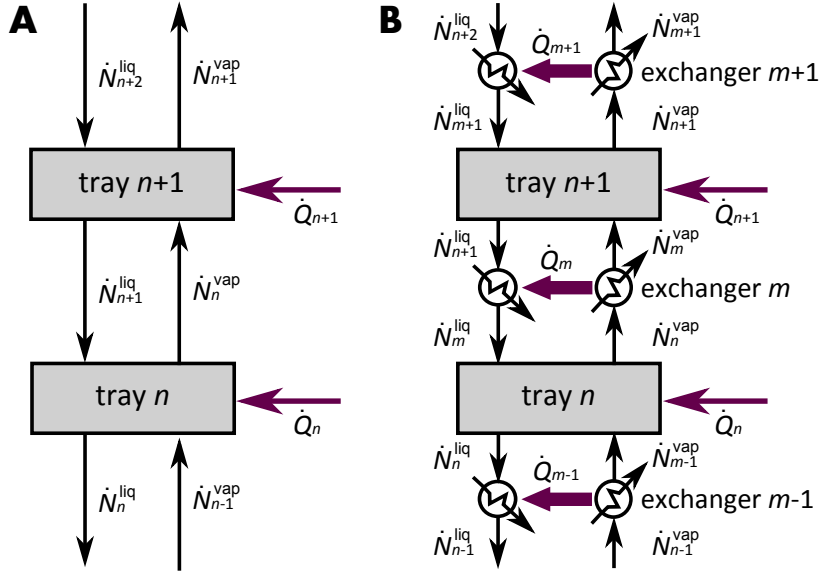


**Fig. 6.5** Schematic illustration of tray  $n$  and neighboring tray  $n + 1$  for the regular formulation of MESH equations (A) and for the case where intermediate heat exchangers  $m - 1$ ,  $m$  and  $m + 1$  are considered (B).

However, the equality constraints that contain the tray models are non-linear equations as derived in the Appendix E.1. The resulting non-linear programming problem (NLP) is given as:

$$\begin{aligned} \min_{\varphi} \quad & f(\varphi) \\ \text{s.t.} \quad & h(\varphi) = \mathbf{0} \\ & \varphi_{lb} \leq \varphi \leq \varphi_{ub} \end{aligned} \quad (6.12)$$

The system of the MESH governing equations is contained in  $h(\varphi)$  and the lower  $\varphi_{lb}$  and upper bounds  $\varphi_{ub}$  correspond to non-negativity constraints and external feed and product specifications.

As an additional benchmark for the FluxMax results, the MESH equations are extended with  $n_{HX} = n_{tray} - 1$  heat exchangers in order to enable heat exchange between vapor and liquid fluxes between trays as depicted in Fig. 6.5 B and derived in the Appendix E.1. Mass and energy balances for the heat exchangers are added to the system of model equations  $h(\varphi)$  and the heat flows  $\dot{Q}_m$  of the  $m$ -th heat exchangers are added as new decision variables. Furthermore, feasibility constraints for the inter-tray heat exchange must be fulfilled:

$$T_n^{vap} \geq T_m^{liq} + \Delta T_{min} \quad m = 1, \dots, n_{HX} \quad (6.13a)$$

$$T_m^{\text{vap}} \geq T_{n+1}^{\text{liq}} + \Delta T_{\text{min}} \quad m = 1, \dots, n_{\text{HX}} \quad (6.13b)$$

These feasibility constraints are added to the optimization problem as inequality constraints  $g(\varphi)$ . They ensure that the temperature from the bottom to the top of the column is decreasing monotonically.

## 6.4 Results

The results are divided into three parts. The first part is the application of the FluxMax approach to classical distillation design tasks. Particularly the influence of the selected discretization is analyzed. In contrast, the second part emphasizes the exploitation of additional degrees of freedom by the FluxMax formulation. It is shown that an improved heat transfer between vapor and liquid streams drastically reduces the energy demand. Since the exploitation of the energy reduction potential requires an improved heat transfer, the third part evaluates implementation of the additional heat transfer and the influence of the minimum driving force of the heat transfer on the required heat exchange area.

### 6.4.1 Application to conventional distillation design tasks

#### Optimal design of distillation processes

Fig. 6.6 depicts the equilibrium diagram as temperature  $T$  versus molar fraction  $x_{\text{CH}_3\text{OH}}$  of the low boiler methanol for a temperature discretization of 17 stages. The heat integration model for identifying classical distillation columns according to Fig. 6.4 A is used. The vapor-liquid area between boiling and dew curve is the attainable region (gray area) of the thermodynamic state space for the column design: All EPNs/TSNs are located in this region. The molar fraction  $x_{\text{H}_2\text{O}} = 1 - x_{\text{CH}_3\text{OH}}$  of the missing component water can easily be calculated. The attainable region is enclosed by the boiling point curve (blue) and the dew point curve (red). In addition, the inlet and desired product specifications are marked as magenta and green dots. The black dots in Fig. 6.6 correspond to the TSNs and thus to the discrete points in the thermodynamic state space, which are connected by the elementary processes heating or cooling in vertical direction and phase separation in horizontal direction (see also Fig. 6.3). The left-hand side of Fig. 6.6 shows the actual state space representation of the optimal pathways according to the considered objective function. The active elementary processes along the different TSNs from the feed TSN – magenta point – to the lower and upper product TSNs – green points – are indicated by the cyan lines.

Once the optimal solution has been found, all liquid and vapour flows entering or leaving a particular tray and the corresponding molar composition are known. This allows the calculation of the actual mixing points (Fig. 6.6 B and D cyan points) at each tray. The

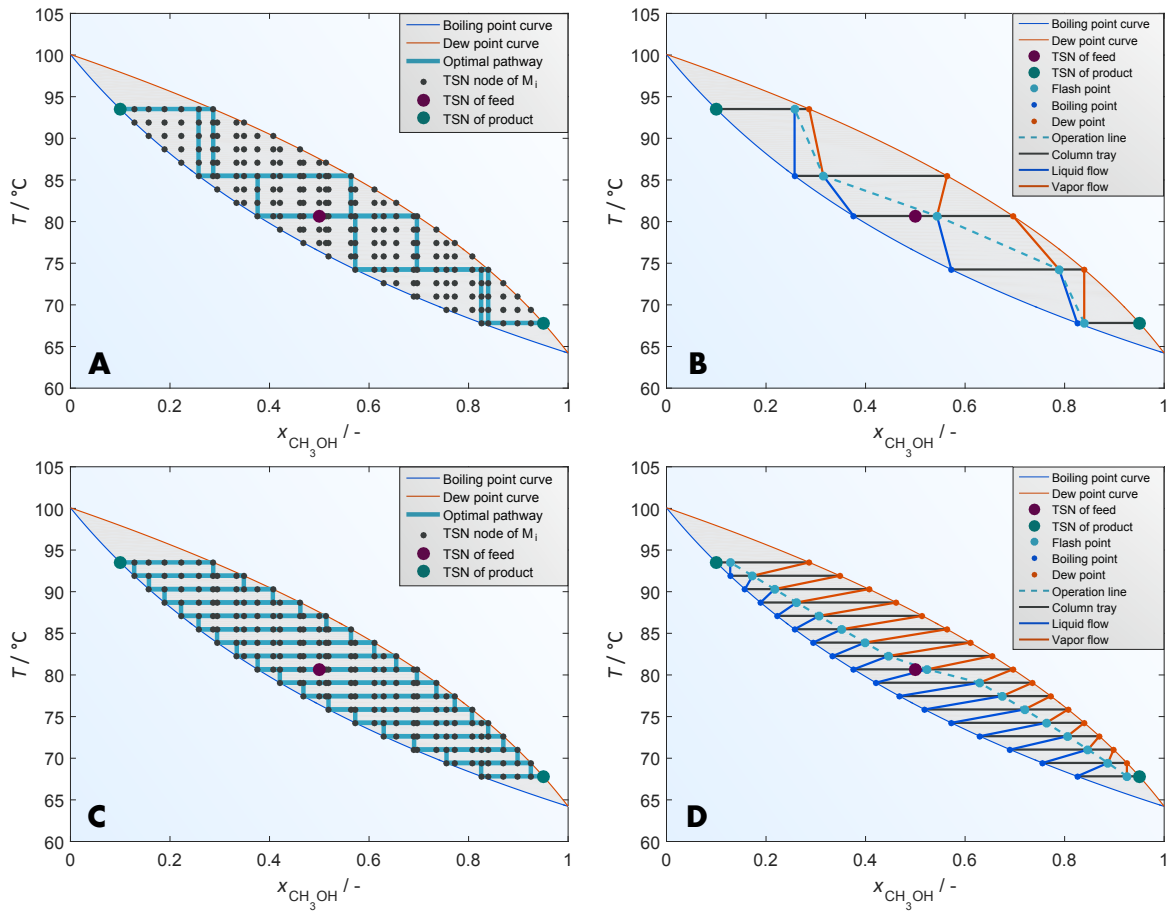


**Fig. 6.6** Optimal pathway within the thermodynamic state space for the two objective functions (Eqs. (6.8) and (6.9); left-hand sides), and corresponding operation line for a temperature discretization of 17 (right-hand sides); minimization of number of trays (A,B), and total energy minimization (C,D).

resulting operation lines (dashed cyan line) are shown on the right-hand side of Fig. 6.6. In addition, the corresponding liquid (red line) and vapor (blue line) flows are shown.

The two upper diagrams (Fig. 6.6 A and B) show the optimal results for the first objective: Minimizing the number of trays (Eq. (6.8)). The optimization algorithm reveals that the separation task in this scenario (Tab. 6.1) requires at least five separation trays. In order to achieve the desired product purification with the minimum number of trays, stages with as different temperatures as possible are selected. The resulting operation line has the shape of a zigzag curve, with the slopes between the first two or the last two trays being as steep as possible. While the number of trays is minimal, the energy duty (534.0 kW/mol<sub>feed</sub>) and the reflux ratio (7.83) are very high. The beginning of each distillation column design is the calculation of the minimum number of stages. This is typically achieved using the Fenske equation [161], but the results in Fig. 6.6 A show, that the FluxMax approach returns the same minimum number of trays.

The lower two plots (Fig. 6.6 C and D) correspond to the most energy efficient column design. As expected, the optimal path is found when phase separation occurs at all possible discrete temperature levels. It can be seen that starting from the TSN of the feed, the mixture is split into the corresponding saturated equilibrium states, which are then cooled or heated to the next possible temperature considered, which represents a different column tray. The resulting operation line in Fig. 6.6 D is located in the stripping section of the column near the boiling point curve and in the rectifying section near the dew point curve. The total energy demand is 36.0 kW/mol<sub>feed</sub> and the reflux ratio is 0.25.

Both results are consistent with the expectation that the total energy demand is inversely proportional to the number of trays. In the following, the FluxMax approach is utilized using additional degrees of freedom. It is shown that improved heat exchange leads to the same energy reduction as an increase in the number of stages. To illustrate the effect for a different number of stages, it is necessary to force the optimizer to select a certain number of trays. However, unlike the MESH equations, FluxMax formulations are based on a flux optimization on a predefined temperature grid. There the energy minimum is always found for the maximum number of stages, which corresponds to the selected temperature discretization as can be seen in Fig. 6.6 C. In order to be able to use the same discretization – which guarantees the comparability of the results – and still force the optimization algorithm to select only a limited number of trays, integer variables  $y_n$  are introduced below for each tray. In this way, the actual number of selected trays  $n_{\text{tray}}$  is limited by the following inequality:

$$\sum_{n=1}^{n_{\text{tray}}} y_n \leq n_{\text{tray}} \quad (6.14)$$

Although the remaining FluxMax formulation remains the same, it is important to note that the following figures are based on a mixed integer linear program (MILP) solved with the help of the efficient MILP solver SCIP [185].

Fig. 6.7 illustrates again the operation lines for the most energy efficient design identified for a discretization of 17 temperature levels. However, unlike Fig. 6.6, the newly added constraints limit the selectable levels to 9 (Fig. 6.7 A), and 11 (Fig. 6.7 B), respectively. Interestingly, the optimization algorithm selects the stages in a way that more trays are active near the feed point and only a few in the remaining stripping and rectifying section. By selecting trays with smaller temperature differences in the feed section of the column, a better approximation to the optimal operating line for the unlimited case is achieved (Fig. 6.6 D). Again, the calculated results correspond well to the known temperature profiles of classical distillation columns [164].

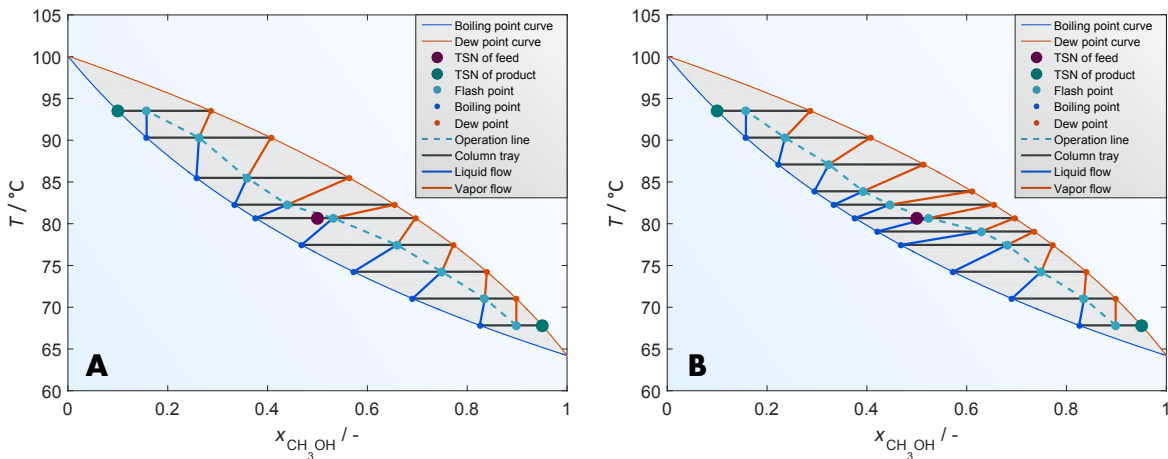


**Fig. 6.7** Operation line for a discretization of 17 temperature levels if the number of selectable tray stages is limited to 9 (A), and 11 (B) .

### Influence of the temperature discretization

While the benefit of the FluxMax formulation is the decoupling of the non-linearities from the optimization step by discretization of the thermodynamic state space, the disadvantage is the grid dependence of the obtained results. Therefore, in the following the energy demand is analyzed as a function of different temperature discretizations, corresponding to the maximum number of trays. Fig. 6.8 shows the influence of the selected temperature discretization on the energy demand for the classical column design task as shown in Fig. 6.4 A. For each discretization – 5, 9, 17, 33 – the temperatures are distributed equidistantly between the desired top and bottom product temperatures. This ensures two prerequisites: i) a separation tray is always considered at the considered feed inlet temperature, and ii) for each finer discretization, the same temperatures of the coarser grids are considered in addition to the newly added temperatures. While the first condition ensures that no pre-heating or pre-cooling of the feed is required, the second condition allows a fair comparison of the different cases. In addition to the results obtained by the FluxMax formulation, the energy duties calculated from the classical MESH equations are shown in Fig. 6.8.

As expected, Fig. 6.8 shows that the calculated total energy demand depends strongly on the discretization. The finer the grid, the more the calculated energy duties correspond to the MESH results. In case of the coarsest discretization of only 5 temperature steps, the calculated energy demand does not depend on the limitation of the selectable stages, because the maximum number of trays is only 5. In the other cases, however, the grid dependency decreases with increasing number of actually selected trays. Even with a discretization of 9 temperature levels, the FluxMax results are quite close to the MESH results if the number of selected trays is bigger than 7. In contrast, the selection of an appropriate grid is crucial if the number of trays is low. However, it is important to note that the

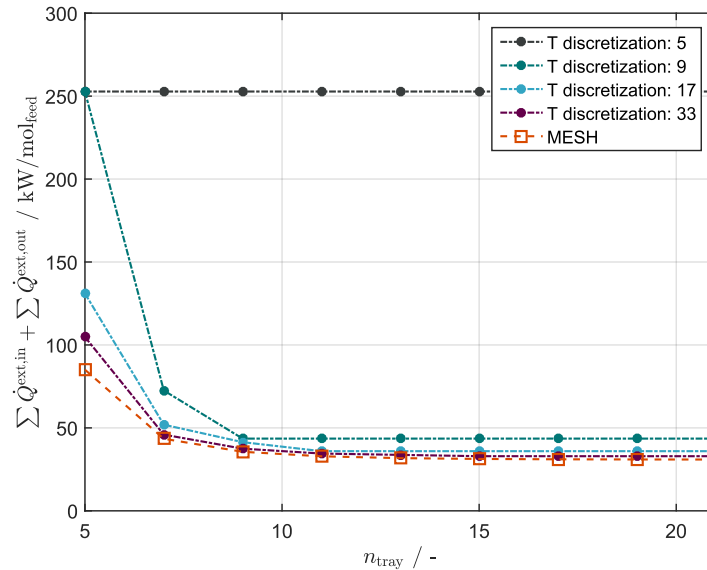


**Fig. 6.8** Influence of number of separation stages on the total energy duty if no additional heat transfer is considered. Illustrated are the results of the FluxMax formulation considering different temperature discretizations (5, 9, 17, and 33 temperature levels) as well as of the classical MESH formulation.

accuracy of the FluxMax formulation can be improved not only by finer grids, but also by the selected temperatures. Both formulations have the same energy requirement when the actual tray temperatures calculated with the MESH equations are used as input for the FluxMax formulation. The discretization procedure with adding new temperature levels is bound to this example. Separation tasks featuring, for example, azeotropic points or other non-ideal behavior may require different discretization schemes.

#### 6.4.2 Energy-efficient designs by additional heat transfer

The following shows the influence of the additional heat transfer options as shown in Fig. 6.4 B and C. Within the FluxMax approach, each mass and heat flux is modeled separately. The formulation thus allows the identification of non-conventional configurations. In the case of the distillation column, the consideration of improved heat transfer between liquid and vapor streams – enabled either by direct or indirect heat integration – results in a lower energy consumption compared to classical column design. Fig. 6.9 illustrates the energy requirements for the configurations with improved heat integration. A theoretical minimum temperature difference of  $\Delta T_{\min} = 0$  K is assumed, which is technically not possible, since it would require an infinitely large heat exchange area. In this way, however, the theoretically maximum amount of heat that can be transferred is evaluated. Later, the influence of different minimum driving forces will be examined in more detail. Furthermore, the energy

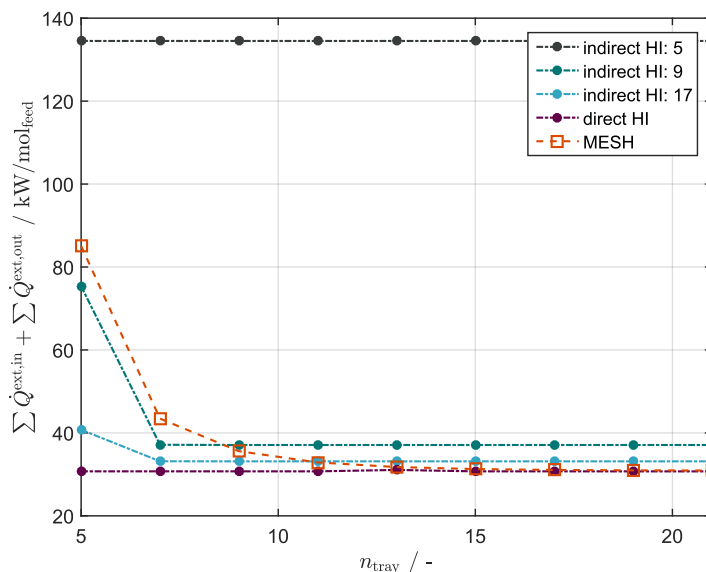


**Fig. 6.9** Influence of number of separation stages on the total energy duty if additional heat transfer is considered. Illustrated are the results of the FluxMax formulation considering different temperature discretizations (5, 9, and 17 temperature levels) as well as of the MESH formulation as a benchmark.

requirements calculated with the MESH equations are presented as a benchmark. For indirect heat integration, the discretization, which corresponds to the number of utility nodes, plays a role: An additional utility node is introduced at the intermediate temperature of two neighboring separation stages. Thus, the more auxiliary nodes are considered, the more additional heat transfer options are available, resulting in lower energy requirements. In any case the energy demand is lower compared to non-heat integrated columns (see Fig. 6.8). Compared to the benchmark case, the largest energy saving potential is observed when the maximum number of stages is small ( $\leq 9$ ). In this range, even rather coarse discretizations lead to more energy efficient configurations: Even a temperature discretization of 9 – corresponding to 17 utility levels – result in a lower energy consumption as the classical MESH design. For a larger number of stages, however, the optimizer cannot find better configurations because the discretization is limited.

However, if direct heat integration is considered, which corresponds to an infinite number of utility nodes, the calculated results are independent of the temperature discretization. For any number of stages, the same theoretically feasible minimum energy requirement is calculated at 30.7 kW for each mole of feed flux, resulting in energy savings of up to 64 % compared to classical MESH designs. The calculated heat integration potential has also been validated using the extended MESH equations, which result in the same results as the direct heat integration approach. Since the energy demand of standard columns decreases rapidly



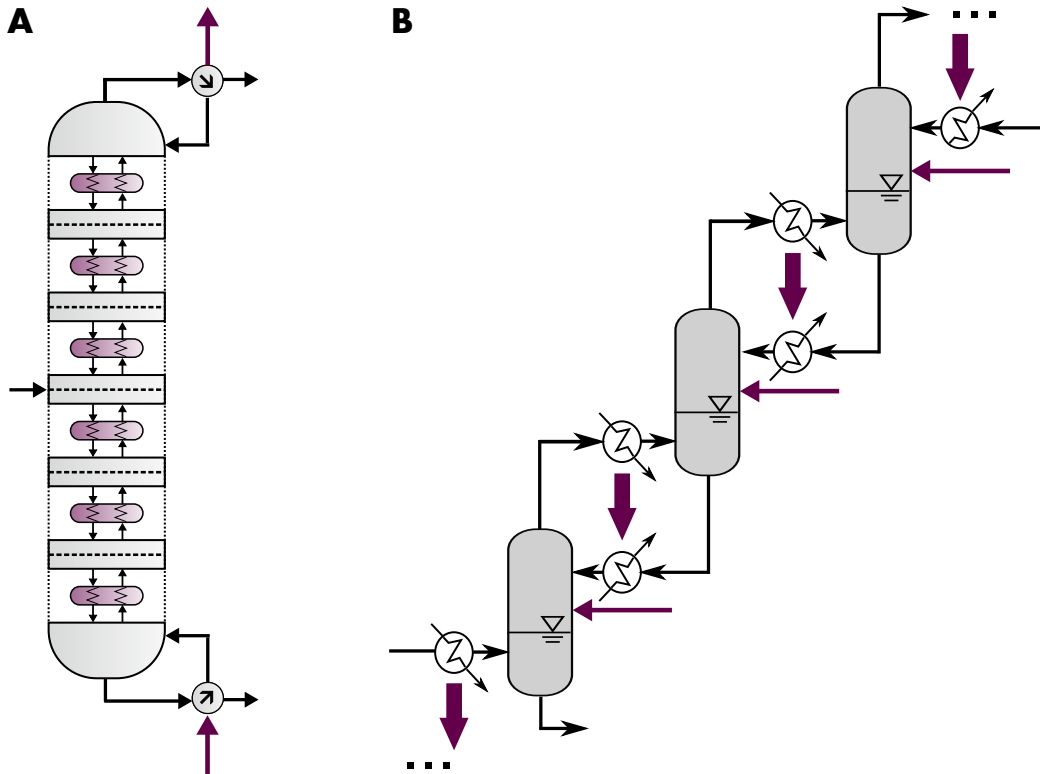


**Fig. 6.10** Schematic illustration of a column with intermediate heat exchangers (A), and the corresponding interpretation as a series of heat integrated flash drums (B).

with an increasing number of stages, the potential for columns with improved heat transfer decreases with each additional tray.

If the direct heat integration result is taken as the minimum energy requirement and thus the most energy efficient configuration, it is evident that an improved heat transfer (at  $\Delta T_{\min} = 0$  K) corresponds to a classical column design with an infinite number of trays. Consequently, there is a trade-off between additional separation stages – corresponding to the column’s vapor/liquid mass transfer area – and additional heat transfer area. Before discussing the influence of considering different minimum driving forces  $\Delta T_{\min}$  on the required heat transfer area, Fig. 6.10 A shows the additional heat transfer within the column schematically. A two-phase heat exchanger transfers the heat provided by the hot vapor stream flowing between two stages to the cold liquid stream flowing in the opposite direction. The practical realization of two-phase heat exchangers is beyond the scope of this work, therefore the interested reader is referred to adequate literature [186, 187]. In contrast to the MESH formulation, the FluxMax formulation is not associated to a particular design. As a consequence, besides the representation as a classic distillation column (Fig. 6.10 A), the resulting configuration can also be interpreted as a series of heat integrated flash drums with intermediate heat exchange (Fig. 6.10 B). The interpretation as flash drums allows a simpler technical realization as well

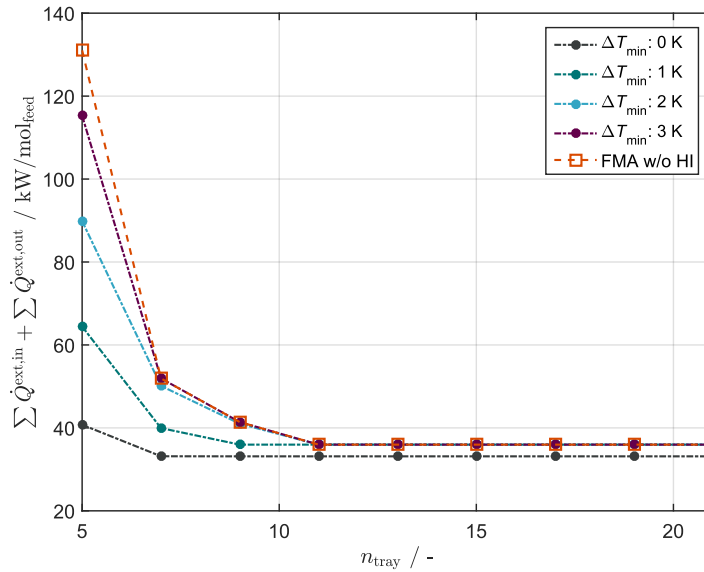


**Fig. 6.11** Influence of the selected minimum temperature difference  $\Delta T_{\text{min}}$  of the additional heat transfer. Illustrated are the heat integrated results for  $\Delta T_{\text{min}} = 0, 1, 2, 3 \text{ K}$  as well as the non-integrated result as a benchmark for discretization of 17 temperature stages.

as the modular design of the separation system. The latter is particularly interesting in the context of R2Chem, where smaller decentralised plants are discussed to make efficient use of excess electrical energy. According to Fig. 6.9 a sequence of a minimum number of flash drums is sufficient to reduce the total energy demand drastically.

### 6.4.3 Implementation of the improved heat transfer

#### Influence of the minimum driving force $\Delta T_{\text{min}}$

In all calculations of this chapter up to this point, a minimum driving force of  $\Delta T_{\text{min}} = 0 \text{ K}$  is assumed. To obtain finite areas, a minimum driving force  $\Delta T_{\text{min}} > 0 \text{ K}$  must be present. Fig. 6.11 illustrates the influence of the assumed minimum temperature difference  $\Delta T_{\text{min}}$  on the actual energy demand. In addition to the results obtained by considering four different minimum driving forces ( $\Delta T_{\text{min}} = 0, 1, 2, 3 \text{ K}$ ), the non-heat integrated case is presented as a benchmark. All results are based on a discretization of 17 temperature levels.

The black curve ( $\Delta T_{\text{min}} = 0 \text{ K}$ ) and the red benchmark curve (non-heat integrated case) are the same as the corresponding curves in Fig. 6.8 and Fig. 6.9. They represent both the best and worst case scenarios for a given temperature discretization. Two observations can be made: i) the bigger the minimum driving force becomes, the bigger the energy duties become and the closer the curve becomes to the benchmark curve, and ii) for a certain number of stages there is no heat integration potential for  $\Delta T_{\text{min}} > 0 \text{ K}$ . Both observations indicate

for the case study under consideration that, on the one hand, there is an enormous energy saving potential for a small number of stages, but that this potential can only be used for very small driving forces. Even at a minimum temperature difference of  $\Delta T_{\min} = 3$  K, which is already very small compared to the usually technically applied minimum driving forces of  $\Delta T_{\min} > 10$  K, the potential almost disappears. However, there may be technical solutions that can exploit the identified energy saving potential. A possible realization of the calculated design could be the concept of horizontal columns, where the contact time between vapor and liquid streams is increased and adjusted by the tilt angle of the column [188, 189].

### Evaluation of the required heat exchanger area

The previously presented results show that improved heat transfer reduces drastically the energy demand of distillation columns. However, the heat has to be transferred across very small temperature differences, which results in a low driving force for the heat transfer and thus large heat exchange areas. The heat exchange area  $A_{(E_j)}^{\text{HX}}$  that is required for each EPN  $E_j$  depends on the sum of received heat fluxes and the corresponding mean logarithmic temperature differences  $\Delta T_{m,(E_j)}^{(E_i)}$  and  $\Delta T_{m,(E_j)}^{(U_l)}$  of the internal heat transfers between EPNs  $E_i$  as well as UNs  $U_l$  towards  $E_j$ . Furthermore, the heat exchanger area is inversely proportional to the heat transfer coefficient  $k^{\text{HX}}$  as given in Eq. (4.19).

The heat transfer coefficient  $k^{\text{HX}}$  depends on the fluids and the type of heat exchanger. A constant value of  $3,000$  W/m<sup>2</sup>K is assumed for the two-phase heat exchange, which corresponds to a vapor-liquid heat transfer in a spiral plate heat exchanger [190]. It is evident that there is a trade-off between an increase in internal heat flows – corresponding to a reduction in operating costs – and more heat transfer area corresponding to an increase in capital costs. A multi-objective optimization is performed by applying the  $\epsilon$ -constraint method [191]. Therefore, one of the competing targets (Eq. (4.19)) is added as an additional constraint to the optimization problem. As a result, the Pareto-optimal point of the second objective (Eq. (6.9)) is calculated. By systematic variation of the heat exchanger area, the Pareto curves for distinct number of stages and a minimum driving force  $\Delta T_{\min} = 0$  are generated and plotted in Fig. 6.12.

The Pareto curves denote the limits at which an improvement of one objective is only possible if the second objective is simultaneously worsened. According to Fig. 6.9 it can be seen that the energy saving potential decreases with an increasing number of stages. Interestingly, the slope of the curves is steepest for small heat exchanger areas. This means that a rather small heat exchanger area leads to a rather large energy saving potential, especially for small columns with a small number of stages. After the first steep decline, the curves become flatter, which corresponds only to a small energy reduction. Consequently, the required area is very high if the full integration potential is to be exploited at the minimum number of stages. The

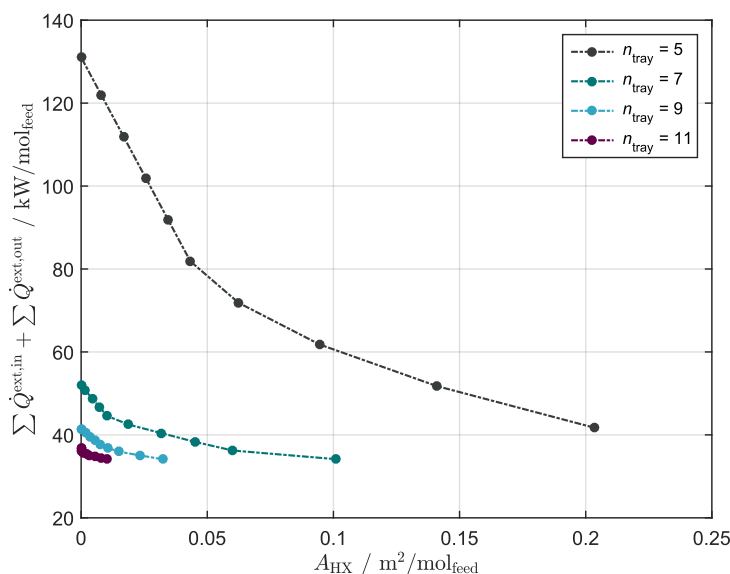


**Fig. 6.12** Pareto curves of the two competing objectives: Minimization of total energy duty and minimization of additional heat transfer area for different number of separation stages: 5, 7, 9, and 11 stages.

heat transfer area required to save a separation tray also becomes smaller for larger columns. While a heat exchange area of almost  $0.14 \text{ m}^2/\text{mol}_{\text{feed}}$  is needed to achieve the same energy demand for 5 stages compared to a column with 7 stages, only  $0.025 \text{ m}^2/\text{mol}_{\text{feed}}$  is sufficient to save two additional trays.

Fig. 6.12 also summarizes the main results of this chapter. It shows that an improved heat exchange reduces the energy demand up to 64 % compared to classic distillation columns, and thus can contribute to the reduction of carbon dioxide emissions. For the case study under consideration, however, heat transfer across very small temperature differences is required, which result in additional heat exchanger areas up to  $0.21 \text{ m}^2$  per mole feed stream. Nevertheless, the separation of different mixtures – with more distant boiling points – could have a greater potential for larger temperature differences and thus less heat exchange area.

## 6.5 Chapter summary

Distillation processes are an essential component of any chemical plant for the separation and purification of condensable mixtures. However, distillation columns account for the largest contribution to the total energy consumption of chemical processes due to their high heat demands. Consequently, there is a strong need for energy efficient column designs to reduce drastically the carbon dioxide emissions and thus to reach the settled climate goals of the chemical industry. In order to achieve optimal designs, the FluxMax approach

decouples process-based non-linearities from the optimization problem by discretizing the thermodynamic state space and representing the distillation process by three elementary processes: Mixing, heating/cooling and phase separation. The versatility of the FluxMax approach was demonstrated by applying two different objective functions: Minimizing i) the number of trays, and ii) the energy demand. As a consequence of the simultaneous consideration of heat integration by introducing inequality constraints, the design space was increased compared to classical design methods based on the MESH equations. A non-conventional design was identified that outperforms classical distillation column designs based on the MESH equations. The last research question (V) was answered by demonstrating that an improved heat transfer between hot vapor streams and cold liquid streams – with the consequence of additional heat exchange area – reduces the energy consumption in the same way as additional separation stages of classical columns. In this way, the idealized design based on the FluxMax formulation reduces the energy consumption by up to 64 % compared to conventional designs. The trade-off between the reduction in energy demand – corresponding to lower operating costs – and the increase in heat exchange area – corresponding to higher capital costs – was analyzed through multi-objective optimization. The MESH equations were extended and used to validate the FluxMax design and proved that the achieved results are thermodynamically consistent. The results underline the strength of the FluxMax approach to design distillation processes with increased degrees of freedom, which allows the identification of highly energy efficient designs.

However, the presented results show that heat must be transferred across very small temperature differences to fully exploit the identified energy reduction potential. Nevertheless, it is possible that separation tasks for other mixtures – with more different boiling points of the pure components – also have a high potential for higher temperature differences, which would lead to a lower requirement of heat exchange area. The practical implementation of the highly energy-efficient designs by using horizontal columns is also possible, which reduces the surface area by improving the heat transfer by extending the contact time of vapor and liquid streams. The identified energy potential is of particular interest for applications with a limited number of trays, e.g. decentralized or modularized container systems, as the FluxMax design can be represented as a cascade of heat-integrated flash drums with intermediate heat exchange.



# Chapter 7

## Conclusions

In this final chapter, the main conclusions are drawn and placed in the broader context of the global challenges facing the world in the context of the energy transition. Of course, research is never complete, and every step towards gaining new insights raises new, unanswered research questions. For this reason, an outlook is provided to indicate possible future research activities that may result from the findings presented in this dissertation.

### 7.1 Summary

Most of the global challenges mentioned in Chapter 1 are caused by the world's unquenchable thirst for energy and the resulting harmful GHG emissions, especially CO<sub>2</sub> emissions. Without strong efforts and effective climate protection measures, the world's population will have less than 10 years to reach the target of 1.5 °C announced in the Paris Agreement and less than 25 years to reach at least the target of 2 °C. For the chemical industry, this means a massive reduction in GHG emissions by substituting fossil-based raw materials with alternative raw materials, such as biomass and CO<sub>2</sub>, and significant improvements in energy efficiency. Both the effective analysis of the current system and the derivation of future strategies for a more sustainable chemical production require the development of novel, powerful computer-aided tools. Such tools must be able to design sustainable and energy-optimized processes across different process hierarchies in order to use renewable energy sources as efficiently as possible. Before the results of the individual chapters are concluded individually, the most important outcomes of this dissertation are summarized below:

- Development of the scale-independent FluxMax approach for process design and synthesis with simultaneous consideration of heat integration by discretization of the thermodynamic state space.

- Thorough evaluation of several target molecules frequently discussed in the context of R2Chem to establish a roadmap for the efficient use of valuable energy from renewable sources.
- Systematic analysis of a variety of raw materials and energy sources to evaluate economically efficient and low-carbon (or even carbon consuming) chemical production networks at the production system level.
- Identification of non-intuitive process configurations by exploitation of synergy effects to drastically reduce energy consumption (and thus CO<sub>2</sub> emissions) at the plant level. The identified process outperforms configurations obtained by sequential design approaches (99 % heat saving compared to 88 %) due to an enhanced heat integration potential.
- Unit design of highly energy-efficient distillation columns, leading to significantly lower energy consumption (up to 64 %) compared to classical designs by exploiting additional degrees of freedom at the process unit level.

## 7.2 FluxMax approach

Today's global challenge to achieve a successful transition from fossil-based to renewable-based chemical production, and thus the need to solve problems at different levels of the process hierarchy, led to the development of the FluxMax approach: The scale-independent methodology for process design and synthesis under simultaneous consideration of heat integration. The introduction of thermodynamic state nodes (TSN), elementary process nodes (EPN), utility nodes (UN), and work utility nodes (WUN) enables the representation of arbitrary chemical processes as a directed graph, with edges corresponding to the mass and energy fluxes to be optimized. All mixtures in the process are uniquely determined by thermodynamic coordinates and thus assigned to a unique TSN. The EPNs facilitate the thermodynamic state change between the TSNs. Therefore each elementary process is described in a uniform way. By introducing a generalized process extent number, a stoichiometric equation is formulated for each elementary process type. The generalized process extent number is also used to formulate a continuous flow optimization problem that identifies the optimal path within the discretized thermodynamic state space. The discretization of the thermodynamic state space effectively decouples the process-based non-linearities from the network optimization problem, leading to a linear feasible region. By adding additional inequality constraints, heat integration is considered as an integrated part of the flow optimization.

In addition to the main features of simultaneously considering heat integration and uniformly representing each chemical process as a directed graph by introducing generalized stoichiometric equations, the FluxMax approach has another important aspect: The FluxMax approach



is independent of the process scale under consideration. EPNs can correspond to: i) whole processes for the optimization of chemical production networks at the production system level, ii) process units for the optimization of chemical processes at the plant level, or iii) elementary processes for the optimization of process units. This is made possible by the uniform description of each type of chemical transition through stoichiometric equations that introduce generalized stoichiometric coefficients  $\chi_{(E_j)}^{(M_i)}$ . The energy requirements – heating, cooling and power supply – are considered by specific heat  $\varphi$  and work  $\omega$ , which can be evaluated a priori by suitable (not-linear) models. In this way, it is also possible to overlap different scales by using rigorous models to describe elementary processes of special interest, while lumped models are used for less important elementary processes. Therefore, the FluxMax approach is a powerful tool that identifies optimal, non-intuitive process paths and process configurations. Especially if the underlying models are highly non-linear, some obstacles of classical non-linear optimization approaches could be overcome at the price of a solution that depends on the discretization of the thermodynamic state space.

The FluxMax approach presented in Chapter 3 was developed in collaboration with Georg Liesche at the MPI Magdeburg and developments to the version presented here have been published in several journal publications and are mainly based on [138, 139]. Especially the heat integration model has been continuously developed further [157].

Future developments of this methodology include the consideration of process-related uncertainties by applying robust or stochastic optimization techniques. The detailed investigation of intelligent grid generations should also be carried out in the future, since discretization plays such a large role for the accuracy of the results and is the limiting factor in terms of computational complexity and time. In particular, the possibility of adaptive grid refinement strategies should be investigated, since initial investigations in the context of this dissertation have led to promising results. Promising future directions regarding the introduction of further nodes, e.g. corresponding to storage tanks, would allow the investigation of a variety of other highly relevant research questions within the context of R2Chem, e.g. the identification of flexible processes considering dynamically changing process conditions (e.g. due to the fluctuating availability of renewable energy sources). Finally, the applicability of the FluxMax approach to further levels of the process hierarchy, such as the phase or molecular level, could be explored. Possible applications are the optimization of reaction networks addressing e.g. selectivity problems, or the optimization of metabolic networks in systems biology.

### 7.3 Production system level

The utilization of alternative raw materials and renewable (surplus) energy for the production of chemicals via the R2Chem path is a promising way to reduce greenhouse gas emissions from the chemical industry. The principal step of the R2Chem concept is the electrochemical

splitting of water into hydrogen and oxygen by electrolysis and the subsequent utilization and/or storage of H<sub>2</sub>. In order to further convert H<sub>2</sub> into hydrocarbons or nitrogen-based carbon compounds, sustainable carbon and nitrogen sources have to be found which result in a higher energy requirement than conventional (fossil-based) resources like coal or natural gas. In conjunction with the first research question (I) raised in Chapter 1, the energy storage efficiency was introduced in Chapter 2 to assess the stored energy in relation to the required input energy in the production of several target molecules, which are often discussed in connection with R2Chem.

Methanol has the second best storage efficiency after H<sub>2</sub>, which makes it an optimal target molecule due to its better storage properties, e.g. CH<sub>3</sub>OH is a liquid at ambient conditions. While the CO<sub>2</sub> source – direct air capture or capture from a concentrated point source – has a significant impact on the total energy consumption, by far the largest energy demand is caused by the water electrolysis for the production of H<sub>2</sub>. It is shown that the substitution of fossil based raw materials by alternative sources is not sufficient as the only measure to sufficiently reduce GHG reduction, but that the energy efficiency of the processes must be increased.

In Chapter 4 the specific costs and specific CO<sub>2</sub> emissions for the target product methanol were systematically assessed for a variety of fossil and renewable raw materials and energy sources. For each combination of raw material and energy source considered, cost-optimal process structures and the associated CO<sub>2</sub> emissions were identified and thus the research questions (II) and (III) were answered. A net consumption of CO<sub>2</sub> by the entire production system is possible if renewable energy sources are used and CO<sub>2</sub> is simultaneously used as a raw material source. Due to the high indirect CO<sub>2</sub> emissions from the energy supply (electricity, heat) a significant carbon footprint is unavoidable when using fossil energy sources. Therefore, not only the economic challenge of using CO<sub>2</sub> as a raw material, but also the ecological impact depends strongly on the energy source used.

It was shown that the combined use of natural gas and CO<sub>2</sub> as a raw material source leads to a very good compromise between production costs and emissions, especially if the required energy is from renewable sources. A multi-objective optimization of the two conflicting targets – costs and emissions – for natural gas fed processes illustrated the trade-off between the two targets. It became clear that it is possible to significantly reduce CO<sub>2</sub> emissions while costs increase only slightly. Only if almost emission-free configurations are pursued do costs increase dramatically. Therefore, the theoretical price of CO<sub>2</sub> certificates, which would be necessary to make nearly emission-free configurations cost-optimal, was further analyzed. Depending on the energy source used, certificate prices were calculated in the range of 50 to 150 €/t<sub>CO2</sub> (current price: 25 €/t<sub>CO2</sub>).

The case study presented is based on the publication [82], which in turn is the result of the developments presented in [106] and [107]. In the context of this dissertation, a similar study was carried out for the formic acid production network by comparing CO<sub>2</sub> and natural gas-fed processes [108]. Also here a net CO<sub>2</sub> consumption is achieved by using renewable energy sources, but the production costs are very high. The reasons are the high costs of electricity generation from renewable energies and the low technology readiness level of the process technologies applied, which result in high investment costs.

Although the application at the production system level is only a coarse estimation due to the lack of detailed process knowledge, both case studies conducted show the main advantage of the FluxMax approach, namely the ability to quickly determine an optimal process system within a superstructure in which many alternative process configurations are embedded. The main result is the fact that a net consumption of CO<sub>2</sub> and thus a real reduction of atmospheric CO<sub>2</sub> is only possible if the energy is completely provided by renewable energies. However, due to the high economic challenges resulting from high electricity prices and the low level of technology, a combination of fossil-based natural gas and renewable energy supply is an economically viable alternative in the transition period, which can drastically reduce CO<sub>2</sub> emissions.

Accordingly, the future application of the developed methodology to different sectors of the energy systems is promising, e.g. the assessment of the future transportation sector or the energy supply of households. Further research questions also arise in the industrial sector, which can be answered by modifying the method accordingly: The consideration of spatial coordinates in addition to the thermodynamic coordinates enables the evaluation of spatially distributed networks. In particular, CO<sub>2</sub> emissions caused by the global distribution of chemicals and corresponding supply chains could be assessed, which would lead to an alternative method for determining the ecological impact of chemical products throughout their entire life cycle. Of particular interest is also the consideration of aspects of the future circular economy by evaluating the possibilities of reusing chemical products after their life cycle as raw materials through intelligent recycling techniques.

## 7.4 Plant level

The application of the FluxMax approach at the plant level is directly motivated by the outcomes at the production system level: Energy consumption is the main cost driver of R2Chem production routes, and the substitution of fossil raw materials by renewable sources is not sufficient as the only measure. Consequently, the aim was to design a highly energy-efficient methanol production process. Methanol synthesis was chosen as a case study because it was present in all optimal process configurations derived in Chapter 4. A sequential approach is normally used to identify energy efficient processes: In a first step, an energetic

objective function is applied to identify processes with low energy consumption, and in a second step the further heat reduction potential is evaluated by performing pinch-based approaches. In contrast, in Chapter 5 the simultaneous approach was applied, where process design and heat integration are considered simultaneously to identify the most energy efficient process.

The simultaneous approach was used to answer the fourth research question (IV): A process was designed in which the reaction takes place at two different reaction temperatures. While additional heating is required to heat the reactor effluent of the high temperature reactor, the heat integration potential is significantly increased: The simultaneous approach resulted in a heat savings potential of almost 99 % compared to 88 % with a sequential approach. Although almost all of the heat required is provided internally, the total energy – heating, cooling and power supply – is only slightly increased from 11 % to 13 %. However, this is not a disadvantage of the approach, but is due to the fact that the total energy demand of the methanol synthesis process is dominated by cooling and power consumption.

In the course of the dissertation, in addition to the presented case study based on [139], the FluxMax approach was also applied to the energy-intensive high-temperature hydrogen cyanide process [138]. The comparison of different reactor concepts – Andrussov and the high and low temperature BMA process – showed the enormous energy saving potential that can be achieved in a simultaneous approach. This shows the strength of the approach for high energy consuming processes, which should be the focus of future applications of the FluxMax approach at the plant level.

Limits are mainly set by the selection of the heat integration approach: While the indirect approach leads to drastically reduced computational effort but a dependence on the discretization of the utilities, the application of the direct approach is limited to simple case studies when heat is transferred at a variety of different temperatures. As already indicated, the consideration of intelligent adaptive grid generation techniques is promising to overcome these obstacles.

## 7.5 Process unit level

While at the plant level, separation was considered only as a simple separation of the condensable methanol from the gaseous compounds by condensation, in real technical applications, product purification accounts for the largest energy requirement of the entire process due to its low energy efficiency. For the fifth research question (V), in Chapter 6 the FluxMax approach was applied at the process unit level to design distillation columns with significantly reduced energy requirements. To achieve optimal designs, the distillation process was represented by three elementary processes: Mixing, heating/cooling and phase

separation. As a consequence of the simultaneous consideration of heat integration by introducing inequality constraints, the design space is increased compared to classical design methods based on the MESH equations. A non-conventional design was identified that outperforms classical distillation column designs based on the MESH equations. It could be shown that an improved heat transfer between hot vapor streams and cold liquid streams – resulting in an additional heat exchange area – reduces the energy consumption in the same way as additional separation stages of classical columns. Thus, the optimized design based on the FluxMax formulation reduces the energy consumption by up to 64 % compared to conventional designs. The trade-off between reducing energy consumption – corresponding to lower operating costs – and increasing the heat exchange area – corresponding to higher capital costs – was analyzed by multi-objective optimization. The MESH equations were extended and used to validate the FluxMax design and to prove that the results obtained are thermodynamically consistent. The results underlined the strength of the FluxMax approach to design distillation processes with increased degrees of freedom, which enables the identification of highly energy-efficient designs.

However, the results presented show that heat must be transferred across very small temperature differences in order to fully exploit the identified energy saving potential. Nevertheless, it is possible that separation tasks of other mixtures – with different boiling points of the pure components – also have a high potential for higher temperature differences, which would lead to a lower demand for heat exchange area. The practical implementation of the highly energy-efficient designs by using horizontal columns is also possible, which reduces the surface area by improving heat transfer by extending the contact time of vapor and liquid streams. The identified energy potential is of particular interest for applications with a limited number of trays, e.g. decentralized or modularized vessel systems, as the FluxMax design can be represented as a cascade of heat-integrated flash drums with intermediate heat exchange.

The presented case study demonstrated the energy saving potential by the invention of new unit concepts [157], after the proof-of-concept of the application to distillation processes was provided in the context of the dissertation [156]. On the process unit level, the proof-of-concept of the proposed methods was so far also provided for the reactor and compressor cascade design of the methanol synthesis [155]. However, further research is needed to clearly investigate the limitations and advantages of the proposed methods compared to classical unit design tools.

## 7.6 Outlook

After summarizing the main findings of this dissertation in the previous sections of this chapter, the final section places the results in the broader context outlined in Chapter 1. All the central research questions raised at the beginning were successfully addressed and

answered. Does this mean that the results of this dissertation are the key to all energy-related global challenges facing humanity? Unfortunately not! But the results can clearly lead to guiding global development in the right direction. A powerful tool was developed that can provide support on many different process levels and for even more research questions.

It can support decision makers by screening and analysing strategic decisions quickly and effectively: In the long term, for a large scale production of chemicals by renewable energy sources, only target molecules with short conversion chains such as  $H_2$  and  $CH_3OH$  should be considered. In particular,  $CH_4$ , often publicized in the context of R2Chem, is unsuitable as a target molecule from an energy point of view and should only be considered for the short to medium term due to the distribution network available in many countries. Apart from the production of these molecules, only chemicals with special functions, such as OME or decane, which are used as substitutes for fossil fuels in long-range vehicles and in aviation, should be produced via the R2Chem route as long as the supply of renewable energy is limited. It is also capable of designing and synthesizing innovative chemical processes: It is essential to consider both the design step and the energy assessment at the same time in order to design highly energy-integrated processes that result in low GHG footprints. Old processes can be retrofitted by smart use of synergies and the linking of suitable processes. In addition, completely new processes can be designed without relying on conventional process configurations, resulting in innovative and non-conventional process systems as well as unit designs.

The results of this dissertation also show the limitations of the potential of the chemical industry in view of the global energy consumption and the corresponding GHG emissions. However, the chemical industry must be considered in a sector-coupled perspective because the chemical industry has a major impact on other sectors: sustainable production of alternative fuels leads to lower GHG emissions from the transport or residential heating sector. The same applies to the sustainable production of consumer goods and the switch from a linear to a circular economy. Nevertheless, the chemical industry will always face economic constraints, as a sustainable transition requires functioning business models.

Consequently, the conclusion of this dissertation is also the recognition that a successful energy transition is only possible if society changes its behavior. Only if the world's thirst for energy is significantly reduced, the earth's resources can be used sustainably. While it may be disappointing to claim that there will be no solution to the global challenges without the efforts of every single human being, I would like to conclude this dissertation in an affirmative way:

*A solution that makes us all responsible also means that each one of us is empowered to take the first step!*

# Appendix A

## Thermodynamic data

Throughout the dissertation, various thermodynamic data is required for the analyses, which is presented in this section. Enthalpies and entropies of pure components are used to calculate the heat and work fluxes. Assuming ideal gas behavior the enthalpy  $h_\alpha$  of a pure component  $\alpha \in \mathcal{A}$  is pressure independent but a function of temperature and can be calculated if a reference enthalpy, e.g. the enthalpy of formation  $\Delta h_{f,\alpha}$  at standard temperature  $T_0 = 298.15$  K is known.

$$h_\alpha(T) = \Delta h_{f,\alpha}(T_0) + \int_{T_0}^T c_{p,\alpha}(T) dT \quad (\text{A.1})$$

For the calculation of the entropy  $s_\alpha \in \mathcal{A}$  of a pure component  $\alpha \in \mathcal{A}$  the temperature and pressure dependence must be considered. Again, the temperature dependence of the entropy against a reference entropy, e.g. the entropy of formation  $\Delta s_{f,\alpha}$  at standard temperature, can be expressed by means of the heat capacity  $c_{p,\alpha}$ .

$$s_\alpha(T, p) = \Delta s_{f,\alpha}(T_0) + \int_{T_0}^T \frac{c_{p,\alpha}(T)}{T} dT - R \int_{p_0}^p \frac{dp}{p} \quad (\text{A.2})$$

In Eqs. (A.1) and (A.2) the standard enthalpy of formation  $\Delta h_{f,\alpha}^\ominus$  and the standard entropy of formation  $\Delta s_{f,\alpha}^\ominus$  are used to determine the reference states:

$$h_\alpha(T_0) = \Delta h_{f,\alpha}^\ominus \quad (\text{A.3a})$$

$$s_\alpha(T_0, p_0) = \Delta s_{f,\alpha}^\ominus \quad (\text{A.3b})$$

Since the heat capacities  $c_{p,\alpha}$  in Eqs. (A.1) and (A.2) are temperature dependent, a functional relationship between heat capacity and temperature is required. Many polynomial fitting approaches of experimentally derived values were published in the literature [192]. In this dissertation, the Shomate-Equation (Eq.(A.4)) was applied with listed parameters from NIST [193].

$$c_{p,\alpha}(T) = A_\alpha + B_\alpha \left( \frac{T}{1000} \right) + C_\alpha \left( \frac{T}{1000} \right)^2 + D_\alpha \left( \frac{T}{1000} \right)^3 + E_\alpha \left( \frac{T}{1000} \right)^{-2} \quad (\text{A.4})$$

The parameters  $A_\alpha$ ,  $B_\alpha$ ,  $C_\alpha$ ,  $D_\alpha$  and  $E_\alpha$  as well as  $\Delta h_{f,\alpha}$  and  $\Delta s_{f,\alpha}$  are given in Tab. A.1 for the pure components relevant in this study. Furthermore, the gravimetric lower heating values  $\Delta h_{u,\alpha}^{\text{mass}}$  are listed.



Tab. A.1 Thermodynamic data.

Component	Formula	Phase	$\Delta h_{f,\alpha}^\ominus$ kJ/mol	$\Delta s_{f,\alpha}^\ominus$ J/molK	$\Delta h_{f,\alpha}^{\text{mass}}$ MJ/kg	$A_\alpha$	$B_\alpha$	$C_\alpha$	$D_\alpha$	$E_\alpha$	References
Ammonia	NH <sub>3</sub>	g	-45.9	192.77	18.6	19.99563	49.77119	-15.37599	1.921168	0.189174	[194]
Carbon	C	s	0	6	32.79	10	0	0	0	0	[195, 196]
Carbon dioxide	CO <sub>2</sub>	g	-393.52	213.79	0	24.99735	55.18696	-33.69137	7.948387	-0.136638	[194]
Carbon monoxide	CO	g	-110.53	197.66	10.10	25.56759	6.09613	4.054656	-2.671301	0.131021	[194]
Decane	C <sub>10</sub> H <sub>22</sub>	g	-249.7	545.8	44.6	-54.44	1122	-703.2	167.4	1.034	[197, 198]
DME	C <sub>2</sub> H <sub>6</sub> O	g	-184.1	266.4	28.4	23.29	169.4	-65.11	8.777	-0.2269	[199-201]
Ethanol	C <sub>2</sub> H <sub>5</sub> OH	g	-234	283.88	27.8	17.03	190.8	-76.42	10.69	0.02886	[193, 202]
Formaldehyde	CH <sub>2</sub> O	g	-115.9	218.95	17.3	34.5	-25.94	120.7	-67.67	-0.0004238	[194]
Formic Acid	HCOOH	g	-378.6	248.7	5.6	29.2	13.88	182.2	-152.6	0.007477	[203, 204, 201]
Hydrogen	H <sub>2</sub>	g	0	130.68	119.97	33.066178	-11.363417	11.432816	-2.772874	-0.158558	[194]
Methane	CH <sub>4</sub>	g	-74.6	186.25	50.01	-0.703029	108.4773	-42.52157	5.862788	0.678565	[194, 205]
Methanol	CH <sub>3</sub> OH	g	-201	239.9	21.13	13.94	111.3	-41.59	5.483	0.05204	[199, 206]
Methanol	CH <sub>3</sub> OH	l	-239.5	127.19	19.93	81.13	0	0	0	0	[207, 208]
OME <sub>n=1</sub>	C <sub>3</sub> H <sub>8</sub> O <sub>2</sub>	g	-348.2	335.72	23.7	51.161	162.44	82.6	-85.1	0	[209-211]
Oxygen	O <sub>2</sub>	g	0	205.15	0	31.32234	-20.23531	57.86644	-36.50624	-0.007374	[194]
Water	H <sub>2</sub> O	g	-241.83	188.84	0	30.092	6.832514	6.793435	-2.53448	0.082139	[194]
Water	H <sub>2</sub> O	l	-285.83	69.95	0	-203.606	1523.29	-3196.413	2474.455	3.855326	[194]



# Appendix B

## Supplement to Chapter 2

There are a number of energetic assessments of different targets in the literature [64, 39, 65, 66, 59, 67], which either directly indicate the specific energy demand  $e_j^{\text{in}}$  of step  $j$  or in the form of a conversion efficiency  $\eta_j$ , which can be used to determine the energy output. For some molecules, however, there is no reliable energy assessment, which is why the procedure for calculating the specific energy requirement is described below.

$e_j^{\text{in}}$  is composed by the reversible (thermodynamic) energy requirement  $e_j^{\text{rev,in}}$  and irreversible energy losses, which can be expressed by the thermodynamic efficiency  $\eta_j^{\text{th}}$  of the process step  $j$  shown in Fig. 2.2.

$$e_j^{\text{in}} = \frac{e_j^{\text{rev,in}}}{\eta_j^{\text{th}}} \quad (\text{B.1})$$

The reversible specific energy demand can be divided into a specific work  $\omega_j^{\text{rev,in}}$  as well as heat demand  $\varphi_j^{\text{rev,in}}$ :

$$e_j^{\text{rev,in}} = \omega_j^{\text{rev,in}} + \varphi_j^{\text{rev,in}} \quad (\text{B.2})$$

An expression for both specific energy demands –  $\omega_j^{\text{rev,in}}$  and  $\varphi_j^{\text{rev,in}}$  – is derived by solving the enthalpy and entropy balance taking into account the differences of enthalpy  $\Delta h_j$  and entropy  $\Delta s_j$  as well as the temperature  $T_j$  of the process step  $j$ :

$$\omega_j^{\text{rev,in}} = \Delta h_j - T_i \Delta s_j \quad (\text{B.3})$$

**Tab. B.1** Comparison of the reversible conversion efficiency  $\eta_j^{\text{rev}}$  and the real conversion efficiency  $\eta_j$  reported in the literature.

Molecule	$\eta_j$	$\eta_j$	$\eta_j^{\text{th}}$	Reference
Methane	0.83	0.76	0.92	[39]
Methanol	0.92	0.84	0.92	[65]
Formaldehyde	0.68	0.58	0.86	[65]

$$\varphi_j^{\text{rev,in}} = T_i \Delta s_j \quad (\text{B.4})$$

The thermodynamic efficiency  $\eta_j^{\text{th}}$  expresses the ratio of reversible energy demand and real energy demand, which can also be expressed by the reversible conversion efficiency  $\eta_j^{\text{rev}}$ :

$$\eta_j^{\text{th}} = \frac{e_j^{\text{rev,in}}}{e_j} = \frac{\eta_j^{\text{rev}}}{\eta_j}, \quad (\text{B.5})$$

where  $\eta_j^{\text{rev}}$  is calculated according to Eq. 2.7.

$$\eta_j^{\text{rev}} = \frac{E_\alpha^{\text{stored}}}{\Delta h_{\text{u},\beta}^{\text{mol}} \dot{N}_\beta + e_j^{\text{rev,in}} \dot{N}_\alpha} \quad (\text{B.6})$$

Tab. B.1 lists the calculated reversible conversion efficiency  $\eta_j^{\text{rev}}$  as well as the real conversion efficiency  $\eta_j$  reported in the literature. Furthermore, the resulting thermodynamic efficiency  $\eta_j^{\text{th}}$  is calculated according to Eq. (B.5). The thermodynamic efficiency  $\eta_j^{\text{th}}$  is approximately 0.9 for the molecules under consideration. Therefore, in this dissertation  $\eta_j^{\text{th}}$  is set to 0.9 for the calculation of the storage efficiency  $\eta_\alpha^{\text{storage}}$  in Tab. 2.2 if the efficiency is not taken from literature.

# Appendix C

## Supplement to Chapter 4

### C.1 Linear fitting parameters for investment cost estimation

At the production system level, a cost estimate proposed by Lange [134] is used, which is linearized by curve fitting. The linear regression parameters  $p_1$  and  $p_2$  (Eq. (4.13)) depend on the estimated energy loss, as shown in Fig. C.1. It can be seen that the linear fitting is in very good accordance with the original estimate, in particular in case of increasing energy losses.

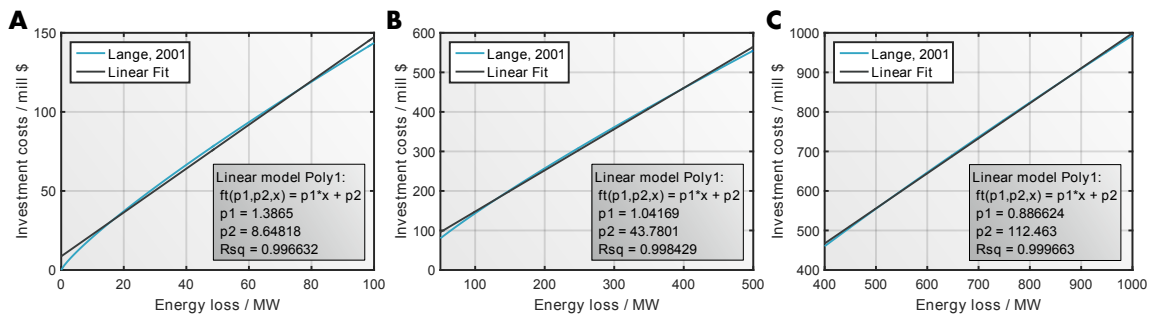


**Fig. C.1** Determination of fitting parameters  $p_1$  and  $p_2$  by linear fitting of investment cost estimation proposed by Lange [134]. Linear fits depend on the estimated energy loss range: A: 0 to 100 MW, B: 0 to 500 MW, and C: 400 to 1,000 MW.

### C.2 Elementary processes at production system level

The elementary processes are described on the production system level by the stoichiometry of the involved chemical reactions. The temperature and pressure levels of the elementary processes are set to the corresponding reaction conditions. Tab. C.1 lists the stoichiometry of the processes together with typical operating windows for temperature and pressure reported in the literature.

Tab. C.1 Overview of considered conversion processes.

Conversion process	Stoichiometry	T / °C	p / bar	References
Ammonia synthesis	$N_2 + 3 H_2O \rightarrow 2 NH_3 + 3/2 O_2$	25...650	1	[212]
AC-Electrolysis	$N_2 + 3 H_2O \rightarrow 2 NH_3 + 3/2 O_2$	25	1	[212, 213]
LT-Electrolysis	$N_2 + 3 H_2O \rightarrow 2 NH_3 + 3/2 O_2$	80	1	[212, 214]
HT-Electrolysis	$N_2 + 3 H_2O \rightarrow 2 NH_3 + 3/2 O_2$	500	1	[212, 215]
Andrussow process	$CH_4 + NH_3 + O_2 \rightarrow HCN + 2 H_2O + H_2$	>1000	1	[216, 217]
Andrussow process	$CH_4 + NH_3 + 3/2 O_2 \rightarrow HCN + 3 H_2O$	>1000	1	[216]
Biological Methane Synthesis	$CO_2 + 2 H_2 \rightarrow CH_4 + O_2$	35	1	[44]
BMA Process	$CH_4 + NH_3 \rightarrow HCN + 3 H_2$	1300	1	[216]
Carbon dioxide electrolysis	$CO_2 \rightarrow CO + 1/2 O_2$	850	1	[52]
HT-Coelectrolysis	$H_2O + CO_2 \rightarrow H_2 + CO + O_2$	850	1	[52]
DME synthesis from methanol	$2 CH_3OH \rightarrow C_2H_6O + H_2O$	250	50	[52]
DME synthesis from syngas	$2 CO + 4 H_2 \rightarrow C_2H_6O + H_2O$	250	50	[218, 52]
DME synthesis from syngas	$3 CO + 3 H_2 \rightarrow C_2H_6O + CO_2$	250	50	[218, 52]
DME synthesis from syngas	$2 CO_2 + 6 H_2 \rightarrow C_2H_6O + 3 H_2O$	200	30	[74, 219]
Dry reforming	$CH_4 + CO_2 \rightarrow 2 H_2 + 2 CO$	700...1000	1	[220-222]
LT-Dry reforming	$CH_4 + CO_2 \rightarrow 2 H_2 + 2 CO$	400...450	1	[223]
Ethanol synthesis from DME	$CO + 2 H_2 + C_2H_6O \rightarrow C_2H_5OH + CH_3OH$	220	15	[224]
Ethanol synthesis from syngas	$2 CO_2 + 6 H_2 \rightarrow C_2H_5OH + 3 H_2O$	270...400	20...90	[225]
Ethylene oxide synthesis from ethanol	$C_2H_5OH \rightarrow C_2H_4O + H_2$	200	1	[226]
Formaldehyde synthesis	$CO_2 + 2 H_2 \rightarrow CH_2O + H_2O$	150	6	[74, 227]
Formic acid synthesis	$CO_2 + H_2 \rightarrow HCOOH$	40...80	100...200	[218, 228-230]
Formic acid synthesis (EC)	$CO_2 + H_2O \rightarrow HCOOH + 1/2 O_2$	80	1	[231]

Tab. C.1 continued: Overview of considered conversion processes.

Conversion process	Stoichiometry	$T / ^\circ C$	$p / \text{bar}$	References
Methane synthesis (Sabatier process)	$\text{CO}_2 + 4 \text{H}_2 \rightarrow \text{CH}_4 + 2 \text{H}_2\text{O}$	250...500	1...13	[232, 233]
Methane synthesis (Sabatier process)	$\text{CO} + 3 \text{H}_2 \rightarrow \text{CH}_4 + \text{H}_2\text{O}$	250...500	1...13	[232, 233]
Methanol synthesis	$\text{CO} + 2 \text{H}_2 \rightarrow \text{CH}_3\text{OH}$	200...300	50...100	[30, 220]
Methanol synthesis	$\text{CO}_2 + 3 \text{H}_2 \rightarrow \text{CH}_3\text{OH} + \text{H}_2\text{O}$	200...300	50...100	[30, 220, 218]
Methylal synthesis (OME <sub>1</sub> )	$\text{CH}_2\text{O} + 2 \text{CH}_3\text{OH} \rightarrow \text{OME}_1 + \text{H}_2\text{O}$	45...100	1...3	[234–237]
Methylal synthesis (OME <sub>1</sub> )	$3 \text{CH}_3\text{OH} + 1/2 \text{O}_2 \rightarrow \text{OME}_1 + 2 \text{H}_2\text{O}$	300	1	[238]
Methylcyclohexane dehydration	$\text{C}_6\text{H}_{11}\text{CH}_3 \rightarrow \text{C}_7\text{H}_8 + 3 \text{H}_2$	450	20	[33, 34]
Oxalic acid synthesis (EC)	$2 \text{CO}_2 + \text{H}_2\text{O} \rightarrow \text{C}_2\text{H}_2\text{O}_4 + 1/2 \text{O}_2$	25	1	[239]
Partial oxidation of methane	$\text{CH}_4 + 1/2 \text{O}_2 \rightarrow \text{CO} + 2 \text{H}_2$	1350...1600	150	[240]
PEM fuel cell	$\text{H}_2 + 1/2 \text{O}_2 \rightarrow \text{H}_2\text{O}$	50...90	1	[241]
Reverse water gas shift	$\text{CO}_2 + \text{H}_2 \rightarrow \text{CO} + \text{H}_2\text{O}$	800	1	[242]
Steam reforming	$\text{CH}_4 + \text{H}_2\text{O} \rightarrow \text{CO} + 3 \text{H}_2$	800...1000	20...40	[240, 220]
EC-Steam reforming	$\text{CH}_4 + \text{H}_2\text{O} \rightarrow \text{CO} + 3 \text{H}_2$	500...600	1	[243, 244]
LT-Steam reforming	$\text{CH}_4 + \text{H}_2\text{O} \rightarrow \text{CO} + 3 \text{H}_2$	400...550	1...1.5	[243]
Thermal methane decomposition	$\text{CH}_4 \rightarrow \text{C} + 2 \text{H}_2$	1250	(0.85)...1	[245]
Toluene hydration	$\text{C}_7\text{H}_8 + 3 \text{H}_2 \rightarrow \text{C}_6\text{H}_{11}\text{CH}_3$	250	30	[33, 34]
Water electrolysis	$\text{H}_2\text{O} \rightarrow \text{H}_2 + 1/2 \text{O}_2$	60	30	[25, 26]
HT-water electrolysis	$\text{H}_2\text{O} \rightarrow \text{H}_2 + 1/2 \text{O}_2$	850	1	[52]
Water gas shift	$\text{CO} + \text{H}_2\text{O} \rightarrow \text{CO}_2 + \text{H}_2$	300...400	1	[246]
LT-water gas shift	$\text{CO} + \text{H}_2\text{O} \rightarrow \text{CO}_2 + \text{H}_2$	60...150	1...5	[247]





# Appendix D

## Supplement to Chapter 5

### D.1 Overview of elementary processes

Examples for selected elementary processes are summarized in Tab. D.1. The resulting balances are listed according to Eq. (D.1) and Eq. (D.2).

$$0 = -\text{sgn}\left(\chi_{(\mathbf{E}_j)}^{(\mathbf{M}_i)}\right) \dot{N}_{(\mathbf{E}_j)}^{(\mathbf{M}_i)} + \chi_{(\mathbf{E}_j)}^{(\mathbf{M}_i)} \dot{\Gamma}_{(\mathbf{E}_j)}. \quad (\text{D.1})$$

$$0 = \left(-\omega_{(\mathbf{E}_j)}^{\text{in}} + \omega_{(\mathbf{E}_j)}^{\text{out}}\right) \dot{\Gamma}_{(\mathbf{E}_j)} + \dot{W}_{(\mathbf{E}_j)}^{\text{ext, in}} - \dot{W}_{(\mathbf{E}_j)}^{\text{ext, out}} \quad (\text{D.2a})$$

$$0 = \left[\varphi_{(\mathbf{E}_j)}^{\text{out}} + \left(1 - \eta_{(\mathbf{E}_j)}^{\text{in}}\right) \omega_{(\mathbf{E}_j)}^{\text{in}} + \left(\frac{1}{\eta_{(\mathbf{E}_j)}^{\text{out}}} - 1\right) \omega_{(\mathbf{E}_j)}^{\text{out}}\right] \dot{\Gamma}_{(\mathbf{E}_j)} - \sum_{U_l \in \mathcal{U}} \dot{Q}_{(U_l)}^{(\mathbf{E}_j)} \quad (\text{D.2b})$$

$$0 = -\varphi_{(\mathbf{E}_j)}^{\text{in}} \dot{\Gamma}_{(\mathbf{E}_j)} + \sum_{U_l \in \mathcal{U}} \dot{Q}_{(U_l)}^{(\mathbf{E}_j)} \quad (\text{D.2c})$$

The first column contains a brief description of the elementary process, followed by the corresponding stoichiometric equation that links different TSNs. The third and fourth columns contain the partial molar balances PMBs and energy balances. Reaction equations for the least complex reaction elementary functions or reactor process units consist generally of an in- and an outlet mixture and require therefore two mass balances according to Eq. (D.1). The assumption of zero work duties allows for a combination of both energy balances Eq. (D.2b) and Eq. (D.2c).

Tab. D.1 Reaction equations, partial molar and energy balances for selected EPNs.

EPN	Stoichiometric equation	Partial molar balance	Energy balance
chemical reaction: $R_j$	$M_1 \longrightarrow \chi_{(R_j)} M_2$	$0 = \dot{N}_{(R_j)}^{(M_1)} - \dot{N}_{(R_j)}^{(M_2)} + \chi_{(R_j)} \dot{I}_{(R_j)}$	$0 = \left( -\varphi_{(R_j)}^{\text{in}} + \varphi_{(R_j)}^{\text{out}} \right) \dot{I}_{(R_j)} + \dot{Q}_{(R_j)}^{\text{ext, in}} - \dot{Q}_{(R_j)}^{\text{ext, out}}$
separation: $S_j$	$M_1 \longrightarrow \chi_{(S_j)}^{(M_2)} M_2 + \chi_{(S_j)}^{(M_3)} M_3$	$0 = \dot{N}_{(S_j)}^{(M_1)} - \dot{N}_{(S_j)}^{(M_2)} - \dot{N}_{(S_j)}^{(M_3)} + \chi_{(S_j)}^{(M_2)} \dot{I}_{(S_j)} + \chi_{(S_j)}^{(M_3)} \dot{I}_{(S_j)}$	$0 = -\varphi_{(S_j)}^{\text{in}} \dot{I}_{(S_j)} + \dot{Q}_{(S_j)}^{\text{ext, in}}$ $0 = \varphi_{(S_j)}^{\text{out}} \dot{I}_{(S_j)} - \dot{Q}_{(S_j)}^{\text{ext, out}}$
adiabatic static mixing: $L_j$	$\chi_{(L_j)}^{(M_2)} M_2 + \chi_{(L_j)}^{(M_3)} M_3 \longrightarrow M_1$	$0 = \dot{N}_{(L_j)}^{(M_2)} - \dot{N}_{(L_j)}^{(M_1)} - \dot{N}_{(L_j)}^{(M_3)} + \chi_{(L_j)}^{(M_2)} \dot{I}_{(L_j)} - \chi_{(L_j)}^{(M_3)} \dot{I}_{(L_j)}$	$-$
adiabatic absorption $A_j$ with entrainer $O_{(A_j)}$	$M_1 + e_{(A_j)} O_{(A_j)} \longrightarrow \left( e_{(A_j)} + \chi_{(A_j)}^{(M_2)} \right) M_2 + \chi_{(A_j)}^{(M_3)} M_3$	$0 = \dot{N}_{(A_j)}^{(M_1)} - \dot{N}_{(A_j)}^{(O)} - \dot{N}_{(A_j)}^{(M_2)} - \dot{N}_{(A_j)}^{(M_3)} - \dot{I}_{(A_j)}$	$-$
adiabatic compression: $C_j$	$M_1 \longrightarrow M_2$	$0 = \dot{N}_{(C_j)}^{(M_1)} - \dot{N}_{(C_j)}^{(M_2)} + \dot{I}_{(C_j)}$	$0 = \omega_{(C_j)}^{\text{in}} \dot{I}_{(C_j)} + \dot{W}_{(C_j)}^{\text{ext, in}}$
economizer edge: $D_j$	$M_1 \longrightarrow M_2$	$0 = \dot{N}_{(D_j)}^{(M_1)} - \dot{N}_{(D_j)}^{(M_2)} - \dot{I}_{(D_j)} + \dot{I}_{(D_j)}$	$0 = \left( -\varphi_{(D_j)}^{\text{in}} + \varphi_{(D_j)}^{\text{out}} \right) \dot{I}_{(D_j)} + \dot{Q}_{(D_j)}^{\text{ext, in}} - \dot{Q}_{(D_j)}^{\text{ext, out}}$
generic elementary function: $G_j$	$M_1 + \chi_{(G_j)}^{(M_2)} M_2 \longrightarrow \chi_{(G_j)}^{(M_3)} M_3 + \chi_{(G_j)}^{(M_4)} M_4$	$0 = \dot{N}_{(G_j)}^{(M_1)} - \dot{N}_{(G_j)}^{(M_2)} - \dot{N}_{(G_j)}^{(M_3)} - \dot{N}_{(G_j)}^{(M_4)} - \dot{I}_{(G_j)}$	$0 = \left( -\omega_{(G_j)}^{\text{in}} + \omega_{(G_j)}^{\text{out}} \right) \dot{I}_{(G_j)} + \dot{W}_{(G_j)}^{\text{ext, in}} - \dot{W}_{(G_j)}^{\text{ext, out}}$ $0 = \left[ \varphi_{(G_j)}^{\text{out}} + \left( 1 - \eta_{(G_j)}^{\text{in}} \right) \omega_{(G_j)}^{\text{in}} \right] + \left( \frac{1}{\eta_{(G_j)}^{\text{out}}} - 1 \right) \omega_{(G_j)}^{\text{out}} \left[ \dot{I}_{(G_j)} - \dot{Q}_{(G_j)}^{\text{ext, out}} \right]$ $0 = -\varphi_{(G_j)}^{\text{in}} \dot{I}_{(G_j)} + \dot{Q}_{(G_j)}^{\text{ext, in}}$

The separation process is described by a TSN that is split into two TSNs. Consequently, three TSN PMBs are required. The generic separator duty does not contain work duties and therefore the energy balance system consists of Eq. (D.2b) and Eq. (D.2c). In case the separator edge represents a  $p, T$  flash, one of the heat duties is unequal zero. In a different scenario this edge may represent a distillation column where both heating and cooling is required for reboiler and condenser duties.

PMBs of an adiabatic static mixing edge  $L_j$  are the reverse of the separation edge. Three TSN PMBs are required and no energy balance is necessary.

An adiabatic absorption edge  $A_j$  is described in line 4 of Tab. D.1. The difference to the regular separation edge is the introduction of an entrainer TSN  $O_{(A_j)}$  that requires an entrainer to feed ratio  $e_{(A_j)}$ . Therefore, an additional PMB is required for the TSN.

The next two line entries comprise an adiabatic compressor  $C_j$  and an economizer  $D_j$ . As no chemical transformation occurs between in- and outlet TSNs the stoichiometric equation becomes trivial and both stoichiometric coefficients are equal to unity. PMBs are necessary, however, in order to identify if the edge is active, to attribute a fixed cost to an edge as explained below and to close the overall molar balance. The adiabatic compression edge requires solely Eq. (D.2a) as an energy balance and the compression duty is obtained directly from the enthalpy difference of in- and outlet TSN. For the economizer Eq. (D.2a) is not required but Eq. (D.2b) and Eq. (D.2c) are combined in a single energy balance where heating and cooling duties are also obtained directly from enthalpy differences of in- and outlet TSN.

The bottom line entry of Tab. D.1 contains a generic elementary process with four participating TSNs, work, heating and cooling duties. Based on this generic elementary process further types of elementary process can be easily derived.

## D.2 Formulation of the linear program

The mass and energy balances presented in sections 2.2 and the temperature constraints for consideration of heat integration presented in section 2.3 serve as equality and inequality constraints of the optimization problem (Eq. 13). These constraints as well as the objective function considered – minimization of the total external energy duty (Eq. 15) – are linear in terms of the fluxes  $\varphi = (\dot{\mathbf{N}}, \dot{\mathbf{F}}, \dot{\mathbf{Q}}, \dot{\mathbf{W}})^\top$ . Thus the entire optimization problem can be formulated as a linear program (LP). The resulting LP is given in Eq. (D.3). The lower and upper bounds correspond to an annual methanol production of 100,000 t<sub>CH<sub>3</sub>OH</sub>/a.

$$\min_{\varphi=(\dot{\mathbf{N}}, \dot{\mathbf{F}}, \dot{\mathbf{Q}}, \dot{\mathbf{W}})^\top} = \sum_{U_i \in \mathcal{U}} \dot{Q}_{(E_j)}^{(U_i)} + \sum_{U_i \in \mathcal{U}} \dot{Q}_{(U_i)}^{(E_j)} + \sum_{E_j \in \mathcal{E}} \dot{W}_{(E_j)}^{\text{ext, in}} \quad (\text{D.3a})$$

s.t. *Equality constraints*

$$\text{Mass balances for each EPN } j \text{ and TSN } i \text{ (Eq. (2))} \quad (\text{D.3b})$$

$$0 = -\text{sgn} \left( \chi_{(\mathbf{E}_j)}^{(\mathbf{M}_i)} \right) \dot{N}_{(\mathbf{E}_j)}^{(\mathbf{M}_i)} + \chi_{(\mathbf{E}_j)}^{(\mathbf{M}_i)} \dot{\Gamma}_{(\mathbf{E}_j)}$$

$$\text{Energy balances for each EPN } j \text{ (Eq. (3) or Eq. (11))} \quad (\text{D.3c})$$

*Indirect heat integration (Eq. (3))*

$$0 = \left( -\omega_{(\mathbf{E}_j)}^{\text{in}} + \omega_{(\mathbf{E}_j)}^{\text{out}} \right) \dot{\Gamma}_{(\mathbf{E}_j)} + \dot{W}_{(\mathbf{E}_j)}^{\text{ext, in}} - \dot{W}_{(\mathbf{E}_j)}^{\text{ext, out}}$$

$$0 = \left[ \varphi_{(\mathbf{E}_j)}^{\text{out}} + \left( 1 - \eta_{(\mathbf{E}_j)}^{\text{in}} \right) \omega_{(\mathbf{E}_j)}^{\text{in}} + \left( \frac{1}{\eta_{(\mathbf{E}_j)}^{\text{out}}} - 1 \right) \omega_{(\mathbf{E}_j)}^{\text{out}} \right] \dot{\Gamma}_{(\mathbf{E}_j)} - \sum_{U_i \in \mathcal{U}} \dot{Q}_{(U_i)}^{(\mathbf{E}_j)}$$

$$0 = -\varphi_{(\mathbf{E}_j)}^{\text{in}} \dot{\Gamma}_{(\mathbf{E}_j)} + \sum_{U_l \in \mathcal{U}} \dot{Q}_{(\mathbf{E}_j)}^{(U_l)}$$

*Direct heat integration (Eq. (11))*

$$0 = \left( -\omega_{(\mathbf{E}_j)}^{\text{in}} + \omega_{(\mathbf{E}_j)}^{\text{out}} \right) \dot{\Gamma}_{(\mathbf{E}_j)} + \dot{W}_{(\mathbf{E}_j)}^{\text{ext, in}} - \dot{W}_{(\mathbf{E}_j)}^{\text{ext, out}}$$

$$0 = \left[ \varphi_{(\mathbf{E}_j)}^{\text{out}} + \left( 1 - \eta_{(\mathbf{E}_j)}^{\text{in}} \right) \omega_{(\mathbf{E}_j)}^{\text{in}} + \left( \frac{1}{\eta_{(\mathbf{E}_j)}^{\text{out}}} - 1 \right) \omega_{(\mathbf{E}_j)}^{\text{out}} \right] \dot{\Gamma}_{(\mathbf{E}_j)}$$

$$- \sum_{U_l \in \mathcal{U}} \dot{Q}_{(U_l)}^{(\mathbf{E}_j)} - \sum_{\mathbf{E}_i \in \mathcal{E}} \dot{Q}_{(\mathbf{E}_i)}^{(\mathbf{E}_j)}$$

$$0 = -\varphi_{(\mathbf{E}_j)}^{\text{in}} \dot{\Gamma}_{(\mathbf{E}_j)} + \sum_{U_l \in \mathcal{U}} \dot{Q}_{(\mathbf{E}_j)}^{(U_l)} + \sum_{\mathbf{E}_i \in \mathcal{E}} \dot{Q}_{(\mathbf{E}_j)}^{(\mathbf{E}_i)}$$

$$\text{Mass balances for each TSN } i \text{ (Eq. (5))} \quad (\text{D.3d})$$

$$0 = \sum_{\mathbf{E}_j \in \mathcal{E}} \text{sgn} \left( \chi_{(\mathbf{E}_j)}^{(\mathbf{M}_i)} \right) \dot{N}_{(\mathbf{E}_j)}^{(\mathbf{M}_i)} + \dot{N}_{\text{ext, in}}^{(\mathbf{M}_i)} - \dot{N}_{\text{ext, out}}^{(\mathbf{M}_i)}$$

$$\text{Energy balances for each UN } l \text{ (Eq. (6))} \quad (\text{D.3e})$$

$$0 = \sum_{\mathbf{E}_j \in \mathcal{E}} \left( \dot{Q}_{(U_l)}^{(\mathbf{E}_j)} - \dot{Q}_{(\mathbf{E}_j)}^{(U_l)} \right) + \dot{Q}_{(U_l)}^{\text{ext, in}} - \dot{Q}_{(U_l)}^{\text{ext, out}}$$

*Inequality constraints*

$$\text{Constraints for heat integration (Eq. (7) and Eq. (9))} \quad (\text{D.3f})$$

$$0 \leq \frac{T_{\text{H, in}}^{\text{max}} - T_{\text{C, in}, (\mathbf{E}_j)} - \Delta T_{\text{min}}}{T_{\text{C, out}, (\mathbf{E}_j)} - T_{\text{C, in}, (\mathbf{E}_j)}} \varphi_{(\mathbf{E}_j)}^{\text{in}} \dot{\Gamma}_{(\mathbf{E}_j)} - \sum_{k_{mj}^H \in \mathcal{K}_m^H} \dot{Q}_{(\mathbf{E}_j)}^{(k_{mj}^H)}$$

$$0 \leq \frac{T_{\text{H, in}, (\mathbf{E}_j)} - T_{\text{C, in}}^{\text{min}} - \Delta T_{\text{min}}}{T_{\text{H, in}, (\mathbf{E}_j)} - T_{\text{H, out}, (\mathbf{E}_j)}} \varphi_{(\mathbf{E}_j)}^{\text{out}} \dot{\Gamma}_{(\mathbf{E}_j)} - \sum_{k_{mj}^C \in \mathcal{K}_m^C} \dot{Q}_{(\mathbf{E}_j)}^{(k_{mj}^C)}$$

*Lower bounds*

$$\text{Non-negativity conditions} \quad (\text{D.3g})$$

$$0 \leq \varphi$$

$$\text{Specification of minimum production of metanol} \quad (\text{D.3h})$$

$$100000 \frac{t_{\text{CH}_3\text{OH}}}{a} \leq \dot{N}_{\text{ext,in}}^{\text{CH}_3\text{OH}}$$

*Upper bounds*

Infinity flux conditions (D.3i)

$$\infty \geq \varphi$$

Specification of maximum production of metanol (D.3j)

$$100000 \frac{t_{\text{CH}_3\text{OH}}}{a} \geq \dot{N}_{\text{ext,in}}^{\text{CH}_3\text{OH}}$$

### D.3 Temperature levels of utilities

In Tab. D.2 the temperature levels of the utilities depending on the number of utilities are listed. The temperature levels result from the equidistant distribution between 5 °C and 420 °C.

**Tab. D.2** Temperature levels of the utilities depending on the number of utilities.

Number of utilities	Temperatures / °C								
2	5	420							
3	5	213	420						
4	5	143	282	420					
5	5	109	213	316	420				
6	5	88	171	254	337	420			
7	5	74	143	213	282	351	420		
8	5	64	124	183	242	301	361	420	

### D.4 Discretization of thermodynamic state space

Fig. D.1 shows the discretization used for the results presented in Fig. 5.10 of chapter 5. The discretization leads to an optimization problem for case A with 51,907 variables and 13,556 constraints (9,956 equality and 3,600 inequality constraints), with the vast majority of variables (35,756) corresponding to internal heat flows.

Case B leads to a similar size of the optimization problem: 51,563 variables (35,504 corresponding to internal heat flows) and 13,556 constraints (9,901 equality and 3,562 inequality constraints).

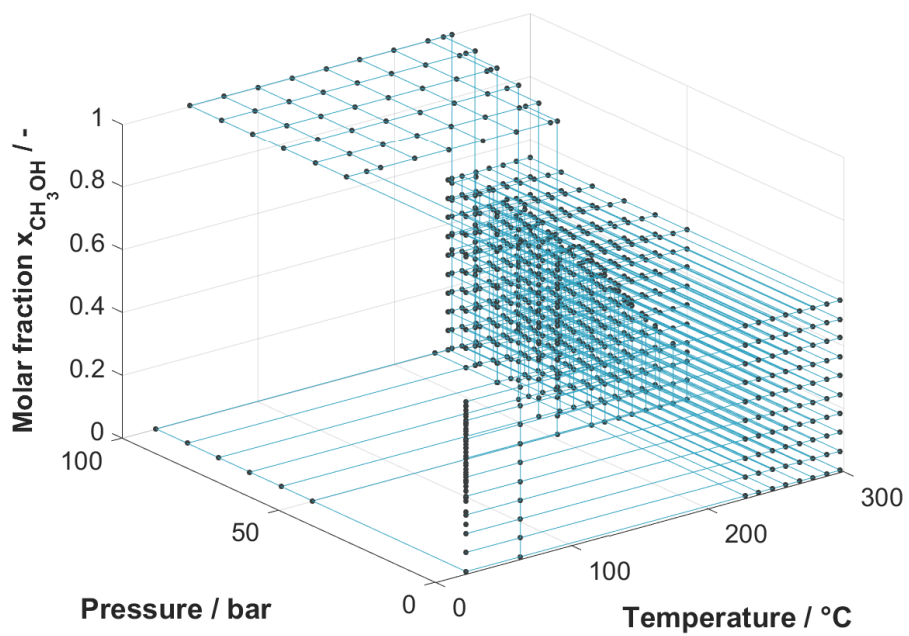


Fig. D.1 Illustration of the discretization of the thermodynamic state space.

# Appendix E

## Supplement to Chapter 6

### E.1 Distillation column design by MESH equations

The classical approach to designing a distillation column is the tray-by-tray formulation and solution of the MESH equations. The MESH equations consider the mass and enthalpy balance on each tray, taking into account the summation condition of the molar fractions. In addition, each tray is considered to be in equilibrium, i.e. outgoing mass flows are considered saturated. Therefore a phase equilibrium condition is required for each tray to determine the ratio between liquid and vapour phase.

#### E.1.1 MESH equations for classic column design

In principle, an external feed stream  $\dot{N}_n^{\text{feed}}$  can enter the tray  $n$ , and liquid  $\dot{N}_n^{\text{liq,out}}$  or vapor product  $\dot{N}_n^{\text{vap,out}}$  can leave the tray to the outside. In addition, there are flows that interact with neighboring trays. These are denoted by the indices  $n - 1$  and  $n + 1$  respectively to indicate the corresponding tray and liq and vap to indicate the phase.

$$\begin{aligned} & \dot{N}_n^{\text{feed}} z_{\alpha,n} + \dot{N}_{n+1}^{\text{liq}} x_{\alpha,n+1} + \dot{N}_{n-1}^{\text{vap}} x_{\alpha,n-1} \\ & = \left( \dot{N}_n^{\text{liq}} + \dot{N}_n^{\text{liq,out}} \right) x_{\alpha,n} + \left( \dot{N}_n^{\text{vap}} + \dot{N}_n^{\text{vap,out}} \right) y_{\alpha,n} \\ & \forall \alpha \in \mathcal{A} \\ & n = 1, \dots, n_{\text{tray}} \end{aligned} \tag{E.1}$$

The molar ratio of a component  $\alpha$  is denoted as  $z$  for a feed stream,  $x$  for a liquid stream and  $y$  for a vapor stream. The trays are considered to be equilibrium stages, which means that the outgoing streams are assumed to be saturated liquid or vapor streams. The equilibrium

constant  $K_{\alpha,n} := y_{\alpha,n}/x_{\alpha,n}$  is defined as the ratio of vapor and liquid molar fraction of the component  $\alpha$  and depends on the pressure  $p_n$  and the temperature  $T_n$  of the tray  $n$ . If ideal conditions are assumed, only the vapor pressure  $p_{\alpha}^{\text{sat}}$  must be known for a given pressure  $p_n$ :

$$K_{\alpha,n} = \frac{p_{\alpha}^{\text{sat}}}{p_n} \quad (\text{E.2})$$

To avoid a total mass balance, summation conditions for the molar fractions  $x_{\alpha,n}$ ,  $y_{\alpha,n}$  and  $z_{\alpha,n}$  of all components  $\alpha$  must be fulfilled for each tray  $n$ :

$$\sum_{\alpha \in \mathcal{A}} x_{\alpha,n} = 1 \quad (\text{E.3a})$$

$$\sum_{\alpha \in \mathcal{A}} y_{\alpha,n} = 1 \quad (\text{E.3b})$$

$$\sum_{\alpha \in \mathcal{A}} z_{\alpha,n} = 1 \quad (\text{E.3c})$$

$$n = 1, \dots, n_{\text{tray}}$$

An enthalpy balance for each tray  $n$  is formulated to take into account the heating and cooling requirements. There are two sources of enthalpy flows: enthalpy transported by mass flows and enthalpy transported by heat flows. The enthalpy of the mixture can be calculated by suitable mixing rules and the enthalpy  $h_{\alpha}$  of the pure components  $\alpha$ . The enthalpy depends on the matter of state – liquid (liq) or vapor (vap) – and can be calculated by suitable equations of state for a given temperature and pressure. In addition, the enthalpy at each tray can be affected by external heat flows which either enter the tray  $\dot{Q}_n^{\text{ext}}$  or leave the tray  $\dot{Q}_n^{\text{out}}$ :

$$\begin{aligned} & \dot{N}_n^{\text{feed}} h_n^{\text{feed}} + \dot{N}_{n+1}^{\text{liq}} h_{n+1}^{\text{liq}} + \dot{N}_{n-1}^{\text{vap}} h_{n-1}^{\text{vap}} + \dot{Q}_n^{\text{ext}} \\ & = \left( \dot{N}_n^{\text{liq}} + \dot{N}_n^{\text{liq,out}} \right) h_n^{\text{liq}} + \left( \dot{N}_n^{\text{vap}} + \dot{N}_n^{\text{vap,out}} \right) h_n^{\text{vap}} + \dot{Q}_n^{\text{out}} \end{aligned} \quad (\text{E.4})$$

$$n = 1, \dots, n_{\text{tray}}$$

### E.1.2 Extension of MESH equations

In addition to comparing the FluxMax results with the classical column design, the MESH equations are used to validate the FluxMax results. However, the FluxMax formulation leads to an increased degree of freedom, in particular it allows heat transfer between vapor and liquid streams entering or leaving the same trays. In order to enable this particular



heat transfer for the MESH formulation as well, the classical formulation is extended in the following. Furthermore, an inequality is introduced which limits the internal heat transfer considering the actual temperature levels and a minimum temperature difference  $\Delta T_{\min}$  of the heat transfer.

The additional degrees of freedom of the FluxMax formulation are given in Fig. 4 (B) of the main manuscript. In contrast to classical columns, the liquid flow  $\dot{N}_{n-1}^{\text{liq}}$  leaving the tray  $n - 1$  does not enter the tray  $n$ , but feeds a heat exchanger  $m$  to obtain heat from the vapor flow  $\dot{N}_j^{\text{vap}}$  which enters the heat exchanger at the other end. While the mass flows remain constant, the temperature levels of the individual flows can change. As a consequence, the enthalpy balances of the individual trays  $n$  must be adjusted accordingly:

$$\begin{aligned}
 & \dot{N}_n^{\text{feed}} h_n^{\text{feed}} + \dot{N}_{n+1}^{\text{liq}} h_m^{\text{liq}} + \dot{N}_{n-1}^{\text{vap}} h_{m-1}^{\text{vap}} + \dot{Q}_n^{\text{ext}} \\
 & = \left( \dot{N}_n^{\text{liq}} + \dot{N}_n^{\text{liq,out}} \right) h_n^{\text{liq}} + \left( \dot{N}_n^{\text{vap}} + \dot{N}_n^{\text{vap,out}} \right) h_n^{\text{vap}} + \dot{Q}_n^{\text{out}} \\
 & n = 1, \dots, n_{\text{tray}} \\
 & m = 1, \dots, n_{\text{HX}}
 \end{aligned} \tag{E.5}$$

In addition to the extended enthalpy balances of the trays, enthalpy balances are formulated for the heat exchangers  $m$ , which are located between trays  $n + 1$  and  $n$ :

$$\begin{aligned}
 & \dot{N}_{n+1}^{\text{liq}} \left( h_{n+1}^{\text{liq}} - h_m^{\text{liq}} \right) = \dot{N}_n^{\text{vap}} \left( h_n^{\text{vap}} - h_m^{\text{vap}} \right) \\
 & n = 1, \dots, n_{\text{tray}} \\
 & m = 1, \dots, n_{\text{HX}}
 \end{aligned} \tag{E.6}$$

From Eq. (E.6) it is evident that the extended model corresponds to the classical MESH equations if the specific enthalpies in the brackets are equal. In this way, the formulation allows the optimization algorithm to either select or omit the additional heat exchange.



# References

- [1] R. Neukom, N. Steiger, J. J. Gomez-Navarro, J. Wang, and J. P. Werner. No evidence for globally coherent warm and cold periods over the preindustrial Common Era. *Nature*, 571(7766):550–554, 2019. doi:10.1038/s41586-019-1401-2.
- [2] UNFCCC. Report of the Conference of the Parties on its Third Session, held at Kyoto from 1 to 11 December 1997. Report, 1998.
- [3] Bundesministerium für Wirtschaft und Energie (BMWi). Energiekonzept für eine umweltschonende, zuverlässige und bezahlbare Energieversorgung (Stand September 2010). 2010.
- [4] UNFCCC. Report of the Conference of the Parties on its twenty-first session, held in Paris from 30 November to 13 December 2015. Report, 2016.
- [5] European Commission. The European Green Deal. Report, 11.12.2019 2019.
- [6] Intergovernmental Panel on Climate Change (IPCC). Global Warming of 1.5 °C. Report, 2018.
- [7] Mercator Research Institute on Global Commons and Climate Change. So schnell tickt die CO<sub>2</sub>-Uhr, accessed: June 2nd 2020. URL <https://www.mcc-berlin.net/de/forschung/co2-budget.html>.
- [8] Fridays for Future (FFF), accessed: June 2nd 2020. URL <https://fridaysforfuture.org/>.
- [9] Bundesministerium für Wirtschaft und Energie (BMWi). Energieeffizienz in Zahlen: Entwicklungen und Trends in Deutschland 2019 (Stand August 2019). 2019.
- [10] A. M. Bazzanella and F. Ausfelder. Low carbon energy and feedstock for the European chemical industry. *DECHEMA Technology Study*, 2017.
- [11] International Energy Agency. Energy Efficiency 2018. Analysis and outlooks , 2018.
- [12] B. Benker, D. Bockey, N. Dahmen, R.-U. Dietrich, M. Form, A. Grewe, A. Günther, B. Heuser, W. Hofer, T. Kuchling, W. Leitner, K. Lucka, A. Martin, D. Meier, J. Michels, G. Muggen, F. Müller-Langer, A. Munack, T. Otto, D. Schieder, J. Seiler, A. Sievers, N. Ullrich, A. Velji, T. Willnerg, and A. Wollmann. Fortschrittliche alternative flüssige Brenn- und Kraftstoffe: Für Klimaschutz im globalen Rohstoffwandel. *DECHEMA Positionspapier*, 2017. URL [https://dechema.de/dechema\\_media/Downloads/Positionspapiere/2017\\_Positionspapier+Alt+Kraftstoffe.pdf](https://dechema.de/dechema_media/Downloads/Positionspapiere/2017_Positionspapier+Alt+Kraftstoffe.pdf).
- [13] A. Kätelhön, R. Meys, S. Deutz, S. Suh, and A. Bardow. Climate change mitigation potential of carbon capture and utilization in the chemical industry. *Proceedings of the National Academy of Sciences*, 116(23):11187–11194, 2019. doi:10.1073/pnas.1821029116.

- [14] F. Ausfelder, C. Beilmann, M. Bertau, S. Bräuninger, A. Heinzl, R. Hoer, W. Koch, F. Mahlendorf, A. Metzethin, M. Peuckert, L. Plass, K. Räuchle, M. Reuter, G. Schaub, S. Schiebahn, E. Schwab, F. Schüth, D. Stolten, G. Teßmer, K. Wagemann, and K.-F. Ziegahn. Energiespeicherung als Element einer sicheren Energieversorgung. *Chemie Ingenieur Technik*, 87(1-2):17–89, 2015. doi:10.1002/cite.201400183.
- [15] Kopernikus Projekte. 1. Roadmap des Kopernikus-Projektes „Power-to-X“: Flexible Nutzung erneuerbarer Ressourcen (P2X). 2018. URL [https://dechema.de/dechema\\_media/Downloads/Positionspapiere/2018\\_Power\\_to\\_X.pdf](https://dechema.de/dechema_media/Downloads/Positionspapiere/2018_Power_to_X.pdf).
- [16] S. R. Foit, I. C. Vinke, L. G. J. de Haart, and R. A. Eichel. Power-to-Syngas: An enabling technology for the transition of the energy system? *Angew Chem Int Ed Engl*, 56(20):5402–5411, 2017. doi:10.1002/anie.201607552.
- [17] A. Otto, M. Robinius, T. Grube, S. Schiebahn, A. Praktiknjo, and D. Stolten. Power-to-Steel: Reducing CO<sub>2</sub> through the integration of renewable energy and hydrogen into the German steel industry. *Energies*, 10(4):451, 2017. doi:10.3390/en10040451.
- [18] M. Ouda, C. Hank, F. Nestler, M. Hadrich, J. Full, A. Schaadt, and C. Hebling. *Power-to-Methanol: Techno-economical and ecological insights*, pages 380–409. Springer Berlin Heidelberg, Berlin, Heidelberg, 2019. doi:10.1007/978-3-662-58006-6\_17.
- [19] S. Schemme, R. C. Samsun, R. Peters, and D. Stolten. Power-to-fuel as a key to sustainable transport systems – An analysis of diesel fuels produced from CO<sub>2</sub> and renewable electricity. *Fuel*, 205:198–221, 2017. doi:10.1016/j.fuel.2017.05.061.
- [20] A. Sternberg and A. Bardow. Life cycle assessment of Power-to-Gas: syngas vs methane. *ACS Sustainable Chemistry & Engineering*, 4(8):4156–4165, 2016. doi:10.1021/acssuschemeng.6b00644.
- [21] M. Thema, F. Bauer, and M. Sterner. Power-to-Gas: Electrolysis and methanation status review. *Renewable and Sustainable Energy Reviews*, 112:775–787, 2019. doi:10.1016/j.rser.2019.06.030.
- [22] Barcelona Declaration – 10th World Congress of Chemical Engineering, 1–5 October 2017. *Chemical Engineering Research and Design*, 129:A1–A2, 2018. doi:<https://doi.org/10.1016/j.cherd.2017.12.035>.
- [23] A. K. Tula, M. R. Eden, and R. Gani. Time for a new class of methods and computer aided tools to address the challenges facing us? *Chemical Engineering Transactions*, 70:7–12, 2018. doi:10.3303/CET1870002.
- [24] A.A. Kiss. Rethinking energy use for a sustainable chemical industry. *Chemical Engineering Transactions*, 76:13–18, 2019. doi:10.3303/CET1976003.
- [25] B. Bensmann, R. Hanke-Rauschenbach, I. K. Pena Arias, and K. Sundmacher. Energetic evaluation of high pressure PEM electrolyzer systems for intermediate storage of renewable energies. *Electrochimica Acta*, 110:570–580, 2013. doi:10.1016/j.electacta.2013.05.102.
- [26] M. Carmo, D. L. Fritz, J. Mergel, and D. Stolten. A comprehensive review on PEM water electrolysis. *International Journal of Hydrogen Energy*, 38(12):4901–4934, 2013. doi:10.1016/j.ijhydene.2013.01.151.
- [27] V. Menon, Q. Fu, V. M. Janardhanan, and O. Deutschmann. A model-based understanding of solid-oxide electrolysis cells (SOECs) for syngas production by H<sub>2</sub>O/CO<sub>2</sub> co-electrolysis. *Journal of Power Sources*, 274:768–781, 2015. doi:10.1016/j.jpowsour.2014.09.158.

- [28] A. Arsalis, A. N. Alexandrou, and G. E. Georghiou. Thermo-economic modeling of a completely autonomous, zero-emission photovoltaic system with hydrogen storage for residential applications. *Renewable Energy*, 126:354–369, 2018. doi:10.1016/j.renene.2018.03.060.
- [29] F. B. Juangsa, L. A. Prananto, Z. Mufrodi, A. Budiman, T. Oda, and M. Aziz. Highly energy-efficient combination of dehydrogenation of methylcyclohexane and hydrogen-based power generation. *Applied Energy*, 226:31–38, 2018. doi:10.1016/j.apenergy.2018.05.110.
- [30] L. K. Rihko-Struckmann, A. Peschel, R. Hanke-Rauschenbach, and K. Sundmacher. Assessment of methanol synthesis utilizing exhaust CO<sub>2</sub> for chemical storage of electrical energy. *Industrial & Engineering Chemistry Research*, 49(21):11073–11078, 2010. doi:10.1021/ie100508w.
- [31] F. Ausfelder, C. Beilmann, M. Bertau, S. Bräuninger, A. Heinzl, R. Hoer, W. Koch, F. Mahlendorf, A. Metzethin, M. Peuckert, L. Plass, K. Räuchle, M. Reuter, G. Schaub, S. Schiebahn, E. Schwab, F. Schüth, D. Stolten, G. Teßmer, K. Wagemann, and K.-F. Ziegahn. Energy storage as part of a secure energy supply. *ChemBioEng Rev*, 4(3):144–210, 2017.
- [32] C. Winnefeld, T. Kadyk, B. Bensmann, U. Krewer, and R. Hanke-Rauschenbach. Modelling and designing cryogenic hydrogen tanks for future aircraft applications. *Energies*, 11(1):105, 2018. doi:10.3390/en11010105.
- [33] M. Taube, D. W. T. Rippin, D. L. Cresswell, and W. Knecht. A system of hydrogen-powered vehicles with liquid organic hydrides. *International Journal of Hydrogen Energy*, 8(3):213–225, 1983. doi:10.1016/0360-3199(83)90067-8.
- [34] G. W. H. Scherer. *Systems and economic analysis of the seasonal storage of electricity with liquid organic hydrides*. Dissertation, 1996.
- [35] D. Teichmann, W. Arlt, P. Wasserscheid, and R. Freymann. A future energy supply based on liquid organic hydrogen carriers (LOHC). *Energy & Environmental Science*, 4(8):2767, 2011. doi:10.1039/c1ee01454d.
- [36] D. Teichmann, K. Stark, K. Müller, G. Zöttl, P. Wasserscheid, and W. Arlt. Energy storage in residential and commercial buildings via liquid organic hydrogen carriers (LOHC). *Energy & Environmental Science*, 5(10):9044, 2012. doi:10.1039/c2ee22070a.
- [37] A. Sternberg and A. Bardow. Power-to-What? – Environmental assessment of energy storage systems. *Energy & Environmental Science*, 8(2):389–400, 2015. doi:10.1039/c4ee03051f.
- [38] G. K. Surya Prakash, G. A. Olah, and A. Goepfert. Beyond oil and gas: The methanol economy. In *ECS Transactions*, volume 35, pages 31–40, 2011. doi:10.1149/1.3645178.
- [39] J. Uebbing, L. K. Rihko-Struckmann, and K. Sundmacher. Exergetic assessment of CO<sub>2</sub> methanation processes for the chemical storage of renewable energies. *Applied Energy*, 233-234:271–282, 2019. doi:10.1016/j.apenergy.2018.10.014.
- [40] J. Bremer, K. H. G. Rätze, and K. Sundmacher. CO<sub>2</sub> methanation: Optimal start-up control of a fixed-bed reactor for power-to-gas applications. *AIChE Journal*, 63(1):23–31, 2017. doi:10.1002/aic.15496.
- [41] D. J. Batstone, J. Keller, I. Angelidaki, S. V. Kalyuzhnyi, S. G. Pavlostathis, A. Rozzi, W. T. M. Sanders, H. Siegrist, and V. A. Vavilin. The IWA anaerobic digestion model No 1 (ADM1). *Water Science and Technology*, 45(10):65–73, 2002. doi:10.2166/wst.2002.0292.

- [42] A. Bensmann, R. Hanke-Rauschenbach, and K. Sundmacher. Reactor configurations for biogas plants – a model based analysis. *Chemical Engineering Science*, 104:413–426, 2013. doi:10.1016/j.ces.2013.09.025.
- [43] K. Koch, M. Lübken, T. Gehring, M. Wichern, and H. Horn. Biogas from grass silage - Measurements and modeling with ADM1. *Bioresource Technology*, 101(21):8158–8165, 2010. doi:10.1016/j.biortech.2010.06.009.
- [44] A. Bensmann, R. Hanke-Rauschenbach, R. Heyer, F. Kohrs, D. Benndorf, U. Reichl, and K. Sundmacher. Biological methanation of hydrogen within biogas plants: A model-based feasibility study. *Applied Energy*, 134:413–425, 2014. doi:10.1016/j.apenergy.2014.08.047.
- [45] J. Fuhrmann, M. Hülsebrock, and U. Krewer. *Energy Storage Based on Electrochemical Conversion of Ammonia*. 2013. doi:doi:10.1002/9783527673872.ch33.
- [46] J. Eppinger and K.-W. Huang. Formic acid as a hydrogen energy carrier. *ACS Energy Letters*, 2(1):188–195, 2016. doi:10.1021/acsenerylett.6b00574.
- [47] K. Räuchle, L. Plass, H. J. Wernicke, and M. Bertau. Methanol for renewable energy storage and utilization. *Energy Technology*, 4(1):193–200, 2016. doi:10.1002/ente.201500322.
- [48] E. Moioli, R. Mutschler, and A. Züttel. Renewable energy storage via CO<sub>2</sub> and H<sub>2</sub> conversion to methane and methanol: Assessment for small scale applications. *Renewable and Sustainable Energy Reviews*, 107:497–506, 2019. doi:10.1016/j.rser.2019.03.022.
- [49] T. A. Adams II, T. Thatho, M. C. Le Feuvre, and C. L. E. Swartz. The optimal design of a distillation system for the flexible polygeneration of dimethyl ether and methanol under uncertainty. *Frontiers in Energy Research*, 6, 2018. doi:10.3389/fenrg.2018.00041.
- [50] M. Martin and I. E. Grossmann. Energy optimization of bioethanol production via gasification of switchgrass. *AIChE Journal*, 57(12):3408–3428, 2011. doi:10.1002/aic.12544.
- [51] P. Sassner, M. Galbe, and G. Zacchi. Techno-economic evaluation of bioethanol production from three different lignocellulosic materials. *Biomass and Bioenergy*, 32(5):422–430, 2008. doi:10.1016/j.biombioe.2007.10.014.
- [52] M. Pozzo, A. Lanzini, and M. Santarelli. Enhanced biomass-to-liquid (BTL) conversion process through high temperature co-electrolysis in a solid oxide electrolysis cell (SOEC). *Fuel*, 145:39–49, 2015. doi:10.1016/j.fuel.2014.12.066.
- [53] J. Burger, M. Siegert, E. Ströfer, and H. Hasse. Poly(oxymethylene) dimethyl ethers as components of tailored diesel fuel: Properties, synthesis and purification concepts. *Fuel*, 89(11):3315–3319, 2010. doi:10.1016/j.fuel.2010.05.014.
- [54] B. Lumpp, D. Rothe, C. Pastötter, R. Lämmermann, and E. Jacob. Oxymethylen ethers as diesel fuel additives of the future. *MTZ worldwide eMagazine*, 72(3):34–38, 2011. doi:10.1365/s38313-011-0027-z.
- [55] N. Schmitz, J. Burger, E. Ströfer, and H. Hasse. From methanol to the oxygenated diesel fuel poly(oxymethylene) dimethyl ether: An assessment of the production costs. *Fuel*, 185:67–72, 2016. doi:10.1016/j.fuel.2016.07.085.
- [56] X. Zhang, A. Kumar, U. Arnold, and J. Sauer. Biomass-derived oxymethylene ethers as diesel additives: A thermodynamic analysis. *Energy Procedia*, 61:1921–1924, 2014. doi:10.1016/j.egypro.2014.12.242.

- [57] *Encyclopedia of electrochemical power sources*, volume Vol. 1. Elsevier Science, 2009. ISBN 9780444520937.
- [58] J. Ren, S. Gao, H. Liang, S. Tan, and L. Dong. *The role of hydrogen energy: Strengths, weaknesses, opportunities, and threats*, pages 1–33. Academic Press, 2017. ISBN 978-0-12-811132-1. doi:10.1016/B978-0-12-811132-1.00001-8.
- [59] D. Krekel, R. C. Samsun, R. Peters, and D. Stolten. The separation of CO<sub>2</sub> from ambient air – A techno-economic assessment. *Applied Energy*, 218:361–381, 2018. doi:10.1016/j.apenergy.2018.02.144.
- [60] N. Böcker, M. Grahl, A. Tota, P. Häussinger, P. Leitgeb, and B. Schmäcker. *Nitrogen*, pages 1–27. Wiley-VCH Verlag GmbH & Co. KGaA, 2013. doi:10.1002/14356007.a17\_457.pub2.
- [61] A. Goeppert, M. Czaun, G. K. Surya Prakash, and G. A. Olah. Air as the renewable carbon source of the future: an overview of CO<sub>2</sub> capture from the atmosphere. *Energy & Environmental Science*, 5(7):7833–7853, 2012. doi:10.1039/c2ee21586a.
- [62] J. C. Abanades, E. S. Rubin, M. Mazzotti, and H. J. Herzog. On the climate change mitigation potential of CO<sub>2</sub> conversion to fuels. *Energy & Environmental Science*, 10(12):2491–2499, 2017. doi:10.1039/c7ee02819a.
- [63] J. Offermann-van Heek, K. Arning, A. Sternberg, A. Bardow, and M. Ziefle. Assessing public acceptance of the life cycle of CO<sub>2</sub>-based fuels: Does information make the difference? *Energy Policy*, 143:111586, 2020. doi:10.1016/j.enpol.2020.111586.
- [64] M. Götz, J. Lefebvre, F. Mörs, A. McDaniel Koch, F. Graf, S. Bajohr, R. Reimert, and T. Kolb. Renewable Power-to-Gas: A technological and economic review. *Renewable Energy*, 85:1371–1390, 2016. doi:10.1016/j.renene.2015.07.066.
- [65] S. Deutz, D. Bongartz, B. Heuser, A. Kätelhön, L. Schulze Langenhorst, A. Omari, M. Walters, J. Klankermayer, W. Leitner, A. Mitsos, S. Pischinger, and A. Bardow. Cleaner production of cleaner fuels: wind-to-wheel – environmental assessment of CO<sub>2</sub>-based oxymethylene ether as a drop-in fuel. *Energy & Environmental Science*, 11(2):331–343, 2018. doi:10.1039/c7ee01657c.
- [66] B. Castellani, S. Rinaldi, E. Morini, B. Nastasi, and F. Rossi. Flue gas treatment by power-to-gas integration for methane and ammonia synthesis – Energy and environmental analysis. *Energy Conversion and Management*, 171:626–634, 2018. doi:10.1016/j.enconman.2018.06.025.
- [67] S. Schiebahn, T. Grube, M. Robinius, L. Zhao, A. Otto, B. Kumar, M. Weber, and D. Stolten. *Power to Gas*, book section 39, pages 813–848. John Wiley & Sons, Ltd, 2013. ISBN 9783527673872. doi:10.1002/9783527673872.ch39.
- [68] K. Wagemann and F. Ausfelder. E-Fuels – Mehr als eine Option. *DECHEMA White Paper*, 2017. URL [https://dechema.de/dechema\\_media/Downloads/Positionspapiere/WhitePaper\\_E\\_Fuels-p-20002780.pdf](https://dechema.de/dechema_media/Downloads/Positionspapiere/WhitePaper_E_Fuels-p-20002780.pdf).
- [69] M. Rumayor, A. Dominguez-Ramos, and A. Irabien. Formic acid manufacture: Carbon dioxide utilization alternatives. *Applied Sciences*, 8(6):914, 2018. doi:10.3390/app8060914.
- [70] European Industrial Gases Association (EIGA). Indirect CO<sub>2</sub> emissions compensation: Benchmark proposal for Air Separation Plants. Report, 2010. URL <https://www.eiga.eu/index.php?eID=dumpFile&t=f&f=3581&token=95e8195add59162bd25aff4554cf2aa64784a1f0>.

- [71] M. Härtl, P. Seidenspinner, G. Wachtmeister, and E. Jacob. Synthetischer Dieselkraftstoff OME1 – Lösungsansatz für den Zielkonflikt NO<sub>x</sub>-Partikel-Emission. *MTZ - Motortechnische Zeitschrift*, 75(7):68–73, 2014. doi:10.1007/s35146-014-0392-7.
- [72] C. Hank, L. Lazar, F. Mantei, M. Ouda, R. J. White, T. Smolinka, A. Schaadt, C. Hebling, and H.-M. Henning. Comparative well-to-wheel life cycle assessment of OME<sub>3–5</sub> synfuel production via the power-to-liquid pathway. *Sustainable Energy & Fuels*, 2019. doi:10.1039/c9se00658c.
- [73] M. Bertau, H. Offermanns, L. Plass, and F. Schmidt. *Methanol: The basic chemical and energy feedstock of the future : Asinger's vision today*. Springer Berlin Heidelberg, Berlin, Heidelberg, 2014. ISBN 9783642397097.
- [74] A. Otto, T. Grube, S. Schiebahn, and D. Stolten. Closing the loop: captured CO<sub>2</sub> as a feedstock in the chemical industry. *Energy & Environmental Science*, 8(11):3283–3297, 2015. doi:10.1039/C5EE02591E.
- [75] K. Roh, R. Frauzem, T. B. H. Nguyen, R. Gani, and J. H. Lee. A methodology for the sustainable design and implementation strategy of CO<sub>2</sub> utilization processes. *Computers & Chemical Engineering*, 91:407–421, 2016. doi:10.1016/j.compchemeng.2016.01.019.
- [76] J. Ott, V. Gronemann, F. Pontzen, E. Fiedler, G. Grossmann, D. B. Kersebohm, G. Weiss, and C. Witte. *Methanol*, pages 1–27. Wiley-VCH Verlag GmbH & Co. KGaA, 2012. ISBN 9783527306732. doi:10.1002/14356007.a16\_465.pub3.
- [77] A. König, K. Ulonska, A. Mitsos, and J. Viell. Optimal applications and combinations of renewable fuel production from biomass and electricity. *Energy & Fuels*, 33(2):1659–1672, 2019. doi:10.1021/acs.energyfuels.8b03790.
- [78] Verband der Chemischen Industrie e. V. Chemie in Zahlen 2019. 2019.
- [79] AG Energiebilanzen. Stromerzeugung nach Energieträgern 1990 - 2019 (Stand Februar 2020). 2019. URL [https://ag-energiebilanzen.de/index.php?article\\_id=29&fileName=ausdruck\\_strez\\_abgabe\\_dez2020\\_anteile\\_.pdf](https://ag-energiebilanzen.de/index.php?article_id=29&fileName=ausdruck_strez_abgabe_dez2020_anteile_.pdf).
- [80] Agora Energiewende. Die Energiewende im Stromsektor: Stand der Dinge 2019. Rückblick auf die wesentlichen Entwicklungen sowie Ausblick auf 2020. 2020. URL [https://static.agora-energiewende.de/fileadmin/Projekte/2019/Jahresauswertung\\_2019/171\\_A-EW\\_Jahresauswertung\\_2019\\_WEB.pdf](https://static.agora-energiewende.de/fileadmin/Projekte/2019/Jahresauswertung_2019/171_A-EW_Jahresauswertung_2019_WEB.pdf).
- [81] A. Voll and W. Marquardt. Reaction network flux analysis: Optimization-based evaluation of reaction pathways for biorenewables processing. *AIChE Journal*, 58(6):1788–1801, 2012. doi:10.1002/aic.12704.
- [82] D. Schack, L. Rihko-Struckmann, and K. Sundmacher. Linear programming approach for structure optimization of Renewable-to-Chemicals (R2Chem) production networks. *Industrial & Engineering Chemistry Research*, 57(30):9889–9902, 2018. doi:10.1021/acs.iecr.7b05305.
- [83] K. Ulonska, M. Skiborowski, A. Mitsos, and J. Viell. Early-stage evaluation of biorefinery processing pathways using process network flux analysis. *AIChE Journal*, 62(9):3096–3108, 2016. doi:10.1002/aic.15305.
- [84] B. Huang, Y. Li, R. Gao, Y. Zuo, Z. Dai, and F. Wang. Simultaneous optimization and heat integration of the coal-to-SNG process with a branched heat recovery steam cycle. *Computers & Chemical Engineering*, 117:117–128, 2018. doi:10.1016/j.compchemeng.2018.02.008.



- [85] N. M. Kaiser, M. Jokieli, K. McBride, R. J. Flassig, and K. Sundmacher. Optimal reactor design via Flux Profile Analysis for an integrated hydroformylation process. *Industrial & Engineering Chemistry Research*, 56(40):11507–11518, 2017. doi:10.1021/acs.iecr.7b01939.
- [86] T. Keßler, C. Kunde, K. McBride, N. Mertens, D. Michaels, K. Sundmacher, and A. Kienle. Global optimization of distillation columns using explicit and implicit surrogate models. *Chemical Engineering Science*, 197:235–245, 2019. doi:10.1016/j.ces.2018.12.002.
- [87] H. Freund and K. Sundmacher. Towards a methodology for the systematic analysis and design of efficient chemical processes. *Chemical Engineering and Processing: Process Intensification*, 47(12):2051–2060, 2008. doi:10.1016/j.cep.2008.07.011.
- [88] A. Peschel, H. Freund, and K. Sundmacher. Methodology for the design of optimal chemical reactors based on the concept of Elementary Process Functions. *Industrial & Engineering Chemistry Research*, 49(21):10535–10548, 2010. doi:10.1021/ie100476q.
- [89] B. Hentschel, A. Peschel, H. Freund, and K. Sundmacher. Simultaneous design of the optimal reaction and process concept for multiphase systems. *Chemical Engineering Science*, 115:69–87, 2014. doi:10.1016/j.ces.2013.09.046.
- [90] J. Maußner, C. Dreiser, O. Wachsen, and H. Freund. Systematic model-based design of tolerant chemical reactors. *Journal of Advanced Manufacturing and Processing*, 1(3), 2019. doi:10.1002/amp2.10024.
- [91] B. Hartono, P. Heidebrecht, and K. Sundmacher. Combined branch and bound method and exergy analysis for energy system design. *Industrial & Engineering Chemistry Research*, 51(44):14428–14437, 2012. doi:10.1021/ie301232t.
- [92] M. Short, A. J. Isafiade, L. T. Biegler, and Z. Kravanja. Synthesis of mass exchanger networks in a two-step hybrid optimization strategy. *Chemical Engineering Science*, 178:118–135, 2018. doi:10.1016/j.ces.2017.12.019.
- [93] F. Friedler, K. Tarjan, Y. W. Huang, and L. T. Fan. Graph-theoretic approach to process synthesis – axioms and theorems. *Chemical Engineering Science*, 47(8):1973–1988, 1992. doi:10.1016/0009-2509(92)80315-4.
- [94] J. Ryu and C. T. Maravelias. Simultaneous process and heat exchanger network synthesis using a discrete temperature grid. *Industrial & Engineering Chemistry Research*, 58(15):6002–6016, 2019. doi:10.1021/acs.iecr.8b04083.
- [95] J. Kim, S. M. Sen, and C. T. Maravelias. An optimization-based assessment framework for biomass-to-fuel conversion strategies. *Energy & Environmental Science*, 6(4):1093–1104, 2013. doi:10.1039/c3ee24243a.
- [96] S. Wilson and V. Manousiouthakis. IDEAS approach to process network synthesis: Application to multicomponent MEN. *AIChE Journal*, 46(12):2408–2416, 2000. doi:DOI 10.1002/aic.690461209.
- [97] B. Linnhoff and J. R. Flower. Synthesis of heat exchanger networks: I. Systematic generation of energy optimal networks. *AIChE Journal*, 24(4):633–642, 1978. doi:10.1002/aic.690240411.
- [98] A. C. Kokossis, M. Tsakalova, and K. Pyrgakis. Design of integrated biorefineries. *Computers & Chemical Engineering*, 81:40–56, 2015. doi:10.1016/j.compchemeng.2015.05.021.

- [99] E. Gencer and R. Agrawal. Toward supplying food, energy, and water demand: Integrated solar desalination process synthesis with power and hydrogen coproduction. *Resources Conservation and Recycling*, 133:331–342, 2018. doi:10.1016/j.resconrec.2018.01.030.
- [100] M. A. Duran and I. E. Grossmann. Simultaneous-optimization and heat integration of chemical Processes. *AIChE Journal*, 32(1):123–138, 1986. doi:DOI 10.1002/aic.690320114.
- [101] H. Cabezas, A. Argoti, F. Friedler, P. Mizsey, and J. Pimentel. Design and engineering of sustainable process systems and supply chains by the P-graph framework. *Environmental Progress & Sustainable Energy*, 37(2):624–636, 2018. doi:10.1002/ep.12887.
- [102] K. Holiastos and V. Manousiouthakis. Infinite-dimensional state-space (IDEAS) approach to globally optimal design of distillation networks featuring heat and power integration. *Industrial & Engineering Chemistry Research*, 43(24):7826–7842, 2004. doi:10.1021/ie010434i.
- [103] V. I. Pichardo, P. and Manousiouthakis. Infinite dimensional state-space as a systematic process intensification tool: Energetic intensification of hydrogen production. *Chemical Engineering Research and Design*, 120:372–395, 2017. doi:10.1016/j.cherd.2017.01.026.
- [104] H. W. Hamacher and K. Klamroth. *Lineare Optimierung und Netzwerkoptimierung*. Vieweg, Wiesbaden, 2006. ISBN 9783834890313. doi:10.1007/978-3-322-91579-5.
- [105] T. F. Long, W. L. Jiao, and G. J. He. RPC Estimation via  $l(1)$ -norm-regularized least squares (L1LS). *Ieee Transactions on Geoscience and Remote Sensing*, 53(8):4554–4567, 2015. doi:10.1109/Tgrs.2015.2401602.
- [106] D. Schack, L. Rihko-Struckmann, and K. Sundmacher. Structure optimization of power-to-chemicals (P2C) networks by linear programming for the economic utilization of renewable surplus energy. *Computer Aided Chemical Engineering*, 38:1551–1556, 2016. doi:10.1016/B978-0-444-63428-3.50263-0.
- [107] D. Schack, L. Rihko-Struckmann, and K. Sundmacher. Economic linear objective function approach for structure optimization of renewables-to-chemicals (R2Chem) networks. *Computer Aided Chemical Engineering*, 40:1975–1980, 2017. URL 10.1016/B978-0-444-63965-3.50331-7.
- [108] D. Schack and K. Sundmacher. Techno-ökonomische Optimierung des Produktionsnetzwerkes für die Synthese von Ameisensäure aus erneuerbaren Ressourcen. *Chemie Ingenieur Technik*, 90(1-2):256–266, 2018. doi:10.1002/cite.201700163.
- [109] R. Schlögl. Sustainable energy systems: The strategic role of chemical energy conversion. *Topics in Catalysis*, 59(8-9):772–786, 2016. doi:10.1007/s11244-016-0551-9.
- [110] K. Roh, J. H. Lee, and R. Gani. A methodological framework for the development of feasible CO<sub>2</sub> conversion processes. *International Journal of Greenhouse Gas Control*, 47:250–265, 2016. doi:10.1016/j.ijggc.2016.01.028.
- [111] U. Arnold, T. Brück, A. de Palmaer, and K. Kuse. Carbon capture and sustainable utilization by algal polyacrylonitrile fiber production: Process design, techno-economic analysis, and climate related aspects. *Industrial & Engineering Chemistry Research*, 57(23):7922–7933, 2018. doi:10.1021/acs.iecr.7b04828.
- [112] M. J. Bidy, R. Davis, D. Humbird, L. Tao, N. Dowe, M. T. Guarneri, J. G. Linger, E. M. Karp, D. Salvachua, D. R. Vardon, and G. T. Beckham. The techno-economic

- basis for coproduct manufacturing to enable hydrocarbon fuel production from lignocellulosic biomass. *ACS Sustainable Chemistry & Engineering*, 4(6):3196–3211, 2016. doi:10.1021/acssuschemeng.6b00243.
- [113] W. Hoppe, S. Bringezu, and N. Thonemann. Comparison of global warming potential between conventionally produced and CO<sub>2</sub>-based natural gas used in transport versus chemical production. *Journal of Cleaner Production*, 121:231–237, 2016. doi:10.1016/j.jclepro.2016.02.042.
- [114] W. Hoppe, N. Thonemann, and S. Bringezu. Life cycle assessment of carbon dioxide-based production of methane and methanol and derived polymers. *Journal of Industrial Ecology*, 22(2):327–340, 2018. doi:10.1111/jiec.12583.
- [115] A. Sternberg, C. M. Jens, and A. Bardow. Life cycle assessment of CO<sub>2</sub>-based C<sub>1</sub>-chemicals. *Green Chemistry*, 19(9):2244–2259, 2017. doi:10.1039/c6gc02852g.
- [116] G. Reiter and J. Lindorfer. Global warming potential of hydrogen and methane production from renewable electricity via power-to-gas technology. *The International Journal of Life Cycle Assessment*, 20(4):477–489, 2015. doi:10.1007/s11367-015-0848-0.
- [117] R. Parajuli, T. Dalgaard, U. Jorgensen, A. P. S. Adamsen, M. T. Knudsen, M. Birkved, M. Gylling, and J. K. Schjorring. Biorefining in the prevailing energy and materials crisis: a review of sustainable pathways for biorefinery value chains and sustainability assessment methodologies. *Renewable and Sustainable Energy Reviews*, 43:244–263, 2015. doi:10.1016/j.rser.2014.11.041.
- [118] A. Giuliano, R. Cerulli, M. Poletto, G. Raiconi, and D. Barletta. Process pathways optimization for a lignocellulosic biorefinery producing levulinic acid, succinic acid, and ethanol. *Industrial & Engineering Chemistry Research*, 55(40):10699–10717, 2016. doi:10.1021/acs.iecr.6b01454.
- [119] E. Zondervan, M. Nawaz, A. B. de Haan, J. M. Woodley, and R. Gani. Optimal design of a multi-product biorefinery system. *Computers & Chemical Engineering*, 35(9):1752–1766, 2011. doi:10.1016/j.compchemeng.2011.01.042.
- [120] O. Onel, A. M. Niziolek, J. A. Elia, R. C. Baliban, and C. A. Floudas. Biomass and natural gas to liquid transportation fuels and olefins (BGTL+C<sub>2</sub>\_C<sub>4</sub>): Process synthesis and global optimization. *Industrial & Engineering Chemistry Research*, 54(1):359–385, 2015. doi:10.1021/ie503979b.
- [121] S. Maronese, A. V. Ensinas, A. Mian, A. Lazzaretto, and F. Marechal. Optimum biorefinery pathways selection using the integer-cuts constraint method applied to a MILP problem. *Industrial & Engineering Chemistry Research*, 54(28):7038–7046, 2015. doi:10.1021/acs.iecr.5b01439.
- [122] P. Cheali, K. V. Gernaey, and G. Sin. Toward a computer-aided synthesis and design of biorefinery networks: data collection and management using a generic modeling approach. *ACS Sustainable Chemistry & Engineering*, 2(1):19–29, 2014. doi:10.1021/sc400179f.
- [123] A. M. Niziolek, O. Onel, M. M. F. Hasan, and C. A. Floudas. Municipal solid waste to liquid transportation fuels – Part II: Process synthesis and global optimization strategies. *Computers & Chemical Engineering*, 74:184–203, 2015. doi:10.1016/j.compchemeng.2014.10.007.
- [124] A. M. Niziolek, O. Onel, Y. Tian, C. A. Floudas, and E. N. Pistikopoulos. Municipal solid waste to liquid transportation fuels – Part III: An optimization-based nationwide supply chain management framework. *Computers & Chemical Engineering*, 2017. doi:10.1016/j.compchemeng.2017.10.034.

- [125] M. Weyland, R. Albert, A. Halatsch, P. Icha, F. Jäger, K. Juhrich, K. Kuhnemann, L. Mohr, C. Mordziol, M. Ollig, D. Osiek, A.-S. Reinhardt, and J. Schuberth. Stromsparen - Schlüssel für eine umweltschonende und kostengünstige Energiewende, 2015. Umweltbundesamt.
- [126] S. Wissel, S. Rath-Nagel, M. Blesl, U. Fahl, and A. Voß. Stromerzeugungskosten im Vergleich, 2008. URL [https://www.ier.uni-stuttgart.de/publikationen/arbeitsberichte/downloads/Arbeitsbericht\\_04.pdf](https://www.ier.uni-stuttgart.de/publikationen/arbeitsberichte/downloads/Arbeitsbericht_04.pdf). Universität Stuttgart, Working Paper.
- [127] U. Nestle and C. Kunz. Studienvergleich: Stromgestehungskosten verschiedener Erzeugungstechnologien, 2014. URL [https://www.enklip.de/projekte\\_23\\_725944286.pdf](https://www.enklip.de/projekte_23_725944286.pdf). Forschungsradar Energiewende.
- [128] H.-J. Wagner, M. K. Koch, J. Burkhardt, T. G. Böckmann, N. Feck, and P. Kruse. CO<sub>2</sub>-Emissionen der Stromerzeugung. *BWK Das Energie-Fachmagazin*, 59(10):44–52, 2007. URL [http://www.vdi.de/fileadmin/vdi\\_de/redakteur\\_dateien/geu\\_dateien/FB4-Internetseiten/CO2-Emissionen%20der%20Stromerzeugung\\_01.pdf](http://www.vdi.de/fileadmin/vdi_de/redakteur_dateien/geu_dateien/FB4-Internetseiten/CO2-Emissionen%20der%20Stromerzeugung_01.pdf).
- [129] P. Icha and G. Kuhs. Entwicklung der spezifischen Kohlendioxid-Emissionen des deutschen Strommix in den Jahren 1990 bis 2015. *Climate Change*, 26:1–27, 2016. URL [https://www.umweltbundesamt.de/sites/default/files/medien/1410/publikationen/2019-04-10\\_cc\\_10-2019\\_strommix\\_2019.pdf](https://www.umweltbundesamt.de/sites/default/files/medien/1410/publikationen/2019-04-10_cc_10-2019_strommix_2019.pdf).
- [130] finanzen.net GmbH. CO<sub>2</sub> European Emission Allowances, accessed: May 21th 2020. URL <https://www.finanzen.net/rohstoffe/co2-emissionsrechte>.
- [131] A. V. Bridgwater. The functional unit approach to rapid cost estimation. *AACE Bulletin*, 18(5):153, 1976.
- [132] H. Gaensslen. Thermal efficiency and production economics of chemical plants. *Chemsa*, 6(1):13–15, 1980.
- [133] M. S. Peters, K. D. Timmerhaus, and R. E. West. *Plant design and economics for chemical engineers*. McGraw-Hill Chemical Engineering Series. McGraw-Hill Education, Singapore, 5 edition, 2003.
- [134] J. P. Lange. Fuels and chemicals manufacturing – guidelines for understanding and minimizing the production costs. *Cattech*, 5(2):82–95, 2001. doi:Doi 10.1023/A:1011944622328.
- [135] A. Bandi and M. Specht. Gewinnung von Methanol aus Biomasse, 2004. URL <https://www.ufop.de/files/9013/3918/4875/Metahnolgewinnung.pdf>.
- [136] F. Ausfelder, A. Bund, A. Fischer, H. A. Gasteiger, T. E. Hamedinger, G. Harp, D. Hoormann, M. Jahn, R. Krähnert, F. Klaucke, F. Köster, U. Krewer, K.-M. Mangold, A. Mitsos, M. Reuter, R. Schütte, T. Sörgel, M. Trennhaus, T. Turek, C. A. Unger, K. Wagemann, M. Waidhas, S. R. Waldvogel, G. Wang, and R. Weber. Elektrifizierung chemischer Prozesse. *DECHEMA Diskussionspapier*, 2015. URL <http://www.dechema.de/2015+Diskussionspapier+Elektrifizierung+Chemischer+Prozesse.html>.
- [137] C. Kunz. Studienvergleich: Entwicklung der Stromgroßhandels- und der CO<sub>2</sub>-Zertifikatspreise, 2013. URL <https://docplayer.org/storage/25/4875049/1616865722/bgsBjjesrSMYpBbGFWOt2A/4875049.pdf>. Forschungsradar Erneuerbare Energien.
- [138] G. Liesche, D. Schack, and K. Sundmacher. The FluxMax approach for simultaneous process synthesis and heat integration: Production of hydrogen cyanide. *AIChE Journal*, 65(7):e16554, 2019. doi:10.1002/aic.16554.

- [139] D. Schack, G. Liesche, and K. Sundmacher. The FluxMax approach: Simultaneous flux optimization and heat integration by discretization of thermodynamic state space illustrated on methanol synthesis process. *Chemical Engineering Science*, 215:115382, 2020. doi:10.1016/j.ces.2019.115382.
- [140] K. Ulonska, A. König, M. Klatt, A. Mitsos, and J. Viell. Optimization of multiproduct biorefinery processes under consideration of biomass supply chain management and market developments. *Industrial & Engineering Chemistry Research*, 57(20):6980–6991, 2018. doi:10.1021/acs.iecr.8b00245.
- [141] S. A. Papoulias and I. E. Grossmann. A structural optimization approach in process synthesis – II: Heat recovery networks. *Computers & Chemical Engineering*, 7(6):707–721, 1983. doi:https://doi.org/10.1016/0098-1354(83)85023-6.
- [142] S. A. Papoulias and I. E. Grossmann. A structural optimization approach in process synthesis – III: Total processing systems. *Computers & Chemical Engineering*, 7(6):723–734, 1983. doi:https://doi.org/10.1016/0098-1354(83)85024-8.
- [143] R. D. Colberg and M. Morari. Area and capital cost targets for heat exchanger network synthesis with constrained matches and unequal heat transfer coefficients. *Computers & Chemical Engineering*, 14(1):1–22, 1990. doi:https://doi.org/10.1016/0098-1354(90)87002-7.
- [144] T. F. Yee, I. E. Grossmann, and Z. Kravanja. Simultaneous optimization models for heat integration – III. Process and heat exchanger network optimization. *Computers & Chemical Engineering*, 14(11):1185–1200, 1990. doi:https://doi.org/10.1016/0098-1354(90)80001-R.
- [145] A. W. Dowling and L. T. Biegler. A framework for efficient large scale equation-oriented flowsheet optimization. *Computers & Chemical Engineering*, 72:3–20, 2015. doi:10.1016/j.compchemeng.2014.05.013.
- [146] A. B. Nagy, R. Adonyi, L. Halasz, F. Friedler, and L. T. Fan. Integrated synthesis of process and heat exchanger networks: algorithmic approach. *Applied Thermal Engineering*, 21(13-14):1407–1427, 2001. doi:Doi 10.1016/S1359-4311(01)00033-3.
- [147] K. Holiastos and V. Manousiouthakis. Minimum hot/cold/electric utility cost for heat exchange networks. *Computers & Chemical Engineering*, 26(1):3–16, 2002. doi:10.1016/S0098-1354(01)00726-8.
- [148] H. Yu, J. Eason, L. T. Biegler, and X. Feng. Simultaneous heat integration and techno-economic optimization of Organic Rankine Cycle (ORC) for multiple waste heat stream recovery. *Energy*, 119:322–333, 2017. doi:10.1016/j.energy.2016.12.061.
- [149] C. Elsidio, A. Mian, and E. Martelli. A systematic methodology for the techno-economic optimization of organic rankine cycles. *4th International Seminar on Orc Power Systems*, 129:26–33, 2017. doi:10.1016/j.egypro.2017.09.171.
- [150] M. Kermani, A. S. Wallerand, I. D. Kantor, and F. Marechal. Generic superstructure synthesis of organic Rankine cycles for waste heat recovery in industrial processes. *Applied Energy*, 212:1203–1225, 2018. doi:10.1016/j.apenergy.2017.12.094.
- [151] R. Holyst and A. Poniewierski. *Thermodynamics for chemists, physicists and engineers*. Springer Netherlands, Dordrecht, 2012. ISBN 978-94-007-2998-8. doi:10.1007/978-94-007-2999-5.
- [152] A. C. Dimian and C. S. Bildea. *Chemical process design: computer-aided case studies*. 2008. ISBN 3527314032.

- [153] S. S. Jogwar and P. Daoutidis. Optimal operation of an energy integrated batch reactor – Feed effluent heat exchanger system. *IFAC-PapersOnLine*, 28(8):1192–1197, 2015. doi:10.1016/j.ifacol.2015.09.130.
- [154] A. C. Dimian and C. S. Bildea. Energy efficient methanol-to-olefins process. *Chemical Engineering Research and Design*, 131:41–54, 2018. doi:10.1016/j.cherd.2017.11.009.
- [155] G. Liesche, D. Schack, K. H. G. Rätze, and K. Sundmacher. Thermodynamic network flow approach for chemical process synthesis. *Computer Aided Chemical Engineering*, 43:881–886, 2018. doi:10.1016/B978-0-444-64235-6.50154-6.
- [156] D. Schack, G. Liesche, and K. Sundmacher. Simultaneous heat and mass flow optimization of a distillation column applying the FluxMax Approach. *Chemical Engineering Transactions*, 76:337–342, 2019. doi:10.3303/CET1976057.
- [157] D. Schack, A. Jastram, G. Liesche, and K. Sundmacher. Energy-efficient distillation processes by additional heat transfer derived from the FluxMax approach. *Frontiers in Energy Research*, 8:134, 2020. doi:10.3389/fenrg.2020.00134.
- [158] European Commission. A clean planet for all a European strategic long-term vision for a prosperous, modern, competitive and climate neutral economy. Report, 28.11.2018 2018. URL <https://eur-lex.europa.eu/legal-content/EN/TXT/PDF/?uri=CELEX:52018DC0773&from=EN>.
- [159] G. M. de Koeijer and S. Kjelstrup. Minimizing entropy production rate in binary tray distillation. *International Journal of Thermodynamics*, 3(3):105–110, 2000.
- [160] I. J. Halvorsen and S. Skogestad. Energy efficient distillation. *Journal of Natural Gas Science and Engineering*, 3(4):571–580, 2011. doi:10.1016/j.jngse.2011.06.002.
- [161] M. R. Fenske. Fractionation of straight-run Pennsylvania gasoline. *Industrial & Engineering Chemistry*, 24(5):482–485, 1932. doi:10.1021/ie50269a003.
- [162] A. J. V. Underwood. Fractional distillation of multicomponent mixtures. *Industrial & Engineering Chemistry*, 41(12):2844–2847, 1949. doi:10.1021/ie50480a044.
- [163] E. R. Gilliland. Multicomponent rectification estimation of the number of theoretical plates as a function of the reflux ratio. *Industrial & Engineering Chemistry*, 32(9):1220–1223, 1940. doi:10.1021/ie50369a035.
- [164] L. T. Biegler, I. E. Grossmann, and A. W. Westerberg. *Systematic methods of chemical process design*. Upper Saddle River, NJ Prentice Hall, 1997. ISBN 0-13-272337-9.
- [165] J. Bausa, R. v. Watzdorf, and W. Marquardt. Minimum energy demand for nonideal multicomponent distillations in complex columns. *Computers & Chemical Engineering*, 20:S55–S60, 1996. doi:[https://doi.org/10.1016/0098-1354\(96\)00020-8](https://doi.org/10.1016/0098-1354(96)00020-8).
- [166] C. Adiche and A. Vogelpohl. Short-cut methods for the optimal design of simple and complex distillation columns. *Chemical Engineering Research and Design*, 89(8):1321–1332, 2011. doi:10.1016/j.cherd.2011.02.014.
- [167] J. A. Caballero and I. E. Grossmann. *Optimization of distillation processes*, pages 437–496. Academic Press, Boston, 2014. doi:10.1016/B978-0-12-386547-2.00011-9.
- [168] M. Ledezma-Martinez, M. Jobson, and R. Smith. Simulation-optimization-based design of crude oil distillation systems with preflash units. *Industrial & Engineering Chemistry Research*, 57(30):9821–9830, 2018. doi:10.1021/acs.iecr.7b05252.

- [169] Z. Jiang, G. M. Ramapriya, M. Tawarmalani, and R. Agrawal. Process intensification in multicomponent distillation. *Chemical Engineering Transactions*, 69:841–846, 2018. doi:10.3303/CET1869141.
- [170] Z. Jiang, G. Madenoor Ramapriya, M. Tawarmalani, and R. Agrawal. Minimum energy of multicomponent distillation systems using minimum additional heat and mass integration sections. *AIChE Journal*, 64(9):3410–3418, 2018. doi:10.1002/aic.16189.
- [171] M. Nakaiwa, K. Huang, A. Endo, T. Ohmori, T. Akiya, and T. Takamatsu. Internally heat-integrated distillation columns: A review. *Chemical Engineering Research and Design*, 81(1):162–177, 2003. doi:10.1205/026387603321158320.
- [172] R. Agrawal and T. F. Yee. Heat-pumps for thermally linked distillation-columns – An exercise for argon production from air. *Industrial & Engineering Chemistry Research*, 33(11):2717–2730, 1994. doi:Doi 10.1021/Ie00035a023.
- [173] A. A. Kiss, S. J. Flores Landaeta, and C. A. Infante Ferreira. Towards energy efficient distillation technologies – Making the right choice. *Energy*, 47(1):531–542, 2012. doi:10.1016/j.energy.2012.09.038.
- [174] C. Cui, Z. Xi, S. Liu, and J. Sun. An enumeration-based synthesis framework for multi-effect distillation processes. *Chemical Engineering Research and Design*, 144: 216–227, 2019. doi:10.1016/j.cherd.2019.02.018.
- [175] C. Cui, H. Yin, J. Yang, D. Wei, J. Sun, and C. Guo. Selecting suitable energy-saving distillation schemes: Making quick decisions. *Chemical Engineering and Processing - Process Intensification*, 107:138–150, 2016. doi:10.1016/j.cep.2016.05.009.
- [176] P. Schäfer, A. Caspari, K. Kleinhans, A. Mhamdi, and A. Mitsos. Reduced dynamic modeling approach for rectification columns based on compartmentalization and artificial neural networks. *AIChE Journal*, 65(5):e16568, 2019. doi:10.1002/aic.16568.
- [177] T. Waltermann and M. Skiborowski. Efficient optimization-based design of energy-integrated distillation processes. *Computers & Chemical Engineering*, 129:106520, 2019. doi:10.1016/j.compchemeng.2019.106520.
- [178] K. P. Papalexandri and E. N. Pistikopoulos. Generalized modular representation framework for process synthesis. *Aiche Journal*, 42(4):1010–1032, 1996. doi:DOI 10.1002/aic.690420413.
- [179] S. R. Ismail, E. N. Pistikopoulos, and K. P. Papalexandri. Modular representation synthesis framework for homogeneous azeotropic separation. *Aiche Journal*, 45(8): 1701–1720, 1999. doi:DOI 10.1002/aic.690450809.
- [180] P. B. Shah and A. C. Kokossis. New synthesis framework for the optimization of complex distillation systems. *AIChE Journal*, 48(3):527–550, 2002. doi:DOI 10.1002/aic.690480311.
- [181] S. Brüggemann and W. Marquardt. Rapid screening of design alternatives for nonideal multiproduct distillation processes. *Computers & Chemical Engineering*, 29(1):165–179, 2004. doi:10.1016/j.compchemeng.2004.07.009.
- [182] I. Heckl, F. Friedler, and L. T. Fan. Solution of separation-network synthesis problems by the P-graph methodology. *Computers & Chemical Engineering*, 34(5):700–706, 2010. doi:10.1016/j.compchemeng.2010.01.019.
- [183] D. R. Stull. Vapor pressure of pure substances. Organic and inorganic compounds. *Industrial & Engineering Chemistry*, 39(4):517–540, 1947. doi:10.1021/ie50448a022.

- [184] D. Ambrose and C. H. S. Sprake. Thermodynamic properties of organic oxygen compounds XXV. Vapour pressures and normal boiling temperatures of aliphatic alcohols. *The Journal of Chemical Thermodynamics*, 2(5):631–645, 1970. doi:10.1016/0021-9614(70)90038-8.
- [185] A. Gleixner, M. Bastubbe, L. Eifler, T. Gally, G. Gamrath, R. L. Gottwald, G. Hendel, C. Hojny, T. Koch, M. E. Lübbecke, S. J. Maher, M. Miltenberger, B. Müller, M. E. Pfetsch, C. Puchert, Daniel Rehfeldt, Franziska Schlösser, Christoph Schubert, Felipe Serrano, Yuji Shinano, Jan Merlin Viernickel, M. Walter, F. Wegscheider, J. T. Witt, and J. Witzig. The SCIP Optimization Suite 6.0. Report, Optimization Online, July 2018. URL [http://www.optimization-online.org/DB\\_HTML/2018/07/6692.html](http://www.optimization-online.org/DB_HTML/2018/07/6692.html).
- [186] V. V. Kuznetsov. *Two-phase heat exchangers*, pages 1473–1500. Springer International Publishing, Cham, 2018. ISBN 978-3-319-26695-4. doi:10.1007/978-3-319-26695-4\_20.
- [187] A. Bejan and A. D. Kraus. *Heat transfer handbook*. Wiley, Hoboken, NJ, 2003. ISBN 0-471-39015-1.
- [188] B. C. Kim, H. H. Chun, and Y. H. Kim. Energy-efficient diabatic distillation using a horizontal distillation column. *Industrial & Engineering Chemistry Research*, 52(42):14927–14935, 2013. doi:10.1021/ie4013997.
- [189] D. J. Jang and Y. H. Kim. A new horizontal distillation for energy saving with a diabatic rectangular column. *Korean Journal of Chemical Engineering*, 32(11):2181–2186, 2015. doi:10.1007/s11814-015-0048-4.
- [190] W. Roetzel and B. Spang. *Typical values of overall heat transfer coefficients*, pages 75–78. Springer Berlin Heidelberg, Berlin, Heidelberg, 2010. ISBN 978-3-540-77877-6. doi:10.1007/978-3-540-77877-6\_6.
- [191] K. Miettinen. *Nonlinear Multiobjective Optimization*. International Series in Operations Research & Management Science. Springer US, New York, NY, 1st ed. 1998 edition, 1998. ISBN 9781461555636.
- [192] R. C. Reid. *The properties of gases and liquids*. McGraw-Hill, New York, 1987. ISBN 978-0070116825.
- [193] NIST. NIST Chemistry WebBook. URL <http://webbook.nist.gov/chemistry/>.
- [194] M.W. Chase Jr. NIST-JANAF Thermochemical Tables. *Journal of Physical and Chemical Reference Data*, 4:1–1951, 1998. doi:10.18434/T42S31.
- [195] Y. Takahashi and E. F. Westrum Jr. Glassy carbon low-temperature thermodynamic properties. *The Journal of Chemical Thermodynamics*, 2(6):847–854, 1970. doi:10.1016/0021-9614(70)90028-5.
- [196] A. Dobrosavljevic, N. Perovic, and K Maglic. Thermophysical properties of POCO AXM-5Q1 graphite in the 300 to 1800 K range. *High Temperatures-High Pressures*, 19:303–310, 1987.
- [197] E. J. Prosen and F. D. Rossini. Heats of combustion and formation of the paraffin hydrocarbons at 25 °C. *Journal of Research of the National Bureau of Standards*, 34(3):263–269, 1945. doi:10.6028/jres.034.013.
- [198] D. W. Scott. Correlation of the chemical thermodynamic properties of alkane hydrocarbons. *The Journal of Chemical Physics*, 60(8):3144–3165, 1974. doi:10.1063/1.1681500.
- [199] W.M. Haynes. *CRC Handbook of Chemistry and Physics, 97th Edition*. CRC Press, 2016. ISBN 9781498754293.



- [200] G. Pilcher, A. S. Pell, and D. J. Coleman. Measurements of heats of combustion by flame calorimetry. Part 2.—Dimethyl ether, methyl ethyl ether, methyl n-propyl ether, methyl isopropyl ether. *Transactions of the Faraday Society*, 60(0):499–505, 1964. doi:10.1039/TF9646000499.
- [201] J. Chao, K. R. Hall, K. N. Marsh, and R. C. Wilhoit. Thermodynamic properties of key organic oxygen compounds in the carbon range C<sub>1</sub> to C<sub>4</sub>. Part 2. Ideal gas properties. *Journal of Physical and Chemical Reference Data*, 15(4):1369–1436, 1986. doi:10.1063/1.555769.
- [202] J. H. S. Green. Thermodynamic properties of organic oxygen compounds. Part 5.—Ethyl alcohol. *Transactions of the Faraday Society*, 57(0):2132–2137, 1961. doi:10.1039/TF9615702132.
- [203] J. P. Guthrie. Hydration of carboxamides. Evaluation of the free energy change for addition of water to acetamide and formamide derivatives. *Journal of the American Chemical Society*, 96(11):3608–3615, 1974. doi:10.1021/ja00818a039.
- [204] R. C. Millikan and K. S. Pitzer. Infrared spectra and vibrational assignment of monomeric formic acid. *The Journal of Chemical Physics*, 27(6):1305–1308, 1957. doi:10.1063/1.1743996.
- [205] J. A. Manion. Evaluated enthalpies of formation of the stable closed shell C<sub>1</sub> and C<sub>2</sub> chlorinated hydrocarbons. *Journal of Physical and Chemical Reference Data*, 31(1):123–172, 2002. doi:10.1063/1.1420703.
- [206] B.J. Zwolinski and L. Beach. *Selected values of properties of chemical compounds*. Thermodynamics Research Center, Texas Engineering Experiment Station, Texas A & M University, 1975.
- [207] J. Chao and F. D. Rossini. Heats of combustion, formation, and isomerization of nineteen alkanols. *Journal of Chemical & Engineering Data*, 10(4):374–379, 1965. doi:10.1021/je60027a022.
- [208] H. G. Carlson and E. F. Westrum Jr. Methanol: Heat capacity, enthalpies of transition and melting, and thermodynamic properties from 5–300 °K. *The Journal of Chemical Physics*, 54(4):1464–1471, 1971. doi:10.1063/1.1675039.
- [209] G. Pilcher and R. A. Fletcher. Measurements of heats of combustion by flame calorimetry. Part 5.—Dimethoxymethane, 1,1-dimethoxyethane. *Transactions of the Faraday Society*, 65(0):2326–2330, 1969. ISSN 0014-7672. doi:10.1039/TF9696502326.
- [210] D. M. McEachern Jr. and J. E. Kilpatrick. Entropy and related thermodynamic properties of dimethoxymethane. *The Journal of Chemical Physics*, 41(10):3127–3131, 1964. doi:10.1063/1.1725685.
- [211] K. G. Joback and R. C. Reid. Estimation of pure-component properties from group-contributions. *Chemical Engineering Communications*, 57(1-6):233–243, 1987. doi:10.1080/00986448708960487.
- [212] I. Garagounis, V. Kyriakou, A. Skodra, E. Vasileiou, and M. Stoukides. Electrochemical Synthesis of Ammonia in Solid Electrolyte Cells. *Frontiers in Energy Research*, 2:1.1–1.10, 2014. doi:10.3389/fenrg.2014.00001.
- [213] R. Lan, J. T. Irvine, and S. Tao. Synthesis of ammonia directly from air and water at ambient temperature and pressure. *Scientific Reports*, 3:1145, 2013. doi:10.1038/srep01145.

- [214] G. C. Xu, R. Q. Liu, and J. Wang. Electrochemical synthesis of ammonia using a cell with a Nafion membrane and  $\text{SmFe}_{0.7}\text{Cu}_{0.3-x}\text{Ni}_x\text{O}_3$  ( $x = 0-0.3$ ) cathode at atmospheric pressure and lower temperature. *Science in China Series B: Chemistry*, 52(8):1171–1175, 2009. doi:10.1007/s11426-009-0135-7.
- [215] X. W. Wang, J. L. Yin, J. H. Xu, H. T. Wang, and G. L. Ma. Chemical stability, ionic conductivity of  $\text{BaCe}_{0.9-x}\text{Zr}_x\text{Sm}_{0.1}\text{O}_3$ -alpha and its application to ammonia synthesis at atmospheric pressure. *Chinese Journal of Chemistry*, 29(6):1114–1118, 2011. doi:10.1002/cjoc.201190209.
- [216] E. Gail, S. Gos, R. Kulzer, J. Lorösch, A. Rubo, M. Sauer, R. Kellens, J. Reddy, N. Steier, and W. Hasenpusch. *Cyano compounds, inorganic*. Wiley-VCH Verlag GmbH & Co. KGaA, 2000. ISBN 9783527306732. doi:10.1002/14356007.a08\_159.pub3.
- [217] A. S. Bodke, D. A. Olschki, and L. D. Schmidt. Hydrogen addition to the Andrussow process for HCN synthesis. *Applied Catalysis A: General*, 201(1):13–22, 2000. doi:10.1016/S0926-860x(00)00419-1.
- [218] G. Centi and S. Perathoner. Opportunities and prospects in the chemical recycling of carbon dioxide to fuels. *Catalysis Today*, 148(3-4):191–205, 2009. doi:10.1016/j.cattod.2009.07.075.
- [219] K. Sun, W. Lu, M. Wang, and X. Xu. Low-temperature synthesis of DME from  $\text{CO}_2/\text{H}_2$  over Pd-modified  $\text{CuO-ZnO-Al}_2\text{O}_3\text{-ZrO}_2/\text{HZSM-5}$  catalysts. *Catalysis Communications*, 5(7):367–370, 2004. doi:10.1016/j.catcom.2004.03.012.
- [220] A. Goepfert, M. Czaun, J. P. Jones, G. K. Surya Prakash, and G. A. Olah. Recycling of carbon dioxide to methanol and derived products – closing the loop. *Chem Soc Rev*, 43(23):7995–8048, 2014. doi:10.1039/c4cs00122b.
- [221] R. Amin, B. Liu, Z. B. Huang, and Y. C. Zhao. Hydrogen and syngas production via  $\text{CO}_2$  dry reforming of methane over Mg/La promoted Co-Ni/MSU-S catalyst. *International Journal of Hydrogen Energy*, 41(2):807–819, 2016. doi:10.1016/j.ijhydene.2015.10.063.
- [222] K. Selvarajah, N. H. H. Phuc, B. Abdullah, F. Alenazey, and D.-V. N. Vo. Syngas production from methane dry reforming over Ni/ $\text{Al}_2\text{O}_3$  catalyst. *Research on Chemical Intermediates*, 42(1):269–288, 2016. doi:10.1007/s11164-015-2395-5.
- [223] L. Yao, J. Shi, H. Xu, W. Shen, and C. Hu. Low-temperature  $\text{CO}_2$  reforming of methane on Zr-promoted Ni/ $\text{SiO}_2$  catalyst. *Fuel Processing Technology*, 144:1–7, 2016. doi:10.1016/j.fuproc.2015.12.009.
- [224] X. Li, X. San, Y. Zhang, T. Ichii, M. Meng, Y. Tan, and N. Tsubaki. Direct synthesis of ethanol from dimethyl ether and syngas over combined H-Mordenite and Cu/ZnO catalysts. *ChemSusChem*, 3(10):1192–9, 2010. doi:10.1002/cssc.201000109.
- [225] L. Lopez, J. Velasco, S. Cabrera, M. Boutonnet, and S. Järas. Effect of syngas conversion and catalyst reduction temperature in the synthesis of ethanol: concentration of water vapor in mesoporous Rh/MCM-41 catalyst. *Catalysis Communications*, 69:183–187, 2015. doi:10.1016/j.catcom.2015.06.015.
- [226] M. J. Lippits and B. E. Nieuwenhuys. Direct conversion of ethanol into ethylene oxide on copper and silver nanoparticles. *Catalysis Today*, 154(1-2):127–132, 2010. doi:10.1016/j.cattod.2010.03.019.
- [227] D. K. Lee, D. S. Kim, and S. W. Kim. Selective formation of formaldehyde from carbon dioxide and hydrogen over PtCu/ $\text{SiO}_2$ . *Applied Organometallic Chemistry*, 15(2):148–150, 2001. doi:10.1002/1099-0739(200102)15:2<148::Aid-Aoc104>3.0.Co;2-N.

- [228] C. Fletcher, Y. Jiang, and R. Amal. Production of formic acid from CO<sub>2</sub> reduction by means of potassium borohydride at ambient conditions. *Chemical Engineering Science*, 137:301–307, 2015. doi:10.1016/j.ces.2015.06.040.
- [229] S. Moret, P. J. Dyson, and G. Laurenczy. Direct synthesis of formic acid from carbon dioxide by hydrogenation in acidic media. *Nat Commun*, 5:4017, 2014. doi:10.1038/ncomms5017.
- [230] C. Hao, S. Wang, M. Li, L. Kang, and X. Ma. Hydrogenation of CO<sub>2</sub> to formic acid on supported ruthenium catalysts. *Catalysis Today*, 160(1):184–190, 2011. doi:10.1016/j.cattod.2010.05.034.
- [231] H.-Y. Kim, I. Choi, S. H. Ahn, S. J. Hwang, S. J. Yoo, J. Han, J. Kim, H. Park, J. H. Jang, and S.-K. Kim. Analysis on the effect of operating conditions on electrochemical conversion of carbon dioxide to formic acid. *International Journal of Hydrogen Energy*, 39(29):16506–16512, 2014. doi:10.1016/j.ijhydene.2014.03.145.
- [232] S. Rönsch, J. Schneider, S. Matthischke, M. Schlüter, M. Götz, J. Lefebvre, P. Prabhakaran, and S. Bajohr. Review on methanation – From fundamentals to current projects. *Fuel*, 166:276–296, 2016. doi:10.1016/j.fuel.2015.10.111.
- [233] F. Koschany, D. Schlereth, and O. Hinrichsen. On the kinetics of the methanation of carbon dioxide on coprecipitated NiAl(O)<sub>x</sub>. *Applied Catalysis B: Environmental*, 181:504–516, 2016. doi:10.1016/j.apcatb.2015.07.026.
- [234] X. Zhang, S. Zhang, and C. Jian. Synthesis of methylal by catalytic distillation. *Chemical Engineering Research and Design*, 89(6):573–580, 2011. doi:10.1016/j.cherd.2010.09.002.
- [235] H. Liu, H. Gao, Y. Ma, Z. Gao, and W. Eli. Synthesis of high-purity methylal via extractive catalytic distillation. *Chemical Engineering & Technology*, 35(5):841–846, 2012. doi:10.1002/ceat.201100446.
- [236] H. Li, H. Song, F. Zhao, L. Chen, and C. Xia. Chemical equilibrium controlled synthesis of polyoxymethylene dimethyl ethers over sulfated titania. *Journal of Energy Chemistry*, 24(2):239–244, 2015. doi:10.1016/s2095-4956(15)60307-2.
- [237] J. Masamoto, J. Ohtake, and M. Kawamura. Process for producing formaldehyde and derivatives thereof, European Patent Office, EP0327343B1, Apr. 1994. URL <https://patentimages.storage.googleapis.com/6f/59/03/d39824c95021e6/EP0327343B1.pdf>.
- [238] Y. Yuan, H. Liu, H. Imoto, T. Shido, and Y. Iwasawa. Performance and characterization of a new crystalline SbRe<sub>2</sub>O<sub>6</sub> catalyst for selective oxidation of methanol to methylal. *Journal of Catalysis*, 195(1):51–61, 2000. doi:10.1006/jcat.2000.2990.
- [239] J. Fischer, T. Lehmann, and E. Heitz. The production of oxalic-acid from CO<sub>2</sub> and H<sub>2</sub>O. *Journal of Applied Electrochemistry*, 11(6):743–750, 1981. doi:Doi 10.1007/Bf00615179.
- [240] R. Reimert, F. Marschner, H.-J. Renner, W. Boll, E. Supp, M. Brejc, W. Liebner, and G. Schaub. *Gas production, 2. Processes*. Wiley-VCH Verlag GmbH & Co. KGaA, 2000. ISBN 9783527306732. doi:10.1002/14356007.o12\_o01.
- [241] A. Heinzl, M. Cappadonia, U. Stimming, K. V. Kordesch, and J. C. T. de Oliveira. *Fuel Cells*. Wiley-VCH Verlag GmbH & Co. KGaA, 2000. ISBN 9783527306732. doi:10.1002/14356007.a12\_055.pub2.
- [242] M. Wenzel, L. Rihko-Struckmann, and K. Sundmacher. Thermodynamic analysis and optimization of RWGS processes for solar syngas production from CO<sub>2</sub>. *AIChE Journal*, 63(1):15–22, 2017. doi:10.1002/aic.15445.

- [243] S. D. Angeli, F. G. Pilitsis, and A. A. Lemonidou. Methane steam reforming at low temperature: Effect of light alkanes presence on coke formation. *Catalysis Today*, 242: 119–128, 2015. doi:10.1016/j.cattod.2014.05.043.
- [244] V. Kyriakou, I. Garagounis, A. Vourros, E. Vasileiou, A. Manerbino, W. G. Coors, and M. Stoukides. Methane steam reforming at low temperatures in a  $\text{BaZr}_{0.7}\text{Ce}_{0.2}\text{Y}_{0.1}\text{O}_{2.9}$  proton conducting membrane reactor. *Applied Catalysis B: Environmental*, 186:1–9, 2016. doi:10.1016/j.apcatb.2015.12.039.
- [245] S. Abanades, H. Kimura, and H. Otsuka. A drop-tube particle-entrained flow solar reactor applied to thermal methane splitting for hydrogen production. *Fuel*, 153:56–66, 2015. doi:10.1016/j.fuel.2015.02.103.
- [246] J. R. Hufton, S. Mayorga, and S. Sircar. Sorption-enhanced reaction process for hydrogen production. *AIChE Journal*, 45(2):248–256, 1999. doi:DOI 10.1002/aic.690450205.
- [247] P. Bender, S. Neuendorf, N.D. Schödel, and H.D. Winkler. Verfahren zur Erzeugung von Wasserstoff mit Hilfe der Wassergas-Shift-Reaktion bei sehr niedrigen Temperaturen, European Patent Office, EP1878782A1, Jan. 2008. URL <https://patentimages.storage.googleapis.com/3d/e8/1d/fab2bc2963530c/EP1878782A1.pdf>.

# List of Figures

1.1	Schematic illustration of the process hierarchies considered in the context of this dissertation. . . . .	3
1.2	Dissertation in a nutshell: Schematic illustration of the structure of this dissertation and indication of the research questions answered. . . . .	5
2.1	Schematic illustration of the R2Chem concept to store electrical energy by chemical conversion of valuable chemicals. . . . .	8
2.2	Schematic illustration of the conversion chain to produce valuable chemicals via the R2Chem pathway. . . . .	11
2.3	Storage efficiency of different target molecules for two carbon dioxide sources: capturing from flue gas and direct air capturing. . . . .	14
2.4	Comparison of annual renewable energy available in Germany and CO <sub>2</sub> emissions with annual productions of H <sub>2</sub> and CH <sub>3</sub> OH. . . . .	15
3.1	Illustration of the three-steps of the FluxMax approach for unit and process design with simultaneous heat integration. . . . .	21
3.2	Grid of thermodynamic state points in the thermodynamic state space with $p$ , $T$ and $\mathbf{x}$ coordinates. . . . .	23
3.3	Schematic illustration of direct and indirect heat integration. . . . .	27
4.1	Schematic illustration of the process design task at the production system level.	36
4.2	Mass conversion along the edges; schematic illustration of a single process consisting of reaction, separation and auxiliary operations used for temperature and pressure adjustment. . . . .	40
4.3	Systematically evaluation of the influence of different sources for feedstock, heat and power supply on the specific production costs and on the specific CO <sub>2</sub> emissions. . . . .	49
4.4	Schematic illustration of optimal process configurations for the different feedstock sources coal (1st row), natural gas (2nd row), biomass (3rd row) and CO <sub>2</sub> (4th row). . . . .	52
4.5	Evaluation of the influence of energy supply sources on the specific costs (left) and on the CO <sub>2</sub> emissions (right). . . . .	53

---

4.6	Analysis of the reforming processes for the conversion of methane into synthesis gas for each combination of heat and power source. . . . .	54
4.7	Flowsheets of the optimal process configuration for the methanol synthesis using methane and carbon dioxide as feedstock sources depending on different reforming processes. . . . .	55
4.8	Pareto optimal curve of multiobjective optimization problem using natural gas as feedstock source and each combination of heat and power source for methanol synthesis. . . . .	56
5.1	Schematic illustration of the process design task at the plant level. . . . .	60
5.2	Schematic illustration of selected EPNs in the discretized thermodynamic state space. . . . .	63
5.3	Boiling temperature of methanol as a function of the pressure. . . . .	67
5.4	Illustration of the pressure dependence of the chemical equilibrium molar fraction of methanol in the reactor $x_{\text{CH}_3\text{OH}}$ (A) and of the boiling temperature of methanol (B). . . . .	70
5.5	Optimal pathway of benchmark case in the discretized state space; corresponding elementary processes are represented along the path. . . . .	73
5.6	Schematic illustration of the optimal process configurations of the benchmark scenario obtained in a sequential procedure. . . . .	75
5.7	Optimal pathway in discretized state space obtained in a simultaneous procedure; optimal pathways for direct (A) and indirect heat integration (B); in addition, external energy demands and heat integration potentials are given. . . . .	77
5.8	Schematic illustration of the optimal process configurations obtained in a simultaneous procedure; for better clarity, only the flowsheet is shown, taking direct heat integration into account. . . . .	79
5.9	Illustration of the external heating requirement as a function of the number of utilities considered. . . . .	80
5.10	Optimal pathway in discretized state space for cases A) $T_{\text{targ}} = 25\text{ }^\circ\text{C}$ , $p_{\text{targ}} = 50\text{ bar}$ and B) $T_{\text{targ}} = 150\text{ }^\circ\text{C}$ , $p_{\text{targ}} = 100\text{ bar}$ . . . . .	82
6.1	Schematic illustration of the process unit design task at the process level. . . . .	86
6.2	Representation of the overall distillation process as a sequence of elementary processes mixing (grey), heating/cooling (magenta) and flash separation (cyan) as well as single tray fluxes. . . . .	87
6.3	Schematic illustration of the FluxMax approach for distillation column design. . . . .	88
6.4	Schematic illustration of the heat integration model for classic distillation columns, and for the exploitation of additional degrees of freedom. . . . .	90

---

6.5	Schematic illustration of tray $n$ and neighboring tray $n + 1$ for the regular formulation of MESH equations (A) and for the case where intermediate heat exchangers $m - 1$ , $m$ and $m + 1$ are considered (B). . . . .	94
6.6	Optimal pathway within the thermodynamic state space for the two objective functions, and corresponding operation line for a temperature discretization of 17. . . . .	96
6.7	Operation line for a discretization of of 17 temperature levels if the number of selectable tray stages is limited to 9 (A), and 11 (B) . . . . .	98
6.8	Influence of number of separation stages on the total energy duty if no additional heat transfer is considered. . . . .	99
6.9	Influence of the number of separation stages on the total energy duty if additional heat transfer is considered. . . . .	100
6.10	Schematic illustration of a column with intermediate heat exchangers (A), and the corresponding interpretation as a series of heat integrated flash drums (B). 101	
6.11	Influence of the selected minimum temperature difference $\Delta T_{\min}$ of the additional heat transfer on the energy demand. . . . .	102
6.12	Pareto curves of the two competing objectives: Minimization of total energy duty and minimization of additional heat transfer area for different number of separation stages: 5, 7, 9, and 11 stages. . . . .	104
C.1	Determination of fitting parameters $p_1$ and $p_2$ by linear fitting of investment cost estimation proposed by Lange [134]. Linear fits depend on the estimated energy loss range: A: 0 to 100 MW, B: 0 to 500 MW, and C: 400 to 1,000 MW. 121	
D.1	Illustration of the discretization of the thermodynamic state space. . . . .	130





# List of Tables

2.1	Overview on different storage molecules. . . . .	8
2.2	Overview on the conversion efficiencies. . . . .	13
2.3	Overview of specific energy inputs required for CCU and air separation. . . . .	13
3.1	Temperature conditions for for classification of heat integration possibility. . . . .	28
4.1	Comparison of different energy sources, their costs and associated CO <sub>2</sub> emissions. . . . .	43
4.2	Definition of scenario. . . . .	44
4.3	Lower and upper bounds. . . . .	44
5.1	Overview of generalized stoichiometric equations and corresponding unit operations of elementary processes considered in this case study. . . . .	62
5.2	Definition of scenario. . . . .	71
5.3	Overview of the external heating and cooling duties of the sequential and simultaneous approach and corresponding saving potentials. . . . .	78
5.4	Utilities and their corresponding temperatures used in the study. . . . .	81
6.1	Scenario definition of methanol-water separation. . . . .	91
6.2	Antoine parameters for pure water and methanol for the relevant temperature range. . . . .	92
A.1	Thermodynamic data. . . . .	117
B.1	Comparison of the reversible conversion efficiency $\eta_j^{\text{rev}}$ and the real conversion efficiency $\eta_j$ reported in the literature. . . . .	120
C.1	Overview of considered conversion processes. . . . .	122
D.1	Reaction equations, partial molar and energy balances for selected EPNs. . . . .	126
D.2	Temperature levels of the utilities depending on the number of utilities. . . . .	129



# Publications and statements of authorship

## Peer-reviewed journal articles

**Schack, D.**, Jastram, A., Liesche, G., Sundmacher, K.: Energy-efficient distillation processes by additional heat transfer derived from the FluxMax approach, *Frontiers in Energy Research*, 8, 134, **2020**. doi:10.3389/fenrg.2020.00134

**Schack, D.** developed the model, carried out the optimizations, analyzed the results and wrote the manuscript.

**Schack, D.**, Liesche, G., Sundmacher, K.: The FluxMax approach: Simultaneous flux optimization and heat integration by discretization of thermodynamic state space illustrated on methanol synthesis process, *Chemical Engineering Science*, 215, 115382, **2020**. doi:10.1016/j.ces.2019.115382

**Schack, D.** and Liesche, G. developed the FluxMax approach with equal contributions and the advice of Sundmacher, K. **Schack, D.** developed the model for the methanol case study, carried out the optimizations, analyzed the results and wrote the manuscript.

**Schack, D.**, Liesche, G., Sundmacher, K.: Simultaneous heat and mass flow optimization of a distillation column applying the FluxMax approach, *Chemical Engineering Transactions*, 76, 337–342, **2019**. doi:10.3303/CET1976057

**Schack, D.** developed the model, carried out the optimizations, analyzed the results and wrote the manuscript.

Liesche, G., **Schack, D.**, Sundmacher, K.: The FluxMax approach for simultaneous process synthesis and heat integration: Production of hydrogen cyanide, *AIChE Journal*, 65(7), e16554, **2019**. doi:10.1002/aic.16554

**Schack, D.** and Liesche, G. developed the FluxMax approach with equal contributions and the advice of Sundmacher, K. **Schack, D.** provided parts of the figures and methods section to the final manuscript.

**Schack, D.** and Sundmacher, K.: Techno-economic optimization of the production network for the synthesis of formic acid from renewables, *Chemie Ingenieur Technik*, 90(1–2), 256–266, **2018**. doi:10.1002/cite.201700163

**Schack, D.** developed the model, carried out the optimizations, analyzed the results and wrote the manuscript.

**Schack, D.**, Rihko-Struckmann, L., Sundmacher, K.: Linear programming approach for structure optimization of Renewable-to-Chemicals (R2Chem) production networks, *Industrial & Engineering Chemistry Research*, 57(30), 9889–9902, **2018**. doi:10.1021/acs.iecr.7b05305

**Schack, D.** developed the model, carried out the optimizations, analyzed the results and wrote the manuscript.

**Special achievement:** Article is awarded as highlighted paper by using the graphical abstract as cover picture of volume 57, issue 30 of *Industrial & Engineering Chemistry Research*.

## Peer-reviewed conference papers

Lueg, L., **Schack, D.**, Örs, E., Schmidt, R., Bickert, P., von Kurnatowski, M., Ludl, P.O., Bortz, M.: Data-driven process design exemplified on the steam methane reforming process, *31th European Symposium on Computer Aided Process Engineering*, Istanbul, Turkey, *Computer Aided Chemical Engineering*. Elsevier, **2021**, accepted paper.

Liesche, G., **Schack, D.**, Rätze, K.H.G., Sundmacher, K.: Thermodynamic network flow approach for chemical process synthesis, *28th European Symposium on Computer Aided Process Engineering*, Graz, Austria, *Computer Aided Chemical Engineering*, 43, 881–886. Elsevier, **2018**. doi:10.1016/B978-0-444-64235-6.50154-6

**Schack, D.**, Rihko-Struckmann, L., Sundmacher, K.: Economic linear objective function approach for structure optimization of renewables-to-chemicals (R2Chem) networks, *27th European Symposium on Computer Aided Process Engineering*, Barcelona, Spain, *Computer Aided Chemical Engineering*, 40, 1975–1980. Elsevier, **2017**. doi:10.1016/B978-0-444-63965-3.50331-7

**Schack, D.**, Rihko-Struckmann, L., Sundmacher, K.: Structure optimization of power-to-chemicals (P2C) networks by linear programming for the economic utilization of renewable surplus energy, *26th European Symposium on Computer Aided Process Engineering*, Portoroz, Slovenia, *Computer Aided Chemical Engineering*, 38, 1551–1556. Elsevier, **2016**. doi:10.1016/B978-0-444-63428-3.50263-0

---

## Conference proceedings

**Schack, D.** and Sundmacher, K.: Renewables-to-Chemicals: Optimaler Prozessentwurf für eine nachhaltige Methanolproduktion unter Einsatz von CO<sub>2</sub>, *Chemie Ingenieur Technik, Special Issue: ProcessNet-Jahrestagung und 33. DECHEMA-Jahrestagung der Biotechnologen 2018*, 90(9), 1135, **2018**. doi:10.1002/cite.201855006

**Schack, D.**, Rihko-Struckmann, L., Sundmacher, K.: Strukturoptimierung von Renewables-to-Chemicals (R2Chem) Netzwerken zur wirtschaftlichen Nutzung erneuerbarer Energien, *Chemie Ingenieur Technik, Special Issue: ProcessNet-Jahrestagung und 32. DECHEMA-Jahrestagung der Biotechnologen 2016*, 88(9), 1343, **2016**. doi:10.1002/cite.201650270

## Further publications

**Schack, D.:** R2Chem: Renewables to valuable chemicals and fuels, *MPI Magdeburg Report 2017 – 2018*, 42–43, Magdeburg, Germany, **2019**.

## Conference contributions

### Oral contributions

Lueg, L., **Schack, D.**, Örs, E., Schmidt, R., Bickert, P., von Kurnatowski, M., Ludl, P.O., Bortz, M.: Data-driven process design exemplified on the steam methane reforming process, *31th European Symposium on Computer Aided Process Engineering*, Istanbul, Turkey, **2021**, accepted as oral presentation.

**Schack, D.**, Liesche, G., Sundmacher, K.: Optimal process design for a sustainable methanol production using renewable energies by applying the FluxMax approach, *2019 AIChE Annual Meeting*, Orlando, USA, **2019**.

Liesche, G., **Schack, D.**, Sundmacher, K.: The FluxMax approach: Integrated process synthesis and heat integration exemplified for the production of hydrogen cyanide, *2019 AIChE Annual Meeting*, Orlando, USA, **2019**.

**Schack, D.**, Jastram, A., Sundmacher, K.: Simultaneous heat and mass flow optimization of a distillation column applying the FluxMax approach, *22nd Conference on Process Integration for Energy Saving and Pollution Reduction*, Agios Nikolaos, Greece, **2019**.

**Schack, D.** and Sundmacher, K.: Optimal process design for a sustainable methanol production using renewable energies by applying the FluxMax approach, *12th European Congress of Chemical Engineering*, Florence, Italy, **2019**.

**Schack, D.**, Sundmacher, K.: E-Fuels: Converting electricity, water and CO<sub>2</sub> into transportation fuels. *1. Workshop zur Nachhaltigkeit in der MPG*, Magdeburg, Germany, **2019**, (Held by Sundmacher, K.).

**Schack, D.**, Liesche, G., Sundmacher, K.: Optimaler Prozessentwurf für eine nachhaltige Methanolproduktion unter Einsatz von CO<sub>2</sub> und erneuerbaren Energien, *Jahrestreffen der ProcessNet-Fachgruppe Energieverfahrenstechnik*, Frankfurt, Germany, **2019**.

Liesche, G., **Schack, D.**, Sundmacher, K.: Integriertes Prozessdesign und Wärmeintegration am Beispiel der Blausäuresynthese, *Jahrestreffen der ProcessNet-Fachgruppe Energieverfahrenstechnik*, Frankfurt, Germany, **2019**.

Liesche, G.; **Schack, D.**; Sundmacher, K.: Integrated process synthesis and heat integration exemplified for production of hydrogen cyanide. *Young Professionals Conference on Process Engineering*, Magdeburg, Germany, **2019**.

**Schack, D.**, Liesche, G., Sundmacher, K.: Renewables-to-Chemicals: Optimaler Prozessentwurf für eine nachhaltige Methanolproduktion unter Einsatz von CO<sub>2</sub>, *ProcessNet-Jahrestagung und 33. DECHEMA-Jahrestagung der Biotechnologen 2018*, Aachen, Germany, **2018**.

**Schack, D.**, Liesche, G., Rätze, K.H.G., Sundmacher, K.: Thermodynamic network flow approach for chemical process synthesis. *28th European Symposium on Computer Aided Process Engineering*, Graz, Austria, **2018**, (Keynote lecture held by K. Sundmacher).

**Schack, D.**, Rihko-Struckmann, L., Sundmacher, K.: Strukturoptimierung von Renewables-to-Chemicals (R2Chem) Netzwerken zur wirtschaftlichen Nutzung erneuerbarer Energien, *ProcessNet-Jahrestagung und 32. DECHEMA-Jahrestagung der Biotechnologen 2016*, Aachen, Germany, **2016**.

**Schack, D.**, Rihko-Struckmann, L., Sundmacher, K.: Structure optimization of power-to-chemicals (P2C) networks by linear programming for the economic utilization of renewable surplus energy. *26th European Symposium on Computer Aided Process Engineering*, Portoroz, Slovenia, **2016**.

## Poster contributions

**Schack, D.**, Rihko-Struckmann, L., Sundmacher, K.: An economic linear objective function approach for structure optimization of renewables-to-chemicals (R2Chem) networks, *27th European Symposium on Computer Aided Process Engineering*, Barcelona, Spain, **2017**.

**Schack, D.**, Rihko-Struckmann, L., Sundmacher, K.: Thermodynamische Analyse der Erzeugung flüssiger Kraftstoffe aus erneuerbarer Energie und Biomasse, *ProcessNet-Jahrestreffen der Fachgruppe "Energieverfahrenstechnik"*, Bonn, Germany, **2015**.

## Invited Talks

Sundmacher, K., **Schack, D.**, Liesche, G.: FluxMax: Process intensification by network flow optimization in the thermodynamic state space. *Process Intensification Colloquium*, Dortmund, Germany, **2019**.

Sundmacher, K., **Schack, D.**, Himmel, A., Bremer, J.: Bilanzierung von CO<sub>2</sub>: Betrachtung des Gesamtsystems. *8. Energiekolloquium der Chemiegesellschaften*, DECHEMA, Frankfurt, Germany, **2017**.





## Schriftliche Erklärung

Ich erkläre hiermit, dass ich die vorliegende Arbeit ohne unzulässige Hilfe Dritter und ohne Benutzung anderer als der angegebenen Hilfsmittel angefertigt habe. Die aus fremden Quellen direkt oder indirekt übernommenen Gedanken sind als solche kenntlich gemacht.

Insbesondere habe ich nicht die Hilfe einer kommerziellen Promotionsberatung in Anspruch genommen. Dritte haben von mir weder unmittelbar noch mittelbar geldwerte Leistungen für Arbeiten erhalten, die im Zusammenhang mit dem Inhalt der vorgelegten Dissertation stehen.

Die Arbeit wurde bisher weder im Inland noch im Ausland in gleicher oder ähnlicher Form als Dissertation eingereicht und ist als Ganzes auch noch nicht veröffentlicht.

Magdeburg, den 06. April 2021

Dominik Schack